Technical Research Report

CTRS-Report
March 2003

THERMAL-HYDRAULIC UNCRETAINTY ANALYSIS IN PRESSURIZED THERMAL SHOCK RISK ASSESSMENT

Methodology And Implementation On Oconee, Beaver Valley, And Palisades Nuclear Power Plants

Y. H. Chang
K. Almenas
A. Mosleh
M. Pour-Gol-Mohammed

CTRS
CENTER FOR TECHNOLOGY RISK STUDIES
A. JAMES CLARK SCHOOL OF ENGINEERING
UNIVERSITY OF MARYLAND AT COLLEGE PARK

THERMAL-HYDRAULIC UNCRETAINTY ANALYSIS IN PRESSURIZED THERMAL SHOCK RISK ASSESSMENT

Methodology And Implementation On Oconee, Beaver Valley, And Palisades Nuclear Power Plants

Y. H. Chang
K. Almenas
A. Mosleh
M. Pour-Gol-Mohammed

March 2004

Report to the RES/NRC

Thermal-Hydraulic Uncertainty Analysis in Pressurized Thermal Shock Risk Assessment

Methodology and Implementation on Oconee, Beaver Valley, and Palisades Nuclear Power Plants

Draft Report

Prepared by

Y.H. Chang
K. Almenas
A. Mosleh
M. Pour-Gol Mohammad

University of Maryland

Prepared for the
U.S. Nuclear Regulatory Commission
March, 2004

Table of Content

List of Figures

List of Tables

1 Introduction

1.1 Background

Before the year of 1978 it was postulated that the most severe thermal shock scenarios were large loss of coolant (LOCA). The large thermal stress on the reactor pressure vessel (RPV) wall alone could cause RPV failure (crack through). The Rancho Seco incident (March 20, 1978) raised concern that secondary system induced RCS over cool down combining with RCS repressurization would result in maximum tensile stress imposed on the inside surface of the RPV. When events such as the Rancho Seco incident combine with reduced RPV wall toughness due to neutron irradiation, it was suspected that small flaws existing on the surface or embedded in the RPV wall could propagate and eventually crack through the wall. Since then pressurized thermal shock (PTS) risk was designated as an unresolved safety issue (A-49)[Rosenthal 2001].

Between 1983 and 1985, the US Nuclear Regulatory Commission (NRC) selected three pressurized water reactors (PWRs) for Integrated Pressurized Thermal Shock (IPTS) analysis. These three plants were: Oconee Unit 1 (B&W), Calvert Cliffs Unit 1 (Combusting Eng.) and H.B. Robinson Unit 2 (Westinghouse).

Results concluded from the PTS study of Calvert Cliffs Unit 1, a Combusting Engineering designed two-loop PWR, are [Selby, Ball et al. 1984]:

- small break LOCA (SBLOCA) occurring during low decay heat conditions were the most significant contributors to the PTS risk
- uncertainty in the RPV flaw density was the most important uncertainty contributor to the overall uncertainty in the risk
- the most important operator action in mitigating PTS risk was controlling repressurization after a rapid cooldown

Results concluded from the PTS study of H.B. Robinson Unit 2, a Westinghouse designed three-loop PWR, are [Selby, Ball et al. 1985]:

- main steam line breaks (MSLB) involving blowdown of more than one stream generator (SG) were the most important contributor to PTS risk
- uncertainty of flaw density on the RPV wall was the most important uncertainty contributor to the overall uncertainty in PTS risk
- The most important operator actions to mitigate the PTS risk were:
  - closing main steam isolation valves (MSIVs) following a small or medium-sized MSLB down stream of MSIVs, and
  - isolating auxiliary feedwater (AFW) to low-pressure SGs following MSLB incidents

In the study of Oconee Unit 1 [Burns, Cheverton et al. 1986], a B&W designed two-hot-leg-and-4-cold-leg PWR, the PTS risk scenarios were grouped into three event categories: MSLB, all turbine bypass valves stuck open, and 2-inch (2E-3m^2) SB LOCA. Conclusions are:

- MSLB was the most significant contributor to the through-the-wall crack (TWC) risk
- the uncertainty of the downcomer temperature was the most important contributor to the overall uncertainty in the risk
- the most important plant features that mitigate the PTS challenge were
  - RPV vent valves
  - Feedwater pumps tripping on high SG levels
- the most important operator action to reduce the PTS challenge was isolating an SG during MSLB

A number of studies had been performed in understanding PTS related risk such as studying thermal hydraulic mixing impacts [Theofanous and Yan 1991; Bass, Pugh et al. 1999], a probabilistic fracture mechanics (PFM) sensitivity study using SBLOCA transients as the leading conditions for the Yankee Rowe Reactor Pressure Vessel [Dickson, Cheverton et al. 1993], assessing the impact of heat transfer coefficient uncertainty [Boyd and Dickson 1999], and international efforts of understanding PTS related materials characteristics [Ikonen 1995; Pugh and Bass 2001]. Results of these studies provide insights for this analysis.

The most recent IPTS study was performed on the H.B. Robinson plant [Palmorse 1999]. Scenarios from four different initiating events were analyzed. The initiating events were SBLOCA (2-inch break) at hot leg and cold leg, double ended MSLB at hot standby, and SG overfeed. It indicated that SBLOCA and MSLB are the two most important PTS risk event initiators. The conclusions indicate that the PTS challenge requires the presence of both thermal stress and pressure stress. Presence of thermal stress alone contributes little to PTS risk.

1.2 Achievements and Observations from this Study

The assessment of PTS risk uncertainty is achieved by the collaboration of multiple disciplines including probabilistic risk assessment (PRA), thermal hydraulic (TH), and PFM. This report discusses the method and results in analyzing TH uncertainty contributing to PTS risk uncertainty. The following are achievements from this study:

- Rediscovered large LOCA as a significant PTS contributor
  Despite PTS initiators having been narrowed down to SBLOCA and MSLB, the TH uncertainty study reassesses the whole event spectrum that could cause PTS risk. Sensitivity assessment identified break size as one of the key parameters. PFM calculation for LOCA at various sizes revealed that large LOCA is one of the significant PTS risk contributors. It indicates that thermal stress alone could cause TWC.
- Revised the Phenomena Identification and Ranking Table (PIRT) process
  A top-to-bottom approach is developed to identify the key parameters. Sensitivity assessment on the parameters could rank the parameters.
- Developed a PTS events classification matrix to facilitate analysis
  A PTS event classification matrix was developed through the top-to-bottom approach to classify event categories for PTS risk analysis. The matrix classifies

events with clear boundary conditions. The classification reduces the number of key parameters needed for analysis, which reduces analysis complexity.

- Developed a method to identify PTS risk representative scenarios
  A sensitivity indicator was identified for measuring sensitivities of individual parameters. Justified assumptions are applied to assess aggregate sensitivity of multiple parameters' combined effect. The PTS risk representative scenarios are identified directly. No numerical processing is required to generate artificial time histories of the three TH parameters relevant to PTS risk for the representative scenarios. The three TH parameters are downcomer fluid temperature (T_{dc}), downcomer pressure (P_{dc}), and the heat transfer coefficient between RPV inner wall and RCS fluid at the downcomer region (h_{dc}).
- Performed a thorough parameter sensitivity assessment
  The one-factor-at-a-time method is used to plan RELAP5 calculations to assess parameters' sensitivities at various boundary conditions. Between 100 and 200 RELAP5 calculations are performed for each plant to assess parameters' sensitivities. After the RPV's conditional probability of failures of these RELAP5 calculations are calculated, the results provide rich information in understanding the relationship between TH behavior and PFM.

Observations from the study are concluded as follows:

- For events with similar TH signature, the effect of P_{dc} uncertainty on PTS uncertainty is small compared with the impact of T_{dc} uncertainty. One exception is the scenarios involving RCS repressurization.
- Scenarios of large LOCA and PZR SRV stuck open and later self reseated are the two most significant PTS risk event categories.
- For PZR SRV stuck open and later self reseated scenarios, the SRV reseat timing and the timing of operator throttle HPI could significantly affect PTS risk.
- Reducing even a quarter of the HPI flow rate in small LOCA scenarios could significantly reduce PTS risk

1.3 Products Requirements and Resources Restrictions

The following lists restrictions applied on the assessment:

- PFM computational input
  With the FAVOR (the PFM computing program) input requirements, a class of scenarios needs to be represented by one or a few representative scenarios. The TH inputs to PFM analysis are the deterministic time histories of T_{dc}, P_{dc}, and h_{dc} of PTS risk representative scenarios and probabilistic distributions of the representative scenarios.
- Resource (i.e., budget) limitations
  - TH uncertainty analysis is constrained to focus only on the PTS-dominant event categories
  - Restriction in the number of representative scenarios could be chosen to represent a huge number of scenarios in the PRA model (181,258 for Oconee, 8,298 for Beaver Valley, and 3,425 for Palisades)
- FAVOR availability

FAVOR was under revision and was not available for production calculation during the method development phase. The relationship between TH behavior and its PFM impacts could not be assessed without FAVOR calculations. In terms of assessing PTS significance from the PFM perspective, only the 300 °F screen criterion is decisive. The other observations are qualitative statements (e.g., RCS repressurization is PTS significant).

- Exclusive of external events
  External events (e.g., fire, earthquake) are not included in the PRA model. Their contributions to PTS risk are not included in the whole project.

1.4 Tasks and Process

PTS uncertainty analysis is a complex issue since it involves various uncertainty sources such as uncertainties in PRA model construction, TH analysis, PFM calculation, and interfaces. It requires collaboration of professionals in different disciplines to achieve the goal. This project aims to develop a systematic way of analyzing PTS uncertainty to be used for the other PWRs. In doing so, the project focuses are divided into three groups, and NRC staff are supervising and coordinating the joint effort among the three groups. The three groups and their responsibilities are discussed in the following:

- PRA group
  The PRA group is composed of professionals from NRC, SNL, INEEL, and SAIC. This group is responsible for interacting with plant staff to construct a PRA model for PTS scenarios. In order to manage the huge number of event sequences generated in the PRA model for further TH uncertainty analysis, a limited number of bins are specified to bin the sequences having similar TH responses. The probability of a bin is the accumulative probabilities of sequences binned to it.
- TH group
  Two subgroups exist for different purpose. This first subgroup assesses validity of the TH program used for the analysis, RELAP5-gamma. The group composes professionals from NRC, ISL (RELAP), LANL (TRAC), Oregon State University (APEX experiments), and UMD (studying downcomer and cold leg flow patterns by using a laser illuminated fluorescent dye and camera system). The second subgroup develops methods to assess TH uncertainty and to identify uncertainty representative scenarios. The group composes experts from NRC and UMD.
- PFM group
  The PFM group is composed of professionals from NRC, ORNL, and UMD. This group is responsible for FAVOR development and computation to assess final PTS risk.

PTS uncertainty includes three types of uncertainty relating to the above three groups and the interfaces between these groups. Figure 1.1 shows the conceptual process to aggregate the uncertainties. The block on left hand side represents the event trees constructed based on the PRA model. In order to manage such a huge number of sequences, a number of bins (typically about 50 bins) are identified. Sequences that have similar TH responses are binned together. Each bin represents an event cluster whose

frequency is an accumulative frequency of the scenarios binning to it. Binning is an iterative process between experts in the PRA, TH, and PFM fields to ensure the bins cover all PTS event categories.

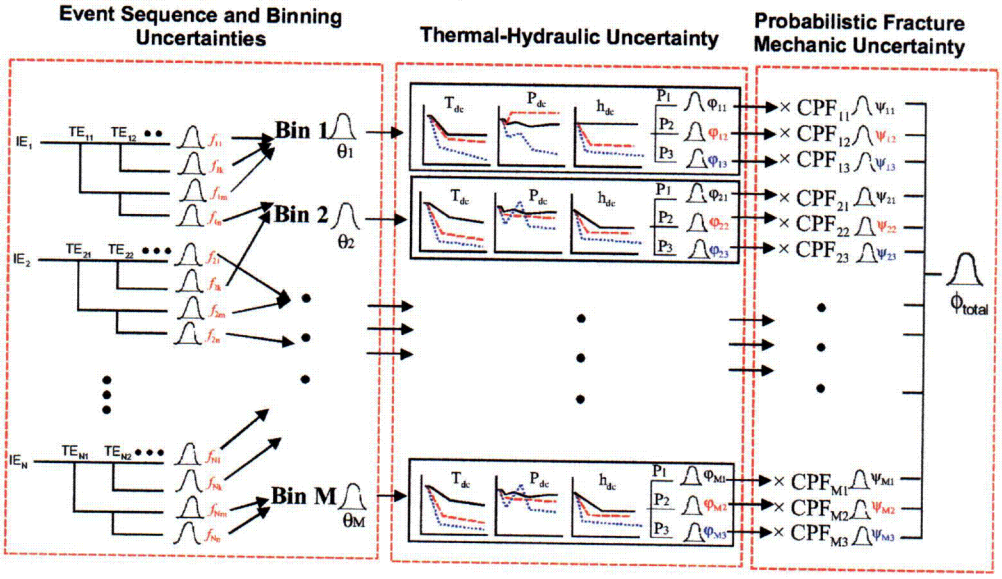

Figure 1.1 The conceptual model of the PTS uncertainty analysis process

Each bin represents an event cluster. TH uncertainty analysis assesses uncertainty of TH behavior (i.e., T_{dc}, P_{dc}, and h_{dc}) and selects a few representative scenarios to represent the PTS risk of each bin. Each representative scenario splits the bin's probability. Typically 3 to 5 scenarios are identified to represent the TH uncertainty of each event category. RELAP5-gamma was used to calculate the representative scenarios to generate time histories of T_{dc}, P_{dc}, and h_{dc}, which along with the probability distribution of the representative scenario, are data required for PFM analysis. PFM analysis is based on the time history of T_{dc}, P_{dc}, and h_{dc} of each representative scenario to calculate its conditional probability of RPV failure (CPF). The FAVOR's post process accumulates the products of event frequencies (probabilities) and CPFs for all representative scenarios to assess total PTS risk.

Constrained by resource limitations, TH uncertainty was performed only on PTS-dominant event categories. For the bins having less PTS risk, the TH uncertainties of these bins were not analyzed. A conservative representative scenario was selected for the bins. The bins having no PTS risk were eliminated from further analysis (Figure 1.2).

C01

At the beginning of the PTS risk assessment process, the PRA group, TH group, and PFM group develop their methods of approach independently. PRA group used a bottom-to-top approach to build a PRA model (i.e., event trees) that differed from the TH group's top-to-bottom approach. However, at the end the two approaches reached the same results in event classification except that there were minor differences in the scope of some event categories. For example, LOCAs are divided into small (less than 2 inches), medium (2 – 6 inches), and large LOCAs (greater than 6 inches) in the PRA model. In TH analysis, LOCA was divided into less than 1.5 inches, between 1.5 and 4 inches, between 4 and 8 inches, and greater than 8 inches, based on their TH similarity. As a result the probability of a PRA bin could be split into two TH event categories, and a TH event category could share probabilities from more than one PRA bin.

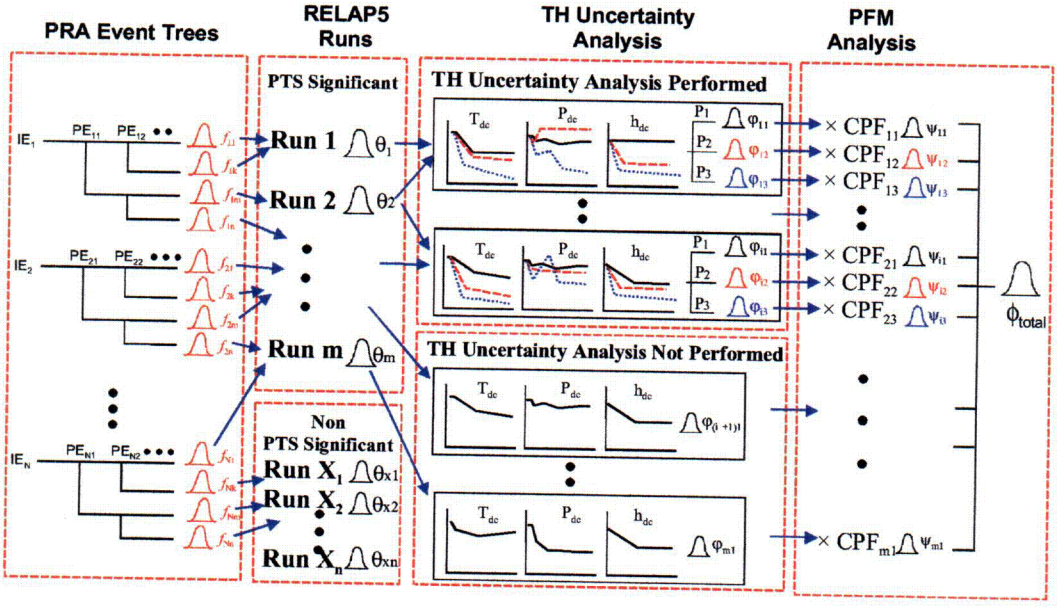

Figure 1.2 The real process of the PTS uncertainty analysis for the Oconee-1 NPP

In this report, Section 2 reviews the most recent IPTS on H.B. Robinson NPP. Section 3 summarizes the task flow for TH uncertainty assessment, which includes identification of factors affecting thermal stress and pressure stress, event classification and identification of the key influencing parameters at the system level, determination of uncertainty analysis scope, sensitivities assessment of influencing parameters, uncertainty assessment, and selection of representative scenarios.

Section 4 discusses identification of factors affecting thermal stress and pressure stress, event classification and identification of the key influencing parameters at the system level, and determination of uncertainty analysis scope. A top-to-bottom approach is used to identify the factors affecting thermal stress and pressure stress. The process

C02

parameters and phenomena at the system level are discussed and their impacts are assessed. As a result a PTS events classification matrix is constructed to facilitate the analysis effort. The matrix classifies PTS event based on the main factors affecting thermal stress and pressure stress. The boundary conditions of each cell within the matrix is clearly defined, which reduces the number of influencing parameters needed to be considered for the analysis and dramatically reduces the analysis effort.

TH uncertainty analysis heavily relies on the RELAP5 computational program. It added another layer of uncertainty, **model uncertainty**, beyond the existing **parameter uncertainty**. Parameter uncertainty relates to the boundary conditions characterizing the transient and is "**what** input to RELAP5". Model uncertainty relates to the appropriateness of RELAP5 used in analyzing the transient and is "**how** RELAP5 models it". Section 5 discusses the model (RELAP5-gamma) uncertainty. Several RELAP5-gamma modeling weaknesses resulting from inherent limitations of RELAP5 are discussed. Some of them are treated explicitly and some of them are not treated. For example, the uncertainty of pluming in the downcomer region, which can not be modeled by the 1-D code, is not treated. The key factors affecting modeling uncertainty are discussed.

Section 6 discusses parameter sensitivity. The event category of primary system losing subcooling is identified as the greatest PTS risk event category. The parameters affecting PTS risk are identified, and their sensitivities are assessed. A sensitivity indicator (T_{sen}) is chosen to measure parameter sensitivities. T_{sen} is calculated by averaging T_{dc} of the first 10,000 seconds of a scenario, and T_{sen} is a surrogate indication of thermal stress. Use of T_{sen} allows identification of the representative scenarios without performing huge number of RELAP5 and FAVOR calculations. A matrix is developed for each plant to assess the T_{sen} of each influencing factor using the one-factor-at-a-time method. T_{sen}s are calculated by RELAP5. Hundreds of RELAP5 calculations are performed for sensitivity assessment of the four plants.

Section 7 discusses analysis results of Oconee-1, Beaver Valley, and Palisades NPPs. Medium LOCA, Large LOCA, and PZR SRVs stuck open and later self reseated scenarios are concluded to be the dominant initiators for PTS risk. Section 8 discusses the relationship between T_{sen} and CPF. In this analysis, the pressure stress uncertainty is limited for each event category. The PTS uncertainty is mainly dependent on the uncertainty of thermal stress. T_{sen} is used as a surrogate thermal stress indicator. It is used to select the representative scenarios. The appropriateness of T_{sen} selection is discussed.

Section 8 discusses the appropriateness of using T_{sen} as the sensitivity indicator. Parameters' sensitivities in T_{sen} and CPF are compared.

Appendix A classifies events from a different perspective. Three types of event categories are identified dependent on the system responses to perturbations. The perturbations could have damped, proportional, or augmented effects on the system. The key factors of different types of effects are discussed. It provides another viewpoint of

classifying TH uncertainty. Appendix B justifies the argument that h_{dc} uncertainty has insignificant contribution to PTS uncertainty.

Appendix B confirms the conclusion reached by Boyd and Dickson [Boyd and Dickson 1999] that energy transfer from the RPV wall is conduction limited over the entire possible range of h(t) values. The evaluation of temperature gradients within the wall then depends principally on the fluid temperature $T_{dc}(t)$, and the uncertainties associated with the evaluation of h(t) have a small influence.

Appendix C reviews the range of temperature differences between the primary system and the secondary side. It concludes that SGs are over designed when the reactor is tripped. The amount of SGs heat capacity is substantial. With a huge amount of heat transfer area, the secondary side becomes the heat source in some transients to moderate the T_{dc} decreasing rate when the primary system is coupling with the secondary system.

Appendix D places the Oconee-1 TH representative scenarios in the PTS event classification matrix. Appendix E is the C++ computer code developed to calculate multiple factors combined effects on T_{sen} and combination probabilities. The results provide a foundation for identifying the uncertainty representative scenarios.

Appendix E lists the RPV conditional probability of failure (CPF) results calculated by the FAVOR code for the parameter sensitivity study. It's a study for validating the appropriateness of use of T_{sen}.

Appendix F lists the RELAP5 calculations performed by ISL and their placement in the PTS event classification matrix.

2 Literature Review and Study Restrictions

This chapter reviews the H.B. Robinson Unit 2 (HBR-2) PTS uncertainty study [Palmorse 1999], which is the most recent NPPs PTS uncertainty study. The HBR-2 PTS uncertainty analysis was in response to the SECY-92-283 regulation guideline, which emphasizes the cold leg stratification impact on PTS challenge. The HBR-2 study does not intend to evaluate the PTS probability for all possible scenarios, instead, a few scenarios concerning cold leg stratification were analyzed, and their TH uncertainties were calculated.

The HBR-2 study modified the Code Scaling, Applicability, and Uncertainty (CSAU) evaluation methodology [Boyack, Catton et al. 1990] to assess TH uncertainty. The original and modified processes of the CSAU methodology are shown in Figures 2.1 and 2.2 respectively. The CSAU methodology was developed with the background of NRC rules approved in 1988 allowing the results obtained from using the best-estimate methods to be used to provide more realistic estimates of plant safety margin. However, the rules also require quantifying the uncertainty of the best-estimate results for comparison with the prescribed acceptance limits provided in the 10 CFR Part 50. The CSAU methodology was developed to quantify the best-estimate method's (code's) uncertainty. A CSAU methodology demonstration was performed, assessing peak clad temperature (PCT) uncertainty in quantifying reactor safety margin. The H.B. Robinson study modified the CSAU methodology and implemented it on PTS uncertainty analysis.

In the HBR-2 study, four specific scenarios were selected for TH uncertainty study: 2-inch diameter cold leg LOCA, 2-inch diameter hot leg LOCA, MSLB from HZP conditions, and SG overfeed. For each scenario, a Phenomena Identification and Ranking Table (PIRT) process, an expert judgment based parameter importance ranking procedure, was first performed to weight parameters. Through the PIRT process, the upper bound, nominal, and lower bound values of each important parameter were identified.

Second, an uncertainty calculation matrix was developed to identify baseline TH runs. In the original CSAU methodology, the surface response methodology was used to design necessary runs, however, the HBR-2 study did not use the surface response methodology. Instead, some important parameters were placed into common groups based on their PTS impact commonalities. Two groups were created based on the parameters with similar impact on RCS injection flow rate (i.e., HPI flow and accumulator pressure) and RCS injection temperature (i.e., HPI temperature and refueling water storage tank (RWST) temperature). Three parameters could not be grouped and were discussed separately. The three parameters are PRV wall heat conductivity, flow distribution and mixing in downcomer, and break flow. An uncertainty calculation matrix was developed based on the impact magnitudes and PTS influence of these two groups and the three individual parameters' directions. The calculation matrix typically includes a nominal run, an extreme mitigate PTS challenge run, an extreme enhance PTS challenge run, and a few other runs varying from the two extreme runs. In totally six RELAP5 runs were

performed to assess PTS uncertainty of 2-inch hot leg LOCA. Different TH calculation codes, such as TRAC-P, REMIX, and COMMIX, were used to validate RELAP5 results.

Finally, a numerical method was used to manipulate the results of the baseline RELAP5 runs to generate new T_{dc}, P_{dc}, and h_{dc}s' time histories to create new scenarios. These new scenarios include selecting the data with the maximum and minimum PTS contribution from all baseline runs for each time step (e.g., lowest T_{dc} and highest P_{dc}) to generate the upper and lower bounds for PTS challenge. The mean scenario is the numerical product of averaging all baseline runs. Uniform distribution was assumed for all parameters' probabilities, thus the distribution between maximum and minimum bounding curves was uniform. The new generated upper, mean, and minimum scenarios represent the 5^{th}, 50^{th}, and 95^{th} percentiles for TH uncertainty, and are used for PFM calculation.

As mentioned above, the uncertainty scenarios representing the 5^{th}, 50^{th}, and 95^{th} percentiles for TH uncertainty are numerically manipulated products rather than real scenarios. For example, the 95^{th} percentile scenarios have the lowest T_{dc} and highest P_{dc} of all baseline scenarios, intended to produce the highest thermal stress and pressure stress in one scenario. In real scenarios, scenarios with lower T_{dc} usually have lower P_{dc}. H.BR-2's approach also overlooks the significant impact of RCS repressurization on PTS risk. RCS repressurization caused by the scenario of PZR SRV stuck open and self reseated in later of the scenario is identified as one of the PTS dominant event categories in the current study.

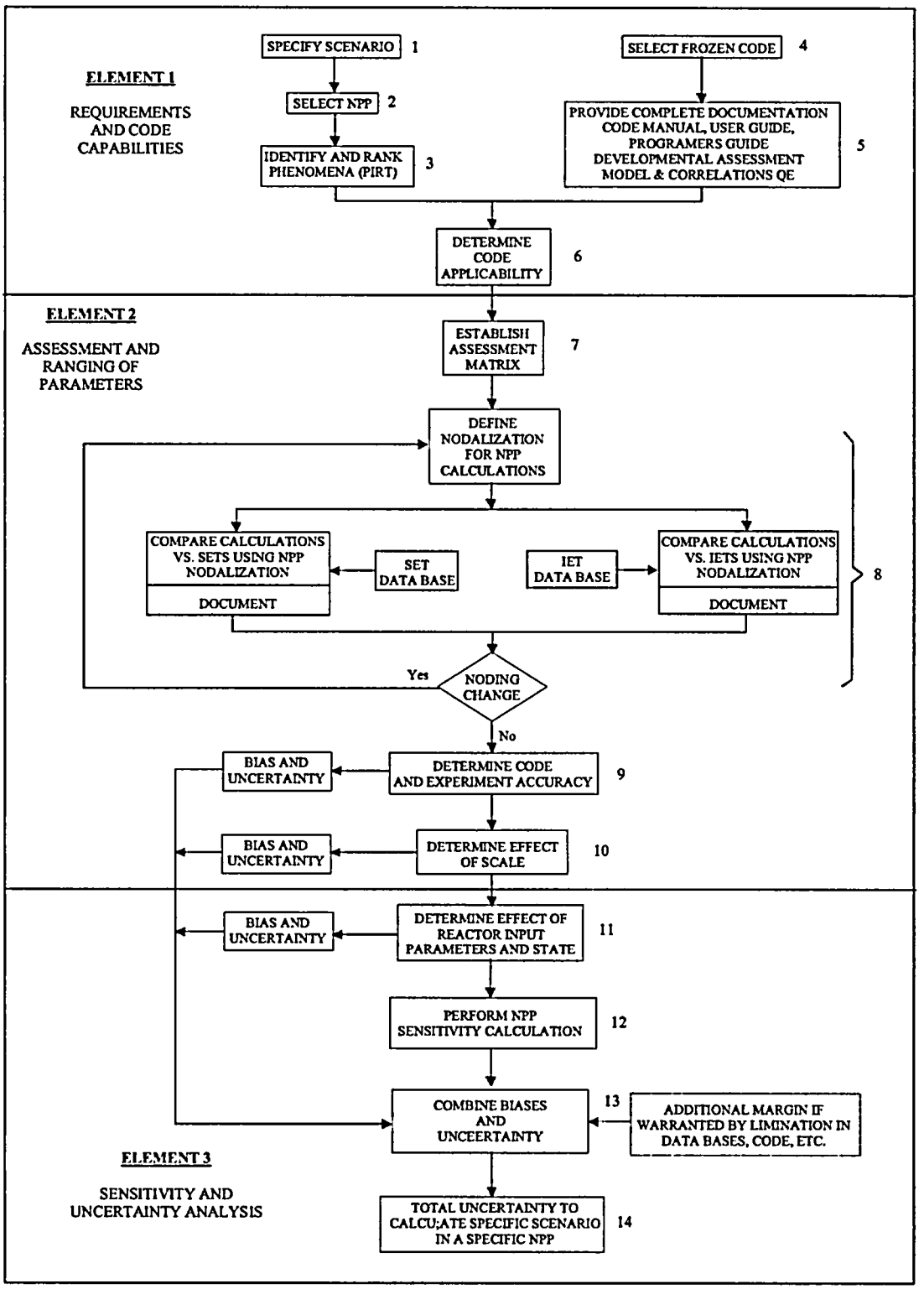

Figure 2.1 The Code Scaling, Applicability and Uncertainty (CSAU) evaluation methodology [Boyack, Catton et al. 1990]

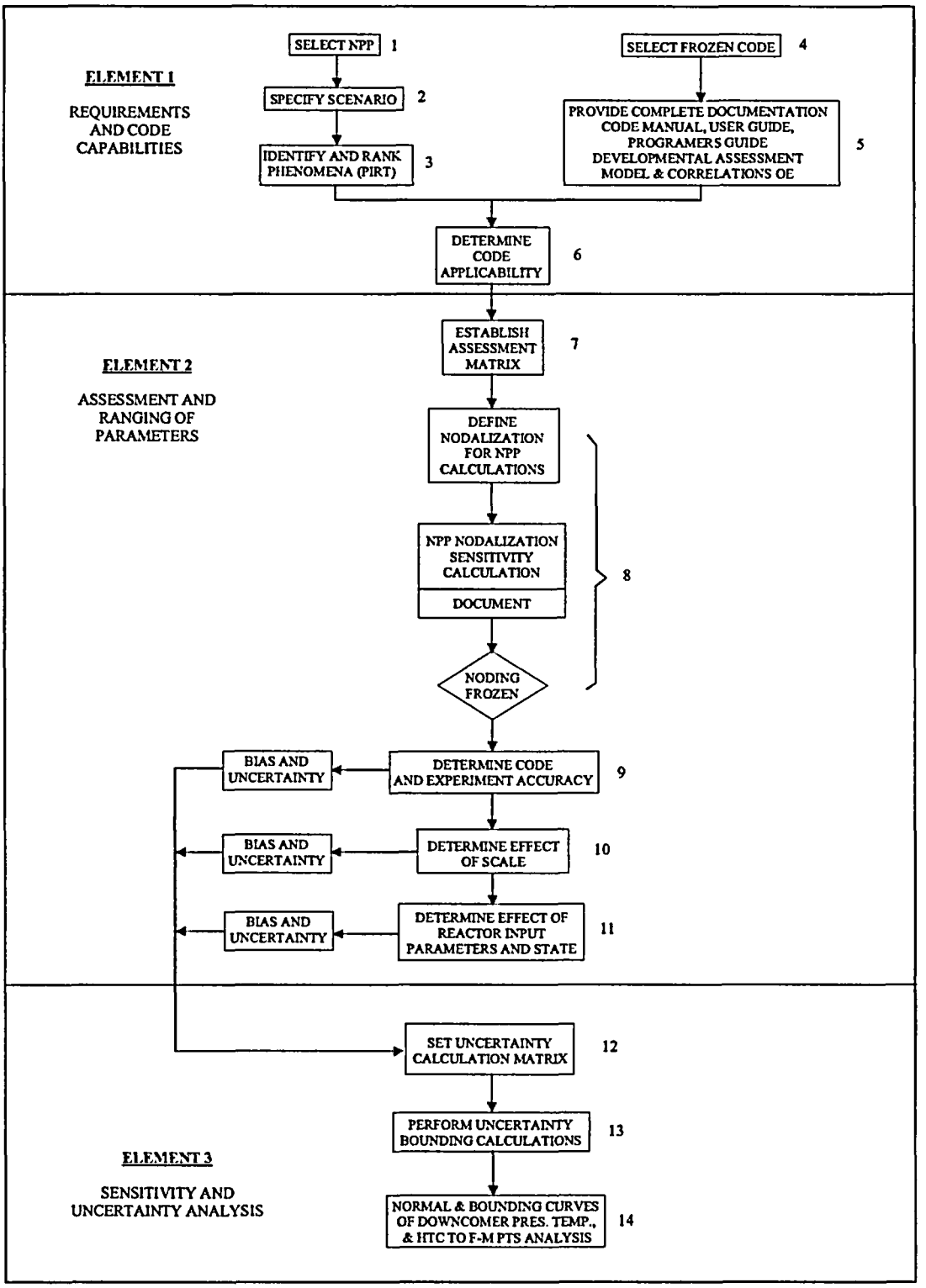

Figure 2.2 Process of the H.B. Robinson Unit-2 PTS uncertainty methodology [Palmorse 1999]

3 TH Uncertainty Assessment Process

This section summarizes the task flow for TH uncertainty assessment, which includes identification of factors affecting thermal stress and pressure stress, event classification and identification of the key influencing parameters at the system level, determination of uncertainty analysis scope, sensitivities assessment, uncertainty assessment, and selection of representative scenarios. These tasks are divided into nine steps. There are iterations between some steps. Some steps require PRA and PFM inputs. Figure 3.1 shows the block diagram of the TH uncertainty assessment process. Steps 1 to 3 are the foundation buildup process for understanding PTS and plant design influencing PTS analysis. The purpose of these steps is to facilitate the analysis effort. The "real" uncertainty analysis starts at Step 4. The following paragraphs provide an introduction to these steps. The detailed process of each step is discussed in the rest of this report.

Step 1 Apply basic principles and plant-specific design characters to identify influencing factors

TH uncertainty deals with the uncertainty of three parameters: the downcomer fluid temperature (T_{dc}), the downcomer pressure (P_{dc}), and the heat transfer coefficient between inner RPV wall and downcomer fluid (h_{dc}).

The impact of h_{dc} on the evaluation of temperature gradients within the RPV wall has been studied [Boyd and Dickson 1999], and it has been concluded that heat transfer to and from the RPV wall is determined primarily by the internal, conductive resistance, that is, energy transfer with the RPV wall is conduction limited. The impact of $h_{dc}(t)$, as well as the computational uncertainties that are associated with $h_{dc}(t)$ is therefore limited. Appendix B of this report provides additional support for this conclusion. As a result, the effort of uncertainty assessment could focus on two parameters only: $T_{dc}(t)$ and $P_{dc}(t)$.

The basic factors affecting an open system's temperature are the heat capacity of the system and the heat sources and heat sinks introduced into the system. For RCS design, downcomer temperature gradient could also be affected by the secondary system thus RCS flow pattern (i.e., forced circulation, natural circulation, and flow stagnation) also is one of the influencing factors. Some plant-specific design could also change the fluid temperature distribution inside the RPV, consequently T_{dc} is affected. For example, the RPV vent valves of the B&W reactor could cause hot water/steam at the core top region to flow to the downcomer region to increase T_{dc}. The five T_{dc}-dependent factors are the following:

- Heat capacity
- Heat source
- Heat sink
- RCS coolant flow rate
- RPV internal fluid/stream energy distribution

The basic factors changing an open system with constant volume pressure are the mass and energy change of the system. For RCS the mass is the coolant in and out of the system. The energy in and out of the system is dependent on the heat sources and heat

sinks of the system. Besides mass and energy, steam condensation occurring in RCS could change reactor pressure. The following are the three P_{dc}-dependent factors:

- Change in RCS coolant inventory
- Change in heat source and heat sinks
- Steam condensation in RCS

The specific parameters relating to factors affecting T_{dc} and P_{dc} could be identified based on system design. Some parameters might require more elaboration to identify the basic parameters. For example, a primary system breach would induce a heat sink to RCS. The basic parameters relating to primary system breach could be breach size and breach location (in hot leg or cold leg sections).

•

Step 2 Construct PTS event classification matrix

Based on the factor that the primary system and secondary system have huge heat capacities, it is necessary to induce a huge heat sink to have PTS. There are a few scenarios could cause a substantial heat sink to have PTS risk. A PTS event classification matrix is constructed based on the scenarios. Three scenarios frame the matrix: breach in primary system, depressurization in secondary system, and overfed secondary system. An additional factor, HPI state, is considered in all scenarios, since the pressure uncertainty is strongly dependent on HPI state for the interest of PTS.

The purpose of the matrix is to facilitate uncertainty analysis in three perspectives. First, through well classified event categories with clearly defined boundary conditions the number of influencing parameters needing to be considered can be reduced. This reduces analysis effort. Second, the matrix provides a framework for analysts to perform scenario propagation. It's especially helpful in identifying operators' actions. Operators' actions are one of the important factors contributing to PTS uncertainty. Third, the matrix provides a framework to perform preliminary screening in order to focus on PTS significant event categories.

Step 3 Apply conservative qualitative screening to identify event categories with PTS potential

This step requires PRA inputs. The PTS event classification matrix provides a framework for preliminary screening to eliminate the PTS-insignificant event categories. Screening criteria could be low event frequency or low fracture mechanics challenge. Since event frequencies of the initiating events that construct the matrix can be roughly estimated, the frequencies of event categories involving one or several combined initiating events can be estimated too. The current screen criterion for event frequency is 1E-8 per reactor year. For the fracture mechanics challenge screening, the event categories that cannot decrease T_{dc} to below 422 °K (300 °F) and cannot cause a T_{dc} cooldown ramp greater than 56 °K/hr (100 °F/hr) are screened out from further analysis.

Step 4 Select dominant event categories for uncertainty analysis

This step requires PRA and PFM inputs. Select one or a few most likely or representative scenarios in each remaining (not screened out) event category to have their

CPF calculated. The CPF information along with the event frequencies could be used to prioritize the event categories for uncertainty analysis. For the analyzed four plants it happens that loss of RCS subcooling due to primary system breach is the dominant event category contributing to PTS-risk. With resource limitations, TH uncertainty analysis is performed on this category only.

Step 5 Refine event categories to bind pressure stress uncertainty
The defined event categories contain a wide range of T_{dc} and P_{dc} uncertainties. It requires finer classification to reduce uncertainty. It is observed that the variation of P_{dc} contributing to PTS uncertainty is much smaller than contribution from T_{dc} uncertainty in an event cluster. The exception is in the scenarios involving RCS repressurization. Event categories could be refined further to eliminate contributions from P_{dc} uncertainty. The uncertainty analysis could focus on T_{dc} uncertainty only. For the scenarios involving RCS repressurization, the T_{dc} uncertainty and P_{dc} uncertainty need to be analyzed separately and combined together to determine the aggregated effect on PTS risk.

For example, the event category of primary system breach causing RCS loss of subcooling includes two types of scenarios: LOCA and PZR valves stuck open. For LOCA scenarios, sensitivity analysis indicates that greater than 1.5-inches LOCA could cause RCS to lose subcooling. LOCA with break size between 1.5 inches and the max possible break size are within the event category. P_{dc} uncertainty in the event category is too large to be neglected. In the analysis, LOCA is further subdivided into three groups dependent on their break sizes: between 1.5 and 4 inches, between 4 and 8 inches, and greater than 8 inches. For PZR SRV stuck open scenarios, RCS repressurization could occur if the valve stuck open reseats during the later of the scenarios. In such situations, P_{dc} uncertainty needs to be taken into consideration. The PZR SRV stuck open scenarios are divided into two groups. The distinction between the two groups is SRV reseating.

Thus five subcategories are generated from the original event category. Only one subcategory requires handling T_{dc} and P_{dc} uncertainties. The other four subcategories deal only with T_{dc} uncertainty. These five categories are listed below:

- LOCA between 1.5-inches and 4-inches (consider only T_{dc} uncertainty)
- LOCA between 4-inches and 8-inches (consider only T_{dc} uncertainty)
- LOCA greater than 8-inches (consider only T_{dc} uncertainty)
- PZR SRV stuck open and remains open till the end of scenario (consider only T_{dc} uncertainty)
- PZR SRV stuck open and self reseated in the middle of the scenario (consider both T_{dc} and P_{dc} uncertainties)

Step 6 Identify sources of uncertainty and corresponding ranges
For each refined event category identified in Step 5, if there are any, identify the key parameters influencing T_{dc} (and P_{dc} if necessary). The system parameters relating to the five T_{dc}-dependent factors and three P_{dc}-dependent factors specified in Step 1 need to be identified. The key parameters affecting T_{dc} and P_{dc} are concluded to be the following: Factors affecting T_{dc} and the key system parameters of the factors:

- Heat capacity

Liquid mass, steam mass, and structure mass of the primary system and secondary system

- Heat source
  Decay heat, RCPs pump heat, structure heat, and PZR heater
- Heat sink
  - Breach size, breach location (i.e., elevation and HL vs. CL), breach flow rate, PZR SRV reseat timing
  - RCS coolant injection temperature, flow rate, timing of injection
  - Energy transferred to the secondary system. Depressurization and overfeeding of the secondary system would induce an excessive heat sink to RCS.
- RCS coolant flow rate
  RCPs' states, flow resistance
- RPV internal fluid/stream energy distribution
  RPV vent valves states (B&W reactor only)

Factors affecting P_{dc} and the key system parameters of the factors:

- Change in RCS coolant inventory
  - Breach size, HPI flow rate, and PZR SRV reseat timing
- Change in RCS energy
- Steam condensation

Uncertainty sources for the above parameters could be from model uncertainty or parameter uncertainty. It is important to identify the common causes for different parameters. For example, the HPI, accumulator, and LPI coolant temperatures vary with seasonal differences. The season is a common factor for the temperatures of the HPI, accumulator, and LPI.

For each identified factor, its range of variation needs to be identified. Its uncertainty is discretely represented by its lower bound, nominal value, and upper bound with appropriate probabilities.

Step 7 Perform sensitivity analysis of each key parameter

Construct a parameter sensitivity assessment matrix based on the nominal range sensitivity analysis (NRSA) method [Cullen and Frey 1999; Frey and Patil 2002] or the one-factor-at-a-time (1-FAT) method. Since break size is an independent parameter, and all the other parameters' sensitivities in T_{sen} are dependent on break size, a parameter's sensitivities have to be assessed at various break sizes. Based on the representative values identified for each parameter in Step 6, a parameter's sensitivities are assessed by RELAP5 calculations.

For example, winter's effect could be assessed by comparing RELAP5 results (i.e., T_{sen}) with RCS injection coolant temperatures of spring/fall and of winter. The difference in T_{sen} is the index of winter's impact.

Step 8 Determine the aggregated uncertainty and select representative scenarios
Linear additive analysis could be used to assess the combined effect of multiple uncertainty sources on T_{sen}. This assumption is valid for the event category of primary system breach being the dominant heat sink. The assumption does not work for scenarios where parameters are strongly dependent on each other.

A small computing program (see Appendix D) is written to estimate the sensitivities of all combinations. The sensitivity of a combination is the accumulative sensitivities of its compositions. The probability of a combination is the product of its compositions' probabilities. These combinations could be plotted in a probabilistic density function (PDF) versus T_{sen} plot as shown in the left hand side of Figure 3.1. Transferring the PDF into a cumulative distribution function (CDF) plot, the representative scenarios can be identified. In the CDF diagram, the distribution less than the 5th percentile and greater than the 95th percentile are cut off from the representative scenarios selection process. The distribution range from the 5th percentile to the 95th percentile is divided equally into several sections, depending on the required detail. Each section generates a representative scenario at the mean distribution. For example, a section's probabilities for the lower and upper bounds are P_L and P_H, respectively. The representative scenario is selected at the $(P_L + P_H)/2$ position. The probability for this representative scenario is $(P_H - P_L)$. The representative scenarios' T_{sen}s can be identified through reflecting the selected percentiles to the CDF curve. Based on the T_{sen}s, the exact combinations of the representative scenarios can be identified from all the combinations (see the right hand side of Figure 3.1). The probabilities of the cut off tails are distributed to the lower bound and upper bound representative scenarios.

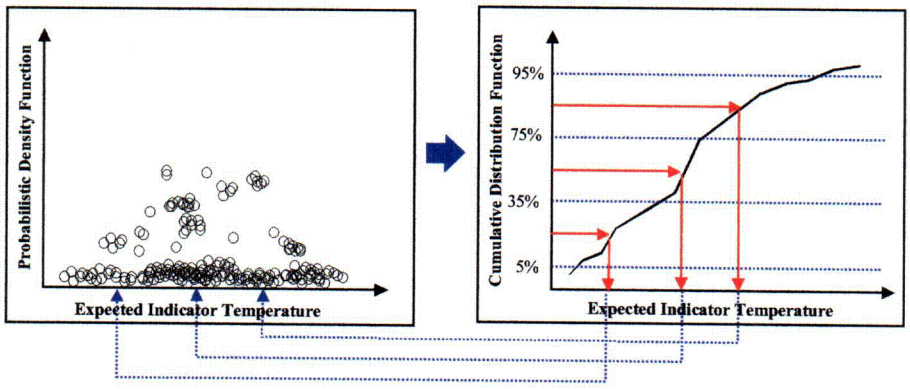

Figure 3.1 The probabilistic density function and cumulative density function diagrams for identification of uncertainty representative scenarios

Step 9 Estimate frequency distribution for each representative TH run
The uncertainty representative scenarios identified in Step 8 shares the event frequency of their represented TH Bin, thus, their frequencies can be calculated by multiplying their probabilities by the frequency of their represented TH scenario. In some cases, there are some differences in scope definition between the PRA group and the TH group, and an

C03

adjustment factor might be needed to make them consistent with each other in probability.

RELAP5 is used to calculate all representative scenarios to generate the time histories of T_{dc}, P_{dc}, and h_{dc} along with the scenarios' probability distributions for PFM analysis.

4 Important PTS Related System Characteristics and Event Classification Matrix

Quantification of the uncertainties of T_{dc}, P_{dc}, and h_{dc} requires a careful assessment of their relative importance and their inter-dependence. These parameters vary in time, and their uncertainty band varies as well, furthermore, for some types of transients, these parameters are not independent, consequently neither are their uncertainties. Section 4.1 discusses the end parameters relating to thermal stress and pressure stress from a TH perspective.

Irrespective of how the PTS significant transient scenarios are initiated, their evolution is dominated by the mass/energy exchange rates imposed on the fluid of the primary system. Therefore, terms in the mass/energy balance of the primary system fluid could be used as classification criteria. The large number of 'event' based scenarios can be classified into a significantly smaller number of categories. Section 4.2 illustrates a simple Oconee-1 plant model to identify the factors that affect T_{dc} and P_{dc}. Section 4.3 discusses the T_{dc} influencing factors, and Section 4.4 discusses the P_{dc} influencing factors. Section 4.5 presents the PTS event classification matrix developed for this study to facilitate analysis.

4.1 PTS Driving Forces from a Thermal Hydraulic Perspective

TH results are employed by PFM to evaluate stresses generated in the RPV wall. The two major stress components are: thermal stress due to the temperature gradient across RPV and pressure stress due to the pressure difference between the internal and external RPV walls. The average temperature of the RPV wall is also important, because it affects its material characteristics. Therefore, from the end use point of view, the three relevant parameters are:

1) the average RPV wall temperature
2) the temperature gradient in the RPV wall
3) the pressure difference across it

Almost all reactor transients that are initiated by some malfunction will eventually lead to a cool-down of the system. In time low T_{dc} values will therefore be present for most transients. The above parameters thus cannot be considered in isolation. PTS relevance is determined by a combination of sufficiently low average wall temperatures with a commensurate total stress composed of thermal stress and pressure stress. Note that the role and importance of the pressure stress depends on just what fracture mode is being determined. The two possibilities are: "crack propagation", that is, propagating a crack until it reaches zero thermal stress position, or "driving the crack through the wall". For the first mode, pressure difference is less important because crack propagation can occur even for zero pressure differences. For the second mode, an appropriate pressure difference is essential, because without it the crack can not move beyond the position of zero thermal stress. FAVOR code defines a through wall crack (TWC) event as when the

RPV wall has been 90% cracked through. In this sense, thermal stress plays a more important role than pressure stress in CPFs calculated by FAVOR.

The T_{dc} and h_{dc} are important in that they provide the boundary conditions for determining the heat flux at the inner RPV wall surface, which in turn determines the time dependent internal temperature gradients. Their relative importance can be assessed by considering the thermal characteristics of the RPV wall. It is a quite thick (on the order of ~0.21 m) C-steel slab, clad on the inside by a thin layer of stainless. The thermal diffusivity of the wall material has a moderate magnitude; as a result, appreciable time periods (on the order of several hundreds of seconds) are required for thermal energy to penetrate into the interior. A quantitative measure of this characteristic is the Bi number (ratio of internal to external resistance to heat transfer). For the RPV wall this index is always well above 1 and for reasonable values of h_{dc} (e.g. ~2000 $W/m^2 K$ or ~630 BTU/ft^2 hr F) can exceed 10. This implies that the energy transfer rate into the wall is determined primarily by the internal resistance. The external resistance ($1/h_{dc}$) has relatively little effect. A recent study has evaluated the effect of h_{dc} [Boyd and Dickson 1999]. A quantitative assessment covering the entire range of fluid conditions is presented in Appendix B. For example, the time by which the centerline temperature changes by 10% of the equilibrium value is ~480 seconds for the high h_{dc} option and ~470 seconds for the low. The studies thus concur that if a physically reasonable value is chosen for the expected flow conditions, the uncertainty contributed by this choice will be small. The effect of h_{dc} is not considered any further in this study.

For the P_{dc} dependence, a distinction must be made between two different classes of transients:

1) Transients for which the primary system remains single phase and subcooled. For these scenarios pressure is determined by boundary conditions imposed on the primary system (e.g. PORV pressure settings, or by operator control). Primary system pressure is then independent of downcomer fluid temperature.

2) Transients for which a two-phase region develops and persists in the primary system. For these conditions the system pressure is equal to the saturation pressure of the fluid located at some high elevation within the system, usually at the top of the RPV. For these conditions $P_{dc} = P_{sat}(T_{hot})$ and is not independent of T_{dc} anymore. The degree of dependences varies. If a sizable circulation rate is maintained $T_{hot} \simeq T_{av} \simeq T_{dc}$ and thus P_{dc} and T_{dc} are coupled along the saturation line. For transients with moderate or low system flows, T_{dc} lags behind T_{hot} by a sub-cooling margin, which depends on the relative HPI and circulation flow rates.

The system pressure can be uncertain for both cases, but a "TH analysis caused uncertainty" can exist only for the second class of transients. For transients of the first type, the uncertainty reduces to the human factor issue of just how the operators will control the pressure. The exception is the case where HPI flow is not controlled, the pressurizer fills, and pressure reaches the PZR PORV set point. When specific cases are considered in this study, the pressure response of the transient is identified, and if it falls

into the 'controlled pressure' category, a 'nominal' pressure trace is evaluated. The uncertainty of P_{dc} time history is dominated by operators' intervention.

The conclusion of this brief review is that of the three "PTS relevant variables", $T_{dc}(t)$ has the largest impact on the generation of thermal stresses in the RPV wall. T_{dc} is a dependent variable, and its value is obtained from the output of a TH code like RELAP5 and is thus dependent both on the boundary conditions characterizing the transient and the appropriateness of the model used in analyzing it. It is therefore subject to both boundary conditions imposed and code related uncertainties that are parameter uncertainty and model uncertainty, respectively. This dependence will be analyzed in subsequent sections. An important conclusion is that time fluctuations of T_{dc}, which are short in comparison to the thermal time constant of the RPV wall, need not be considered.

The conclusion based on the relative magnitude of time constants has important consequences. As will be shown, most of the TH time constants that characterize the primary system (e.g. the fluid circulation time constant, and the thermal time constant across the SG tubes) are shorter then the thermal time constant of the RPV wall. This means that from the PTS point of view a computed result obtained by a mass/energy balance (rather than instantaneous mass/energy transfer rates) is adequate in most cases. System codes perform balance calculations accurately. Note, this does not imply that "code related" uncertainties are not present. Such uncertainties exist in any computation of mass/energy exchange rates. However, if the time constants characterizing these rates are smaller then the thermal time constants of the RPV wall, the actual transfer rates (as long as they are in the appropriate range) contribute little to the uncertainty of the result. What matters is the equilibrium state of the system which is determined by the heat capacity and the magnitude of the sink and source terms. The uncertainty of the computed result is then directly related to the uncertainty of these parameters.

4.2 A Simple Oconee Nuclear Power Plant System Model

A useful standard that can be used to compare the magnitudes of the mass/energy source and loss terms is the heat capacity of the primary system and its components. Fig 4.1 shows a generic schematic of the Oconee-1 nuclear plant that groups basic components into control volumes suitable for PTS analysis. Starting from the grouping most important to PTS issues these components are:

1) The downcomer and the pump discharge side of the cold legs
2) The RPV minus the downcomer
3) The hot legs, the primary system of the steam generator and the pump suction side of the cold legs
4) The pressurizer and the surge line.

The combined component blocks 1 through 3 represent the normal 'circulating' side of the primary system. The diagram indicates the location of the principal energy source and sink. These are: core power or decay energy ($\dot{Q}_{dec}$) and the energy transferred to the

steam generators ($\dot{Q}_{SG}$). In addition, the locations at which mass/energy interchange can take place during transients are shown. This includes:

- HPI and accumulator liquid feed into the primary system
- cold or hot leg break
- PZR PORV and PZR SRV at the top of the pressurizer
- RCP's which are relevant not just because they greatly increase circulation but also because they represent a significant energy source.

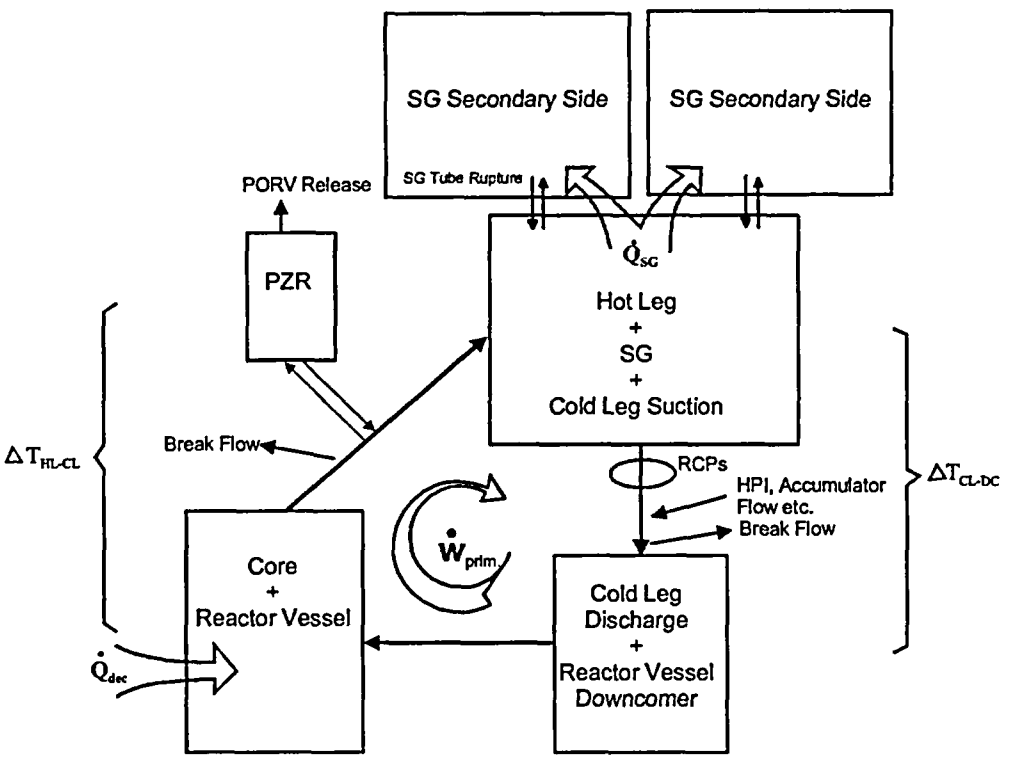

Figure 4.1 Schematic of PWR relative heat capacities and mass/energy sink/source terms

The reason it is valid to simplify an NPP to the simple model is that the ELAP5 running results that shows even in the liquid solid natural circulation mode, the RCS coolant flow rate is large enough to assume the coolant is well mixed in each volume shown in Figure 4.1. For PTS concern at single-phase, the RCS pressure remains at the PZR PORV open pressure. The T_{dc} and h_f are related. From the TH point of view we can derive the generic T_{dc} change rate from the following Equation.

$$\frac{dT_{dc}}{dt} \pm \delta = \frac{(\dot{Q}_{dec} \pm \delta) - (\dot{w}_{hpi} \pm \delta) \times \{[h_f(T_i) \pm \delta] - [h_f(T_o) \pm \delta]\} + (\dot{Q}_{pump} \pm \delta) - (\dot{Q}_{brk} \pm \delta) - (\dot{Q}_{SG} \pm \delta)}{[M_{prm,f} \times Cp_f(T_{av}) + (M_{Int.met} + Fac \times M_{Ext.met}) \times Cp_{met}(T_{av})] \pm \delta_{mcp}}$$

(Eq 4.1)

Where:

$\dot{Q}_{dec}$ = decay energy rate (MW)

$\dot{w}_{hpi}$ = HPI flow rate (kg/s)

$h_f(T_i)$ = liquid enthalpy at entering temperature $\overline{T}_i$ (MJ/K)

$h_f(T_o)$ = liquid enthalpy at exiting temperature $\overline{T}_o$ (MJ/K)

$\dot{Q}_{pump}$ = energy generated by RCPs

$\dot{Q}_{brk}$ = energy lost from the primary system breach

$\dot{Q}_{SG}$ = energy transferred to the two steam generators

$M_{prim,f}$ = mass of primary liquid

$M_{Int.met}$ = mass of internal metal

$M_{Ext.met}$ = mass of external metal

$Cp(T_{av})$ = Heat capacities of respective material at T_{av}

δ_{mcp} = the variation of the effective metal heat capacity

Fac = fraction of external metal that adds to the effective heat capacity

δ = the uncertainty associated with the respective terms.

Equation 4.1 can be seen as a generic equation for anticipating the magnitude of dT_{dc}/dt, however, the B&W reactor has a special design feature, in that the reactor vessel vent valves (RVVVs) were evaluated to have significant influence on T_{dc}. The RVVVs impact needs to be considered. In order to simply the PST uncertainty study, Equation 4.1 can be used for the PRA group to pre-screen or merge the huge number of event sequences. The uncertainty of the dT_{dc}/dt comes from the heat sources and sinks identified in equation 4.1 and the RVVVs. All the single phase scenarios, either from the operators' interaction with the plant or the component failures, can be concluded to change these parameters' quantities and induced timing.

The uncertainty induced by the TH code or expert judgments need to be studied further. The most important energy sink is the exchange rate with the steam generators $\dot{Q}_{sg}$ and the break flow through the primary system breach. In most cases, HPI is the dominant mass injection to maintain RCS pressure in the PTS event interval of interest. The T_{dc} and P_{dc} influencing factors are discussed in detail in Section 4.3 and 4.4.

4.3 Downcomer Temperature Influencing Factors

From the point of view of the local fluid temperature, the primary circuit of a PWR can be considered as a series of volumes having large heat capacities. The primary fluid circulates sequentially through these volumes and energy is added and/or subtracted as it moves through them. The variation in the local temperature will depend upon:

A) the relative magnitude of the heat sources or sinks (relative to the heat capacity of the volume and energy distribution)
B) the rate of energy addition or subtraction (relative to the circulation rate)

Items A and B indicate the heat capacity, heat sink, heat source, energy distribution, and RCS coolant flow rate are the factors affecting downcomer temperature. Varying these factors will therefore encompass all possible transient scenarios. These boundary conditions can be imposed (e.g. by an accidental event or by operator action), or they can be triggered and/or modulated by the state of the primary system (e.g. initiation and flow rate of HPI). The schematic shown in Figure 4.1 provides the basis for classifying the PTS significant transients, analyzing how the uncertainties are associated with boundary conditions, and transforming TH analysis into uncertainties of the PTS relevant parameters that are T_{dc}, P_{dc}, and h_{dc}.

A list of these five T_{dc} influencing factors with their relevant components/system state and phenomena follows.

- **Heat Capacities**
  - Primary system heat capacity including liquid, steam, structure
  - Secondary system heat capacity including liquid, steam, structure
- **Heat sources**
  - Decay heat
  - RCPs
- **Heat sinks**
  - Primary system breach
  - SGs
  - HPI
  - Core flood tank/Accumulator
  - LPI
- **RCS coolant flow rate**
  - RCPs
- **RPV energy distribution**
  - RVVVs: mixing of core water in downcomer
  - RCS flow interruption-and-resumption caused by vapor in candy cane
  - Boiling-condensation

The component/system states and the phenomena of the above five groups are discussed in detail in the following sections. The other parameters considered that have little impact on T_{dc} are not in the above list. For example, the PZR heaters generate about 1.6 MW, however, the PZR heater has little impact on T_{dc}.

4.3.1 Heat Capacities

The primary circuit of the simple Oconee NPP model described in Section 4.2 is depicted as a series of interconnected heat capacity blocks. The heat capacity of these blocks together with the rate of fluid circulation limits the rate at which both the average and the local fluid temperature can change.

Table 4.1 shows the overall mass and heat capacity of the Oconee-1 primary system for single phase and two phase conditions at an average temperature of 560 °K (~550 °F). The unsurprising conclusion to be gained from the table is that the numbers are large. It implies that only commensurately large energy removal rates can produce rapid temperature decreases. The quoted heat capacities will change somewhat with the average temperature of the plant, but the change is moderate. Thus for an average temperature of 500 °K (~440 °F) the values decrease by ~5%.

Table 4.1 Inventory and Heat Capacity of Oconee-1 Primary System

State of Primary	Liquid		Vapor			Combined Heat Cap (MJ/K)	
	Mass (kg)	Heat Cap. (MJ/K)	Mass (kg)	Heat Cap. (MJ/K)	Evap Energy (MJ)	Vapor + Liquid	Vapor + Liquid + Metal
Liquid Solid	2.57E5*	1360**	--	--	--	1360	1690
25% Steam	1.93E5	1080	3170	16	4760	1030	1360
50% Steam	1.29E5	680	6350	32	9520	710	1040

*Without pressurizer

**Evaluated at p = 71 bar (1043 psi), T_{SAT} = 560 °K, T_{CL} = 530 °K

SGs provide extra heat capacity. The amount of SGs' heat capacity is substantial when the secondary system becomes a heat source in some transients to moderate the rate of decrease of T_{dc}. By design, after the reactor trips, the SGs' water levels are maintained at about 30 inches high if RCPs are running, and they are maintained at 240 inches high if RCPs are tripped. The heat capacity of an SG with water levels of 30 inches and 240 inches are 121 MJ/K and 282 MJ/K, respectively. These are about 12% and 27% of the RCS heat capacity in the situation where 50% of the RCS inventory is filled with steam.

4.3.2 Heat Sources

A decay heat curve is dependent on the operation time interval and the reactor power before the reactor trips. Figure 4.2 shows three decay heat trends of reactor tripped at: after having been operated for an infinite time interval, after having been operated 10 hours, and hot zero power(or warm start up). The decay heat trends of having been operated for an infinite time interval and of hot zero power are used as the upper and lower bounds for this study. Each RCP generates about 5.5 MW when it is running. Four RCPs generate total energy of 22 MW. Tripping RCPs not only reduces 22 MW immediately but also changes the RCS circulation flow pattern from forced circulation to natural circulation or to flow stagnation. The flow pattern change enhances the reduction of the heat sources' impact on decreasing T_{dc}.

4.3.3 Heat Sinks

Three important heat sinks that impact on T_{dc} are discussed: primary system breach, secondary system malfunction, and RCS coolant injection.

Heat Sink Induced by Primary System Breach

The primary system breach could be LOCA (e.g., hot leg LOCA, cold leg LOCA), SGTR, or primary system valves (e.g., PZR PORV, PZR SRVs) stuck open. Oconee-1 has a 1.1-inches PZR PORV and two 1.8-inches PZR SRVs. Figures 4.3, 4.4, and 4.5 show the enthalpy flows of various breach sizes and locations calculated by RELAP5. All these calculations assume that there are no other system failures, no operators' actions, and no valve being reseated once the valve is stuck open. SGTR event does not cause significant T_{dc} decrease.

Heat Sinks induced by the Secondary System

The SGs of a nuclear power plant are designed to be capable of removing ~150% of the full nominal power. This means that for accidental conditions when power is supplied by core decay heat, SGs are hugely 'over-designed'. In effect, the available heat transfer surface for those conditions is ~100 times larger then would be required. This large miss-match of the energy source and the available heat transfer area has several important consequences:

a) For a transient in which the SG operation is unimpeded and controlled, it is the SG conditions that overwhelmingly determine the fluid condition in the primary system if they are coupled. Changes in values of primary system boundary conditions have little impact.
b) For a transient in which the SGs malfunction, the fluid conditions in the primary respond closely to the changes occurring in the SG if they are coupled.
c) For transients in which the primary system and secondary systems become 'de-coupled, the temperature response in the primary assumes a qualitatively different trend.

The observations listed above are the basis for a classification of uncertainties presented in Table 4.2 Another consequence of SG importance is that a large number of PTS relevant scenarios are initiated or compounded by SG malfunction. A schematic representation of the boundary conditions that can be imposed on the once-through steam generator (OTSG) and their locations are shown in Figure 4.6 The figure illustrates that though the possible ways in which malfunctions could occur is large, the impact that they have on the SG can be reduced to the variation of four independent boundary conditions. These are: the feed water flow rate ($\dot{W}_{fwd}$), the feed water temperature (T_{fwd}), the flow area available for the exiting steam (A_{flow}), and the location at which feed water is introduced. The effect that these boundary conditions have on the primary system is determined by TH analysis which combines their influence into a single time varying parameter - the SG energy transfer rate ($\dot{Q}_{sg}(t)$).

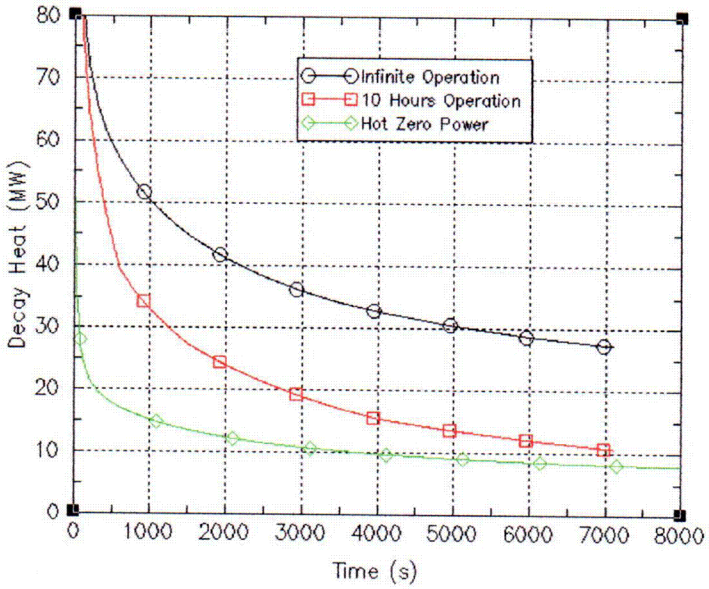

Figure 4.2 The decay heat trends of reactor being tripped at having been operated for infinite time interval, having been operated for 10 hours, and hot zero power.

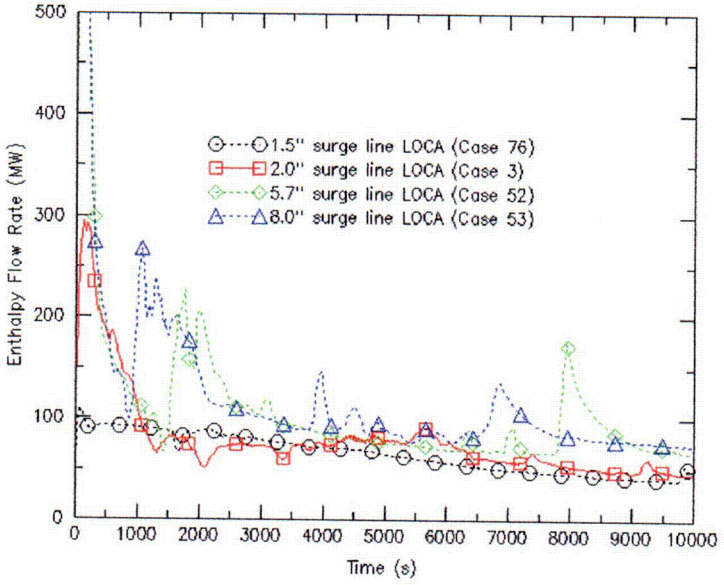

Figure 4.3 The enthalpy flows of different sizes surge line break. Assume all other systems function properly, and there are no operators' actions involved.

cof

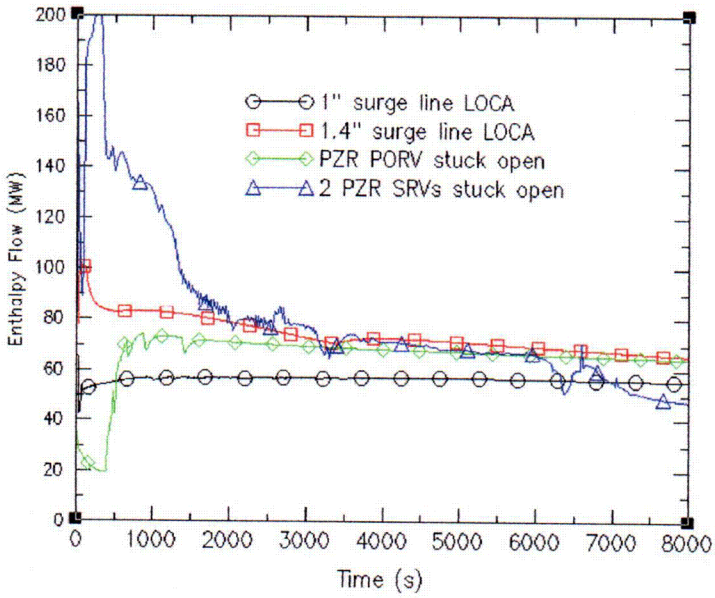

Figure 4.4 The enthalpy flows of different sizes of surge line break and pressurizer valves stuck open. Assume all other systems function properly, and there are no operators' actions involved.

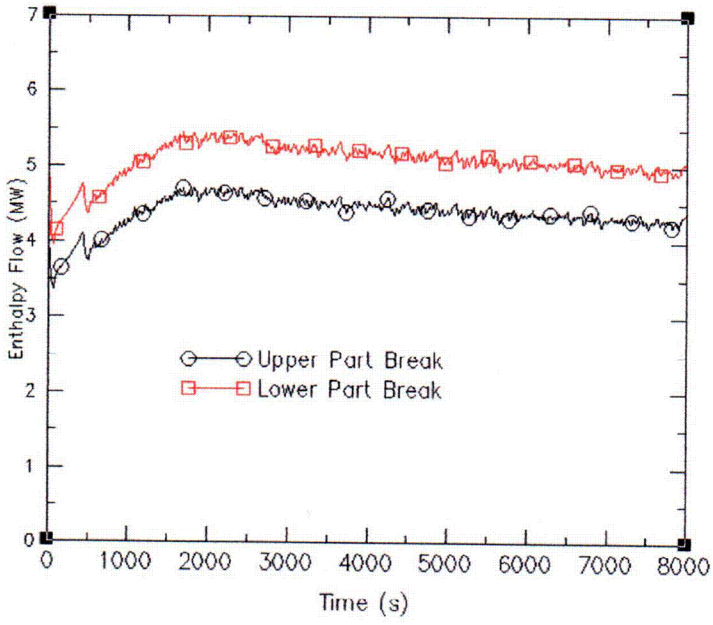

Figure 4.5 The enthalpy flows of one tube double ended guillotine break. Assume all other systems function properly, and there are no operators' actions involved.

A quantitative overview of the temperature difference between the secondary and primary systems for a range of operational conditions is presented in Appendix C. It is shown that for a broad range of conditions, this ranges from less then 0.5 °K for transients with operating RCP's to ~3 °K for unfavorable low flow conditions. The analysis includes the uncertainties associated with the evaluation of h_{eff} across the SG tubes.

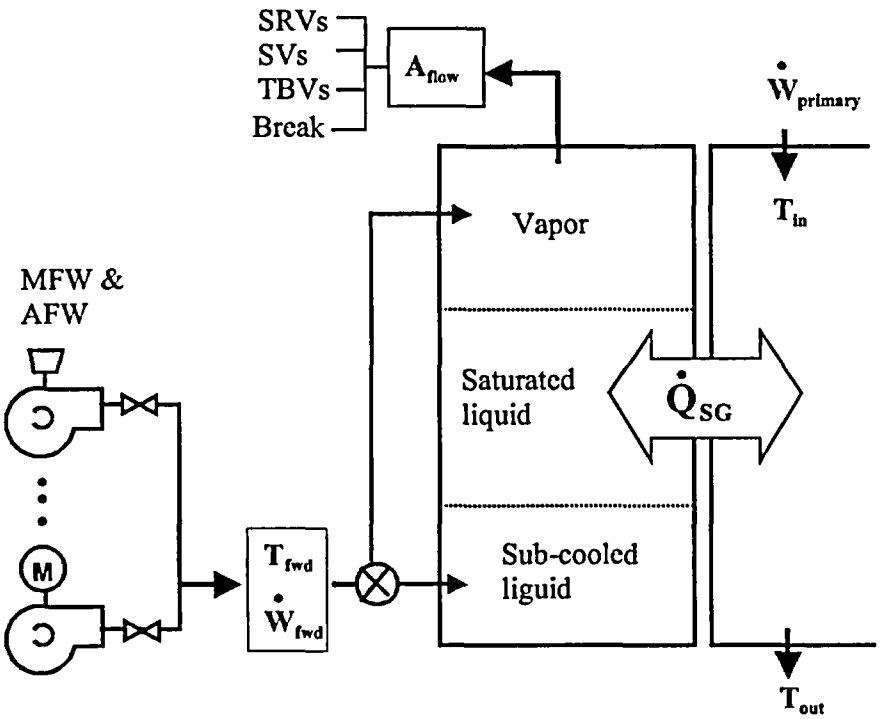

Figure 4.6 Types and location of boundary conditions for OTSG

For some transients (e.g. MSLB) the SGs' heat capacities are of interest. Table 4.2 provides upper limit estimates of the total energy that can be removed during the initial phase of an MSLB event for representative OTSG and U-tube type steam generators. The maximum flashing rate is limited by the rate at which the primary system flow can supply the necessary energy. A bounding estimation shown in the last column is obtained by assuming that the boiling heat transfer coefficient on the secondary system is large, and the resistance to heat transfer consists of the resistance of the tube metal and of the convective resistance of the primary system. As shown in Table 4.2, though the total amount of energy that can be removed in this manner is sizable, due to the very large heat capacity of the primary system, the resulting temperature decrease is relatively modest. This leads to the conclusion that even for MSLB break events, the important cool down phase occurs after the highly dynamic events immediately following the rupture. The initial cool down caused by the flashing of the SG inventory provides an initial temperature drop, but does not produce temperatures which are 'PTS relevant, except that the uncontrolled feedwater flow system keeps pumping water into SGs.

Table 4.2 Energy Removal Capacity & Upper Bound of Energy Removal Rates for MSLB Events

	Initial secondary system. inventory (kg)	Amount left after 380K is reached	Energy required to evaporate unflashed liquid	δT of primary system due to evaporate	Maximized energy removed rate (MJ/s.SG)
OTSG-SG (Oconee)	27200	18240	4080 MJ	-24 K	19.5
U-tube SG (Zion)	43000	28300	6340 MJ	-28 K	60.9

The secondary system malfunctions causing large amounts of heat transfer from the primary system to the secondary system include secondary system breach (e.g., MSLB, TBVs stuck open etc.) or excessive feedwater overfed SGs. For Oconee-1 any of the two main steam lines is about 31.5-inches in diameter. Each MSLB has two 4.3-inches turbine bypass valves (TBVs) and eight 4.4-inches SG Safety valves. Figure 4.7 shows the magnitude of heat transferred rate from the primary system to the secondary system of one SG at different sizes of secondary system breach

Figure 4.8 shows the heat transfer rate of an SG overfed by AFW and MFW. The AFW water source is from the coolant storage tank with nominal temperature 70 °F. The MFW water source is from the main condenser; its temperature normally decreases from 450 °F to 100 °F in four hours. This water temperature difference causes a larger heat transfer rate for AFW overfeed events than for MFW overfeed events.

Heat Sink due to Primary System Coolant Injection

The heat capacities shown in Table 4.1 can be placed in context by comparing them to energy gain/loss rates of RCS after a reactor trip. Table 4.3 shows the decay energy source at three time periods after the reactor is tripped (this is the full power, maximized source) and four representative HPI flow and enthalpy removal rates. HPI flow is inversely proportional to system pressure and therefore has a low value at the pressure of the PORV set points (~30 kg/sec for Oconee). To provide a broader indication, a simple time dependent scenario is assumed in which the pressure decreases from 60 to 20 bar (~ 900 to ~300 psi) in 3000 sec. The table shows the corresponding HPI flows and the negative enthalpy addition obtained by assuming that break flow exits at the average temperature of the system. This simple comparison shows that for the quoted pressures, the negative enthalpy of HPI flows is almost twice as large as the decay energy and can cool the entire system. The last two columns provide bounding values for HPI cooling. The downcomer fill time is the time in which the HPI flow could displace the volume of the downcomer if there were no system flows at all. The last column provides an estimate of the energy removal capacity of the SGs for the conditions where the difference between primary system temperature and the secondary system temperature at OTSG exit ($T_{prim} - T_{sec}$) is 5.5 °K. The potential heat sink is then seen to exceed $\dot{Q}_{dec}$ by a factor of ~ 3. Figure 4.9 shows the RELAP5 calculation of HPI contributed negative energy flow into the downcomer region.

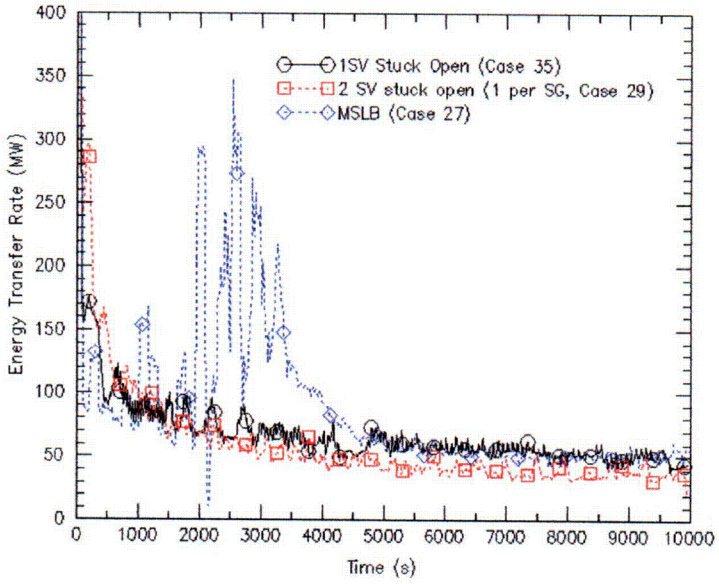

Figure 4.7 Heat transfer rate from the primary system to the secondary system of an SG at different secondary system breaches. No operators' actions are involved.

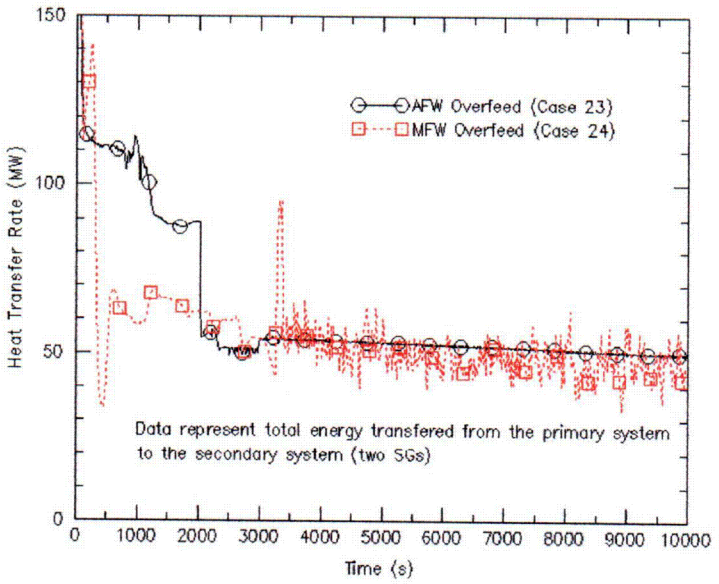

Figure 4.8 Heat transfer rate from the primary system to the secondary system of an SG when the SG is overfed by MFW and AFW. No operators' actions are involved.

C06

Table 4.3 Energy source/sink magnitudes for Oconee

Time after trip (sec.)	System P* Bar (psi)	HPI flow rate (kg/s) 3 pumps	Energy source/sink (MW)		Downcomer + Cold Leg fill time (sec.)	SG energy removing rate for δT= 10 F (5.5k) (MW)
			$\dot{Q}_{decay}$	$\dot{Q}^{*}_{HPI}$		
1000	60 (870)	67	48	-70	400	150
2000	46 (670)	71	40	-74	380	125
4000	20 (290)	77	33	-81	350	115
2000	170(2460)**	30	40 + 22***	-31	900	325

*$\dot{Q}_{HPI} = \dot{w}_{HPI} \times [h_f(T_{SAT}) - h_f(T_{HPI})]$

**PZR PORV setting

***decay heat + pump power

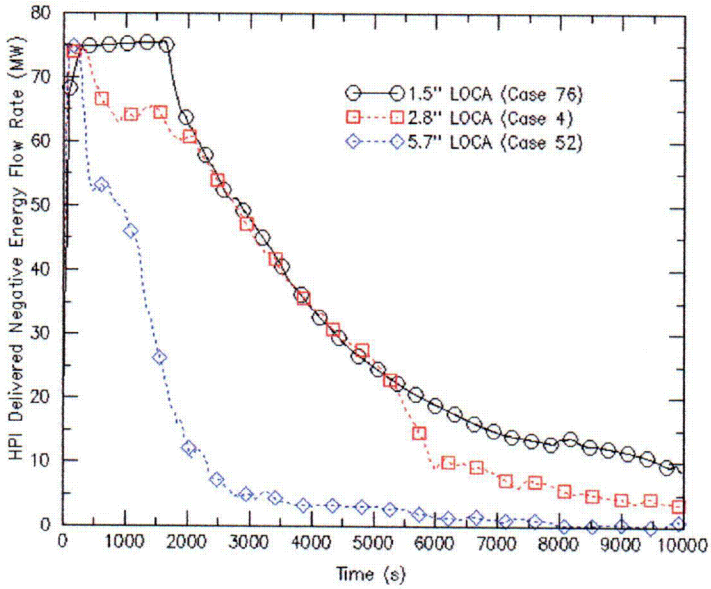

Figure 4.9 RELAP5 calculation of HPI contributed negative energy flow rate into the downcomer for different sizes of LOCA. $\dot{Q}_{HPI} = \dot{w}_{LPI} \times [h_f(T_{DC}) - h_f(T_{HPI})]$

The core flood tanks (CFTs) and the low pressure inject (LPI) also inject negative heat sources into RCS. CFTs are activated when RCS pressure is below 4.1 Mpa (596 psia). Oconee-1 has two CFTs with a total of about 57.2 cubic meters (2020 cubic feet) of coolant. As the HPI, the CFT flow rate is dependent on the primary system pressure. Figure 4.10 shows the two CFTs' total energy absorption rate at different break size LOCAs.

Two LPI pumps can deliver a huge amount of coolant into RCS in a short period of time. However, due to their low activating pressure (1.5 Mpa or 215 psia) the LPI was not considered as a PTS influencing factor in the past PTS uncertainty studies. Figure 4.11 shows the two LPI pumps' total energy absorption rate at different break size LOCAs.

C07

4.3.4 RCS Coolant Flow Rate

The cool down rates in the downcomer will depend strongly upon the circulation flow of the system. This can be very large (with the pumps operating), large (for liquid solid natural circulation), or moderate (for various two-phase flow regimes), as characterizes an OTSG plant. Flow rates, associated inventory exchange time constants and component velocities for these conditions are presented in Table 4.4.

Table 4.4 Fluid circulation time constants for Oconee

	Flow Rate (kg/s)	System Exchange Time (without PZR)	$V_{cold\ leg}$ (m/s)	$V_{downcomer}$ (m/s)
RCPs Operating	17900	14 sec	15.5	7.0
Nat. C. Single ph.				
Qdec @ 1000 s	420	610 sec	0.33	0.15
4000s	290	860 sec	0.22	0.11
Two-ph $\alpha = 0.25$	83	40 min	0.06	0.3
Two-ph $\alpha = 1$ *BCM	24	95 min	0.02	0.008

The system exchange time constant has significant influence on T_{dc} (Table 4.4). When RCPs are running, the RCS coolant is well mixed thus T_{dc} is less likely to decrease fast. Figure 4.12 shows the low decay heat (hot zero power) as an additional factor impacting T_{dc} for the scenario of PZR PORV fully stuck open and reseated 400 seconds after its stuck open. The HPI keeps injecting coolant into RCS even after PZR PORV is reseated. Figure 4.13 shows that RCPs-off enhances the HZP and HPIs' impact on T_{dc}.

Figure 4.12 shows that the RCS circulation speed could have significant T_{dc} impact when the primary system breach is the dominant heat sink. However, in a scenario where the secondary system is the dominant heat sink changing RCS circulation from forced circulation to natural circulation, the circulation speed does not have much impact on T_{dc}. Figure 4.13 shows T_{dc} trends of varying HPI and RCPs' states of SG overfed scenarios (the SG water level is maintained at 100% wide range level). It shows the summation impact of individual HPI and RCPs' impact is about equal to the simultaneous HPI and RCPs' impact.

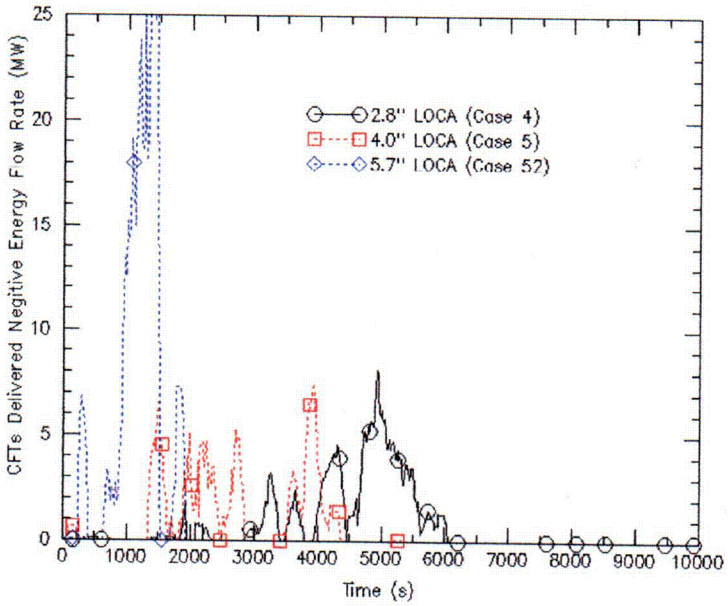

Figure 4.10 The CFTs negative energy contribution rate at different sizes of LOCA events. Assume no other components and systems failure beside pipe break, and there is no operators' action. $\dot{Q}_{CFT} = \dot{w}_{CFT} \times [h_f(T_{DC}) - h_f(T_{CFT})]$

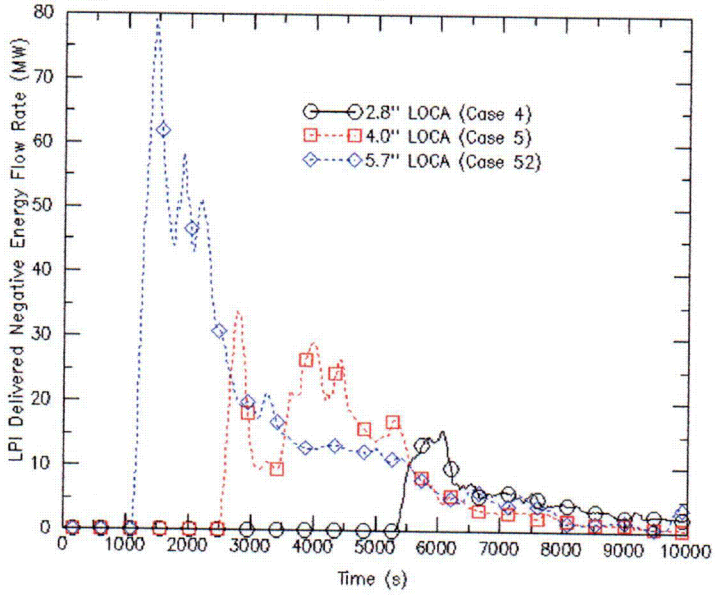

Figure 4.11 The LPI total negative energy contribution to downcomer at different sizes of LOCA events. Assume no other components and system failures beside pipe break, and there is no operator's actions. $\dot{Q}_{LPI} = \dot{w}_{LPI} \times [h_f(T_{DC}) - h_f(T_{LPI})]$

4.3.5 RPV Energy Distribution

For transients during which the primary system is partly voided, a vapor-liquid interface is present that could discontinue the internal flow path and bring about changes in the break flow rate and local fluid composition. For OTSG type plants like Oconee these flow states will be especially pronounced if the break energy flow is smaller then $\dot{Q}_{\ldots}$ or for transients during which HPI fails on demand.

Figures 4.14 and 4.15 illustrate schematically the unique geometrical features of an OTSG type plant like Oconee, which determine the inventory dependent flow states. Figure 4.14 represents the side view of a scaled facility and is used because it clearly exhibits the vertical characteristics of the OTSG flow geometry. The key geometric features that influence the response of reduced inventory states are:

1) The tall vertical section of the hot leg (HL) which turns through a 180° angle (the 'candy cane') before entering the superheated end of the OTSG. The candy cane is the highest elevation of the primary system and is filled with hot water from the core region. As system pressure decreases, hot water at this location will be the first to flash. If sufficient vapor is generated to fill the upper portion of the candy cane, flow in the HL can be interrupted.

2) The large vertical dimension of the OTSG leads to a relatively high loop seal at the suction side of RCPs. Note that before the cold leg (CL) turns into the horizontal segment that enters the downcomer, it rises above the CL entrance in the RPV, so that there is a short descending CL segment. The HPI nozzles are located in this segment.

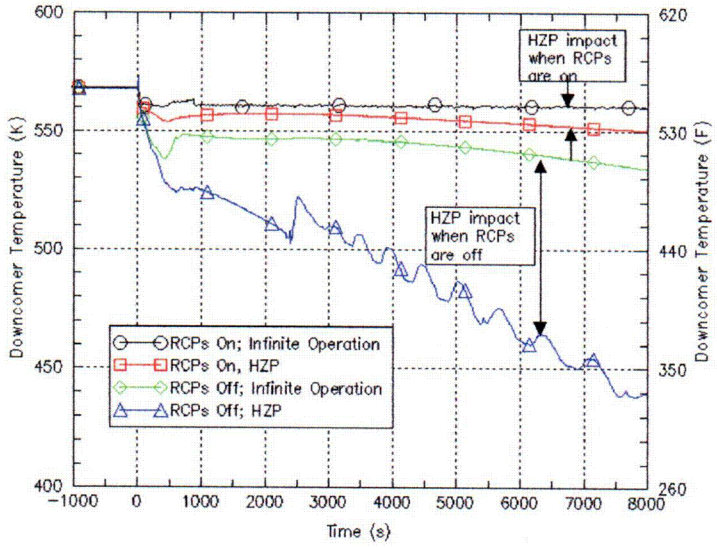

Figure 4.12 The downcomer temperature curves at feed-and-bleed scenarios where decay heat and RCPs state are varied. The PZR PORV stuck opens and stays fully open for the first 400 seconds after reactor trips.

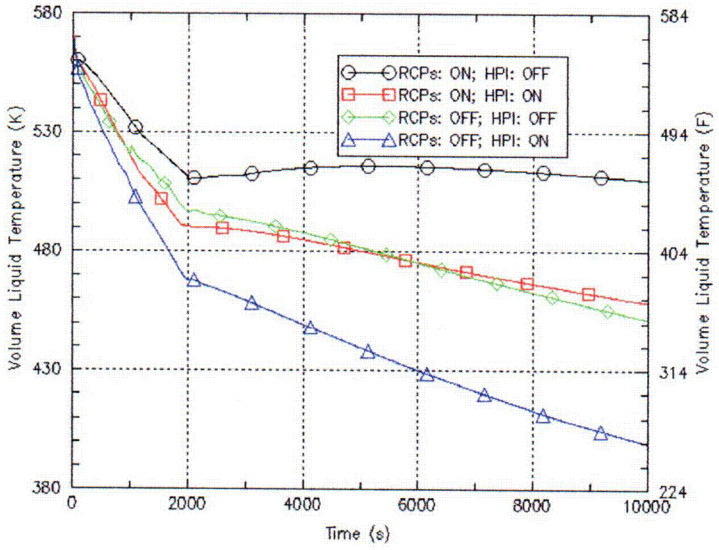

Figure 4.13 The T_{dc} trends of different combination of RCPs and HPI states of the scenario in which reactor trips followed by two SGs overfed event (SGs water levels maintain at 100% high).

C09

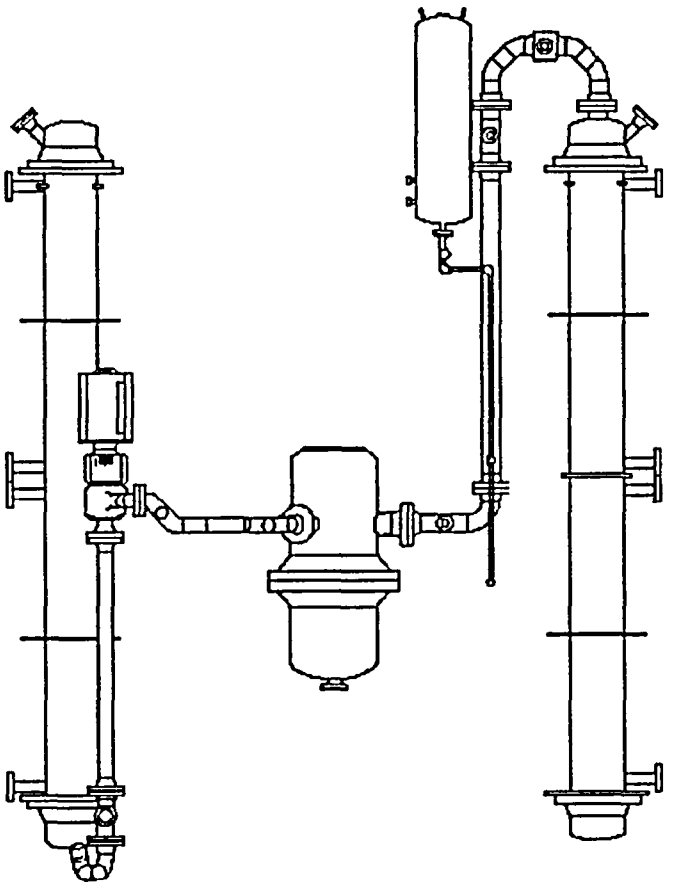

Figure 4.14 Side view of a one through steam generator nuclear power plant flow geometry

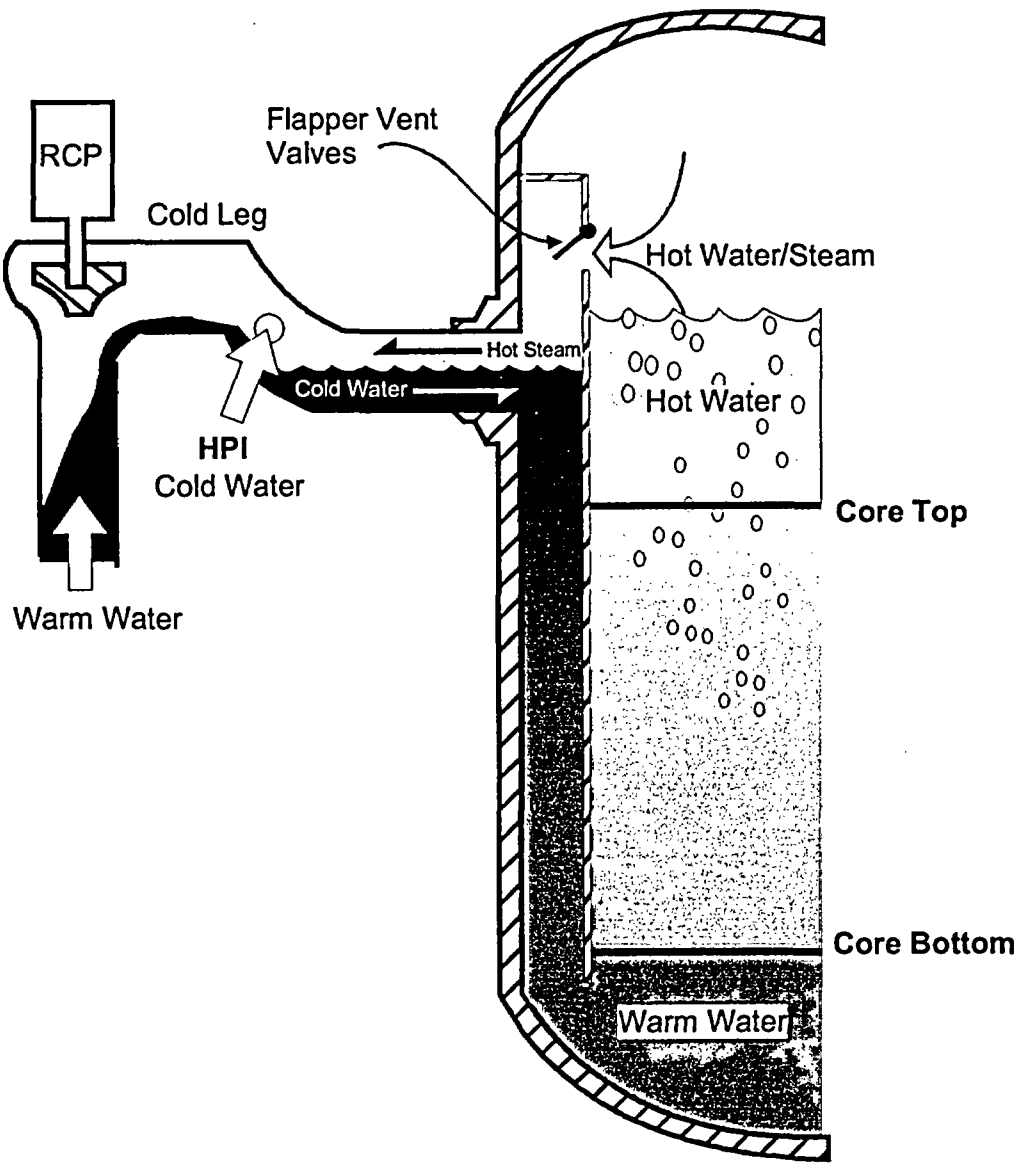

Figure 4.15 Steam-hot & cold water interface in reactor pressure vessel and cold leg.

3) Six RVVV's located in the core barrel above the HL and CL entrance elevation. These are flapper type valves attached to the outside of the core barrel that under normal operation are closed. When the core-to downcomer pressure differential reverses, they open allowing hot water and/or steam to penetrate directly into the upper region of the downcomer.

Figure 4.16 shows the enthalpy delivered from the upper core to the downcomer through RVVVs at various sizes of LOCA based on RELAP5 calculation. It shows that the enthalpy transferring rate is not large but due to the enthalpy that is deposited in the downcomer directly it could significantly affect T_{dc}.

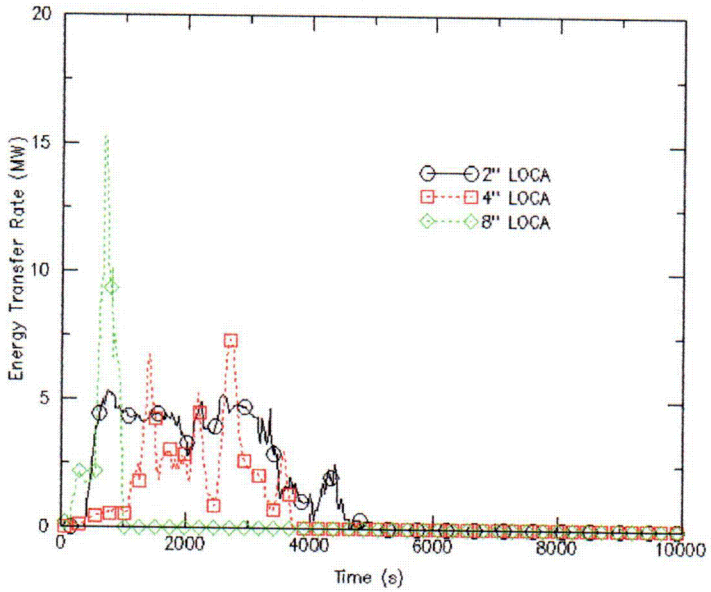

Figure 4.16 The energy delivered from RVVVs to the downcomer region for different sizes of LOCA based on RELAP5 calculation. $\dot{Q}_{RVVVs} = \dot{w}_{RVVVs} \times [h_f(T_{Rcupper\ plenum}) - h_f(T_{dc})]$

4) RELAP5 calculation shows that there is recirculation flow between the two cold legs in the same loop after RCS lost subcooling. This flow behavior is identified as a numerical calculation error (numerical driven flow). This problem is resolved by assigning high reverse flow resistant constants for all RCPs.

4.4 Downcomer Pressure Influencing Factors

The sources affecting P_{dc} could be classified into three categories: change in RCS coolant inventory, change in RCS energy, and short term steam condensation. These categories and their system related factors/components are listed as the following:

- Change in RCS coolant inventory
  - HPI
  - Primary system breach
- Change in RCS energy
  - Heat sources
  - Heat sinks
- Short term rapid RCS steam condensation
  - PZR spray
  - Mixing of core water in downcomer (steam condensation)

- Boiling-condensation

These three categories and their related system factors are discussed in the following sections.

4.4.6 Change in RCS Coolant Inventory

HPI is the main component injecting coolant into RCS to maintain RCS pressure in most RCS cooldown scenarios. Figure 4.17 shows the RCS pressure trends at different sizes of primary system breach. In the nominal situation, Oconee-1's HPI is able to maintain RCS subcooling up to about 1.5-inches LOCA.

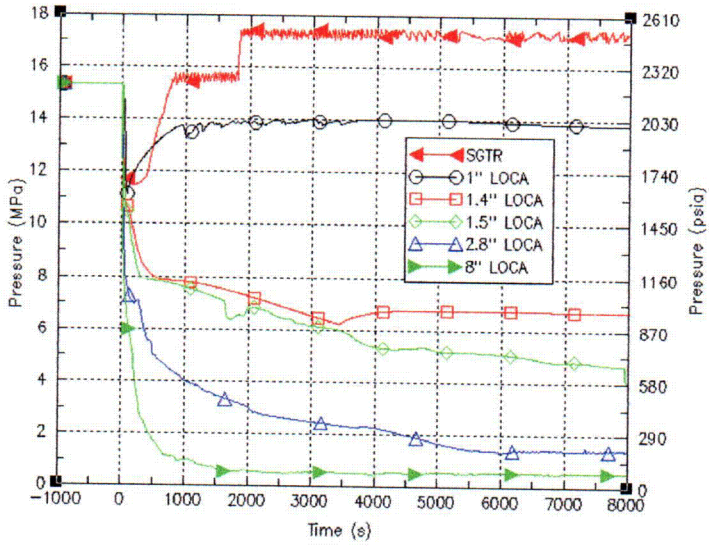

Figure 4.17 The RCS pressure trends of different sizes of surge line LOCA. Assume no other component/system failure, and no operators' actions.

4.4.7 Change in RCS Energy

RCS can be seen as a sealed container containing water and steam. Energy imposed into or removed out this container will change RCS' void fraction, consequently P_{dc} is affected. However, in comparison with the effect from changing RCS inventory, the change of RCS energy has much less impact on P_{dc}.

4.4.8 Short Term Rapid RCS Steam Condensation

The short-term steam condensation phenomena occur within restricted boundary conditions for a short time interval during transients. Such a short term effect on P_{dc} is considered to have little effect on PTS risk uncertainty.

4.5 PTS Event Classification Matrix

Concluding from the above analysis, a PTS event classification matrix (Table 4.5) is created to facilitate TH uncertainty analysis. The matrix uses key influencing factors affecting T_{dc} and P_{dc} discussed in Sections 4.2 and 4.3 as its framework. Varying these

C11

factors' values or states would have significant effect on PTS risk. The less critical PTS risk related parameters are discussed with in the framework.

When a scenario has a system/component state change, causing the scenario's classification to change from one sub-category to another, this scenario is placed in the sub-category with the largest heat sink. For example, a scenario with stuck open and reseated SRV is placed in the category where SRV is stuck open without being reseated, since this creates a greater heat sink than if SRV is closed.

PTS requires rapid T_{dc} decrease and reaches minimum temperature below 422 °K (300 °F). Only the primary system breach or the secondary system failure (i.e., depressurization and overfeed) induced heat sinks could reach this criteria. All PTS events must include either primary system breach, or a secondary system failure, or both of them. These two factors (primary system state and secondary system state) are used as the two dimensional framework of the matrix.

Figures 4.18 and 4.19 show the expected RCS temperature decrease and increase caused by the major heat sinks and source (decay heat), by assuming the RCS heat capacity is constant at 1690 MJ/K, which is conservative. These two figures show that the heat sinks caused by primary system breach and secondary system depressurization dominate the impact of the decay heat.

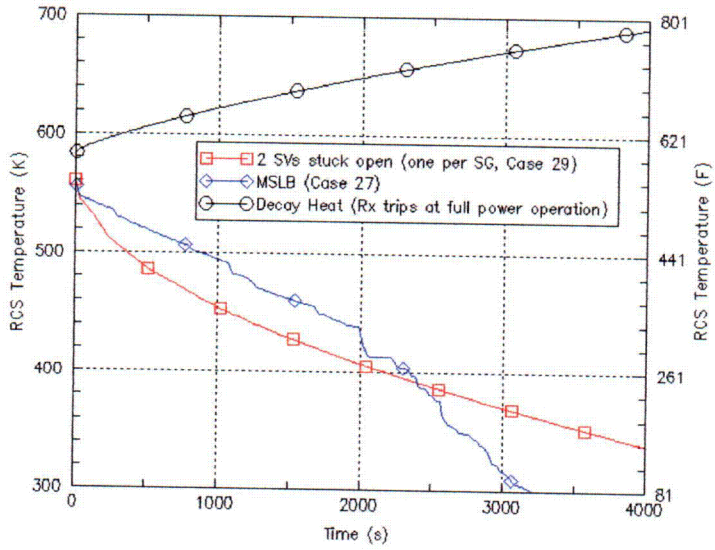

Figure 4.18 The expected RCS temperature decrease and increase trends of LOCA and decay heat, by assuming RCS heat capacity is constant at 1690 MJ/K.

C12

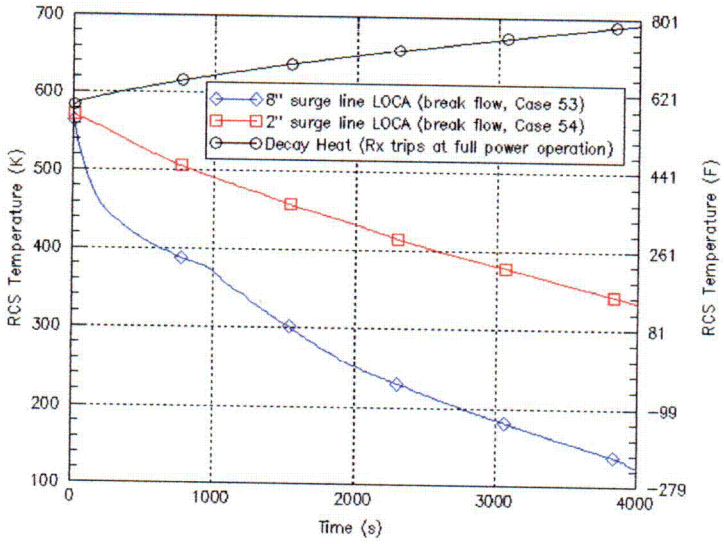

Figure 4.19 The expected RCS temperature decrease and increase trends of the secondary system breach and decay heat by assuming RCS heat capacity is constant at 1690 MJ/K.

As shown in Table 4.5, in the PTS event classification matrix, the primary system state is divided into three sections: intact, breach without losing RCS subcooling, and breach causing RCS loss of subcooling. The RCS subcooling is dependent on whether HPI can compensate for the break flow. For Oconee-1, HPI can compensate for up to 1.5-inches LOCA. However, this study uses whether HPI flow is greater than the break flow for scenario classification. This classification has two advantages. First, an RCP's state can be determined. An RCPs is tripped when RCS losses subcooling. For the scenarios that HPI flow is greater than break flow, RCS subcooling is maintained as a result of the RCPs running (assuming everything functions as designed). For the scenarios that break flow is greater than HPI flow, the RCPs are expected to be tripped. Second, an operator's actions can be determined. There is no need for operators to throttle HPI if the break flow is greater than HPI flow. This reduces the uncertainty of the operator's action for controlling HPI flow rate. The operator's action for controlling HPI flow rate and the RCPs' states are two important parameters in PTS risk, reduction of the two parameters' uncertainties reduces analysis complexity.

Secondary system failure includes the secondary system breach (e.g., MSLB, TBVs stuck open) and SG overfeed (by MFW and EFW). As discussed before, SGs could become a heat source to RCS in the scenarios in which RCS breach is the dominant heat sink or one SG malfunction is the dominant heat sink. For example, for an MSLB transient, the SG in the break loop is a heat sink to RCS. The intact SG later becomes a heat source to RCS that moderates the T_{dc} decreasing rate. The heat capacity of an SG is significant. One SG breach would have the broken SG as a heat sink and the intact SG as a heat source. Two SGs breach would induce two heat sinks to RCS. Two SGs breach scenarios will have a more severe impact on T_{dc} than one SG breach scenarios thus two SGs breach are separated from one SG breach scenarios.

Figure 4.20 shows the difference in total net energy transferred from the primary system to the secondary system for the two-SG-SVs-stuck-open events. Comparing the two SVs are at the same SG and at different SG (one valve in each SG), the primary system transferred a larger amount of energy to the secondary system in the latter case (one valve at each SG).

Sensitivity studies of SG overfed scenarios show that only rare excessive SG overfed scenarios could become PTS significant. There is no need to distinguish whether one or two SGs have been overfed.

The above discussion frames the dominant sources affecting T_{dc}. The P_{dc} uncertainty also needs to be considered in all situations. HPI flow rate is the dominant parameter affecting P_{dc} uncertainty in many PTS relevant scenarios. Four different HPI states are modeled: full injection without (operator's) throttling, activated and throttled (to control flow), not demanded or failed, and failed-and-recovered. These four different HPI states are a subset of each event category classifying dominant scenarios affecting T_{dc} (see Table 4.5).

Table 4.6 shows the expected RCPs and the HPI state in different categories of the PTS event classification matrix. In the situation where the primary system is intact or HPI flow rate is greater than break flow rate, RCPs will keep running. Failure on either HPI or RCPs would invalidate statements in Table 4.6. However, failure of either component has low probability. The scenarios involving failure of RCPs or HPI might have probabilities that are too low to be on the radar screen for further analysis.

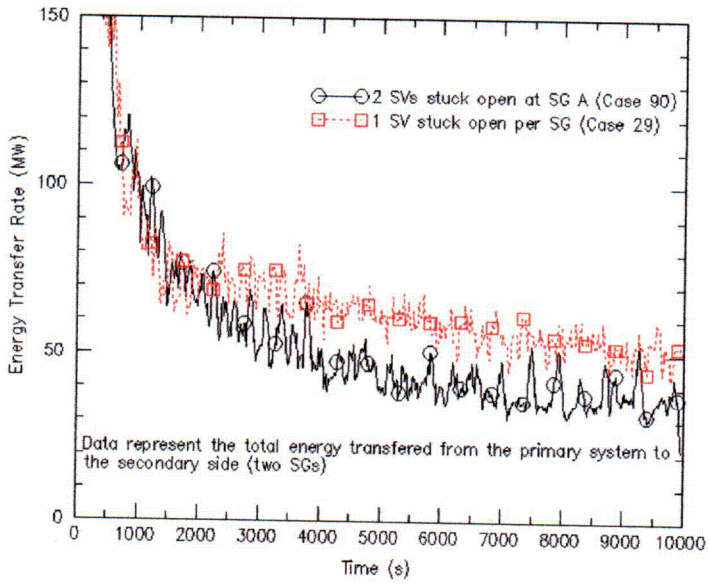

Figure 4.20 The total net energy transferred from the primary system to the secondary system of two two-SG-SVs-stuck-open events. One event has two stuck open SVs located at the same SG, and the other event has one SV stuck open at each SG (total two SGs).

C14

Table 4.5 The PTS event classification matrix

Primary Side State / Secondary system State	Intact	Breached	
		HPI Flow > Break Flow (Break Size <~ 1.5 inch)	HPI Flow < Break Flow (Break Size >~ 1.5 inch)
Nominal	Not PTS concern	A2B1_1	A3B1_1
		A2B1_2	A3B1_2
		A2B1_3	A3B1_3
		A2B1_4	A3B1_4
One SG Breach	A1B2_1	A2B2_1	A3B2_1
	A1B2_2	A2B2_2	A3B2_2
	A1B2_3	A2B2_3	A3B2_3
	A1B2_4	A2B2_4	A3B2_4
Two SGs Breach	A1B3_1	A2B3_1	A3B3_1
	A1B3_2	A2B3_2	A3B3_2
	A1B3_3	A2B3_3	A3B3_3
	A1B3_4	A2B3_4	A3B3_4
SG(s) Overfed	A1B4_1	A2B4_1	A3B4_1
	A1B4_2	A2B4_2	A3B4_2
	A1B4_3	A2B4_3	A3B4_3
	A1B4_4	A2B4_4	A3B4_4
SG(s) Breach + SG(s) Overfed	A1B5_1	A2B5_1	A3B5_1
	A1B5_2	A2B5_2	A3B5_2
	A1B5_3	A2B5_3	A3B5_3
	A1B5_4	A2B5_4	A3B5_4

1. Character 'A' represents the primary system state, which has three variables: 1, 2, and 3 representing states of intact, HPI-recoverable breach, and Non-HPI-recoverable breach, respectively.
2. Character 'B' represents the secondary system state, which has five variables: 1 to 5 representing states of nominal, one SG breach, two SG breach, SG(s) overfed, and combination of SG(s) breach and SG(s) overfed.
3. The final digit at the end of each legend represents the HPI state. It has a variation from 1 to 4 representing HPI is activated and not throttled, HPI is activated and throttled, HPI fails or is not demanded, and HPI failed and recovered, respectively.
4. The primary system 'intact' state includes the primary system small leakage that can be made up by the make up and letdown flow.

Table 4.6 RCPs and HPI nominal states

Primary Side State / Secondary system State	Intact	Breached	
		HPI Flow > Break Flow (Break Size <~ 1.5 inch)	HPI Flow < Break Flow (Break Size >~ 1.5 inch)
Nominal	Not PTS concern	1. RCP will not trip by design 2. HPI is activated 3. Throttling HPI is required	1. RCPs Trip 2. HPI is activated 3. No throttling HPI is required
One SG Breach	1. RCPs will not trip 2. HPI may or may not be activated 3. Throttling HPI is required if HPI is activated		
Two SGs Breach			
SG(s) Overfed			
SG(s) Breach + SG(s) Overfed			

Placing PRA's bins in the PTS event classification matrix is sown in Table 4.7. The value in the bracket of each bin is the total of the event frequencies binning to the bin. Summation of the bins' frequencies for the same event category would indicate the importance of the event category from PRA perspective. About 100 bins are generated. Some of them are eliminated from further analysis due to either low event frequencies or low PFM challenges. Table 4.7 lists only the 47 bins that passed the prescreening process.

Table 4.7 Preliminary TH runs for binning PRA event sequences and their event frequencies (after the screening process)

Primary Side State / Secondary system State	Intact	Breached	
		Break Size <~ 1.5" Breach flow could be compensated by HPI	Break Size > ~1.5" Breach flow cannot be compensated by HPI
Nominal			[2.6e-4] 3 (2" surge line) [6.2e-6] 70 (#3, HZP) [3.0e-5] 52 (5.656" surge line) [6.0e-7] 73 (#52 + HZP) [4.0e-6] 53 (8" surge line) [8.0e-8] 132 (#53 + HZP) [4.0e-4] 34 (PZR-SRV, 2.54") [7.6e-5] 106 (2.828" surge line + HZP) [2.9e-5] 41 (PZR-SRVs reseat at 100 minutes) [1.8e-6] 42 (#41 + HZP)
			[1.1e-3] 83 (PZR SRV SO. SRV reseated at 100 min, HPI throttled 1 min after 5F subcool and 100" PZR level) [2.0e-4] 92 (#83 + HZP) [3.4e-5] 84 (PZR SRV SO. SRV reseated at 100 min, HPI throttled 10 min after 5F subcool and 100" PZR level) [6.2e-6] 93 (#84 + HZP) [1.1e-3] 85 (PZR SRV SO. SRV reseated at 50 min, HPI throttled 1 min after 5F subcool and 100" PZR level) [2.0e-4] 94 (#85 + HZP) [3.4e-5] 86 (PZR SRV SO. SRV reseated at 50 min, HPI throttled 10 min after 5F subcool and 100" PZR level) [6.2e-6] 95 (#86 + HZP)
One SG Breach		[5.6e-8] 8 (1" surge line + 1 SG SV SO) [1.0e-7] 28 (F&B, 1SG SV SO) [1.1e-7] 30 (#28 + HZP)	
	[2.1e-6] 27(MSLB) [4.0e-7] 101(#27 + HZP) [1.2e-6] 37 (1 SG SV SO + HZP)	[4.8e-7] 12 (1" surge line, 1SG SV SO) [7.0e-7] 90 (2 SG SVs SO, HPI throttled @ 20 min after it can be throttled) [2.1e-7] 102 (#90 + HZP) [6.1e-5] 91 (SGA TR+ 1SGB SV SO and reseated @ 10 min after initiation + RCP tripped @ 1 min + HPI throttled @ 10 min after it can be throttled) [5.0e-8] 103 (#91 + HZP) [2.3e-7] 99 (MSLB + HPI throttled 20 min after it can be throttled) [2.3e-7] 100 (#99 + HZP)	

Two SGs Breach		[2.7e-7] 29 (2 SG SVs SO) [5.0e-9] 31 (#29 + HZP)	
	[1.4e-5] 36 (2SVs SO) [2.6e-6] 38 (#36 + HZP)		
		[3.1e-8] 15 (1" + 4 TBVs fully SO + No HPI) [1.8e-8] 74 (#15 + HZP)	[3.1e-6] 81 (2" surge line, 4 TBVs opened @ 15 min)
		[2.7e-8] 44 (1" LOCA + HPI F&R @2250s, 4 TBVs fully open) [1.3e-7] 75 (#44 + HZP) [3.1e-6] 82 (1" + 4 TBVs Opened @ 15 min, HPI recovered when CFTs are 50% discharged, HPI throttled @ 50 min)	[2.4e-7] 87 (PZR SRV SO, HPI fail, 4 TBVs opened @ 15 min, HPI was recovered when CFT was 50% discharged; HPI was throttled @ 20 min after being available) [4.2e-8] 96 (#87 + HZP) [7.4e-7] 88 (PZR SRV SO, HPI fail, 4 TBVs opened @ 15 min, HPI was recovered when CFT were 50% discharged; SRV reseated 5 min after HPI was recovered, HPI throttled 1 min after being available). [1.3e-7] 97 (#88 + HZP)
SG(s) Overfeed			
SG(s) breach + SG(s) Overfed	[1.2e-6] 89 (F&B + 4 TBVs are opened and HPI is throttled after RCS pressure reaches 2275 psi) [6.6e-8] 98 (#89 + HZP)		

HZP: Hot zero power
SG SV SO: Steam generator safety valve stuck open
TBV: Turbine bypass valve
F&R: feed-and-bleed (HPI injects coolant and RCS coolant leaks through the PZR PORV)
PZR SRV: pressurizer safety relief valve
The value inside the bracket is the bin's frequency.
The underlined digit is the identification of the bin corresponding TH run
The value inside the parentheses is the brief description of the TH run
*as a substitute of PZR SRVs stuck open without being reseated (Case 34) plus HZP

Table 4.8 shows the summation event frequencies of bins in each event category. The category of primary system breach causing RCS loss of subcooling with a nominal secondary system state dominates in event frequency of PTS-risk scenarios. The other PTS significant event categories are having secondary system breach, and a combination of primary system breach and secondary system breach. This study performs TH uncertainty analysis on the bolded event category. This category contains about 94% of the total event occurrences of the PTS-risk scenarios. FAVOR code was used to calculate the CPF of the bins. The results also suggest that the selected event categories dominate PTS-risk from PFM perspective.

Figure 4.21 shows the principles of PRA event tree construction. The event trees are constructed with a bottom-to-top approach in a process that is independent from constructing the PTS event classification matrix. Coincidentally, the top events are consistent with the main parameters used in constructing the PTS event classification matrix. The consistency between the event trees construction (from a bottom-to-top approach) and the PTS event classification matrix (from a top-to-bottom approach) provides additional confidence in the matrix construction.

Table 4.8 The summation of event frequency in the PTS event classification matrix

Primary Side State / Secondary system State	Intact	Breached	
		Break Size <~ 1.5" Breach flow could be compensated by HPI	Break Size > ~1.5" Breach flow cannot be compensated by HPI
Nominal			8.1e-4 2.7e-3
One SG Breach	3.7e-6	2.7e-7 6.3e-5	
Two SGs Breach	1.7e-5	2.8e-7 4.9e-8 3.3e-6	3.1e-6 1.2e-6
SG(s) Overfed			
SG(s) Breach + SG(s) Overfed	1.3e-6		

TH uncertainty analysis is performed in the bold circled area.

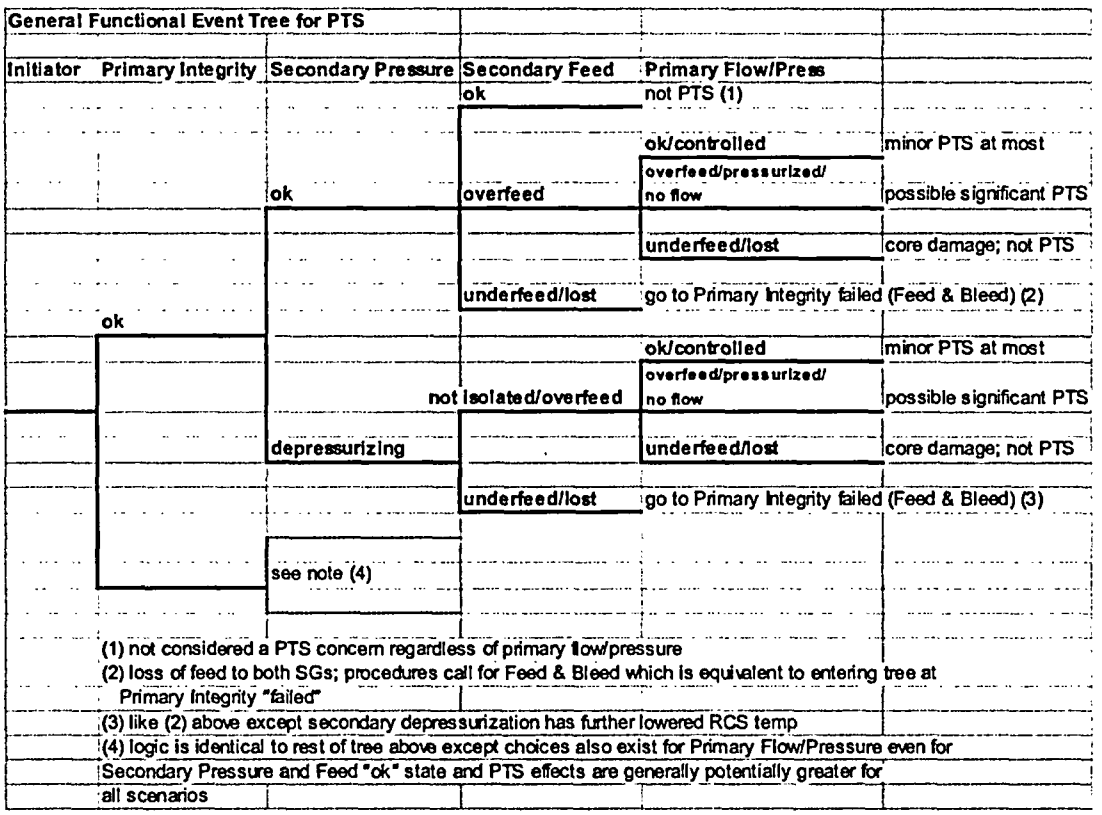

Figure 4.21 An overview of the PRA event tree approach in modeling PTS scenarios.

5 Model Uncertainty Characteristics

Model uncertainty discussed in this section is limited to the appropriateness of the use of RELAP5 in analyzing the transient. It includes two types of uncertainty. The first type of uncertainty relates to RELAP5 internal modeling and results from RELAP5 inherent limitations. The limitations and their treatments are follows:

- One-dimensional code
  The three dimensional fluid flux behavior (e.g., plume) inside the downcomer region cannot be modeled well. By comparing RELAP5 simulation results with the results of the experimental, Computational Fluid Dynamic (CFD), and Oregon State APEX program, it has been shown that the influence of the one-dimensional restriction is small.
- Volume averaged calculation
  The non-physical phenomena associated with volume-averaged system codes are numerically induced oscillations. Comparison of RELAP5 results with results of the experimental, CFD, and Oregon State APEX program have shown that the influence of the volume averaged calculation is small.
- Empirical correlations
  Some uncertainties relating to use of empirical correlations (e.g., calculation of choked flow rate) are discussed in later sections. The important correlations are treated explicitly in the analysis.

The second type of uncertainty relates to the nodalization choice of the RELAP5 input deck. The input deck is a product evolved from the Oconee TH analysis of PTS sequences (Fletcher et al., 1984), the B&W safety report [Hanson, Meyer et al. 1987], and the SCDAP/RELAP5 Oconee model description [Determan and Hendrix 1991]. It was revised in 1994 [Quick 1994]. For this study, since the downcomer region is the area of interest, multiple channels are added into the input to the input deck along with numerous modifications [Arcieri, Beaton et al. 2001]. The nodalization is considered to have reached its optimal level. Finer nodalization is not expected to generate significant results. The uncertainty contributed by the nodalization is concluded to be small.

This section discusses the model uncertainty sources and their characteristics, in order to provide understanding for developing a simple and acceptable method to quantify the model uncertainty. This section does not intend to provide a detailed uncertainty assessing method for the best-estimate code, RELAP5-gamma. Section 5.1 discusses the main phenomena that RELAP5 calculation subjects to large uncertainty. Section 5.2 discusses uncertainty associated with calculation of the two-phase choked flow rate. Section 5.3 discusses uncertainties of flow oscillation and flow driven by numeric flaws. Section 5.4 lists the specific items relating to modeling uncertainty treated in this study.

5.1 Important Phenomena that RELAP5 Code Calculation Subjects to Uncertainty

The answer to the question "what is the contribution of TH uncertainties to the overall uncertainty of the P_{dc} and T_{dc} parameters" is relatively complicated. It is difficult to provide an overall answer because, as shown in the Table 5.1, the code's ability to properly evaluate the states differs significantly.

Table 5.1 Ability of RELAP5 to evaluate inventory dependent two-phase flow states.

Phenomena	Plant type	Ability of RELAP5 to model	Effect on T_{dc} and P_{dc}
1.Flow interruption by vapor in candy cane	OTSG	Poor	Short term increase of P_{dc} and decrease of T_{dc}
2. Interruption-resumption flow	OTSG	Not able	Periodic fluctuation of P_{dc} promotes mixing therefore higher average T_{dc}
3. Boiling-condensation mode	OTSG	Good	Significantly lower P_{dc}. Low loop flow thus lower T_{dc}
4. Mixing of core and downc region fluid (inertial & nat-c through RVVV)	OTSG, & U-tube	Moderate	Increases T_{dc}. Small effect on P_{dc}
5. Reflux condensation	U-tube	Poor	Reduces P_{dc}. Reduces C.L. flow therefore lower T_{dc}
6. Temporary heat sink loss due to mismatch of sec.-prim. liquid levels	OTSG	Moderate	Short term P_{dc} increase & flow stagnation. Short term T_{dc} decrease
7. Heat sink loss due to $P_{prim} < P_{sec}$ Caused by $\dot{Q}_{dec} < \dot{Q}_{brk}$	U-tube & OTSG	Moderate. Bounded by choked flow limits.	P_{dc} rises & flow stagnates, lower T_{dc}

The capability of system codes, such as RELAP5, to evaluate physically realistic TH characteristics for the above outlined modes of energy/mass transfer and inventory loss varies significantly. RELAP5 is a one-dimensional code, employing volume averaged parameters, it is thus to be expected that operational regimes characterized by stratified flows and influenced by three dimensional flow geometry discontinuities will not be properly reproduced. For example, the intermittent flow-stagnation periods during the Interruption-resumption mode (IRM) depends on the position of the collapsed liquid level in the RPV relative to the upper and lower elevations of the hot leg entrance. Such inherently three-dimensional flows cannot be represented adequately by a one-dimensional code. On the other hand, if vapor-liquid separation in horizontal channels is not a dominant phenomenon, or if separation is nearly complete and leads to single phase (vapor or liquid) flows (e.g. the boiling-condensation mode), then system response is reproduced moderately well.

Not all of the uncertainties associated with two-phase flow phenomena and their computation influence the PTS relevant parameters in an un-favorable direction. Several of the phenomena (e.g. operation in the IRM and internal circulation through the

RVVV's) generate more mixing and thus higher downcomer fluid temperatures. A list of the characteristic two-phase flow phenomena along with a qualitative assessment of system code capability to evaluate them is presented in Table 5.1 The table is meant to be inclusive and does not take into account the occurrence probability of the listed phenomena. The question "how do the noted computational short comings influence the uncertainty margin of evaluated PTS relevant results" must be posed by weighing its relevance to the PTS issue. In this respect it is noted that most of the phenomena which cannot be reproduced adequately either have short time constants (short compared to the PTS relevant time constants), or from the PTS concern point of view, they have a 'beneficial' effect. Especially beneficial are flow states that are inherently dynamic. They lead to chugging and to condensation induced flow surges that churn the primary system inventory and promote mixing.

The TH phenomenon, which can lead to long-term flow stagnation and thus impact T_{dc} in a PTS relevant manner, applies to transients for which $\dot{Q}_{\text{...}} < \dot{Q}_{\text{...}}$ (listed at the bottom of the table). The major contribution to the TH analysis uncertainty for such transients is the computation of the mass/energy loss term through the break. These computational uncertainties can be separated into two major components. First is the uncertainty introduced by the fluid conditions of the 'break node'. This uncertainty is strongly dependent on the location (especially the elevation) of the break. Second is the modeling uncertainties associated with the computation of a two-phase choked flow. These two items are correlated.

5.2 Uncertainties Associated With Two-Phase Choke Flow

Modeling of two-phase choked flow has been important to reactor safety analysis from the very beginning, consequently extensive benchmarking and verification efforts of computational models have been carried out. Reviews of these studies are available in a number of survey papers [Weisman and Tentner 1978; Rosdahl and Caraher 1986], a recent example being the study by Queral et al. [Queral, Mulas et al. 2000], which includes quantitative comparisons of the Marviken experimental data base with two models used in recent RELAP5 versions (Ransom-Trapp [Ransom and Trap 1980] and Henry-Fauske [Henry and Fauske 1971]). It would appear that the availability of such an extensive database should make it possible to provide a reasonable assessment of modeling uncertainty. That is true for situations where the boundary conditions are accurately known, however, this condition does not apply for an accidental break. An analysis that claims to evaluate the uncertainty associated with accidental breaks must consider the wide spectrum of locations, sizes and types of possible breaks that are actually possible, as well as code calculation error.

A relevant conclusion of the code calculation uncertainty is that though two-phase critical flow is an adequately modeled phenomenon (on the order of ±10 to 15% precision) for well known fluid conditions and specific physical characteristics of the flow path, this accuracy cannot be expected for generic small breaks. For such breaks there is no alternative but to include the uncertainties imposed by the range of break characteristics by assigning a broader uncertainty band to the break size.

Flow stagnation becoming possible is quite dependent on the relative magnitudes of the primary system mass/energy loss and source terms. The difficulty in putting them into practice is that over the duration of an SB-LOCA transient, these terms are in a sense "a moving target', because both the source terms and the loss terms change with time and system pressure. A serious additional complication is that the choked break flow mass/energy loss term is burdened with large aleatory and modeling uncertainties. The simplification of a complex problem is a desirable goal, however, when dealing with a parameter depending on several time varying conditions, simplification has inherent limits. The computed choke flow rate through an accidentally generated break is such a parameter. An overview of its range of variation is provided in Figures 5.1 to 5.7.

The figures present computed choked flow mass/energy loss rates as a function of upstream pressure, quality, and break size. In order to span the entire possible range of modeling uncertainty, two 'limiting' models as well as two 'best-estimate' models are used in the computations. The models differ principally in the assumptions determining the approach to thermal equilibrium in the 'throat' of the break opening. For two-phase fluids an approach to thermal equilibrium in a decreasing pressure gradient requires both mass and energy transfer between the phases. These processes take time; therefore how close they can come to equilibrium conditions depends on the spatial distribution of the pressure gradient along the flow path. Two models employing bounding assumptions can bracket the range of this dependence.

The lower limit is provided by the Homogeneous Equilibrium Model (HEM). As the name implies, this model assumes that, as the fluid flows from the upstream pressure to the throat pressure, the two phases remain in thermal and mechanical equilibrium. It results in the lowest possible density of the fluid at the throat and thus also in the lowest mass flux.

The upper limit is set by the bounding assumption that the fluid composition does not change at all as it moves through the pressure gradient of the break. In effect, as the name by which this model is identified implies, its state remains 'frozen'. The fluid density at the throat and therefore also the flow rate are maximized.

The actual flow rate will fall somewhere between the two limits. For sharp, 'orifice' like flow path's and for low initial quality, the flow rate will be closer to the boundary set by the 'frozen' model, and for longer flow paths and higher qualities it will move toward the value given by the HEM assumption. The figures also show two 'best estimate' models that have been implemented in RELAP5. Up to ~1998, RELAP5 versions for over a decade relied on the Ransom-Trapp model. The 'beta' version released in ~1998 included the option for using the earlier Henry-Fauske model. In the 'gamma' version (released June 1999), the Henry-Fauske model became the default model.

The models differ in their approach to evaluating thermal and mechanical equilibrium (characterized by the 'slip' ratio) at the throat of the break. As illustrated in the figures, when the upstream condition is saturated (or sub-cooled) water, the computed results move closer to the values obtained by the 'frozen' bounding option. The Ransom-Trapp

model results allow more equilibration and therefore in most cases lie below the rates computed by the Henry-Fauske model. Recent studies [Queral, Mulas et al. 2000] using large scale data for verification have concluded that the Henry-Fauske model is preferable. Such a conclusion is justified if the flow path through the break approximates orifice conditions, however, it should not be uncritically applied to the 'generic' accidental small break. In fact, if the break flow has more time to equilibrate (e.g. the flow from a sheared smaller diameter pipe), than the Ransom-Trapp model is preferable. The spread between the results obtained from the two 'best-estimate' models provides an illustration of the modeling uncertainty associated with this computation.

Figures 5.1 and 5.2 show computed choked mass and enthalpy flow rates for a 2-inch in diameter break (break area is 0.002027 m^2) for saturated water as a function of upstream compartment pressure. Besides the two limiting and two 'best estimate' model results, the range of the relevant source terms is superimposed on the figures. The indicated range of the HPI flow rate (Figure 5.1) depends on the system pressure and can vary from ~40 kg/s at the PORV set point pressure up to ~80kg/s at low system pressures (below ~20 bar). The range of $\dot{Q}_{dec}$ (Figure 5.2) depends on time after scram, thus for the Oconee plant the equilibrium $\dot{Q}_{dec}$ decreases from ~50 MW (15 min after shutdown) to ~28 MW ~2 hrs after shutdown For all SB-LOCA's, the pressure of the primary system will first drop rapidly to the saturation pressure (~72 bar). What happens subsequently depends, as has been outlined, on the relative mass/energy source and sink terms. Figures 5.1 and 5.2 show that if the effective break size is ~0.00203 m^2 and if the HPI's have been activated, then the question whether the primary system will experience a net loss of inventory depends on the nature of the break. For breaks that lead to a critical flow rate approaching the HEM model limit (e.g. the shearing of a smaller pipe at a location so that the sheared pipe segment L/D is >10), net inventory loss will not occur and the primary system can be repressurized. However, net energy loss (Figure 5.2) will proceed, so that the system liquid temperature will continue to drop until saturation temperatures in the range of 50 to 30 bar are approached (540 to 505 °K). The main point of this example is that the question of whether and at what rate cool down and depressurization will be calculated, and thus also the question of whether flow stagnation is possible, depends on the choice of the computational models and thus also on the combination of model and 'type of break' uncertainties.

A more comprehensive overview of the critical flow model dependent range of break sizes is obtained by plotting the mass/energy flow rates for fixed up-stream conditions against the break area. Figures 5.3 to 5.6 show the mass/energy flow rates at two representative pressures: 70 bar (~1028 psi) the saturation pressure at operating conditions, and 20 bar (290 psi), a pressure at the low end from the PTS concern point of view.

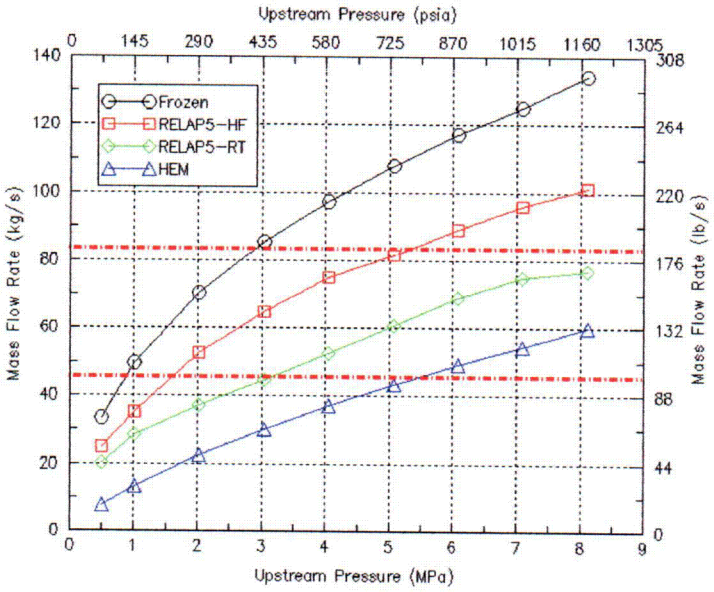

Figure 5.1 Choked mass flow rates vs. pressure. (Saturated liquid 2-inch break, break area = 0.00203 m^2). The region between two dashed lines is the anticipated region where flow stagnation and resumption could occur.

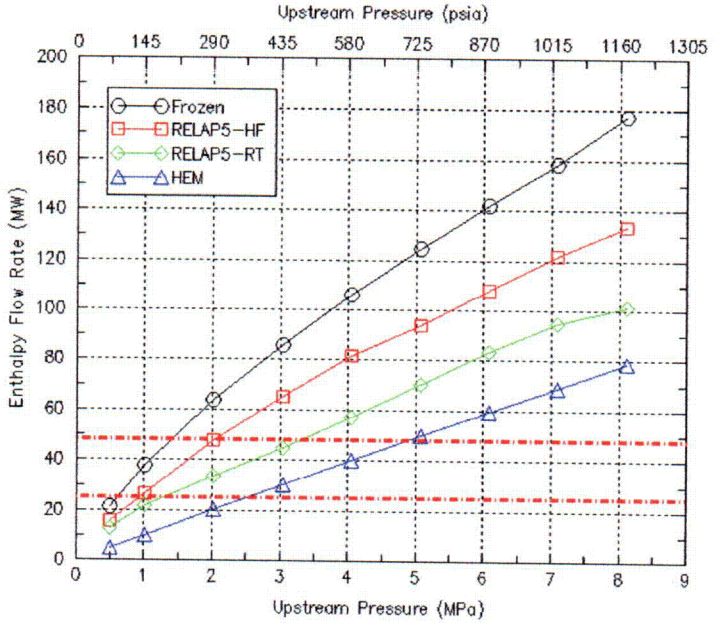

Figure 5.2 Choked enthalpy flow rates vs. pressure. (Saturated liquid 2-inch break, break area = 0.00203 m^2). The region between two dashed lines is the anticipated region where flow stagnation and resumption could occur.

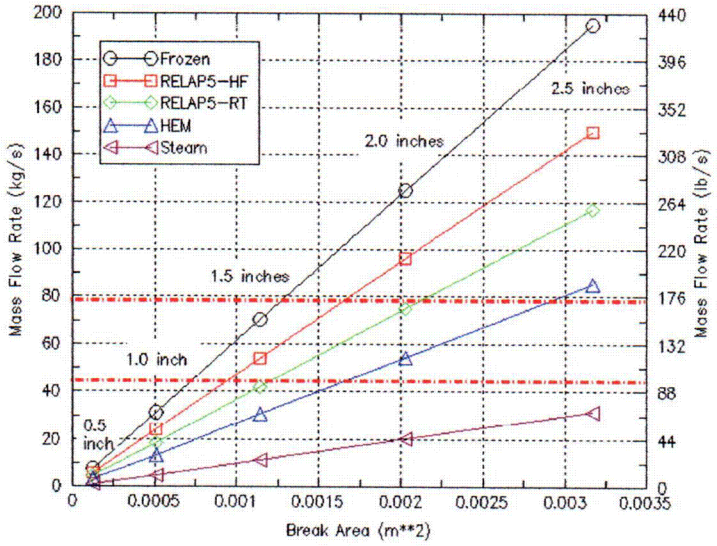

Figure 5.3 Choked mass flow rates as a function of break area; Upstream condition 7 MPa (1028 psia), T_{SAT} = 559 K (546 F) The region between two dashed lines is the anticipated region where flow stagnation and resumption could occur.

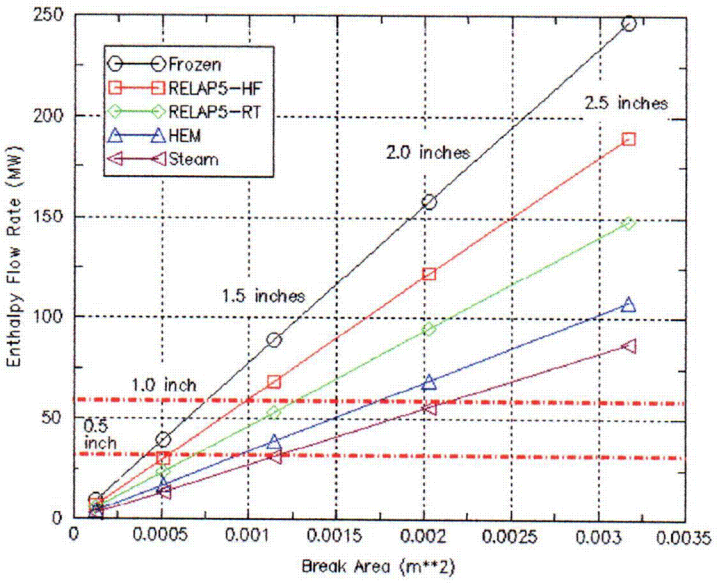

Figure 5.4 Choked enthalpy flow rates as a function of break area; Upstream condition 7 MPa (1028 psia), T_{SAT} = 559 K (546 F) The region between two dashed lines is the anticipated region where flow stagnation and resumption could occur.

C16

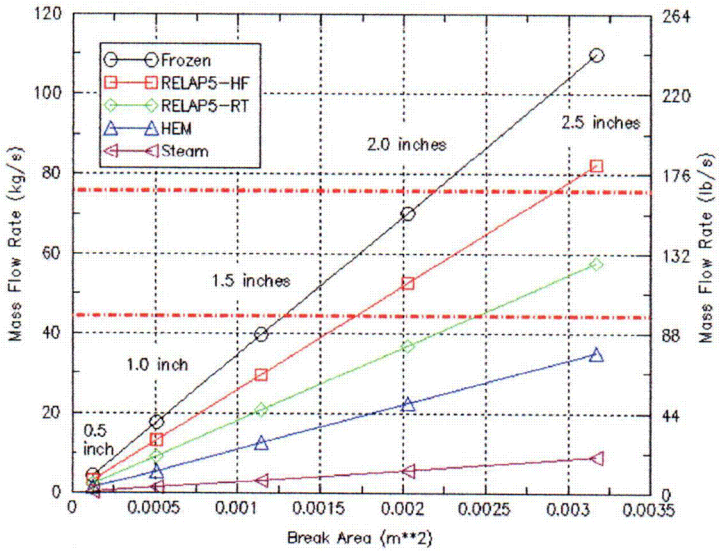

Figure 5.5 Choked mass flow rates as a function of break area; Upstream condition 2 MPa (290 psia), T_{SAT} = 486 K (414 F) The region between two dashed lines is the anticipated region where flow stagnation and resumption could occur.

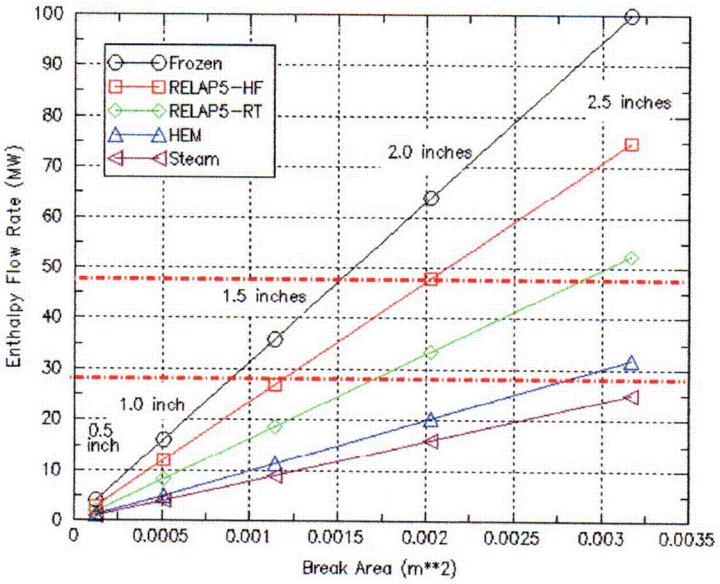

Figure 5.6 Choked enthalpy flow rates as a function of break area; Upstream condition 2 MPa (290 psia), T_{SAT} = 486 K (414 F) The region between two dashed lines is the anticipated region where flow stagnation and resumption could occur.

C17

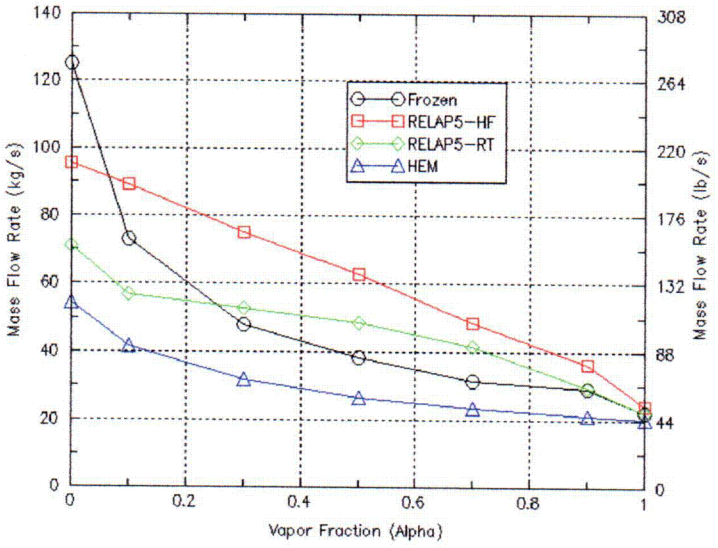

Figure 5.7 Choked mass flow rates as a function of steam fraction (upstream P = 7 MPa, 2-inch in diameter break)

The figures illustrate that the spread caused by model uncertainties is wide. Figures 5.3 and 5.4 can be used for estimating the size of the largest break which, independent of model uncertainties and the physical characteristics of the break, would lead to depressurization, as well as the size of the smallest break for which, given that HPI's are operating, depressurization would not occur. The analogous at a pressure of 20 bars (Figures 5.5 and 5.6) provide an indication of how far the inventory and pressure can decrease before the source/sink terms reach a new balance.

A summary of break size ranges as well as the equivalent break diameters (in inches) as estimated from the figures, is listed in table 5.3. The first row (at a P=70 bar) provides an estimate of the break size ranges that will initiate depressurization, and the second row (P = 20 bar) is an indication of how far depressurization can proceed. The break size range in table 5.3 is quite wide. It ranges from an equivalent diameter of ~3.2-inches down to an equivalent of ~0.65-inches in diameter. This reflects both the large differences that are possible in the characteristics of the break and the margin of uncertainty associated with the modeling of two-phase choked flow.

Note that, as specified by Table 5.2, the provided estimates apply for conditions where the fluid upstream from the break is saturated liquid. An additional source of uncertainty, which changes with elevation and inventory depletion and is thus also a 'moving target', is the state of the break compartment fluid. For low elevations the fluid could be sub-cooled, leading to larger flows, and at higher elevations it could become two-phase which would reduce the break flow rates. The sub-cooled mass flow rate does not exceed the bounding 'frozen' model limit presented in the figures, and the enthalpy flow rate will be lower. This change will thus not adversely alter the estimates shown in table 5.3. On the other hand, if the break compartment fluid becomes two-phase, then the flow rate

decreases, and the 'maximum' break size for which depressurization will not take place increases.

An illustration is provided in Figure 5.7 that shows calculated break flow rates as a function of the upstream fluid vapor fraction for a constant pressure of 70 bar. Depending on the model employed, the flow rate is seen to decrease by a factor of ~6 to ~3 as the upstream fluid condition passes from saturated liquid to steam. As should be expected, the models converge to the same value as α approaches 1. The trends in the range $0 > \alpha > 1$ point out some un-physical aspects of the models. Thus results obtained by the 'frozen' model, which represented the upper bound for saturated water, are seen to fall below those obtained by both 'best estimate' models. This is caused by the 'frozen' model assumption that both phases are accelerated to the same 'throat' velocity. On the other hand, the non-equilibrium best estimate models use a slip ratio that minimizes momentum by preferentially accelerating the lighter phase. A computational shortcoming not evident in the figure is that for several intermediate α values, the Ransom-Trap model as implemented in RELAP5 produces oscillations. The values shown in the figure are averages.

Table 5.2 Bounding Range of Break Sizes for Two-Phase Choked Flow (Oconee-1)

		Low flow limitation: HEM		High flow limitation: 'Frozen'	
		Mass Flow $\dot{W}_{brk} > \dot{W}_{HPI}$	Energy Flow $\dot{Q}_{brk} > \dot{Q}_{HPI}$	Mass Flow $\dot{W}_{brk} > \dot{W}_{HPI}$	Energy Flow $\dot{Q}_{brk} > \dot{Q}_{HPI}$
70 bar	Area (cm^2)	30 – 17	17 – 10	12 – 8	7 - 4
	Eq D (in)	2.4 – 1.4	1.4 - .8	1 - 0.65	0.6 – 0.4
20 bar	Area (cm^2)	40 - 36	21 -18	21 - 18	14 - 9
	Eq D (in)	3.2 - 2.9	1.7 - 1.4	1.7 - 1.4	1.2 - 0.7

5.3 Uncertainties of Flow Oscillation and Numerical Flaw

A fundamental issue in REALP5 code development has been the fact that the six-equation set used to describe the mass/energy/momentum balances of both phases is "ill-posed". This is a broad subject that has been dealt with in depth in many excellent studies [Mahaffy 1981; Ransom and Hicks 1984]. In the RELAP5 code several steps are taken to reduce the consequences of this problem. The most relevant are the incorporation of a numerical viscosity in the time advancement algorithm that dampens high frequency oscillations and prioritization of the precision with which the conservation equations are evaluated. The prioritization is based on the argument that from the point of view of safety related parameters, it is most important to conserve both mass and energy. Therefore transfer of mass/energy between volumes always takes place at the same time (implicit method) in the time advancement scheme. The transfer of momentum is assigned a lower level priority and includes some explicit components.

Such prioritization is necessary because one of the most persistent and commonly occurring non-physical phenomena associated with volume-averaged system codes are numerically induced oscillations. They can occur for a variety of conditions and have a range of causes. A commonly occurring type of oscillation is driven by step transitions of fluid condition dependencies between flow regimes and/or transitions between empirical correlations. This is exacerbated by the circumstance that both the flow regimes and the correlations are chosen explicitly. For many years significant code development effort has been directed toward incorporating various time and spatial averaging schemes to reduce the magnitude of this generic problem and thus make the code more 'robust'. These efforts have been largely successful and in the present version of the code, numerical oscillations rarely grow to such an extent as to terminate its operation. RELAP5 is presently remarkably 'robust', however the price of this achievement is that the code has become less 'transparent'. This is especially true regarding numerical oscillations, as in many cases it is difficult to diagnose their precise cause and to distinguish them from oscillations which have a physical basis.

The important question regarding numerically induced phenomena is how and to what extent they influence the computed parameters of interest and thus contribute to their uncertainty. The two main PTS relevant parameters P_{dc} and T_{dc} depend on the overall system mass/energy balance and on the distribution of the mass/energy within the system. The priority assigned in the evaluation of the conservation equations assures that in spite of potential numerical fluctuation of flows, mass and energy are conserved. However, the distribution of both quantities within the system can be influenced by un-physical flows. This can happen in two basic ways:

1) An un-physical variation of the circulation flow rate in time
2) Un-physical flow mixing, that is fluid is moved back and forth between adjoining regions, (e.g. the core region and the downcomer)

Note, that there is an additional way that improperly evaluated internal flows can impact the parameters of interest, namely, they could affect the magnitude of the energy/mass sink and source terms, particularly the outflow rate through breaks. There is a limited range of system inventory states, in which the geometric discontinuities of the flow system (e.g. the exit elevation of the hot legs from the upper plenum) can induce changes in flow mode and local fluid composition. This, in turn, can influence the computed break flow rate, especially if the break occurs at higher elevations.

Two examples are presented to illustrate both modes: a computed oscillation that has a physical basis but is enhanced by the volume-averaging feature of the code, and a numerically induced flow in parallel channels.

5.3.1 An Example of An Oscillation With A Physical Basis

The flow states that are not evaluated properly are inherently dynamic. They lead to chugging and to condensation induced flow surges that churn the primary system inventory and promote mixing. It is to be expected that in general there will be more mixing in the three-dimensional actual NPP than in a simulation provided by a one-

dimensional model. In this respect the limitations of RELAP5 are more likely to be in the 'conservative' direction, that is, they will underestimate the degree of inter-region mixing. Of special importance in this respect is the code's ability to evaluate the mixing that occurs between the core region and the downcomer

Figure 5.8 shows the RELAP5 computed downcomer cool-down rates of a 'feed-and-bleed' transient, accompanied by loss of the SG heat sink (due to failure of feed-water). As shown in the figure, for this transient the computed T_{dc} oscillates with a period of ~200 s and an amplitude of ~5 K. The answer to the question whether this is a physical or a numerical oscillation is that it is probably a mixture of both. Though the figure depicts a two-phase condition, the flow geometry applies for single phase flows as well. As shown in the figure, HPI flow enters the cold legs ~1m upstream of the downcomer entrance. At this location it meets the warmer circulatory flow, mixes with it to some degree and proceeds towards the downcomer. For a constant HPI rate of flow, the average temperature and density of the fluid stream entering the downcomer will depend on the relative flow rates of the two streams. At low circulation flows the will be cooler, and at high circulation flows it will be warmer.

A component of the driving force for natural circulation flow is the density difference between the downcomer fluid and the fluid on the other side of the baffle in the core region. Assume now that we pick up the development of the cycle depicted in Figure 5.8 at the point in time that T_{dc} decreases. As the downcomer fluid cools, its density increases, increasing the natural circulation driving force. Circulation flow then increases, and the fluid temperature in the cold leg starts to rise because the constant HPI flow rate now mixes with a larger volume of warm circulation flow. When this warmer water starts to penetrate into the downcomer, the driving force is decreased, and the circulation flow drops. There is thus a negative feedback with a time lag between circulation flow and temperature.

Figure 5.9 shows the coolant velocities in all cold legs. As illustrated, the velocities remain positive for all cold legs and vary in magnitude from ~ 0.6 to ~0.3 m/s. Finally Figure 5.10 shows an expanded time segment on which the temperature oscillations in the downcomer and the cold leg velocities are superimposed. This illustrates that the cycles of both variables are indeed out of phase and thus substantiates the proposed explanation.

In the presented example, the code generated oscillation had a physical basis, however, this does not guarantee that the actual phenomenon would have the same period or magnitude. Because of the volume averaged character of the code; the HPI and circulation streams are modeled to be continuously mixed, whereas in reality flow separations (hot water over cold) could occur. The question of how this impacts PTS concerns can be answered by considering the oscillation period and the RPV thermal time constant (~200 s vs. ~400 s). The difference is sufficiently large that a time average of T_{dc} is adequate. This is obtained by the overall energy mass balance, and depends on the average rate of re-circulation flow and HPI flow. Therefore the oscillation, including its possible numerical component, does not contribute an additional uncertainty component.

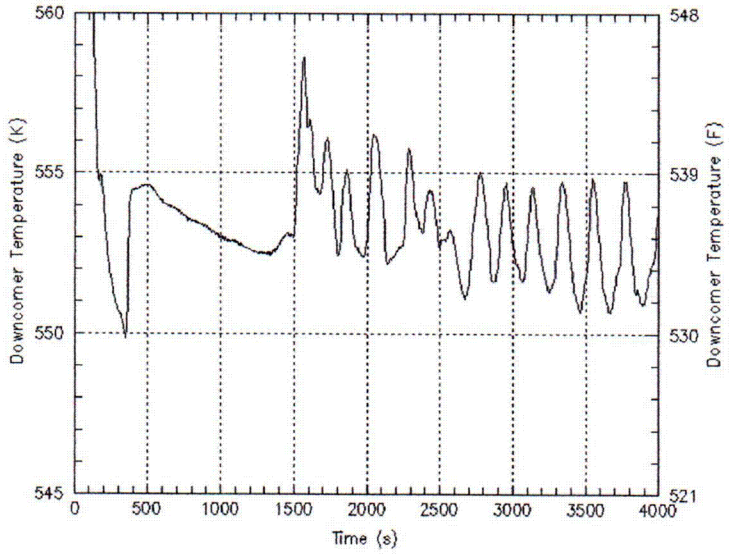

Figure 5.8 T_{dc} oscillation during a 'feed-and-bleed' transient with loss of heat sink

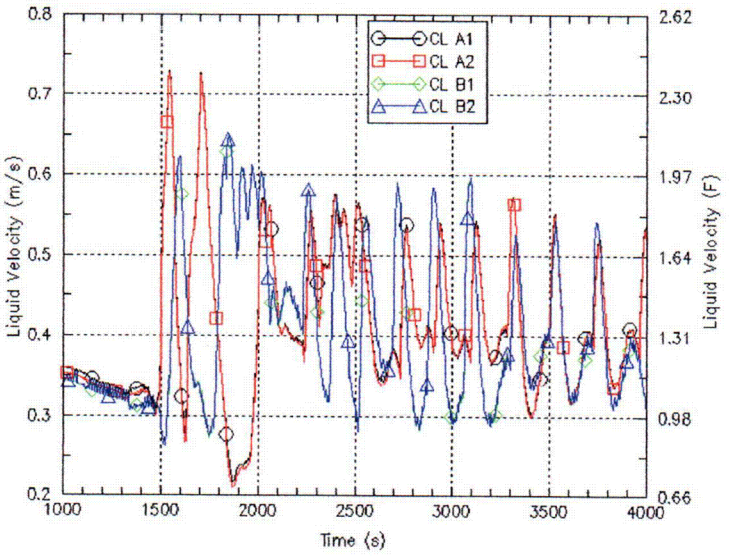

Figure 5.9 Cold leg flow velocities (feed&bleed transient with loss of heat sink)

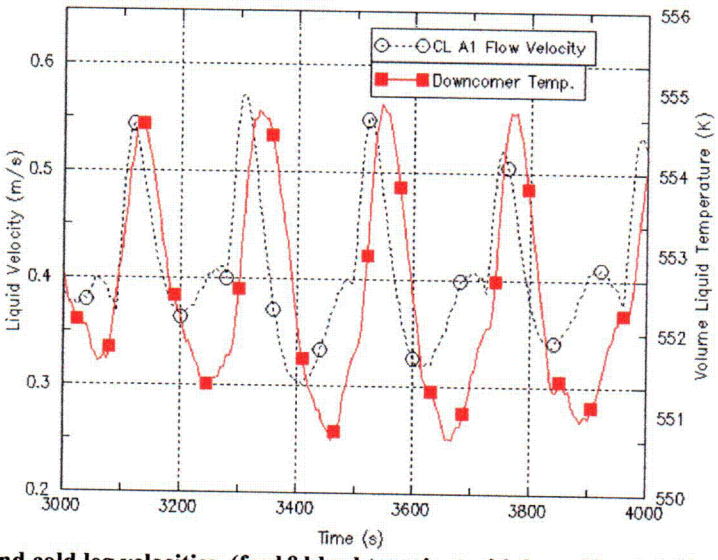

Figure 5.10 T_{dc} and cold leg velocities. (feed&bleed transient with loss of heat sink)

5.3.2 An Example of Numerically Induced Flow

The influence of code numeric on the evaluation of flows becomes more pronounced as the momentum imparting, driving forces decrease. This can become especially apparent if the flow geometry includes parallel flow channels with similar flow resistance. In the model of the Oconee NPP, the two cold legs returning flow from the SG provide just such an example. Anomalous flows in the cold legs can be expected for transients when the RCP's are tripped and the natural circulatory driving force becomes small. This numerical problem has been observed in previous studies of RELAP5 computation [Riemke and Johnsen 1994]. The explanation proposed by the developers is that the iterative algorithm used to invert matrices deals with the volume-averaged nodes sequentially. The inevitable sequential nature introduces asymmetries (through numerical round off) even for flow geometries that are in other respects completely symmetric. When dissipative terms are small, the round off differences can accumulate during the iteration process and produce macro differences in the computed flows.

An illustration of such flows is presented in Figure 5.11. It shows the flow rates in cold legs A1 and A2 for a .148e-2 m^2 break size (equivalent to 1.71-inches in diameter) after the SG heat sink is lost. The only potential driving force for natural circulation for such conditions would be the density difference between the fluid in the downcomer and the core region, but once vapor in the RPV region reaches the hot leg entrance this driving force is not available. The numerical flow shown in Figure 5.11 passes water through the upper downcomer region where it is partially heated by steam entering this region through RVVV's. This warmer water is then mixed with HPI flow and as a result the computed T_{dc} transient will be higher than would be the case if there were no numerical circulation.

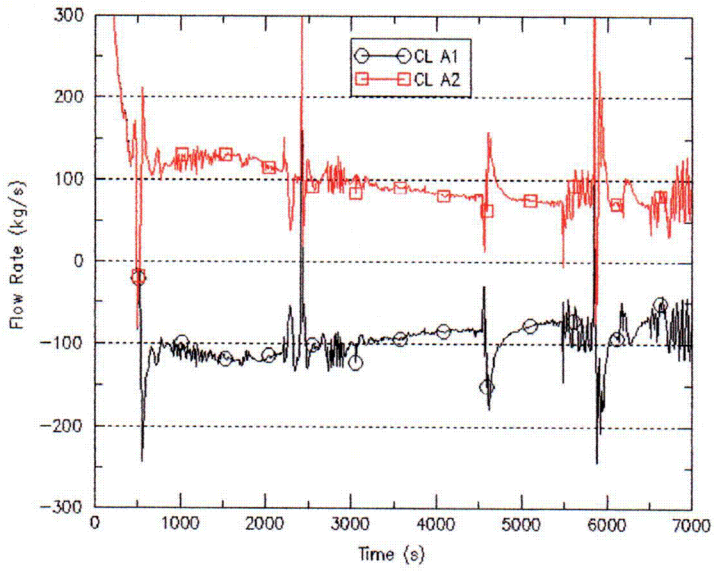

Figure 5.11 Flow rates in cold-legs A1 and A2 in a .148e-2 m^2 break size LOCA (equivalent to 1.71-inch in diameter)

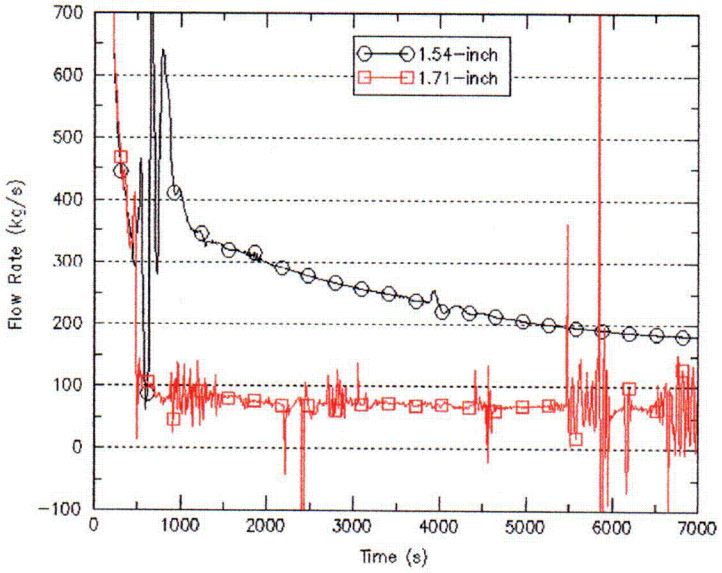

Figure 5.12 Flow rates in hot-leg A of two LOCA events with different break sizes

Figure 5.12 shows the flow rate in hot leg A for two break sizes: the 1.71-inch break utilized in Figure 5.11 and a somewhat smaller break having an equivalent diameter of 1.54-inches. As figure 5.12 shows, for the larger break size the re-circulation flow along the hot leg decreases to zero at ~ 500 sec. The quite sizable flow rate of ~100kg/s in the positive direction (RPV to SG) in cold leg A1 is offset by an equivalent flow in the negative direction (SG to RPV) in cold leg A2. Both cold legs are at the same elevation

thus there is no physical driving force which can propel this flow. The conclusion is that, as diagnosed by Riemke [Riemke and Johnsen 1994], it is generated by round off errors and the asymmetry of the matrix inversion routine. In their discussion of the problem, the code developers make a further comment that this anomaly will have no effect on the evaluation of most TH parameters of interest. Since the anomaly does not alter the overall energy/mass balances, this is true for the wide majority of cases. In this respect parameters of interest to the PTS issue are an exception.

The magnitude of this influence is illustrated in Figure 5.13. It shows two computed T_{dc} traces which differ only in the presence of the numerical flow circulating along both cold legs. For the lower trace this flow is eliminated by specifying a very large 'backwards' flow resistance for the RCP region. As long as flow is in the 'positive' RPV-to-SG direction this artificial input feature does not alter the computed result, however, it prevents the development of an un-physical 'backward' flow.

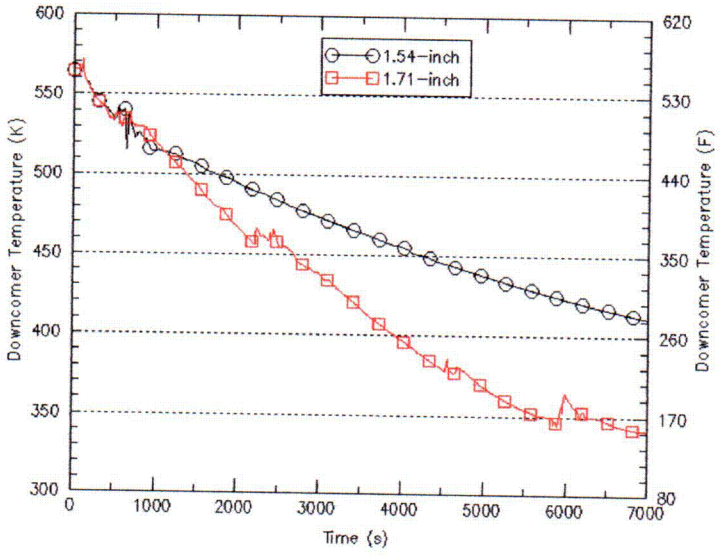

Figure 5.13 Effect of numerical parallel channel flow on T_{dc}

5.4 Treatments of Model Uncertainty

From an implementation perspective, even with the above mentioned limitations, the RELAP5-gamma can simulate the real scenarios well. Only for certain phenomena does the RELAP5-gamma have large uncertainty in reflecting reality. These phenomena and their treatments are listed as follows:

- Evaluation of out-flow rate, especially for two-phase choke flow
  It's complex to change RELAP5 internal flow rate modeling from one model to another. Instead, an increase and a decrease of 30% of the break area with use of the same choked flow rate calculation model are assigned to cover the flow rate uncertainty.

C22

- Modeling RVVVs states
  The uncertainty is due to how RELAP5 models the pressure difference between the two sides of RVVV (upper core region and downcomer). The uncertainty of RVVVs' states is bounded between fully close and fully open.
- Flow driven by numerical flaw
  The unrealistic recirculation flow between the two parallel cold legs of the same loop is eliminated by applying high reverse flow resistances in all RCPs.
- Flow Resistance
  The shear force at the interface between liquid and steam in two-phase scenarios could affect coolant flow rate. There is uncertainty in RELAP5 modeling the flow drag force. A 200% flow resistance is used to model the resistance deviation.
- Heat transfer coefficient
  The heat transfer coefficient between the internal system structure and the RCS coolant is calculated dependent on the heat transfer coefficient mode determined by RELAP5. It is difficult to change the actual heat transfer coefficient calculated by RELAP5. Instead changes are performed in varying the fouling factor for each heat structure in the RELAP5 input deck except core, SG tubes, pressurizer heater, and feedwater heater. A 30% increase and decrease of the heat transfer coefficient is used as the uncertainty boundary.

The above treatments on model uncertainty along with treatments of parameter uncertainty (discussed in Section 6) are combined to assess the aggregated TH uncertainty.

6 Parameter Uncertainty and Uncertainty Assessment

The parameters affecting PTS risk differ from one event category to another. The parameters discussed in this section only focus on the event category of RCS loss of subcooling due to primary system breach with nominal secondary system response. As discussed in Section 4, within this event category, a two-phase region is developed and persists in the primary system. The system pressure is equal to the saturation pressure of the fluid located at some high elevation within the system, usually at the top of the RPV. As a result P_{dc} is not independent of T_{dc} anymore. An exception is the scenario of PZR SRV stuck open and later self reseated. In this scenario, if the operator does not control HPI flow in time the RCS could become subcooled again. In such a situation, a P_{dc} transient is independent from T_{dc}. This leaves only one parameter that determines Pdc uncertainty: the timing of the operators throttling HPI flow.

Section 6.1 discusses preliminary screening of parameters affecting T_{dc}. It utilizes the five types of T_{dc} influencing factors to identify parameters at system level applicable for implementation. Section 6.2 describes the finite discrete probabilistic distribution (DPD) method and its implementation. Section 6.3 discusses selection of a sensitivity indicator to represent the sensitivity of a parameter. A parameter's sensitivity to PTS risk is represented by the difference of the sensitivity indicators of the nominal scenario and of the scenarios with the parameter's value at its upper and lower bounds. Use of the sensitivity indicator is a surrogate indication of a parameter's PTS risk contribution to reduce analysis effort. A significant number of RELAP5 calculations are performed to assess key parameters' sensitivities. The assessment also includes the parameters relating to model uncertainty (discussed in Section 5). Section 6.4 discusses sensitivity study results and DPD representation of all key parameters to assess aggregated uncertainty. The linear additive method is used for the uncertainty aggregation. This subsection also provides self justification of use of the linear additive assumption. Section 6.5 discusses key parameters' rankings.

6.1 Identification of T_{dc} Influencing Parameters

The five T_{dc} influencing factors identified in Section 4 and the parameters associated with them are discussed here. For convenience, the model uncertainty related parameters identified in Section 5.4 are placed in the same category.

- **Heat Capacities**
  The primary parameters in this category are the amounts of liquid and steam and structure (containing structure heat) of the primary and secondary systems. These parameters are dependent on the RELAP5 input deck construction to represent the plant. With use of standard nodalization, the uncertainty in this category is expected to be small.

- **Heat sources**
  - Decay heat
    The decay heat curve is dependent on the operation time interval and reactor power before the reactor trips. For simplicity three decay heat curves are used

to represent decay heat uncertainty instead of using operation time interval and reactor power before reactor trip as the basic parameters. The three representative decay heat curves are for the reactor tripping at full power operation (assuming reactor has been operated for infinite amount of time before trip), at .7% of full power, and at .2% of full power. The .7% and .2% of full power curves represent the event occurring at the warm startup stage with different refueled state. For Oconee-1, only reactor tripped at full power operation and .2% power curves are modeled. When three curves are used, PRA conclude 98%, 1%, and 1% probabilities for reactor trip at full power operation, .7% power, and .2% power, respectively. When two curves are used, the probabilities of reactor trip at full power operation and .2% power are 98% and 2%, respectively.

- RCPs
  Some plants have trip logic to trip RCPs automatically. Some plants rely on operator action to trip RCPs. In general, the RCPs tripping criterion is RCS loss of subcooling. In the PRA model, the probability of RCPs tripping after RCS loss of subcooling is very high. In this study it is assumed that RCPs trip at RCS loss of subcooling.

- System Structure Heat
  As discussed in Section 5, the component heat transfer coefficient, affected by the heat transfer coefficient mode determined by RELAP5, would affect the rate of heat transfer from system structure to RCS coolant. A ±30% of heat transfer coefficient uncertainty is used in this study. The component heat transfer coefficient is a parameter relating to model uncertainty.

- **Heat sinks**
  - Primary system breach
    Breach location and breach size are the key parameters. Breaks occurring at hot leg and cold leg would yield significant differences in TH response. PZR SRV is another breach location that could cause RCS loss of subcooling. The break size for LOCA scenarios causing RCS loss of subcooling could range from about 1.5-inches to the maximum size of break (i.e., double-ended LOCA at hot leg). For PZR SRV stuck open scenarios, the break size could range from a substantial size of valve open area, that creates breach flow greater than HPI flow, to the maximum valve open area.

    For a fixed break size, as mentioned in Section 5, there is uncertainty in RELAP5 calculated break (choked) flow. This uncertainty is a model uncertainty. A ±30% break flow difference is used to represent the uncertainty of the RELAP5 calculated break flow rate.

  - SGs
    The boundary conditions clearly specify that the secondary system is in the nominal condition. In this event category, the primary system breach is the

dominant heat sink. The SGs will become heat sources to RCS. The uncertainty of heat transfer from the secondary system to the primary system is dependent on RELAP5 modeling.

- HPI, Core flood tank (CFT)/Accumulator, and LPI
  Four types of factors relate to the RCS coolant injection system: function states (fail on demand), flow rate, coolant temperature, and activation timing. These four properties are discussed as follows:

  System Functional State
  System failure (complete failure or partial failure) could reduce the flow rate dramatically. It has the most significant impact on RCS risk. However, these systems are relatively reliable and have small failure probabilities. For example, the failure probability of HPI failed-on-demand is about 2E-3. Combined with initiating event frequencies and other system failures, scenarios with multiple failures have very low frequencies. From PRA perspective, such scenarios have negligible PTS risk. From PFM perspective, failure of the RCS coolant injection system would reduce the T_{dc} cooldown rate that reduces PTS risk. The sensitivity of HPI failure has been analyzed, but HPI failure as well as accumulator failure and LPI failure are not included in the uncertainty analysis.

  Flow Rate
  The flow rates of the three RCS coolant injection systems are primarily dependent on the RCS pressure. The flow rate versus pressure curves entered in the RELAP5 input deck are the main uncertainty source. A ±10% flow difference is applied for HPI flow to treat HPI flow rate uncertainty. The flow rate uncertainties of the accumulator (or core flood tank) and LPI are considered to have small impact on PTS risk. They are not included in further uncertainty analysis.

  Flow Temperature
  RCS injection coolant temperature varies throughout the year. Seasonal dependence is the common factor for the coolant temperatures of the three injection systems. Three sets of temperatures representing their coolant temperatures in summer, spring/fall, and winter are the representative temperatures with .25, .5, and .25 probabilities, respectively. Condensate Booster Pumps are activated to provide sump recirculation for the HPI coolant source while the refueling water storage tank (RWST) is running out of water. Sump recirculation allows HPI and LPI tap water to supply the main steam condenser. It would increase the injection coolant temperature. Sump recirculation is activated later in the scenario in which RCS temperature is fairly stable. It is expected to have little impact on PTS risk. The state of sump recirculation is treated deterministically.

  Injection Timing

The activation timing of HPI and LPI are dependent the system logic setting. For the PTS scenario, low RCS pressure usually is the factor to activate HPI and LPI. The pressure settings for activating HPI and LPI are considered as having small uncertainty. Activation timing of the CFT or accumulator is dependent on whether the CFT or accumulator pressure becomes greater than RCS pressure. The CFT or accumulator pressure could vary. A ±50 psi uncertainty is applied to model CFT activation timing.

- **RCS coolant flow rate**
  - RCPs states: The RCPs states have been discussed in the Heat Source category section.

  - RCS flow resistance
    For the analyzed event category, RCPs are expected to be tripped due to loss of RCS subcooling. The RCS coolant flow mode becomes natural circulation or even flow stagnation. Flow resistance between liquid and steam could affect the coolant flow rate. A 100% increase of flow resistance is applied to assess the impact of flow resistance.

- **RPV energy distribution**
  - RVVVs' states
    As discussed in Section 5, RVVVs could cause mixing of hot core water/steam in the downcomer to increase downcomer fluid temperature. There is uncertainty in RELAP5 modeling of the RVVVs states. Uncertainty ranging from fully closed to fully open is used in this study.
  - Flow interruption-and-resumption and Boiling-condensation
    These two phenomena occur at very specific boundary conditions, and the phenomena last only for a short period of time during real transients. Their impact on PTS risk is considered as small.

6.2 Finite Discrete Uncertainty Representation

The discrete Probabilistic Distribution (DPD) method is used in this study to represent a continuous distributed parameter's value by some representative values. Each value has an attached probability. The representative values usually include the lower bound value, nominal value, and upper bound value. The selection of representative values of the parameters has been discussed in Section 6.1. Table 6.1 lists the representative values and probabilities of these parameters.

6.3 Sensitivity Indicator

A parameter's sensitivity in PTS risk analysis is measured by the differences of the sensitivity indicators of the nominal scenario and of the scenarios with the parameter's value at its upper and lower bounds. The sensitivity indicator also is used as an indication to select the TH uncertainty representative scenarios. Based on the events classified in the PTS event classification matrix (see Section 4), the sensitivity indicator represents only T_{dc} impact on PTS risk. T_{dc} ramp and the lowest T_{dc} with associated timing are the key factors affecting PFM results. The averaged downcomer temperature

of the first 10,000 seconds of a scenario is selected as the sensitivity indicator (T_{sen}). The sensitivity indicator is meaningful only by comparing the difference between two scenarios' sensitivity indicators to represent the sensitivity in the differences of the two scenarios.

Table 6.1 The representative values and corresponding probabilities of the key parameters for TH uncertainty analysis of the Oconee NPP.

	Factors	Value 1 (lower Bound) Probability	Value 2 (Nominal) Probability	Value 3 (Upper Bound) Probability
Parametric (Boundary Condition) Uncertainty	Break Size	N number of representative break sizes	--	--
		Proportional to represented percentage of break area	--	--
	Break Location	Cold Leg 0.5	Hot Leg 0.5	-- --
	*Decay Heat	Nominal 0.98	0.7% 0.01	0.2% 0.01
	**Season	Winter 0.25	Spring/Fall 0.5	Summer 0.25
	High Pressure Injection System Flow Rate	90% 0.1	Nominal 0.8	110% 0.1
	Core Flood Tanks Pressure	50 psi less 0.1	Nominal 0.8	50 psi more 0.1
	Sump recirculation	If break size > ~4" 1.0	If break size < ~4" 0.0	
RELAP5 Code Model Uncertainty	Reactor Vessel Vent Valves State	Fully close 0.25	Nominal 0.5	Fully open 0.25
	Component Heat Transfer Rate	70% of nominal value 0.1	Nominal 0.8	130% of nominal value 0.1
	Flow Resistance	200% of nominal value 0.1	Nominal 0.9	-- --
	Break (choked) Flow Rate (by Changing Break Area)	70% of nominal value 0.25	Nominal (100%) 0.5	130% of nominal value 0.25
	Flow driven by numerical flaw	High cold legs reverse flow resistance 1.0	-- --	-- --

*Applied only on LOCA. PRA method treats HZP explicitly in the initiating events of reactor trip with PZR SRV stuck open.
**In winter, t(HPI) = 4.4 °C (40 °F), t(CFT) = 21.1 °C (70 °F), and t(LPI) = 4.4 °C(40 °F) for Oconee-1
**in summer, t(HPI)= 29.4 °C (85 °F), t(CFT) = 37.8 °C (100 °F), and t(LPI) = 29.4 °C (85 °F) for Oconee-1
**in spring and fall, t(HPI) = 21.1 °C (70 °F), t(CFT) = 26.7 °C (80 °F), and t(LPI) = 21.1 °C (70 °F) for Oconee-1

The nominal range sensitivity analysis (NRSA) method [Cullen and Frey 1999; Frey and Patil 2002] is used to assess parameters' sensitivities. In the NRSA method, the variation of each parameter is represented by finite values. The parameter process starts by calculating the base result with all parameters at their nominal values (the most likely values). Then it calculates the result again by changing one-and-only-one parameter's value while the other parameters remain at their nominal values. The difference between the new result and the base result is the sensitivity of the parameter varying from its nominal value to the specified value. This process continues until the sensitivities of all the representative values of all the parameters have been assessed. Such a change of one factor at a time is also called a 1-FAT (one-factor-at-a-time) method, except the NRSA requires all the other parameters to remain at their nominal values, while one parameter changes its value from its nominal. For a complete analysis, the total number of

sensitivity assessments is "N+N–1", which is an abbreviation of "$N_1 + \sum_2^M (N_i - 1)$".

Where M is the total number of parameters, and N_i is the number of representative values of the *i*-th parameter. For example, for four parameters (the M) with three representative values each (the lower bound, nominal, and upper bound; the N_i), the number of sensitivity assessments is 9 (3 + 2 + 2+ 2).

Using the NRSA method to assess parameters' sensitivities is concluded in the following steps. First, for a given initiating event, all key parameters are at their nominal values as the initial condition. Perform RELAP5 calculation based on the initial condition to obtain the T_{sen} of the scenario. The T_{sen} is used as a reference indicator ($T_{sen, ref}$). Second, using the same initial condition, except changing the interested parameter's value from its nominal value to its upper bound value, run another RELAP5 calculation to obtain another T_{sen} ($T_{sen, upper}$). The difference between $T_{sen, upper}$ and $T_{sen, ref}$ is the sensitivity of changing the parameter's value from its nominal value to its upper bound value. Third, repeat the second step, expect change the parameter's value from its upper bound to its lower bound. The difference between $T_{sen, lower}$ and $T_{sen, ref}$ is the sensitivity of changing the parameter's value from its nominal value to its lower bound value. Finally, repeat the second and third steps for all parameters.

All the parameters' sensitivities are strongly dependent on the break size, as it has been known that T_{dc} has less uncertainty for large LOCA than small LOCA. Thus, there should be more than one $T_{sen, ref}$ to represent the "nominal" T_{sen}s at different break sizes. As a result there are more than one set of $T_{sen, upper}$ and $T_{sen, lower}$ to represent a parameter's sensitivities at different break sizes. Table 6.2 shows the T_{sen} of the key parameters of the Oconee-1 plant. Although sump recirculation would significantly affect T_{sen}, sump recirculation has little impact on PTS risk, so the sensitivity results shown in Table 6.2 have sump recirculation disabled. Not all data shown in Table 6.2 is calculated. The uncalculated data can be estimated by interpolation or extrapolation, or based on TH judgment.

6.4 Uncertainty Assessment and Identification of Representative Scenarios

Since the RPV water level does not fall below the bottom of the cold leg, the downcomer is always full of water. The heat capacity in the downcomer is roughly constant. All parameters affecting T_{dc} can be seen as inducing heat sources or heat sinks into the downcomer. Their combined effect on T_{dc} can be interpreted as the net energy change impact on T_{dc}. The combined impact of multiple factors on T_{dc} would be close to adding all parameters' individual effects together. As shown in Equation 6.2, the effect of changing a parameter's value from its nominal value to another can be calculated by the difference of T_{sen} in these two scenarios. Multiple parameters' combined effects are calculated by Equation 6.3. For example, changing the RCS injection temperature from spring/fall (nominal) temperature to winter temperature makes an X degree difference in T_{sen}. Changing the decay heat curve from reactor tripping at full power operation (nominal) to low decay heat makes a Y degree difference in T_{sen}. Combining winter

temperature and low decay heat effects, the equation expects an X + Y degree difference in T_{sen}.

Table 6.2 The key parameters' sensitivities assessing matrix of the primary system breach events of Oconee-1. The default break location is the surge line except for the parameter indicated as Cold Leg LOCA. The temperature is the T_{sen} in Kelvin.

	Break Size (inch-diameter) [m^2] / Parameters' Values	1.5" [1E-3]	2" [0.002]	2.8" [4E-3]	4" [8E-3]	5.7" [1.6E-2]	8" [3.2E-2]
	Nominal	414	394	388	363	329	317
Season	Winter*	402	--	374	--	314	314
	Summer*	--	--	395	--	336	317
CPF	P(CFT) += 50 psi	--	--	386	--	--	--
	P(CFT) -= 50 psi	--	--	389	--	--	--
HPI State and Flow Rate	110% m(HPI) RCPOFF	401	--	380	--	--	--
	90% m(HPI)	416	--	402	--	--	--
	HPI Failed and Recovered (@~7000 sec)	--	--	491	--	--	317
	HPI Failed and Recovered (@~1000 sec)	--	--	400	--	--	--
	HPI Failed and Recovered (@~2000 sec)	--	--	416	--	--	--
	100 % HPI Failed	--	--	500	403	328	319
	25% HPI Failed	446	453	442	--	--	--
	50% HPI Failed	514	511	467	--	--	--
Decay Heat	HZP	398	--	349	--	321	312
Vent Valve State	Vent Valve Close	--	--	362	345	--	--
	Vent Valve 2/6 Open	--	--	406	--	--	--
	Vent Valve 4/6 Open	--	--	410	--	--	--
	Vent Valve 6/6 Open	--	--	413	371	--	--
Numerical Mixing	High CL Reverse Flow Resistance	400	372	370	356	--	311
Component Heat Transfer Coefficient	130% Components Heat Transfer Coefficient	--	400	396	--	331	--
	70% Components Heat Transfer Coefficient	--	387	380	--	324	--
Flow Resistance	200% Loop Flow Resistance	--	395	--	--	--	--
	200% Bypass Flow Area	--	396	--	--	--	--
	Zero Bypass Flow Area	--	375	--	--	--	--
Heat Structure	No heat structure	--	369	--	--	--	--
Break Location	Cold Leg LOCA	--	455	412	376	345	317

*In winter, t(HPI) = 4.4 °C (40 °F), t(CFT) = 21.1 °C (70 °F), and t(LPI) = 4.4 °C(40 °F) for Oconee-1 plant
in summer, t(HPI)= 29.4 °C (85 °F), t(CFT) = 37.8 °C (100 °F), and t(LPI) = 29.4 °C (85 °F) for Oconee-1 plant
in spring and fall, t(HPI) = 21.1 °C (70 °F), t(CFT) = 26.7 °C (80 °F), and t(LPI) = 21.1 °C (70 °F) for Oconee-1 plant

The probability of a combination is the probability product of each parameter's value applied (Equation 6.4). For the above example, the probability of the event occurring during winter is α, and the probability of the event occurring during low decay heat operation is β. The probability of the combination is $\alpha\beta$.

$$\Delta T_{sen(i,j)} = T_{sen,(i,j)} - T_{sen,ref} \quad \textbf{(Equation 6.1)}$$

where

$T_{sen,(I,J)}$: T_{sen} of changing parameter-i's value from its nominal value to j-th representative value.

$T_{sen,ref}$: T_{sen} of the nominal scenario

$\Delta T_{sen,(i,j)}$ = the sensitivity of parameter-I changing its value from nominal to the j-th representative value

$$\Delta T = \sum_{i=1}^{M} \Delta T_{sen,(i,j)} \quad \textbf{(Equation 6.2)}$$

where
ΔT = the combined sensitivity of multiple parameters. M is the total number of key parameters
$\Delta T_{sen,(i,ji}$ = the individual parameter's sensitivity at its j-th representative value. The value j is a random number.

$$Prob[\Delta T] = \prod_{i=1}^{M} Prob(T_{sen,(i,j)}) \quad \textbf{(Equation 6.3)}$$

Where
Prob[ΔT]: the probability of the combined scenario
M: the total number of key parameters
Prob[$T_{sen,(I,j)}$]: the probability of the i-th parameter at its j-th representative value

Apply Equations 6.2 to 6.4 to assess all combinations' sensitivities and probabilities. Each combination has a T_{sen} and a probability. The data can be plotted in a probabilistic density function (PDF) versus T_{sen} diagram. The diagram can be transferred to a cumulative density function (CDF) versus T_{sen} diagram. The representative scenarios are identified from the CDF diagram. The PDF and CDF diagrams are shown in the left hand side and right hand side of Figure 6.1. To identify the representative scenarios, first, decide the number of scenarios for uncertainty representation based on T_{sen} range. Cut the two 5% tails off and evenly divide the remaining 90% space into equivalent areas according to the specified number of representations. The T_{sen} of a representative scenario can be identified by the T_{sen} reflected by using the mean percentile of a divided region through the CDF curve as seen in the CDF diagram of Figure 6.1. The corresponding combination of the identified T_{sen}s could be found from all combinations displayed in the PDF diagram of Figure 6.1.

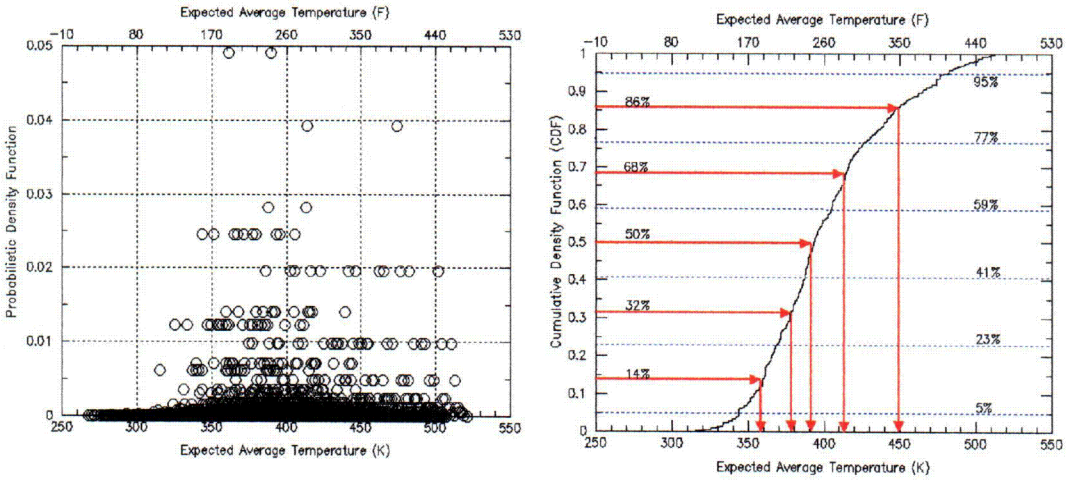

Figure 6.1 the probabilistic density diagram and cumulative density diagram for identifying the uncertainty representative scenarios. The "expected average temperature" is the sensitivity indicator (T_{sen}).

The probability of each representative scenario would be 90% divided by the number of representative scenarios. Since the two 5% tails are cut off from the selection the upper bound and lower bound representative scenarios each share an additional 5% of probability. At this point, the representative scenarios are identified and their proportional probabilities are calculated. RELAP5 calculations are performed to calculate the time histories of T_{dc}, P_{dc}, and h_{dc} of these scenarios. The PRA group distributes appropriate event frequencies to each representative scenario. The TH and PRA data are inputs for PFM calculation.

A 2.8-inch surge line LOCA scenario is selected to validate the linear additive assumption. The validation method uses the T_{sen} ($T_{sen, ref}$) of the nominal scenario (2.8-inch LOCA) as a reference point to select five different combinations whose T_{sen}s are expected to be about ($T_{sen, ref}$ – 100 °F), ($T_{sen, ref}$ – 50 °F), ($T_{sen, ref}$), ($T_{sen, ref}$ + 50 °F), and ($T_{sen, ref}$ + 100 °F). Thus, a 200 °F (111 °K) range is covered. Each T_{sen} representative combination can be identified based on the T_{sen}s assessed for all combinations using the linear additive method. Based on these identified combinations, RELAP5 calculations are performed to obtain the T_{sen}s. Table 6.3 shows the five combinations and the comparison of the T_{sen}s based on the linear additive assumption and resulting from RELAP5 calculations. The plots are shown in Figure 6.2. The 45 degree line in Figure 6.2 represents the perfect scenarios in which the expected values are same as the RELAP5 calculated values. The solid dots represent the realities. The differences between the solid dots and the squares on the 45 degree line are the deviations of the assumption from reality. Figure 6.2 shows that the linear additive assumption is applicable.

C23

Table 6.3 The list of RELAP5 runs for validating the assumption of linear sensitivity addition for multiple parameters interaction for a 2.8-inch in diameter surge line LOCA.

No.	Parameters' values description (expect the parameters using their nominal values)	Expected T_{scn} (°K)	RELAP5 Calculated T_{scn} (°K)	$T_{scn,\,cal} - T_{scn,\,exp}$ (°K)
1	Winter; p(CFT) + 50 psi; 70% A_{brk}; RVVVs Close; 70% HTC	331.7	345.3	13.6
2	Summer; RVVVs Close; 200% flow resistance	360.0	362.3	2.7
3	p(CFT) + 50 psi; 110% m(HPI); 70% A_{brk}; 130% HTC	387.6	391.4	3.8
4	Summer; p(CFT) + 50 psi ; 90% m(HPI); 130% Abrk ; RVVVs fully Open; 200% flow resistance	415.5	406.9	-8.6
5	Summer; 90% m(HPI); 70% A_{brk}; RVVVs fully Open; 130% HTC	438.2	448.8	10.7

The RELAP5 calculated average first 10,000 seconds T_{dc} of a nominal 2.8-inch surge line LOCA is 388 °K

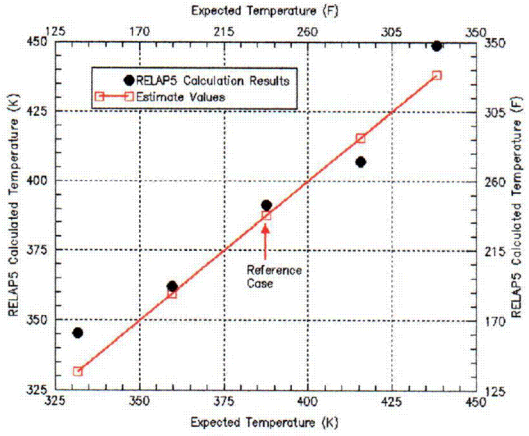

Figure 6.2 Comparing T_{sen}s calculated based on linear additive assumption and based on RELAP5 calculation for a 2.8-inch in diameter surge line LOCA.

6.5 Parameters Ranking

The sensitivity assessment results shown in Table 6.2 can be used as a basis for assessing parameter importance for the designated event category. It is important to note that the parameters only reflect the impact of T_{dc}. The P_{dc} impact by HPI throttling timing in RCS repressurization scenarios is not included.

Figures 6.3 to 6.5 show the key parameters ranking at break sizes of 2.8, 5.7, and 8 inches in diameter (4E-3, 1.6E-2, and 3.2E-2 m^2, respectively). For greater than 8 inches LOCA, the PTS consequence is not sensitive to uncertainty of any parameters. The higher ΔT_{sen} indicates that the effect is good for PTS (less thermal stress). For example, failure of HPI at a 2.8-inch LOCA (4E-3 m^2) increases T_{sen} more than 100 °K, which is expected to reduce thermal stress dramatically. Three observations are made from the figures. First, parameters' sensitivities decreased when break size increased. It is as expected. For example, Figure 6.3 shows that failing of HPI could increase T_{sen} more than 100 °C when the primary system breach size is 4E-3m^2 (2.8 inches in diameter), however, failing of HPI has little impact when break size is greater than 1.6E-2 m^2 (Figures 6.5, and 6.6). Another example is that the LOCA occurring at HZP operation could cause a decrease in T_{sen} of about 40 °C, in comparison with the LOCA occurring at

C24

full power operation, when the break size is 2.8 inches (4E-3 m^2); however, HZP becomes insignificant when the break size is greater than 5.7 inches (1.6E-2 m^2). These observations show that the sensitivity is strongly dependent on the break size. Second, the parameter importance rank varies at different break sizes. The relative importance of two parameters could be different at different break sizes. Third, some parameters changed their PTS impact vector direction when the break sizes changed. The third observation is related to the parameters' dependencies. For example, at small LOCA scenarios the RCS remains at high pressure preventing CFTs and LPI from activating when HPI fails on demand, as a result, T_{sen} is higher than for the nominal scenario. However, at a certain range of break size, HPI failed-on-demand would induce faster CPFs and LPI activation, as a result, T_{sen} is lower than for the nominal scenario.

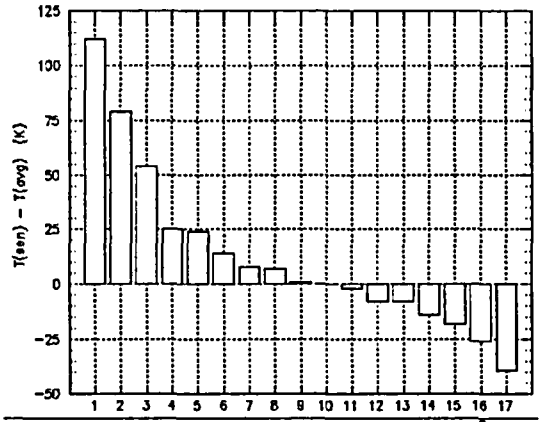

Figure 6.3 The parameter ranking at a 4E-3 m^2 (2.8 inches in diameter) LOCA (default break location is surge line)

1	100% HPI fail
2	50% HPI fail
3	25% HPI fail
4	RVVVs Open
5	CL LOCA
6	90% m(HPI)
7	130% CHTC
8	Summer
9	P(CFT) -= 50 psi
10	Nominal
11	P(CFT) += 50 psi
12	110% m(HPI)
13	70% CHTC
14	Winter
15	High CL rev. K
16	RVVV Close
17	HZP

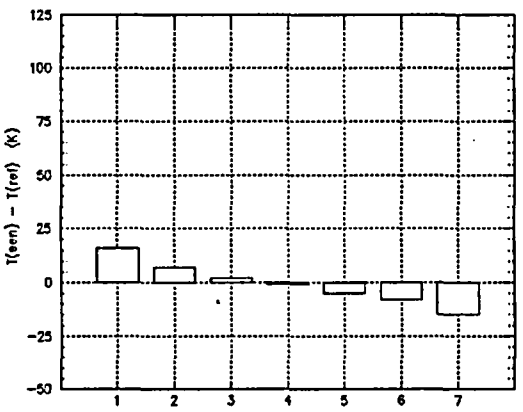

Figure 6.4 The parameter ranking for a 1.6E-2 m^2 (5.7 inches in diameter) LOCA(default break location is surge line).

1	CL LOCA
2	Summer
3	130% CHTC
4	100% HPI fail
5	70% CHTC
6	HZP
7	Winter

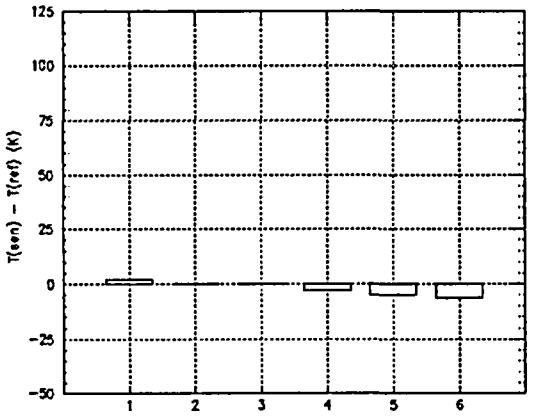

1	HPI fail
2	Summer
3	CL LOCA
4	Winter
5	HZP
6	High CL rev. K

Figure 6.5 The parameter ranking for a 3.2E-2 m^2 (8 inches in diameter) LOCA(default break location is surge line). Assume no component or system failure, and no operators' action for the reference

7 Results of Thermal Hydraulic Uncertainty Assessment

The TH analysis results for Oconee-1, Beaver Valley, and Palisades are discussed in this section. For all three plants, uncertainty analyses are performed for the event category of RCS loss of subcooling due to primary system breach with nominal secondary system state. This event category includes LOCA scenarios and PZR valves stuck open scenarios. The event category is subdivided into five subcategories. The uncertainty of each subcategory is assessed separately. A few representative scenarios are identified for each subcategory. The five subcategories are:

- LOCA with break size between ~1E-3 m^2 and 8E-3 m^2 (~1.5 and 4 inches in diameter)
- LOCA with break size between 8E-3 m^2 and 3.2E-2 m^2 (4 and 8 inches in diameter)
- LOCA with break size larger than 3.2E-2 m^2 (8 inches in diameter)
- PZR SRVs stuck open and remaining open accident with total valves open area greater than ~1E-3 m^2 (~1.5 inches in diameter)
- PZR SRVs stuck open and reseated accident with total valves open area greater than ~1E-3 m^2 (~1.5 inches in diameter)

The minimum break size and PZR valve open area that induce breach flow greater than HPI flow, causing RCS loss of subcooling are similar for all plants with small variation. For convenience, the representative values of key parameters and their probabilities is shown in Table 7.1.

Table 7.1 The representative values and corresponding probabilities of the key parameters for TH uncertainty analysis of the Oconee NPP.

	Factors	Value 1 (lower Bound) Probability	Value 2 (Nominal) Probability	Value 3 (Upper Bound) Probability
Parametric (Boundary Condition) Uncertainty	Break Size	N number of representative break sizes	--	--
		Proportional to represented percentage of break area	--	--
	Break Location	Cold Leg 0.5	Hot Leg 0.5	-- --
	*Decay Heat	Nominal 0.98	0.7% 0.01	0.2% 0.01
	Season	Winter 0.25	Spring/Fall 0.5	Summer 0.25
	High Pressure Injection System Flow Rate	90% 0.1	Nominal 0.8	110% 0.1
	Core Flood Tanks Pressure	50 psi less 0.1	Nominal 0.8	50 psi more 0.1
	Sump recirculation	If break size > ~4" 1.0	If break size < ~4" 0.0	
RELAP5 Code Model Uncertainty	Reactor Vessel Vent Valves State	Fully close 0.25	Nominal 0.5	Fully open 0.25
	Component Heat Transfer Rate	70% of nominal value 0.1	Nominal 0.8	130% of nominal value 0.1
	Flow Resistance	200% of nominal value 0.1	Nominal 0.9	-- --
	Break (choked) Flow Rate (by Changing Break Area)	70% of nominal value 0.25	Nominal (100%) 0.5	130% of nominal value 0.25

	Flow driven by numerical flaw	High cold legs reverse flow resistance	--	--
		1.0	--	--

*For Oconee, only one low decay heat curve is used.

7.1 Oconee-1 TH Uncertainty Representative Scenarios

Table 7.2 shows the sensitivity data calculated byRELAP5. The data are used for uncertainty assessment of all event categories for the Oconee-1 plant. The data not listed could be estimated by interpolation, extrapolation, or judgment based on TH behavior.

Table 7.2 The key parameters sensitivities assessing matrix of the primary system breach events of Oconee-1. The default break location is surge line except for the parameter indicated as Cold Leg LOCA. The temperature is the T_{sca} in Kelvin.

	Break Size (inch-diameter) [m^2] / Parameters' Values	1.5" [1E-3]	2" [0.002]	2.8" [4E-3]	4" [8E-3]	5.7" [1.6E-2]	8" [3.2E-2]
	Nominal	414	394	388	363	329	317
Season	Winter*	402	--	374	--	314	314
	Summer*	--	--	395	--	336	317
CPF	P(CFT) += 50 psi	--	--	386	--	--	--
	P(CFT) -= 50 psi	--	--	389	--	--	--
HPI State and Flow Rate	110% m(HPI) RCPOFF	401	--	380	--	--	--
	90% m(HPI)	416	--	402	--	--	--
	HPI Failed and Recovered (@~7000 sec)	--	--	491	--	--	317
	HPI Failed and Recovered (@~1000 sec)	--	--	400	--	--	--
	HPI Failed and Recovered (@~2000 sec)	--	--	416	--	--	--
	100 % HPI Failed	--	--	500	403	328	319
	25% HPI Failed	446	453	442	--	--	--
	50% HPI Failed	514	511	467	--	--	--
Decay Heat	HZP	398	--	349	--	321	312
Vent Valve State	Vent Valve Close	--	--	362	345	--	--
	Vent Valve 2/6 Open	--	--	406	--	--	--
	Vent Valve 4/6 Open	--	--	410	--	--	--
	Vent Valve 6/6 Open	--	--	413	371	--	--
Numerical Mixing	High CL Reverse Flow Resistance	400	372	370	356	--	311
Component Heat Transfer Coefficient	130% Components Heat Transfer Coefficient	--	400	396	--	331	--
	70% Components Heat Transfer Coefficient	--	387	380	--	324	--
Flow Resistance	200% Loop Flow Resistance	--	395	--	--	--	--
	200% Bypass Flow Area	--	396	--	--	--	--
	Zero Bypass Flow Area	--	375	--	--	--	--
Heat Structure	No heat structure	--	369	--	--	--	--
Break Location	Cold Leg LOCA	--	455	412	376	345	317

*In winter, t(HPI) = 4.4 °C (40 °F), t(CFT) = 21.1 °C (70 °F), and t(LPI) = 4.4 °C(40 °F) for Oconee-1 plant
in summer, t(HPI)= 29.4 °C (85 °F), t(CFT) = 37.8 °C (100 °F), and t(LPI) = 29.4 °C (85 °F) for Oconee-1 plant
in spring and fall, t(HPI) = 21.1 °C (70 °F), t(CFT) = 26.7 °C (80 °F), and t(LPI) = 21.1 °C (70 °F) for Oconee-1 plant

1.5 – 4 inches (1E-3 m^2 - 8E-3 m^2) LOCA

Three representative break sizes are selected for this event category: 1.5, 2.8, and 4 inches in diameter (1E-3, 4E-3, and 8E-3 m^2, respectively). Each of them shares 1/3 of

the probability. HPI failure is not considered since the low HPI failure probability combined with the low initiating event probability would make such events have a frequency below the screen criteria. Table 7.3 lists the parameters included for each break size. Some parameters have insignificant sensitivity at certain break sizes and are not included in the analysis.

The numbers in parentheses in the first column in Table 7.3 are the number of representative values of the parameter, whose values are shown in Table 7.1. For example, the break location has two variations: breaking at hot leg and breaking at cold leg. For 1E-3m^2 LOCA, there are 972 combinations since it contains two parameters with two variations and five parameters with three variations (i.e. $2^2 \times 3^5 = 972$). The 4E-3m^2 LOCA has 5832 combinations ($2^3 \times 3^6$), and the 8E-3m^2 LOCA has 324 combinations ($2^2 \times 3^4$). There are 7128 combinations (972 + 5832 + 324) in total. The event descriptions, probabilities, and expected T_{sen} of the 7128 scenarios are calculated based on the linear additive method. Figures 6.1 and 6.2 are the PDF and CDF plots of the 7128 combinations. The probabilities are calculated based on the individual parameter's probability indicated in Table 7.1.

Table 7.3 The influential parameters of LOCA between 1E-3 m^2 and 8E-3m^2. The numbers in the parentheses are the number of the representative values of the parameter

Key Parameters	Break Size(3)		
	1E-3m^2 (1.5")	4E-3m^2 (2.8")	8E-3m^2 (4")
Break Location (2)	√	√	√
Decay Heat (2)	√	√	√
Season (3)	√	√	√
HPI Flow Rate (3)	√	√	insignificant
CFTs pressure (3)	Insignificant	√	Insignificant
RVVVs state (3)	√	√	√
Component Heat Transfer Rate (3)	√	√	√
Flow Resistance (2)	Insignificant	√	Insignificant
Break Flow Rate (3)	√	√	√

Five TH uncertainty representative scenarios are selected for this category. The probabilities of these five representative scenarios are calculated based on the following process. First, since the T_{sen} of the two tails could have a large deviation from the linearly additive rules, the two tails, smaller than the 5th percentile and larger the 95th percentile, are cutoff from the representative scenarios selection process. Their probabilities are later added to the most similar representative scenarios after these representatives are identified. The remaining 90 percent of the distribution, between the 5th and 95th percentiles, is evenly divided into 5 regions. For each of the five regions, the mean percentile is selected, giving the five representatives. These five scenarios are the 14th, 32nd, 50th, 68th, and 86th percentiles of the distribution as shown in Figure 7.2. Each representative has a probability of .18 which is .9 divided by 5. The 14th and the 86th percentiles' representatives are the most likely scenarios for the two cutoff tails. Each of them is added an additional 5 percent probability to cover the tails probability. The corresponding probabilities of the 14th, 32nd, 50th, 68th, and 86th representatives are .23, .18, .18, .18, and .23.

The T_{sen} of the five representatives could be found by projecting the 5 representatives from percentile to temperature as shown in Figure 7.3 (from the horizontal arrows to vertical arrows). The expected T_{sen} difference of the two edge representatives (14^{th} and 86^{th} percentiles) is about 80 °C. Comparing this with the 111 °C variation in the linearity verification (Figure 6.2), it is expected that the assumption of the proportional additive would have reasonable accuracy.

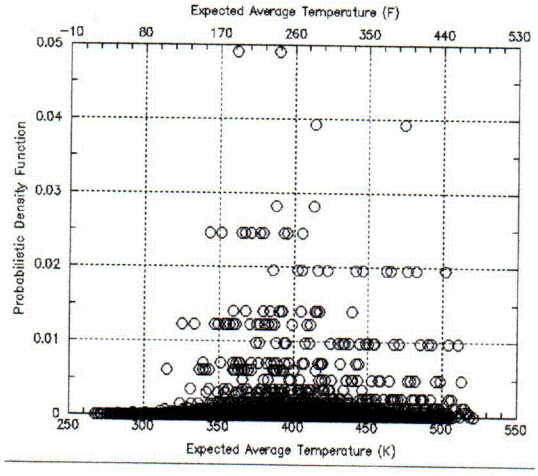

Figure 7.1 the probability distribution of the T_{sen} of LOCA between 1E-3 m^2 and 8E-3 m^2 (1.5 and 4 inches in diameter). There are 7128 combinations in total.

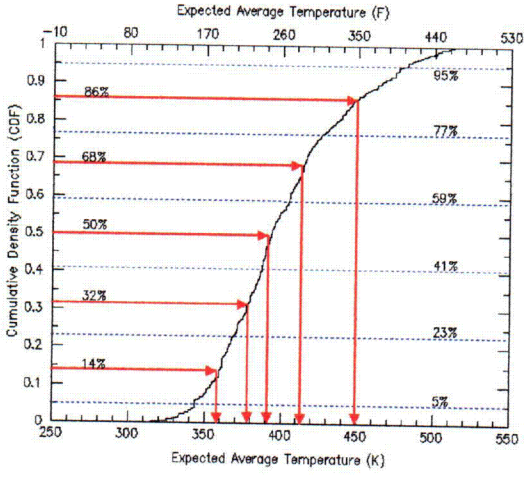

Figure 7.2 The cumulative density function and the identification of the uncertainty representative scenarios of LOCA between 1E-3 m^2 and 8E-3 m^2 (1.5 and 4 inches in diameter).

Based on the identified five T_{sen}, the five representative scenarios could be identified from the 7128 combinations. Table 7.4 lists the five representative scenarios and their

C25

probabilities. Figures 7.3 and 7.4 are the time histories of T_{dc} and P_{dc} of the five representative scenarios calculated by RELAP5

Table 7.4 The boundary conditions of the five uncertainty representative scenarios of LOCA between 1E-3 m^2 and 8E-3 m^2 (1.5 and 4 inches in diameter). All of the five representatives have high cold leg reverse flow resistance applied.

#	TH Bin #	Probability	Scenario Specification Descriptions
1	145	0.23	1E-3 m^2 cold leg LOCA with increased 30% break area Winter*
2	142	0.18	4E-3m^2 surge line with 30% reduced break area
3	141	0.18	4E-3m^2 surge line with 30% increased break area
4	172	0.18	8E-3m^2 cold leg LOCA
5	154	0.23	8E-3m^2 surge line LOCA with 30% reduced break area RPV Vent Valves Closed

*In winter, t(HPI) = 4.4 °C (40 °F), t(CFT) = 21.1 °C (70 °F), and t(LPI) = 4.4 °C(40 °F);
in summer, t(HPI)= 29.4 °C (85 °F), t(CFT) = 37.8 °C (100 °F), and t(LPI) = 29.4 °C (85 °F);
in spring and fall, the nominal season, t(HPI) = 21.1 °C (70 °F), t(CFT) = 26.7 °C (80 °F), and t(LPI) = 21.1 °C (70 °F)

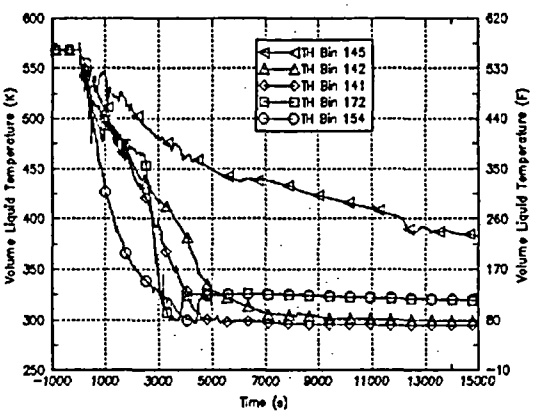

Figure 7.3 The five T_{dc} traces of the TH uncertainty representatives of LOCA between 1E-3 m^2 and 8E-3 m^2 (1.5 and 4 inches in diameter)

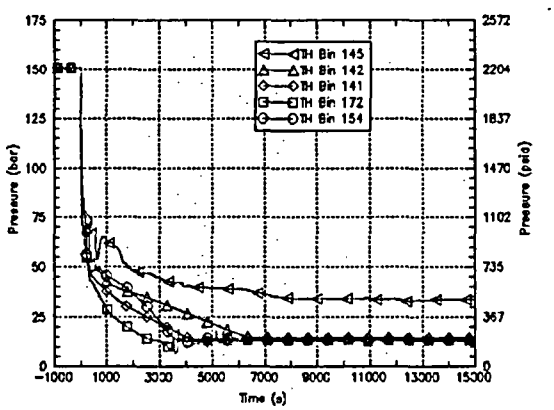

Figure 7.4 The five T_{dc} traces of the TH uncertainty representatives of LOCA between 1E-3 m^2 and 8E-3 m^2 (1.5 and 4 inches in diameter)

4 – 8 Inches (8E-3 m^2 - 3.2E-2 m^2) LOCA

Three representative break sizes are selected in this category: 8E-3 m^2, 1.6E-2 m^2, and 3.2E-2 m^2 (4, 5.7, and 8 inches in diameter, respectively). For the three representative break sizes, three factors' effects might not be negligible for some break sizes. These factors are: break location, season, and low decay heat. Table 7.5 shows the parameters included in the TH uncertainty assessment at different break sizes. The total sample size is 336 ($2^2 \times 3^5 + 2 \times 3 + 2 \times 3$). The PDF and CDF diagrams are shown in Figures 7.5 and 7.6. Three representative scenarios are selected (Figure 7.6). These three scenarios happen to be the nominal scenarios of 8E-3 m^2, 1.6E-2 m^2, and 3.2E-2 m^2 (4, 5.7, and 8 inches in diameter, respectively) hot leg LOCAs. Their probabilities are 0.35, 0.3, and 0.35, respectively. The scenario descriptions of these three representative scenarios and their corresponding TH bins are shown in Table 7.6. Their T_{dc} and P_{dc} plots are shown in Figures 7.7 and 7.8, respectively.

Table 7.5 The influential parameters of LOCA between 8E-3 m^2 and 3.2E-2m^2. The numbers in the parentheses are the number of the representative values of the parameter.

Key Parameters	Break Sizes		
	8E-3m^2 (4 inches)	1.6E-2m^2 (5.7 inches)	3.2E-2m^2 (8 inches)
Break Location (2)	√	√	√
Decay Heat (2)	√	insignificant	Insignificant
Season (3)	√	√	√
HPI Flow Rate (3)	Insignificant	Insignificant	insignificant
RVVVs state (3)	√	insignificant	Insignificant
Component Heat Transfer Rate (3)	√	Insignificant	Insignificant
Flow Resistance (2)	insignificant	insignificant	Insignificant
CFTs pressure (3)	insignificant	insignificant	Insignificant
Break Flow Rate (3)	√	insignificant	insignificant

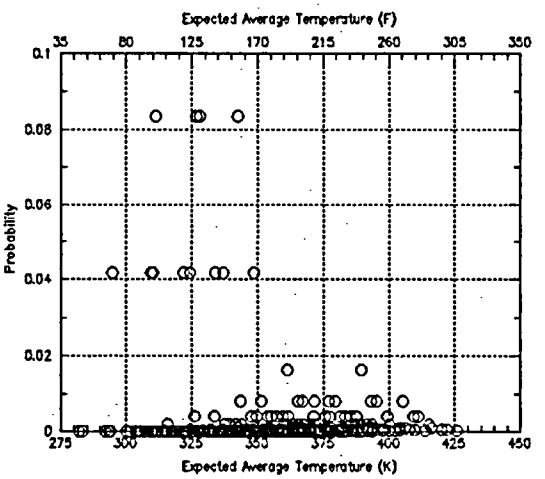

Figure 7.5 The probability distribution of the T_{sat} of LOCA between 8E-3 m^2 and 3.2E-2m^2 (4 and 8 inches in diameter, respectively). There are 336 combinations in total.

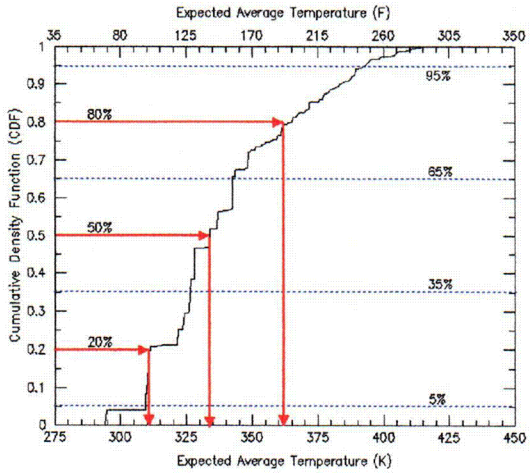

Figure 7.6 The cumulative distribution function and the identification of the three representative scenarios of LOCA between 8E-3 m^2 and 3.2E-2 m^2 (4 and 8 inches in diameter).

Table 7.6 The boundary conditions of the five uncertainty representative scenarios of LOCA between 8E-3 m^2 and 3.2E-2 m^2 (4 and 8 inches in diameter). All of the three representatives have high cold leg reverse flow resistance applied.

#	TH Bin #	Probability	Scenario Description
1	178	0.35	8E-3 m^2 (4 inches) surge line LOCA + Sump recirculation
2	160	0.3	1.6E-2 m^2 (5.7 inches) surge line LOCA + Sump recirculation
3	164	0.35	3.2E-2 m^2 (8 inches) surge line LOCA + Sump recirculation

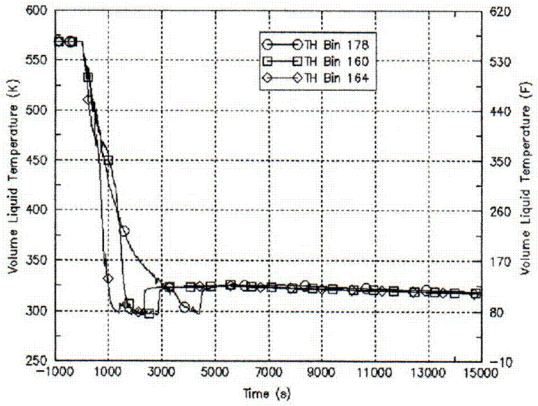

Figure 7.7 The three downcomer temperature traces of the TH uncertainty representatives of LOCA between 8E-3 m^2 and 3.2E-2 m^2 (4 and 8 inches in diameter)

C26

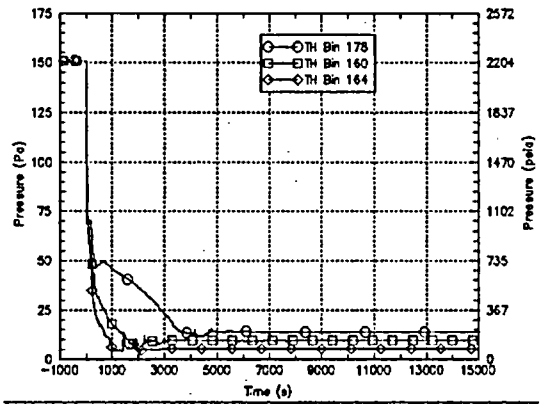

Figure 7.8 The three downcomer pressure traces of the TH uncertainty representatives of LOCA between 8E-3 m^2 and 3.2E-2 m^2 (4 and 8 inches in diameter)

Greater than 8 Inches (8E-3 m^2) LOCA

T_{dc} uncertainty is very limited for greater than 8E-3 m^2 LOCA. Only one representative scenario is selected in this category: 16 inches (0.13 m^2) LOCA (Table 7.7). The T_{dc} and P_{dc} time histories of this scenario are shown in Figure 7.9.

Table 7.7 The boundary conditions of the five uncertainty representative scenarios of LOCA with break size greater than 3.2E-2 m^2 (8 inches in diameter).

#	TH Bin #	Probability	Scenario Description
1	156	1.0	.13 m^2 (16 inches) surge line LOCA + Hi CL Rev. K + Sump recirculation

PZR SRV Stuck Open without Valve Reseating

This discussion is limited to the total PZR SRV stuck open area being greater than 8E-3 m^2 (1.5 inches in diameter), such that HPI can not make up break flow to maintain RCS pressure. There is one PORV (6.1E-4 m^2 or 1.1 inches in diameter) and two SRVs (1.8E-2 m^2 or 1.8 inches in diameter each) in PZR of the Oconee-1 NPP. The probability of two valves simultaneously stuck open events is too small to be considered, according to the PRA assessment. The PZR PORV's capacity is too small to be PTS concern. Thus, this category only analyzes one SRV stuck open with sufficient open area, greater than 1E-3 m^2 (1.5 inches in diameter), and the stuck open valve remaining open till the end of the scenario.

The process of identifying the uncertainty representative scenarios is similar to the process of identifying the LOCA representative scenarios. There are some unique influential factors in this category. First, the break location is specific. Unlike the LOCA being able to occur at hot leg and cold leg, the SRV stuck open location is only at the top of PZR. There is no variation for break location. Second, the SRV has different flow resistance in comparison with LOCA breaks, thus, even though they have the same break sizes, their flow rates are different. Third, the decay heat is explicitly modeled by PRA

event trees for the PZR SRV stuck open scenarios. There is no decay heat uncertainty considered in the analysis.

Two break areas representing the lower bound and upper bound are used: 8E-3 m^2 and 1.8E-2 m^2 (1.5 and 1.8 inches in diameter correspondingly). The parameters' sensitivities obtained through the LOCA scenarios (Table 7.2) can be used based on the equivalent LOCA sizes having the same amount of break flow as the two SRV open sizes. By interpolating and extrapolating data in Table 7.2, the data can be used for uncertainty assessment.

The key parameters are listed in Table 7.8. Three representative cases are selected from the 486 combinations, whose scenario descriptions are shown in Tables 7.9 and 7.10 for reactor trips during full power operation and low decay heat operations, respectively. Their time histories of T_{dc} and P_{dc} are shown in Figure 7.10 and 7.11, respectively.

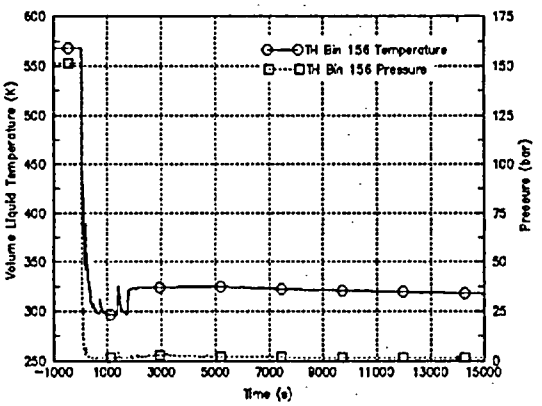

Figure 7.9 $T_{dc}(t)$ and $P_{dc}(t)$ of the .013 m^2 (16 inches in diameter) hot leg LOCA, which is the TH uncertainty representatives scenario of greater than 3.2E-2 m^2 (8 inches in diameter) LOCA

Table 7.8 The list of influential parameters of scenarios of PZR SRV stuck open without reseating. The numbers in the parentheses are the number of the representative values of the parameter.

	Break Sizes	
	8E-3 m^2 (1.5 inches)	1.8E-2 m^2 (1.8 inches)
Decay Heat (1)	Explicitly modeled by PRA Model	Explicitly modeled by PRA Model
Season (3)	√	√
HPI Flow Rate (3)	√	√
RVVVs state (3)	√	√
Component Heat Transfer Rate (3)	√	√
Flow Resistance (1)	Insignificant	Insignificant
CFTs pressure (1)	Insignificant	insignificant
Break Area (3)	√	√

Table 7.9 The TH uncertainty representative scenarios of reactor trips during full power operation causing PZR SRV stuck open and remaining open and their probabilities for the Oconee NPP

#	TH Bin #	Probability	Brief Scenario Description
1	148	0.35	SRV open area = 1.5" + Comp. HTC *= 130%, RCPs trip
2	147	0.3	Summer
3	146	0.35	SRV open area *= 70% + summer + VV Close

Table 7.10 The TH uncertainty representative scenarios of reactor trips during hot zero power operation causing PZR SRV stuck open and remaining open and their probabilities for the Oconee NPP

#	TH Bin #	Probability	Brief Scenario Description
1	171	0.35	SRV open area = 1.5" + Comp. HTC *= 130%, RCPs trip + low decay heat
2	170	0.3	Summer + low decay heat
3	169	0.35	SRV open area *= 70% + summer + VV Close + low decay heat

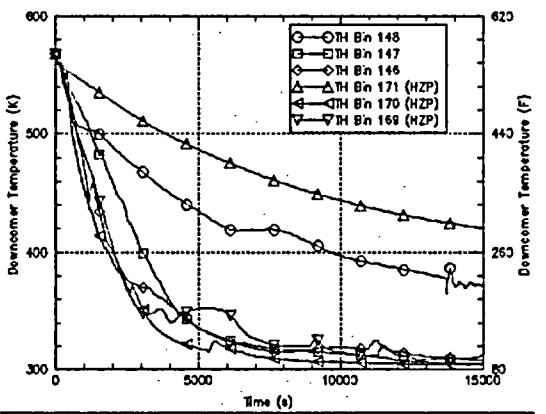

Figure 7.10 The downcomer temperature traces of the six representative scenarios of PZR SRV stuck open and remaining open.

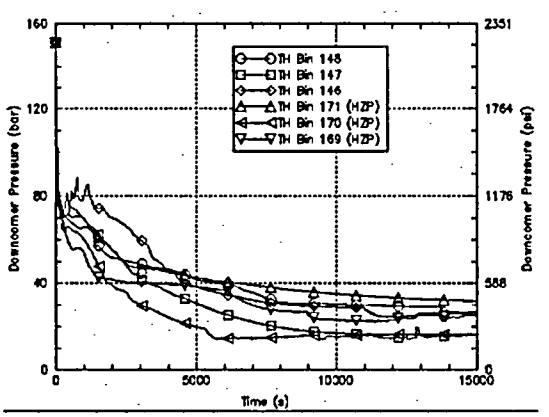

Figure 7.11 The downcomer pressure traces of the six representative scenarios of PZR SRV stuck open and remaining open.

PZR SRV Stuck Open and Self Reseated

Reseating a stuck open SRV has two important effects on the PTS context. First, it removes the dominant heat sink. It would significantly increase RCS temperature. Second, primary system breach is sealed, however the HPI has been activated. It requires an operator's action to throttle HPI to prevent RCS repressurization, which has a significant contribution to PTS risk. Unlike previous event categories analyzing only T_{dc} uncertainty, this event category needs to analyze both T_{dc} and P_{dc} uncertainties.

P_{dc} uncertainty is mainly dependent on the timing of operator throttling of HPI. The PRA group uses three HPI throttling timings: within 1 minute, within 10 minutes, and never throttled with respective probabilities of 97%, 2%, and 1%.

Beside the T_{dc} uncertainty analyzed in Section 7.1.4, the timing of PZR SRV being reseated is an additional factor contributing to T_{dc} uncertainty. In the PRA model the SRV reseat timing is represented by reseating at 50 minutes and at 100 minutes after SRV stuck open. The probability of each representative reseat timing is 0.5. Combining effects of reseat timing, represented by two values, and the other factors, represented by the three representative scenarios (20^{th}, 50^{th}, and 80^{th} percentiles in Section 7.1.4) there are six (2×3) combinations in total to represent the thermal stress uncertainty.

Since reseating RCS would change the course of T_{dc} dramatically, the T_{sen}s in Table 7.2 are not appropriate for the analysis. Instead the lowest T_{dc} is a more appropriate indication. Table 7.11 lists the six combinations and their differences in lowest T_{dc}s. It shows that the SRVs' reseated timing dominates T_{dc} uncertainty. In order to reduce the number of representative scenarios, two out of six are selected representing T_{dc} uncertainty: SRV reseated at 50^{th} and 100^{th} minutes with all the other factors at their nominal values.

The two selected T_{dc} uncertainty representative scenarios need to be combined with three P_{dc} uncertainty representative scenarios to form total uncertainty representative scenarios. Table 7.12 shows the six combinations and their probabilities. Since the PRA model separates full decay heat scenarios from low decay heat scenarios, there are six representative scenarios each for full decay heat and for low decay heat. Figures 7.12 and 7.13 show the T_{dc} and P_{dc} time histories of reactor tripped during full power operation. Figures 7.14 and 7.15 are the T_{dc} and P_{dc} time histories of reactor tripped with low decay heat.

Table 7.11 the six combinations for T_{dc} uncertainty representation of the SRV stuck open and reseated events.

#	ΔT_{min} (K)	Descriptions
1	-8	20^{th} percentile + SRV reseated at 100 minutes
2	0	50^{th} percentile + SRV reseated at 100 minutes
3	6	80^{th} percentile + SRV reseated at 100 minutes
4	76	20^{th} percentile + SRV reseated at 50 minutes
5	83	50^{th} percentile + SRV reseated at 50 minutes
6	90	80^{th} percentile + SRV reseated at 50 minutes

Table 7.12 The TH uncertainty representative scenarios and their probabilities of the reactor trips during full power operation causing PZR SRV stuck open and reseated later by itself of the Oconee-1 NPP

#	TH Bin #	Probability	Brief Scenario Description
1	112	0.485	SRV reseated @ 100 min; HPI throttle at 1 minute after it can be throttled
2	113	0.01	SRV reseated @ 100 min; HPI throttle at 10 minute after it can be throttled
3	109	0.005	SRV reseated @ 100 min; HPI is not throttled
4	114	0.485	SRV reseated @ 50 min; HPI throttle at 1 minute after it can be throttled
5	115	0.01	SRV reseated @ 50 min; HPI throttle at 10 minute after it can be throttled
6	149	0.005	SRV reseated @ 50 min; HPI is not throttled

Table 7.13 The TH uncertainty representative scenarios and their probabilities of the reactor *tripping during hot zero power operation causing PZR SRV stuck open and reseated later by itself* for the Oconee-1 NPP

#	TH Bin #	Probability	Brief Scenario Description
1	121	0.485	SRV reseated @ 100 min; HPI throttle at 1 minute after it can be throttled + low decay heat
2	122	0.01	SRV reseated @ 100 min; HPI throttle at 10 minute after it can be throttled + low decay heat
3	165	0.005	SRV reseated @ 100 min; HPI is not throttled + low decay heat
4	123	0.485	SRV reseated @ 50 min; HPI throttle at 1 minute after it can be throttled + low decay heat
5	124	0.01	SRV reseated @ 50 min; HPI throttle at 10 minute after it can be throttled + low decay heat
6	168	0.005	SRV reseated @ 50 min; HPI is not throttled + low decay heat

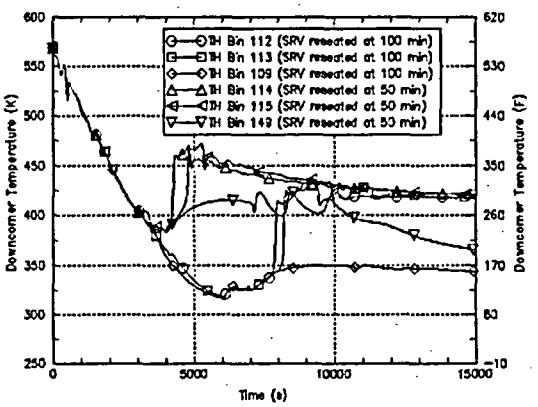

Figure 7.12 The downcomer temperature time history of the event in which the reactor tripped during full power operation coupled with SRV stuck open and reseated later.

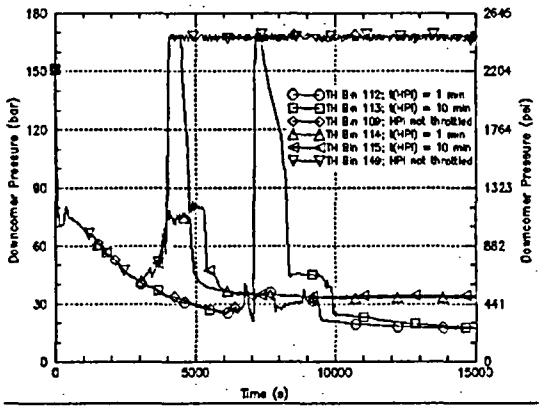

Figure 7.13 The downcomer pressure time history of the event in which the reactor tripped during full power operation coupled with SRV stuck open and reseated later.

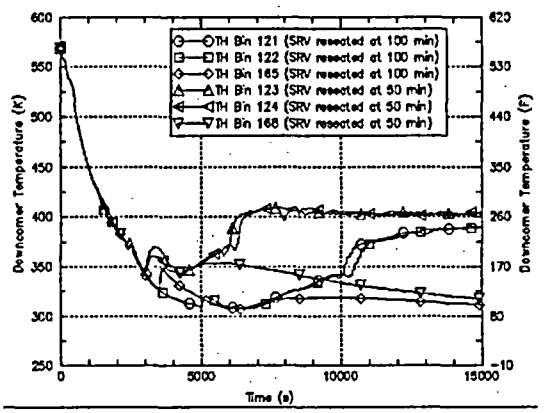

Figure 7.14 The downcomer temperature time history of the event in which the reactor tripped during hot zero power operation coupled with SRV stuck open and reseated later.

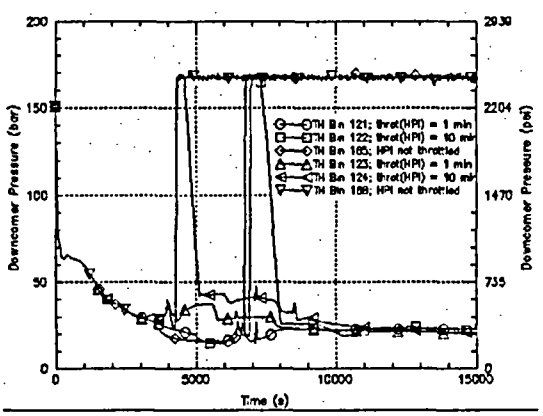

Figure 7.15 The downcomer pressure time history of the event in which the reactor tripped during hot zero power operation coupled with SRV stuck open and reseated later.

7.2 Beaver Valley TH Uncertainty Representative Scenarios

The same process utilized to identify Oconee-1 uncertainty representative scenarios can be applied to identify the representative scenarios for the Beaver Valley plant. Table 7.14 shows the sensitivity data calculated by RELAP5 for Beaver Valley. The probability of each representative value is listed in Table 7.1. The classification of events is identical to the Oconee-1 analysis.

Table 7.14 The parameters' sensitivities for the Beaver Valley NPP based on the nominal range sensitivity analysis. The values inside parentheses are T_{sen} (in Kelvin).

	Break Size m^2 (inches in diameter)							
	1E-3 (1.4")	2E-3 (2")	4E-3 (2.8")	8E-3 (4")	1.6E-2 (5.7")	3.2E-2 (8")	1 SRV SO 2.2E-3 (2.1")	2 SRVs SO 4.4E-3 (3")
Nominal	459	377	336	319	313	300	393	349
Winter*	457	366	333	318	316	297	388.2[&]	346[&]
Summer*	460	370	344	331	318	303	393[&]	355[&]
110% m(HPI)	--	362	334	--	--	--	379'	345[&]
90% m(HPI)	466	373	341	--	--	--	396[&]	354[&]
100 % HPI Failed	521	496	432	--	--	--	--	--
low decay heat (0.7%)	360	348	325	312	304	299	351[&]	334[&]
low decay heat (0.2%)	353	337	320	309	302	298	341[&]	322[&]
130% Components Heat Transfer Coefficient	462	374	342	324	--	300	396[&]	355[&]
70% Components Heat Transfer Coefficient	455	362	331	321	--	--	385[&]	345[&]
130% Break Area	--	329	325	307	300	301	--	327[&]
70% Break Area	--	359	359	323	306	306	--	359[&]
Cold Leg LOCA	455	453	415	369	347	340	--	--

*Water temperature during Summer: T(HPI)= 55°F, T(ACCU)= 105°F ,T(LPI)= 55°F
*Water temperature during Spring/fall: T(HPI)= 50°F, T(ACCU)= 90°F ,T(LPI)= 50°F
*Water temperature during winter: T(HPI)= 45°F, T(ACCU)= 75°F ,T(LPI)= 45°F
' Extrapolated data
[&] Interpolated data

7.2.1 *1.4 – 4 Inches (1E-3m^2 - 8E-3 m^2) LOCA*

Table 7.15 shows the probabilities for different representative break sizes used in the analysis. Table 7.16 lists the parameters that are included in the analysis. There are 1296 combinations in total for the four representative break sizes. The PDF and CDF distributions are shown in Figures 7.16 and 7.17.

Table 7.15 The specific parameter representative values and probabilities for LOCA size between 1.4 inches and 4 inches.

Factors	Value 1	Value 2	Value 3	Value 4
	Probability	Probability	Probability	Probability
Break Size	1.4"	2.0"	2.8"	4.0"
	0.15	0.25	0.30	0.30

Table 7.16 The list of influential parameters considered for each break size from 1.4 to 4 inches in diameter LOCA. The numbers in parentheses represent the number of representative values for the parameter.

	Break Size (4) m^2 (inches in diameter)			
	1E-3 (1.4")	2E-3 (2.0")	4E-3 (2.8")	8E-3 (4")
Break Location (2)	√	√	√	√
Decay Heat (3)	√	√	√	√
Season (3)	√	√	√	√
HPI Flow Rate (3)	√	√	√	insignificant
Component Heat Transfer Rate (3)	√	√	√	√
Break Area (3)	insignificant	√	√	√

Five representative scenarios are identified as shown in Figure 7.17. The scenario descriptions and scenario probabilities are shown in Table 7.17. The Tdc and Pdc time histories are shown in Figures 7.18 and 7.19, respectively.

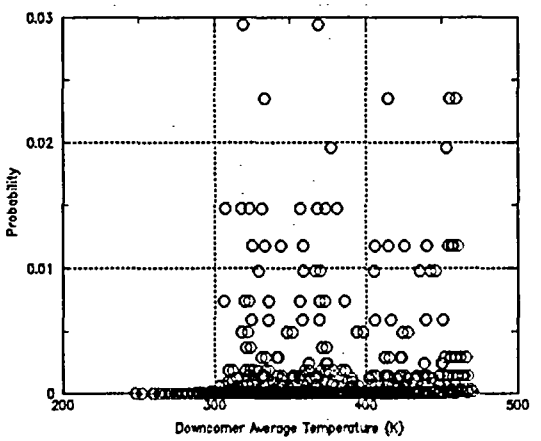

Figure 7.16 The probability distribution of the representative scenarios of LOCA between 1E-3m^2 and 8E-3m^2 (1.4 and 4 inches in diameter).

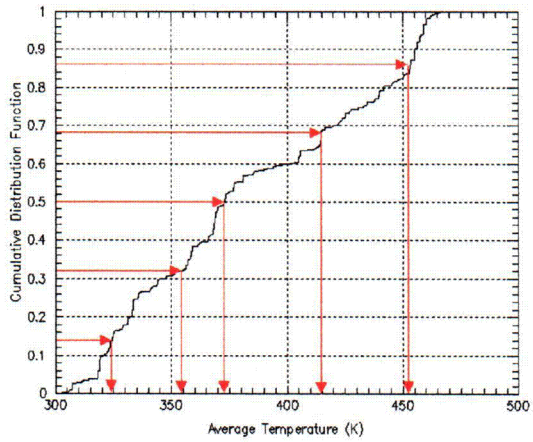

Figure 7.17 The cumulative distribution function and the five representative scenarios for LOCA between 1E-3m^2 and 8E-3m^2 (1.4 and 4 inches in diameter).

Table 7.17 The Boundary conditions of the five uncertainty representative cases for LOCA between 1E-3m^2 and 8E-3m^2 (1.4 and 4 inches in diameter)

#	TH Bin #	Probability	Brief Scenario Description
1	2	0.23	1E-3 m^2 (1.4") cold leg LOCA in winter
2	115	0.18	4E-3 m^2 (2.8") cold leg LOCA
3	3	0.18	2E-3 m^2 (2") surge line LOCA; 90% of nominal HPI flow rate
4	114	0.18	4E-3 m^2 (2.8") surge line LOCA in summer; with 130% component heat transfer coefficient
5	56	0.23	8E-3 m^2 (4") surge line LOCA in summer; reactor trips at hot zero power operation (0.7% of full power)

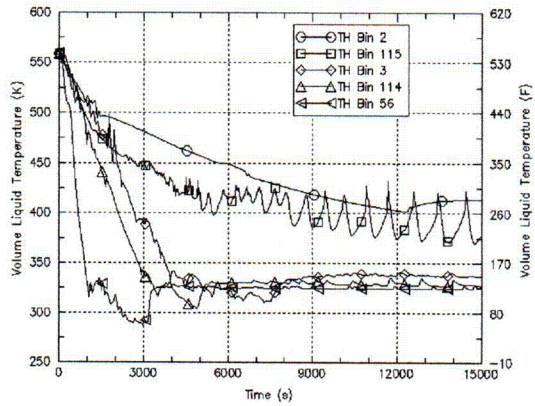

Figure 7.18 The T_{dc} traces of the five TH uncertainty representatives of the event category of LOCA between 1E-3 m^2 and 8E-3 m^2 (1.4 and 4 inches in diameter) of the Beaver Valley NPP

C27

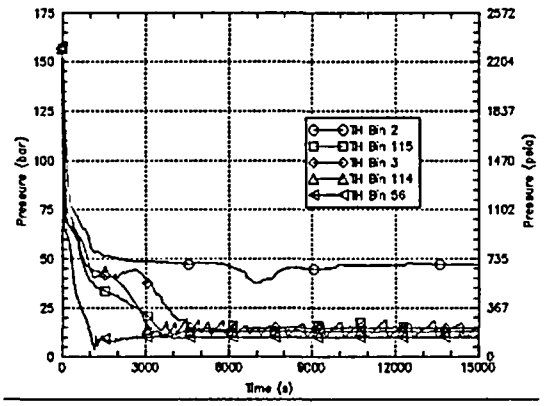

Figure 7.19 The P_{dc} traces of the five TH uncertainty representatives of the event category of LOCA between 1E-3 m^2 and 8E-3 m^2 (1.4 and 4 inches in diameter) of the Beaver Valley NPP

7.2.2 *4 – 8 Inches (8E-3m^2 and 3.2E-3 m^2) LOCA*

Table 7.18 shows the probabilities for different representative break sizes of the category of LOCA with break size between 8E-3m^2 and 3.2E-2 m^2 (4 inches and 8 inches in diameter). Table 7.19 shows the parameters used in the calculation. The total number of combinations is 270. Figures 7.20 and 7.21 are the PDF and CDF diagrams. The descriptions and probabilities of the three representative scenarios are shown in Table 7.20. The T_{dc} and P_{dc} time histories are shown in Figures 7.22 and 7.23, respectively.

Table 7.18 The specific parameter representative values and probability for LOCA size between 4 inch and 8-inch.

Factors	Value 1 Probability	Value 2 Probability	Value 3 Probability
Break Size	4" 0.35	5.7" 0.30	8" 0.35

Table 7.19 The list of influential parameters considered for each break size for LOCA between 8E-3 m^2 and 3.2E-2 m^2 (4 and 8 inches in diameter). The numbers in the parentheses are the number of representative values of the parameter.

	Break Sizes m^2 (inches in diameter)		
	8E-3 (4")	1.6E-2 (5.7")	3.2E-3 (8")
Break Location (2)	√	√	√
Decay Heat (3)	√	√	√
Season (3)	√	√	√
HPI Flow Rate (3)	Insignificant	Insignificant	Insignificant
Component Heat Transfer Rate (3)	√	Insignificant	Insignificant
Break Area (3)	√	√	√

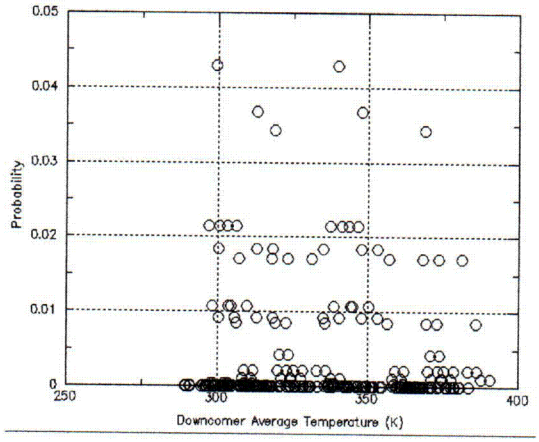

Figure 7.20 The probability distribution of the representative scenarios of LOCA between 8E-3 m^2 and 3.2E-2 m^2 (4 and 8 inches in diameter).

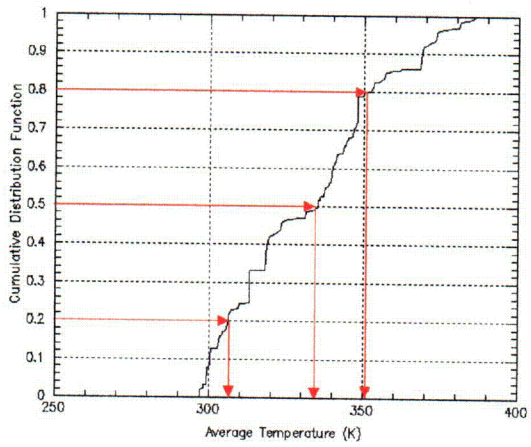

Figure 7.21 The cumulative distribution function and the three representative scenarios for LOCA between 8E-3 m^2 and 3.2E-2 m^2 (4 and 8 inches in diameter).

Table 7.20 The Boundary conditions of the three uncertainty representative cases of LOCA between 8E-3 m^2 and 3.2E-2 m^2 (4 and 8 inches in diameter)

ID	TH Bin #	Probability	Brief Scenario Description
1	117	0.35	5.7" cold leg LOCA in summer
2	116	0.3	5.7" cold leg LOCA; with 30% reduced break area
3	7	0.35	8" surge line LOCA; with 30% reduced break area

C28

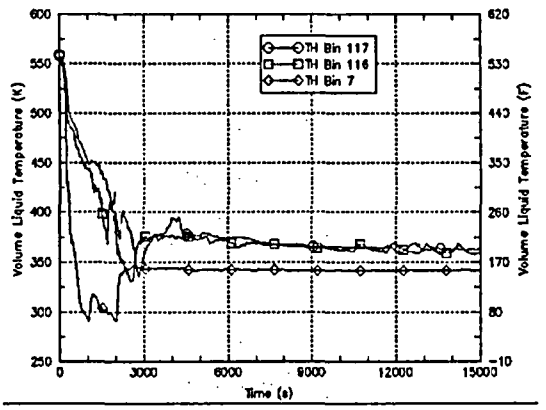

Figure 7.22 The three T_{dc} traces of the TH uncertainty representatives of the event category of LOCA between 8E-3 m^2 and 3.2E-2 m^2 (4 and 8 inches in diameter) of the Beaver Valley NPP

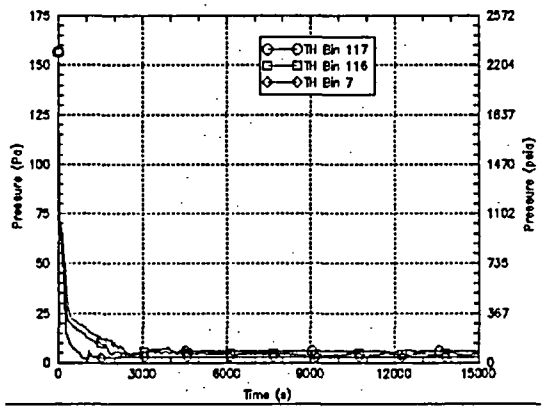

Figure 7.23 The three P_{dc} traces of the TH uncertainty representatives of the event category of LOCA between 8E-3 m^2 and 3.2E-2 m^2 (4 and 8 inches in diameter) of the Beaver Valley NPP

7.2.3 *Greater Than 8 Inches (3.2E-2 m^2) LOCA*

One representative scenario is used: 16 inches (1.3E-1 m^2) hot leg LOCA. Table 7.21 is the event description. The T_{dc} and P_{dc} time histories are shown in Figure 7.24.

Table 7.21 The Boundary conditions of the uncertainty representative case for larger than 8-inch LOCA TH uncertainty analysis

#	TH Bin #	Probability	Brief Scenario Description
1	9	1.0	16" hot leg LOCA

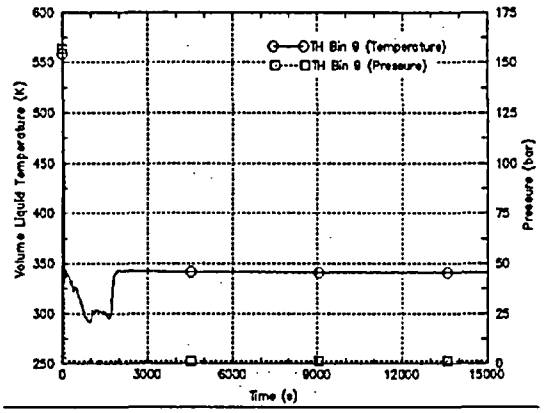

Figure 7.24 The T_{dc} and P_{dc} traces of the 1.3E-1 m^2 (16 inches in diameter) LOCA of the Beaver Valley NPP

7.2.4 *PZR Valve(s) Stuck Open and Remaining Open*

The PRA model indicates that the probabilities of more than one PZR valve stuck open scenarios can not be neglected. The analysis becomes more complex when there are two kinds of valves involved, PZR PORV and PZR SRV, and each kind of valve has different flow capacities. In addition, there are scenarios of no valves reseated, one valve reseated, and two valves reseated that dramatically increase analysis complexity compared with Oconee-1 analysis. In the PRA model, the scenarios with full decay heat are separated from low decay heat scenarios. For low decay heat scenarios, there is uncertainty of being at .7% and .2% of full power decay heat that is not explicitly treated in the PRA model. Thus, the uncertainty analysis separates full decay heat analysis from low decay heat analysis.

Reactor Trips at Full Power Operation

In the PRA model, three types of valve opening combinations are considered:

- 1 SRV stuck open
- 2 SRVs stuck open
- 2 PORVs stuck open

For scenarios of valves stuck open and remaining open, the above three combinations are discussed together, since the valve open area is stochastic and should be continuously distributed. The total open area of two simultaneously stuck open valves could be smaller than one fully opened valve. The analysis becomes more complex by dealing with two kinds of valves, PORVs and SRVs, which have different flow capacities. PRA data regarding valve stuck open frequencies are required for the analysis. All the event frequencies used in the following discussion are based on the PRA preliminary results.

For the scenarios of two simultaneously stuck open valves, it's possible that one valve could be reseated later on in the scenario, while the other valve remains stuck open until the end of the scenario. In order to determine the class of such a scenario, one reseated

and one remaining open, the T_{dc} trends of these scenarios are compared with the no valve reseated scenario. Figure 7.25 shows the T_{dc} time histories of the comparison. The results show that there is little difference in the T_{dc} trends between scenarios where one of the two valves reseated and the scenarios where none valve reseated. Thus, one valve stuck open scenarios are discussed separately from the two valves stuck open scenarios. For one valve stuck open scenarios, the valve could remain open or reseated at later of the scenario. The one valve stuck open and reseated scenarios are discussed in Section 7.2.5. The two valves stuck open scenarios include none of the two valves reseated, one of the two valves reseated, and both valves reseated. The both valves reseated scenarios are discussed in Section 7.2.5. The scenarios of one of the two stuck open valves reseated are classified in the same category as none of the two stuck open valves reseated based on the T_{dc} similarity shown in Figure 7.25.

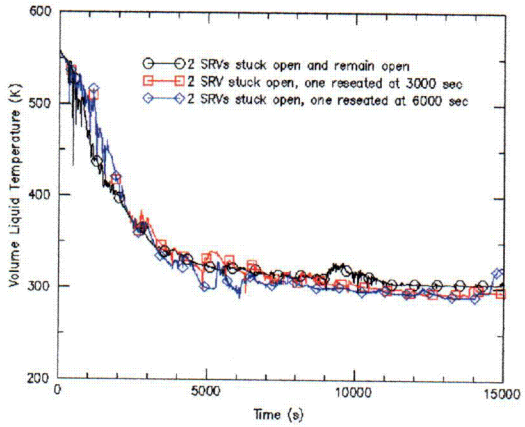

Figure 7.25 The T_{dc} trends of three sub-scenarios of the two SRVs simultaneously stuck open scenario. All the three scenarios have one valve remaining stuck open until the end of the scenario. The difference is in the other valve reseated at 50 minutes, reseated at 100 minutes, and never reseated.

The base frequencies of one SRV, two SRVs, and two PZR PORVs stuck open are 1.6E-3, 1.6E-5, and 3.3E-6, respectively. The relevant frequencies of the sub-scenarios of the PZR valve stuck open scenarios are (according to the PRA data):

- 1 SRV SO that stays open: 1.6E-3 × 0.25* = 4.0E-4 (per/year)
- 2 SRVs SO that stay open: 1.6E-5 × 6.25E-2 = 1.0E-6 (per/year)
- 2 SRVs SO with one reseated: 1.6E-5 × 3.75E-1 = 6.0E-6 (per/year)
- 2 PORVs SO that stay open: 3.3E-6 × 0.5 = 1.65E-6 (per/year)

*The probability of the valve being reseated is 75%

The uncertainty analysis of above four scenarios is same as LOCA analysis. The probability ratios of one SRV stuck open, two SRVs stuck open, and two PORVs fully open are 97.88: 1.71: 0.41. Since the one SRV stuck open scenario dominates the probability, for simplicity, the break size is represented by two values: one SRV fully stuck open and two SRVs fully stuck open with probability of 97.9% and 2.1% as shown in Table 7.22. The results obtained from such a simplification would be conservative.

C29

Table 7.22 The specific parameter representative values and probabilities for primary system valve stuck open without reseating

#	Break Size	Probability
1	2.2E-3 m^2 (One SRV fully open)	0.979
2	4.6E-3 m^2 (Two SRVs fully open)	0.021

Table 7.23 lists the parameters for uncertainty analysis. Applying the probabilities in Table 7.1, the PDF and CDF plots are shown in Figures 7.26 and 7.27. Figure 7.26 shows that there is a probability gap between one and two valve stuck open scenarios. One valve stuck open scenarios share about a probability of 98%. The two valve stuck open scenarios will not be in the representative scenarios due to their relatively low probabilities, in comparison with one valve stuck open scenarios. The PDF diagram (Figure 7.26) is used to identify the representative scenarios. A representative scenario of two valves stuck open, even with relatively low probability, is specified as a representative scenario as shown in Figure 7.26. Table 7.24 shows the probabilities and descriptions of the two representative scenarios.

Table 7.23 The list of influential parameters for assessing TH uncertainty of PZR valves stuck open during full power operation. The numbers in the parentheses are the number of representative values of the parameter

Key Parameters for each break size	1 SRV Fully Open	2 SRV Fully Open
Season (3)	√	√
HPI Flow Rate (3)	√	√
Component Heat Transfer Rate (3)	√	√
Break Area (3)	--	√

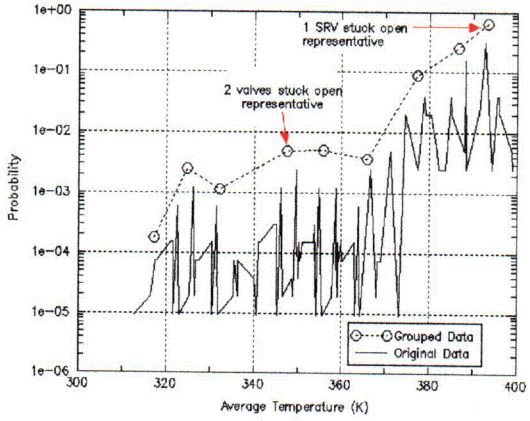

Figure 7.26 The probability distribution of the representative scenarios of PZR valves stuck open and not reseated occurring during full power operation.

C30

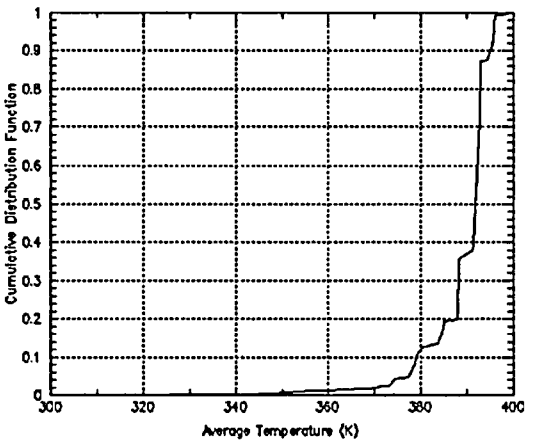

Figure 7.27 The cumulative distribution function of the PZR valves stuck open and not reseated event that occurs during full power operation.

Table 7.24 The Boundary conditions of the three uncertainty representative cases for one PZR valve Stuck open without reseating events TH uncertainty analysis (Full power)

#	Description	Distributed Probability
U1	1 PRZ SRV Stuck Open (fully open)	97.9%
U2	2 PRZ SRV Stuck Open (fully open)	2.1%

Reactor Trips at Hot Zero Power Operation

For the scenarios of PZR valves stuck open during low decay heat operation, the TH uncertainty assessment is similar to that for the valve stuck open during full power operation. The decay heat curves for Beaver Valley are represented by two curves: .7% and .2% of full operation power. The probability of each situation is .5. Table 7.25 shows the representative values and probabilities of break size and decay heat. Figures 7.28 and 7.29 are the PDF and CDF diagrams. Two representative scenarios are identified and shown in Table 7.26. Factors of 0.564 (= 1 – 0.0107/0.0245) and 0.782 (= 1 – 0.0107/0.0490) need to be multiplied for one and two SRVs stuck open scenarios respectively, since we are only interested in the stuck open area greater than 1E-3 m^2 (1.5 inches in diameter) instead of the full spectrum of valve open area.

Table 7.25 The specific parameter representative values and probabilities for primary system valve stuck open without reseating when reactor trips at hot zero power operation

Factors	Value 1 Probability	Value 2 Probability
Break Size	2.2E-3 m^2 (One SRV fully open) 0.979	4.6E-3 m^2 (Two SRV fully open) 0.021
Decay heat	0.7% of full power 0.5	0.2% of full power 0.5

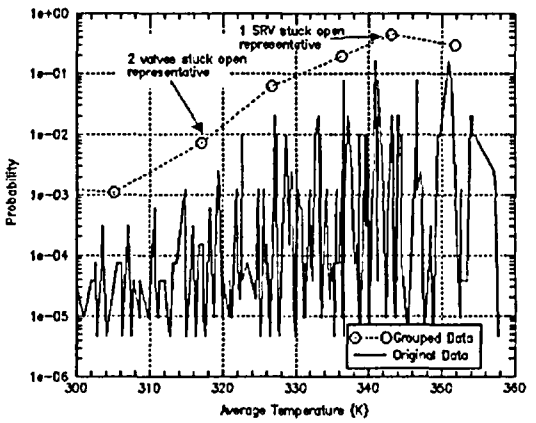

Figure 7.28 The probability distribution of the representative scenarios of PZR valves stuck open and not reseated occurring during hot zero power operation.

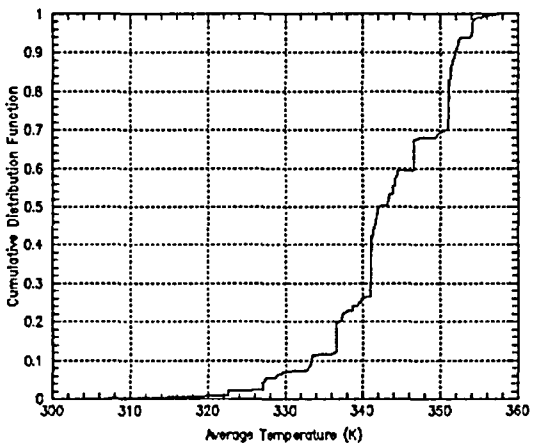

Figure 7.29 The cumulative distribution function of the PZR valves stuck open and not reseated occurring during hot zero power operation

Table 7.26 The Boundary conditions of the three uncertainty representative cases for one PZR valve stuck open without reseating events TH uncertainty analysis (Hot Zero Power)

#	Description	Distributed Probability
U3	1 PRZ SRV Stuck Open (fully open; 0.2% low decay heat	97.9%
U4	2 PRZ SRV Stuck Open (fully open) ; 0.2% low decay heat	2.1%

Adjustment of PRA Probability to be Consistent with Valves Open Area

The above analysis mixes one valve and two valves stuck open scenarios, however in the PRA model the one valve stuck open and two valves stuck open scenarios are explicitly modeled in the PRA event tree. TH uncertainty analysis is based on the total valve open area, however the PRA model is based on how many valves are stuck open. There is

inconsistency is the scope, since two simultaneously partially stuck open valves have a total open area that is not necessarily larger than a single full-open stuck open valve. In order to assign the correct probability to the two representative scenarios in Table 7.27, the probabilities in the PRA model need to be adjusted.

It is assumed that the probability of a valve open area is uniformly distributed. For a one valve stuck open scenario, Figure 7.30 shows the probability distribution of valve open area from zero to its maximum size (2.2E-3 m^2 or 2.4E-2 ft^2). Since the area less than 1E-3m^2 is not of interest to the analysis, the valve open area is divided into two regions as shown in Figure 7.30. The area **A**, ranging between zero and 1E-3m^2, is not of PTS interest. The area **B**, ranging between 1E-3m2 and the maximum valve open area, is the area of PTS interest. Thus, a factor of 0.564 ($= \frac{B}{A+B}$) needs to be multiplied by the final PTS probability for the one SRV stuck open without reseating scenario.

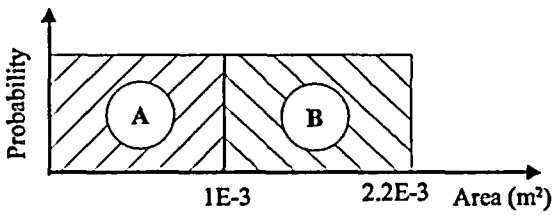

Figure 7.30 The uniform probability distribution of a valve stuck open area. Region A is not of PTS interest. Region B is of PTS interest.

For the two valves stuck open scenarios, the open area range is between zero and two valves fully open. The probability of the total valve open area is a triangle distribution as shown in Figure 7.31 assuming the probability of a valve's open area is uniformly distributed. In Figure 7.31, the region **C** is not of interest to the analysis due to its small open area (less than 1E-3m^2). Region **D** should be represented by an SRV fully stuck open scenario. Only region **E** should be represented by a two valves simultaneously stuck fully open scenario. A factor of 0.5 ($= \frac{E}{C+D+E}$) should be multiplied for the two valves stuck open scenarios in the PRA model to reflect only the portion **E**, which would be applied to the TH representative scenario of two valves simultaneously stuck fully open scenarios (Scenario U4 in Table 7.26). Region **D** shares a 0.4 probability($= \frac{D}{C+D+E}$). Region **D** should be represented by one valve stuck open (Scenario U3 of Table 7.26). Table 7.27 shows the equations for adjusting probabilities of PRA scenarios to be consistent with TH uncertainty definition.

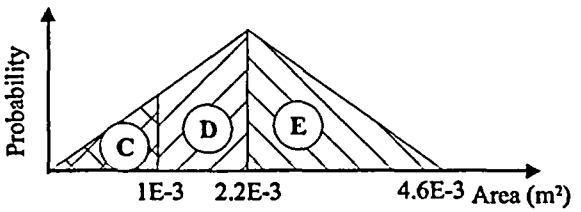

Figure 7.31 The probability distribution of the total open area of two valves stuck open. Region C is not of PTS concern. Region D is represented by one SRV fully stuck open. Region E is represented by two SRVs fully stuck open.

Table 7.27 The two representative scenarios and their probabilities for the scenarios of PZR valves stuck open and remaining open.

Representative Scenario	Probability
1 SRV fully stuck open	0.564 × Probability(1 SRV SO & remain open) + 0.4 × Probability(2 SRVs SO & at least one valve remains open)
2 SRVs fully stuck open	0.5 × Probability(2 SRVs SO & at least one valve remains open)

7.2.5 *One and Two PZR Valves Stuck Open and Reseated*

In this category, the scenarios with two valves stuck open and reseated assume that the two valves were stuck open and reseated simultaneously. As discussed before, the PZR valve reseat scenarios need to consider two additional key parameters: valve reseat timing and timing of HPI shut off. Unlike the Oconee plant, there is no HPI flow rate control mechanism for Beaver Valley thus the HPI can only be either fully injected or completely shut off.

Two valve reseat timings are specified in the PRA model: 50 minutes and 100 minutes. Each has a probability of .5. Figures 7.23 and 7.24 show the valve reseat timing and the number of stuck open valves that have an equivalent level of PTS contribution. Thus, four T_{dc} uncertainty representative scenarios are specified::

- 1 SRV stuck open and reseated at 50 minutes
- 1 SRV stuck open and reseated at 100 minutes
- 2 SRV stuck open and reseated at 50 minutes
- 2 SRV stuck open and reseated at 100 minutes

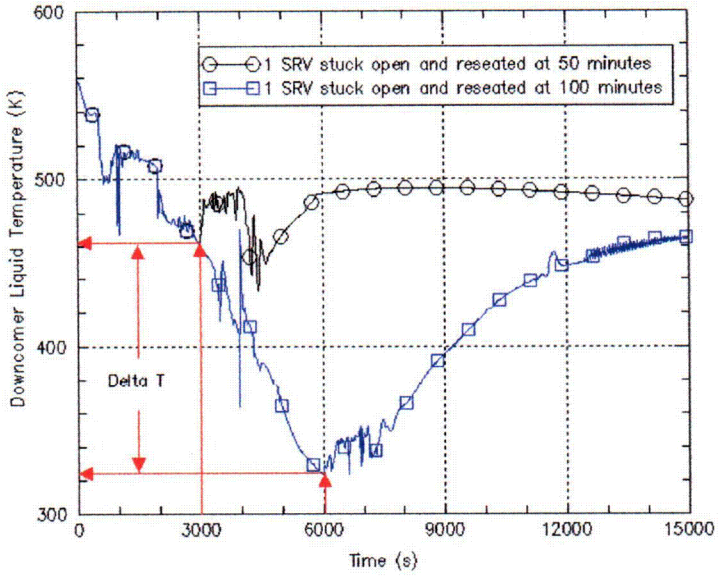

Figure 7.32 The T_{dc} trends of one SRV stuck open and reseated at 50 and 100 minutes (NRC runs #59 and #60).

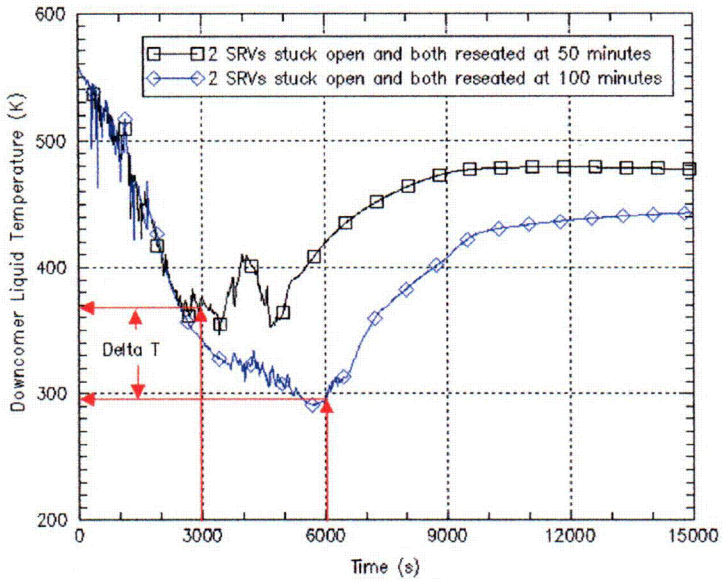

Figure 7.33 The T_{dc} trends of two SRVs stuck open and reseated at 50 and 100 minutes (NRC runs #66 and #67).

Besides T_{dc} uncertainty, P_{dc} uncertainty is dominated by HPI shutoff time. Three representative timings are specified in the PRA model. The timings and probabilities are as the follows:

C31

- HPI shutoff within 1 minute: .906
- HPI shutoff between 1 minute and 10 minutes: .092
- HPI never being shutoff: 1E-3

Combining T_{dc} uncertainty and P_{dc} uncertainty, Tables 7.28 and 7.29 are the representative scenarios and probabilities for one valve and two valves stuck open and reseated scenario.

Table 7.28 The conditional probabilities of the representative scenarios of one SRV stuck open and reseated scenarios. Reactor trips at full power operation.

#	Reseat time (minute) [Probability] (A)	HPI shutoff time (minute) [Probability] (B)	Decay Heat (C)	Distributed Probability (A×B×C)	Descriptions
U9	50 [0.5]	1 [0.906]	Nominal [1.0]	4.53E-01	SRV reseat at 50 minutes; HPI shutoff at 1 minutes
U10		10 [0.092]		4.60E-02	SRV reseat at 50 minutes; HPI shutoff at 10 minutes
U11		Infinite [1E-3]		5.00E-04	SRV reseat at 50 minutes; HPI is not shutoff
U12	100 [0.5]	1 [0.906]		4.53E-01	SRV reseat at 100 minutes; HPI shutoff at 1 minutes
U13		10 [0.092]		4.60E-02	SRV reseat at 100 minutes; HPI shutoff at 10 minutes
U14		Infinite [1E-3]		5.00E-04	SRV reseat at 100 minutes; HPI is not shutoff

Table 7.29 The conditional probabilities of the representative scenarios of two PZR valves stuck open and reseated scenarios. Reactor trips at full power operation.

#	Reseat time (minute) [Probability](A)	HPI throttling time (minute) [Probability] (B)	Decay Heat (C)	Distributed Probability (A×B×C)	Description
U21	50 [0.5]	1 [0.906]	Nominal [1.0]	4.53E-01	SRV reseat at 50 minutes; HPI shutoff at 1 minutes
U22		10 [0.092]		4.60E-02	SRV reseat at 50 minutes; HPI shutoff at 10 minutes
U23		Infinite [1E-3]		5.00E-04	SRV reseat at 50 minutes; HPI is not shutoff
U24	100 [0.5]	1 [0.906]		4.53E-01	SRV reseat at 100 minutes; HPI shutoff at 1 minutes
U25		10 [0.092]		4.60E-02	SRV reseat at 100 minutes; HPI shutoff at 10 minutes
U26		Infinite [1E-3]		5.00E-04	SRV reseat at 100 minutes; HPI is not shutoff

For reactor tripped at low decay heat operation, decay heat uncertainty needs to be considered. Table 7.30 shows the key parameters' values and probabilities. The representative scenarios for one and two valves stuck open and reseated later scenarios during low decay heat situations are listed in Tables 7.31 and 7.32, respectively.

Table 7.30 The unique parameter representative values and probabilities for primary system valve stuck open and reseated

Factors	Value 1 Probability	Value 2 Probability	Value 3 Probability
Break Size	4.6E-3m^2		
	1.0		
Decay Heat	Nominal	low decay heat 0.2%	low decay heat 0.7%
	0.8	0.1	0.1
Valves Reseating Time	50 minutes	100 minutes	
	0.5	0.5	
HPI Shutoff Time	1 minute	10 minutes	Not shutoff
	0.906	0.092	1E-3

Table 7.31 The conditional probabilities of the representative scenarios of one SRV stuck open and reseated scenarios. Reactor trips at hot zero power operation.

#	Reseat time (minute) [Probability] (A)	HPI throttling time (minute) [Probability] (B)	Decay Heat [Probability] (C)	Distributed Probability (A×B×C)	Description (low decay heat for all scenarios)
U15	50 [0.5]	1 [0.906]	0.2% power [1.0]	4.53E-01	SRV reseat at 50 minutes; HPI throttled in 1 minutes
U16		10 [0.092]		4.60E-02	SRV reseat at 50 minutes; HPI throttled in 10 minutes
U17		Infinite [1E-3]		5.00E-04	SRV reseat at 50 minutes; HPI is not throttled
U18	100 [0.5]	1 [0.906]		4.53E-01	SRV reseat at 100 minutes; HPI throttled in 1 minutes
U19		10 [0.092]		4.60E-02	SRV reseat at 100 minutes; HPI throttled in 10 minutes
U20		Infinite [1E-3]		5.00E-04	SRV reseat at 100 minutes; HPI is not throttled

Table 7.32 The conditional probabilities of the representative scenarios of two PZR valves stuck open and reseated scenarios. Reactor trips at hot zero power operation.

#	Reseat time (minute) [Probability](A)	HPI throttling time (minute) [Probability] (B)	Decay Heat (C)	Distributed Probability (A×B×C)	Description (low decay heat for all scenarios)
U27	50 [0.5]	1 [0.906]	0.2% power [1.0]	4.53E-01	SRV reseat at 50 minutes; HPI shutoff at 1 minutes
U28		10 [0.092]		4.60E-02	SRV reseat at 50 minutes; HPI shutoff at 10 minutes
U29		Infinite [1E-3]		5.00E-04	SRV reseat at 50 minutes; HPI is not shutoff
U30	100 [0.5]	1 [0.906]		4.53E-01	SRV reseat at 100 minutes; HPI shutoff at 1 minutes
U31		10 [0.092]		4.60E-02	SRV reseat at 100 minutes; HPI shutoff at 10 minutes
U32		Infinite [1E-3]		5.00E-04	SRV reseat at 100 minutes; HPI is not shutoff

Concluding the analyses in 7.2.4 and 7.2.5, Tables 7.33 to 7.37 list the representative scenarios and estimate frequencies for all PZR valve stuck open scenarios.

Table 7.33 The TH uncertainty representative scenarios of the event category of PZR valves stuck open without reseating and their probabilities of the Beaver Valley NPP

ID	Frequency**	Brief Scenario Description
14	2.23E-4	1 SRV SO and remaining open, full power
72	5.14E-7	1 SRV SO and remaining open, full power, no HPI
34	4.95E-7	2 SRVs SO and remaining open, full power
65	1.04E-9	2 SRVs SO and remaining open, full power, no HPI
66	1.18E-7	2 SRVs SO and one reseated at 50 minutes, full power
67	1.18E-7	2 SRVs SO and one reseated at 100 minutes, full power
83	3.51E-6	2 PORVs SO and remaining open, full power
31	3.10E-7	Open all PZR PORVs and HPI on with loss of feed water
94	4.10E-5	1 SRV SO and remaining open, low decay heat
73	6.55E-8	1 SRV SO and remaining open, low decay heat, no HPI, all ASDVs are open 5 minutes after HPI fails to start
64	8.67E-8	2 SRVs SO and remaining open, low decay heat
92	2.13E-7	2 SRVs SO and one reseated at 50 minutes, low decay heat
93	2.13E-7	2 SRVs SO and one reseated at 100 minutes, low decay heat
76	1.06E-4	2 PORVs SO and remaining open, low decay heat

** PRA results, BV-m.xls, Oct. 8, 2002

Table 7.34 The TH uncertainty representative scenarios of the event category of one PZR valve stuck open and reseated later by itself and their probabilities when reactor trips during full power operation of the Beaver Valley NPP

ID	Frequency**	Brief Scenario Description
59	3.46E-4	1 SRV stuck open; reseated at 50 minutes; HPI has not been throttled
95	1.34E-4	1 SRV stuck open; reseated at 100 minutes; HPI is throttled at 1 minute after it can be throttled
96	1.87E-4	1 SRV stuck open; reseated at 100 minutes; HPI is throttled at 10 minutes after it can be throttled
60	2.15E-5	1 SRV stuck open; reseated at 100 minutes; HPI has not been throttled
82	1.51E-6	1 SRV stuck open, no HPI, all ASDVs are open 5 minutes after HPI fails to start

** PRA results, BV-m.xls, Oct. 8, 2002

Notes: 1 SRV stuck open and reseated at 50 minutes and that HPI is throttled at 1 and 10 minutes are eliminated due to low event frequencies

Table 7.35 The TH uncertainty representative scenarios of the event category of one PZR valve stuck open and reseated later by itself and their probabilities when reactor trips during hot zero power operation of the Beaver Valley NPP

ID	Frequency**	Brief Scenario Description
99	2.59E-5	1 SRV stuck open; reseated at 50 minutes; HPI is throttled at 1 minute after it can be throttled; low decay heat
101	3.09E-5	1 SRV stuck open; reseated at 50 minutes; HPI is throttled at 10 minutes after it can be throttled; low decay heat
97	3.74E-6	1 SRV stuck open; reseated at 50 minutes; HPI has not been throttled; low decay heat
98	2.59E-5	1 SRV stuck open; reseated at 100 minutes; HPI is throttled at 1 minute after it can be throttled; low decay heat
100	3.09E-5	1 SRV stuck open; reseated at 100 minutes; HPI is throttled at 10 minutes after it can be throttled; low decay heat
71	3.74E-6	1 SRV stuck open; reseated at 100 minutes; HPI has not been throttled; low decay heat

** PRA results, BV-m.xls, Oct. 8, 2002

Table 7.36 The TH uncertainty representative scenarios of the event category of two PZR valves stuck open and reseated later by themselves and their probabilities when reactor trips during full power operation of the Beaver Valley NPP

ID	Frequency**	Brief Scenario Description
61	1.79E-6	2 SRV stuck open; reseated at 50 minutes; HPI has not been throttled
86	6.84E-7	2 SRV stuck open; reseated at 100 minutes; HPI is throttled at 1 minute after it can be throttled
87	9.98E-7	2 SRV stuck open; reseated at 100 minutes; HPI is throttled at 10 minutes after it can be throttled
62	1.08E-7	2 SRV stuck open; reseated at 100 minutes; HPI has not been throttled
68	1.33e-8	2 SRV stuck open; no HPI, all ASDVs are open 5 minutes after HPI fails to start

** PRA results, BV-m.xls, Oct. 8, 2002

Notes: 2 SRV stuck open and reseated at 50 minutes and that HPI is throttled at 1 and 10 minutes is eliminated due to low event frequencies

Table 7.37 The TH uncertainty representative scenarios of the event category of two PZR valves stuck open and reseated later by themselves and their probabilities when reactor trips during hot zero power operation of the Beaver Valley NPP

ID	Frequency**	Brief Scenario Description
88	1.33E-7	2 SRV stuck open; reseated at 50 minutes; HPI is throttled at 1 minute after it can be throttled; low decay heat
90	1.65E-7	2 SRV stuck open; reseated at 50 minutes; HPI is throttled at 10 minute after it can be throttled; low decay heat
69	2.09E-8	2 SRV stuck open; reseated at 50 minutes; HPI has not been throttled; low decay heat
89	1.33E-7	2 SRV stuck open; reseated at 100 minutes; HPI is throttled at 1 minute after it can be throttled; low decay heat
91	1.65E-7	2 SRV stuck open; reseated at 100 minutes; HPI is throttled at 10 minute after it can be throttled; low decay heat
70	2.09E-8	2 SRV stuck open; reseated at 100 minutes; HPI has not been throttled; low decay heat

** PRA results, BV-m.xls, Oct. 8, 2002

7.3 Palisades TH Uncertainty Representative Scenarios

This section discusses the TH uncertainty representative scenarios of the Palisades NPP. Instructed by the PRA group, the uncertainty study scope for the Palisades NPP is limited to the LOCA relevant scenarios. The PZR valves stuck open scenarios do not need to be analyzed. Table 7.38 shows the parameters sensitivities calculated by RELAP5. The probabilities of the representative values are listed in Table 7.1.

The LOCA scenarios are divided into three categories dependent on the breach size: between 1.4 and 4 inches (1.1E-3 m^2 - 8E-3m^2), between 4 and 8 inches (8E-3 m^2 - 3.2E-2 m^2), and greater than 8 inches (3.2E-2 m^2). Since the process of identifying the TH representative scenarios is the same as the process used for the other two plants, the process is not repeated here.

Table 7.38 The sensitivity runs matrix of the Palisade PTS study for primary side breach related scenarios. The values are the average downcomer temperature of the first 10,000 seconds in Kelvin.

	Break Size m^2 (inches in diameter)					
	1E-3 (1.4")	2E-3 (2")	4E-3 (2.8")	8E-3 (4")	1.6E-2 (5.7")	3.2E-2 (8")
Nominal	482	427	391	350	320	310
Winter*	476	419	374	334	304	294
Summer*	490	437	404	364	333	325

110% m(HPI)	478	422	386	--	--	--
90% m(HPI)	488	432	397	--	--	--
100 % HPI Failed	550	532	501	--	--	--
low decay heat (0.7%)	450	406	364	333	319	310
low decay heat (0.2%)	416	380	351	330	318	309
130% Components Heat Transfer Coefficient	486	433	402	355	--	--
70% Components Heat Transfer Coefficient	479	425	389	346	--	--
70% Break Area	--	440	415	370	334	313
130% Break Area	--	418	373	338	314	309
Cold Leg LOCA	491	465	430	373	352	332

*Winter [T(HPI)= 4.4 °C/40 °F, T(LPI)= 4.4 °C/40 °F]
*Summer [T(HPI)= 37.8 °C/100 °F, T(LPI)= 37.8 °C/100 °F]
*Spring/Fall [T(HPI)= 21.1 °C/70 °F, T(LPI)= 21.1 °C/70 °F]

7.3.1 1.4 and 4 inches (1.1E-3 m^2 - 8E-3m^2) LOCA

Figures 7.34 and 7.35 are the PDF and CDF plots. The representative scenario descriptions are shown in Table 7.39. Figures 7.36 and 7.37 are the T_{dc} and P_{dc} time histories of the representative scenarios, respectively.

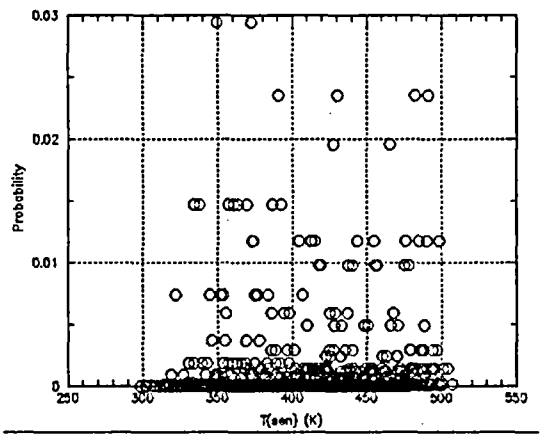

Figure 7.34 The T_{sen} probability distribution for the event category of LOCA between 1.4-inch and 4 inches of the Palisades NPP

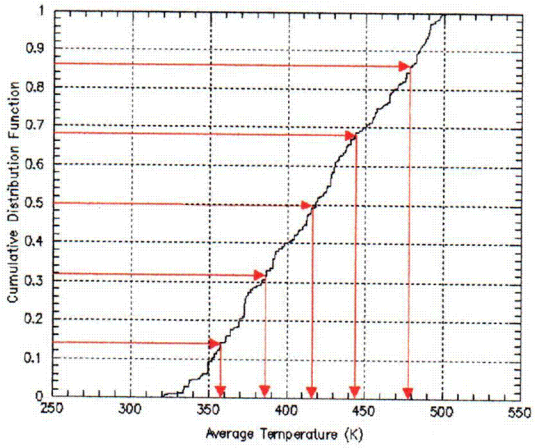

Figure 7.35 The T_{sen} cumulative probability distribution for the event category of LOCA between 1.4 inches and 4 inches for the Palisades NPP and the identification of the representative scenarios

Table 7.39 The Boundary conditions of the five uncertainty representative cases for 1.4inch to 4-inch LOCA TH uncertainty analysis

#	TH Bin #	Probability	Brief Scenario Description
1	2	0.23	1.4" surge line LOCA
2	61	0.18	2.8" surge line LOCA in summer
3	60	0.18	2" surge line LOCA in winter
4	59	0.18	4" cold leg LOCA in summer
5	58	0.23	4" cold leg LOCA in winter

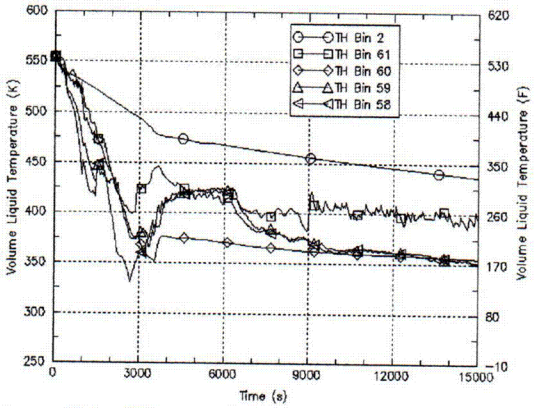

Figure 7.36 The five T_{dc} traces of the TH uncertainty representatives of the event category of LOCA between 1E-3 m^2 and 8E-3 m^2 (1.4 and 4 inches in diameter) for the Palisades NPP

C32

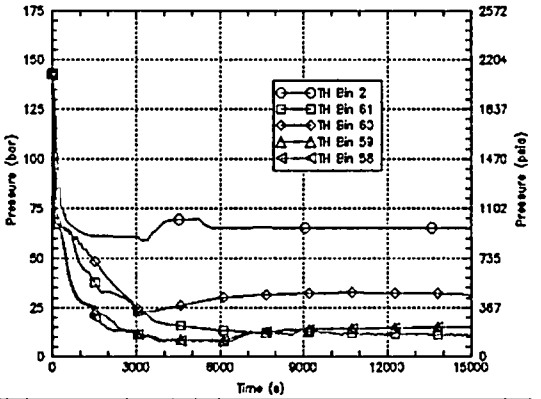

Figure 7.37 The five P_{dc} traces of the TH uncertainty representatives of the event category of LOCA between 1E-3 m^2 and 8E-3 m^2 (1.4 and 4 inches in diameter) for the Palisades NPP

7.3.2 4 and 8 inches (8E-3 m^2 – 3.2E-2 m^2) LOCA

Figures 7.38 and 7.39 are the PDF and CDF plots. The representative scenario descriptions are shown in Table 7.40. Figures 7.41 and 7.42 are the T_{dc} and P_{dc} time histories of the representative scenarios, respectively.

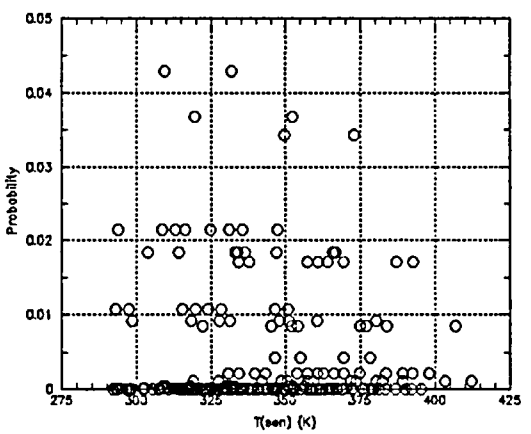

Figure 7.38 The average T_{dc} probability distribution for the event category of LOCA between 8E-3 m^2 and 3.2E-2 m^2 (4 to 8 inches in diameter) for the Palisades NPP

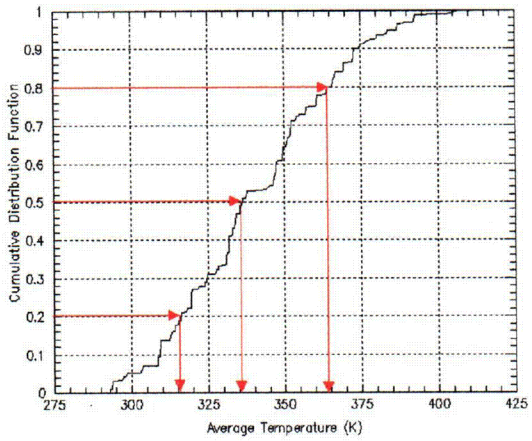

Figure 7.39 The average T_{dc} cumulative probability distribution for the event category of LOCA between 8E-3 m^2 and 3.2E-2 m^2 (4 to 8 inches in diameter) for the Palisades NPP and the identification of the representative scenarios

Table 7.40 The Boundary conditions of the three uncertainty representative cases for 4 inches to 8 inches LOCA TH uncertainty analysis

#	TH Bin #	Probability	Brief Scenario Description
1	64	0.35	4" surge line LOCA in summer
2	63	0.3	5.7" cold leg LOCA in winter
3	62	0.35	8" cold leg LOCA in winter

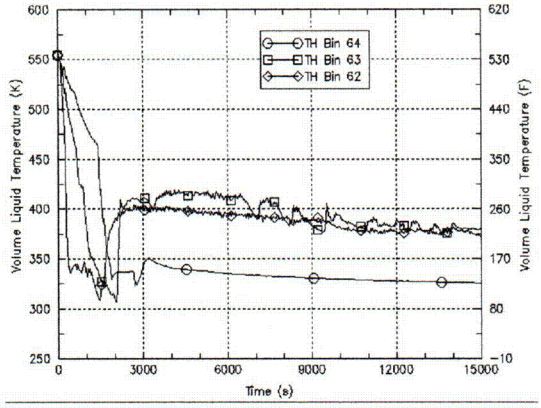

Figure 7.40 The three T_{dc} traces of the TH uncertainty representatives of the event category of LOCA between 8E-3 m^2 and 3.2E-2 m^2 (4 and 8 inches in diameter) for the Palisades NPP

C33

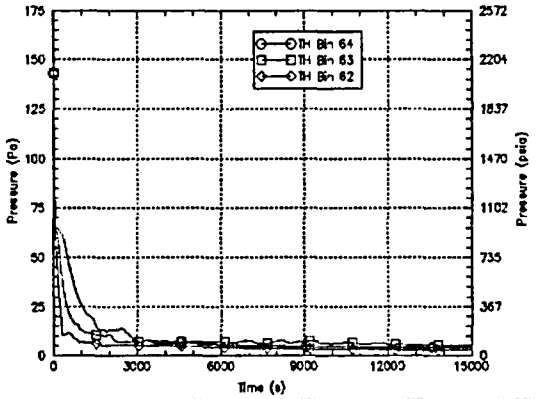

Figure 7.41 The three P_{dc} traces of the TH uncertainty representatives of the event category of LOCA between 8E-3 m^2 and 3.2E-2 m^2 (4 and 8 inches in diameter) for the Palisades NPP

7.3.3 Greater than 8 inches (3.2E-2 m^2) LOCA

The only representative scenario is a16 inches hot leg LOCA (Table 7.41). The T_{dc} and P_{dc} time histories are plotted in Figure 7.42.

Table 7.41 The Boundary conditions of the uncertainty representative case for larger than 8 inches LOCA TH uncertainty analysis

#	TH Bin	Probability	Brief Scenario Description
1	40	1.0	16" surge line LOCA

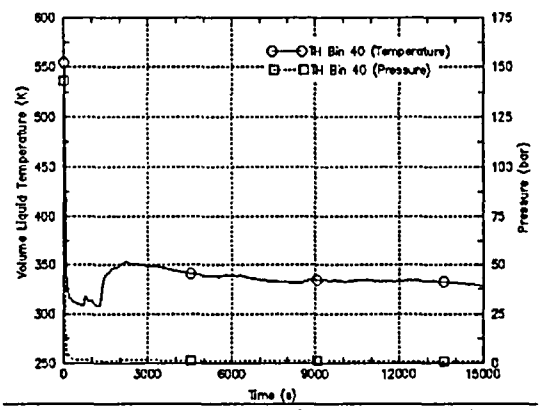

Figure 7.42 The T_{dc} and P_{dc} traces of the TH uncertainty representatives of the event category of LOCA greater than 8E-3 m^2 (8 inches in diameter) for the Palisades NPP

8 Discussion

The sensitivity indicator (T_{sen}) is used as a surrogate indication of a parameter's sensitivity in thermal stress contributing to PTS risk. In this report, the T_{sen} is used as the PTS sensitivity indicator for various reasons. First, thermal-hydraulic behavior of an NPP is better understood than fracture mechanics behavior. Second, during the development of the TH uncertainty methodology, the official PFM code, FAVOR, was not able to produce productive runs. The FAVOR code was available to generate production calculations after the TH uncertainty assessment method had been developed.

It is important to examine the relationship between T_{sen} and CPF in order to validate the appropriateness of using T_{sen} as the indicator for the selection of the representative scenarios for TH uncertainty. Section 8.1 shows the sensitivity assessment matrix with T_{sen}s and CPFs calculated. The data in the matrix is the foundation for the following discussions. Section 8.2 compares parameters' sensitivities in T_{sen} and in CPF. Section 8.3 discusses parameters' importance rankings based on T_{sen} and based on CPF.

It is important to notice that the FAVOR results used in the discussion were calculated in late December 2002 for a parameter sensitivities study. Since then FAVOR has been through a few modifications. There might be inconsistencies between the CPFs used in this section and those in the official PFM report for the same scenario. The CPF data in the official PFM report should be used for any data conflict. The CPIs and CPFs of the sensitivity study are shown in Appendix F.

8.1 Sensitivity Assessment Matrix

Table 8.1 shows the sensitivity assessment matrix. Each cell contains two values. In a cell, the value on the top is T_{sen}, and the value on the bottom is CPF. The parameter sensitivities are evaluated at six different sizes of LOCA: 1E-3, 2E-3, 4E-3, 8E-3, 1.6E-2, and 3.2E-2 square meters (equivalent to 1.5, 2, 2.3, 4, 5.7, and 8 inches in diameter). The first row, "nominal", is the baseline scenarios. All parameters are at their nominal values for the specified break size. The T_{sen} and CPFs are calculated by RELAP5 and FAVOR, respectively.

The sensitivity of a parameter is dependent on break size. Table 8.1 can be used to examine the trend. It also could be used to compare sensitivities of different parameters at a fixed break size. Such comparison could be used for parameter importance ranking.

Table 8.1 The sensitivity assessment matrix for the Oconee-1. The top value in each cell is the T_{sat}. The value at the bottom is the CPF.

#		Break Size m^2 (inches in diameter)					
		1E-3 (1.5")	2E-3 (2")	4E-3 (2.8")	8E-3 (4")	1.6E-2 (5.7")	3.2E-2 (8")
1	Nominal	414 0	394 4.1e-10	388 5.2e-8	363 4.4e-7	329 7.4e-7	317 7.7e-7
2	Winter*	402 1.3e-10	--	374 9.8e-8	--	314 3.5e-7	314 1.3e-8
3	Summer*	--	--	395 2.5e-8	--	336 2.0e-8	317 2.9e-8
4	P(CFT) += 50 psi	--	--	386 1.2e-9	--	--	--
5	P(CFT) -= 50 psi	--	--	389 6.0e-8	--	--	--
6	110% m(HPI) RCPON	521 0	--	402 8.5e-8	--	--	--
7	110% m(HPI) RCPOFF	401 2.5e-11	--	--	--	--	--
8	90% m(HPI)	416 1.8e-13	--	380 1.0e-7	--	--	--
9	HPI Failed and Recovered (@~7000 sec)	--	--	491 0	--	--	317 2.0e-8
10	HPI Failed and Recovered (@~1000 sec)	--	--	400 1.8e-8	--	--	--
11	HPI Failed and Recovered (@~2000 sec)	--	--	416 2.3e-8	--	--	--
12	100 % HPI Failed	--	--	500 0	403 2.8e-7	328 8.6e-7	319 1.5e-7
13	25% HPI Failed	446 0	453 1.9e-12	442 2.1e-8	--	--	--
14	50% HPI Failed	514 0	511	467 6.1e-11	--	--	--
15	low decay heat	490 0	--	349 4.3e-8	--	321 3.3e-8	312 1.1e-6
16	Vent Valve Close	--	--	362 0	345 0	--	--
17	Vent Valve 2/6 Open	--	--	406 0	--	--	--
18	Vent Valve 4/6 Open	--	--	410 0	--	--	--
19	Vent Valve 6/6 Open	--	--	413 0	371 4.7e-9	--	--
20	High CL Reverse Flow Resistance	400 1.4e-9	372 1.6e-8	370 9.6e-9	356 1.1e-6	--	311 4.5e-7
21	130% Components Heat Transfer Coefficient	--	400 1.2e-10	396 3.3e-8	--	331 1.5e-6	--
22	70% Components Heat Transfer Coefficient	--	387 1.3e-10	380 1.2e-7	--	324 9.1e-8	--
23	200% Loop Flow Resistance	--	395 4.8e-10	--	--	--	--
24	200% Bypass Flow Area	--	396 0	--	--	--	--
25	Zero Bypass Flow Area	--	375 0	--	--	--	--
26	No heat structure	--	369 4.5e-8	--	--	--	--
27	Cold Leg LOCA	--	455 0	412 0	376 1.4e-11	345 5.2e-9	317 1.2e-7

*In winter, t(HPI) = 4.4 °C (40 °F), t(CFT) = 21.1 °C (70 °F), and t(LPI) = 4.4 °C(40 °F);
in summer, t(HPI)= 29.4 °C (85 °F), t(CFT) = 37.8 °C (100 °F), and t(LPI) = 29.4 °C (85 °F);
in spring and fall, t(HPI) = 21.1 °C (70 °F), t(CFT) = 26.7 °C (80 °F), and t(LPI) = 21.1 °C (70 °F)

8.2 *Sensitivity: Trend and Comparison*

This section discusses the sensitivity trends and comparisons between T_{sen} and mean CPF. In general, a smaller T_{sen} would correspond to a larger mean CPF. Thus, the opposite trends are expected for T_{sen} and CPF. All the CPFs are calculated based on the embrittlement map used in these analyses, which corresponds to 60 effective full power years (EFPY) of Oconee-1 plant operation, calculated by FAVOR code. Each PFM result has reached its CPF convergence. The TH results are calculated by RELAP5-gamma. The following subsections discuss the sensitivities of different parameters.

8.2.1 Sensitivity of Break Size

Increasing break size would decrease both the RCS' temperature and pressure, which increases thermal stress but reduces pressure stress on the RPV wall. The sensitivity trends of the T_{sen} and mean CPF at different break sizes are shown in Figure 8.1. The trends are the baseline trend. It is a reference for assessing a parameter's sensitivity in discussions in the later sections.

The trend contradicts the previous understanding of PTS. In the previous PTS uncertainty studies [Boyd, 1998 #563;Burns, 1986 #564;Fletcher, 1984 #573], it was believed that PTS should have presence of both thermal stress and pressure stress. Thus, the previous PTS studies focused on small LOCA and MSLB related scenarios. The large LOCA scenarios were not expected to be PTS significant due to lack of pressure stress, and were excluded from the previous PTS analyses. Figure 8.1 shows that the mean CPF does not decrease with increased break size. It indicates that thermal stress alone can cause RPV wall failure. NRC further assessed the CPF of 16 inches LOCA, and its mean CPF has the same magnitude as 8 inches LOCA. Figures 8.2 to 8.4 are the time histories of T_{dc}, P_{dc}, and h_{dc} of these scenarios, respectively.

Figure 8.1 shows that based on the specified material strength, the CPF is sensitive to break size when the break size is less than 8E-3 meter square (4 inches in diameter). The CPF increases three orders of magnitude when the break size increases from 2E-3 m^2 (2 inches in diameter) to 8E-3 m^2 (4 inches in diameter). The CPF increases less than an order of magnitude when the break size increases from 8E-3 m^2 (4 inches in diameter) to 3.2E-2 m^2 (8 inches in diameter). The T_{sen} trend is similar to the flipped mean CPF trend with a different scale.

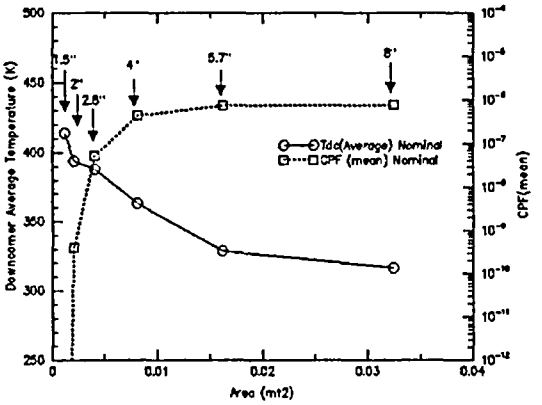

Figure 8.1 The T_{sat} and mean CPFs trends of varying sizes of LOCA for the Oconee NPP. The mean CPF is calculated by FAVOR based on the embrittlement map used in these analyses, corresponding to 60 effective full power years (EFPY). The high cold leg reversal flow resistances and sump recirculation are applied in these scenarios. The TH results are calculated by RELAP 5.

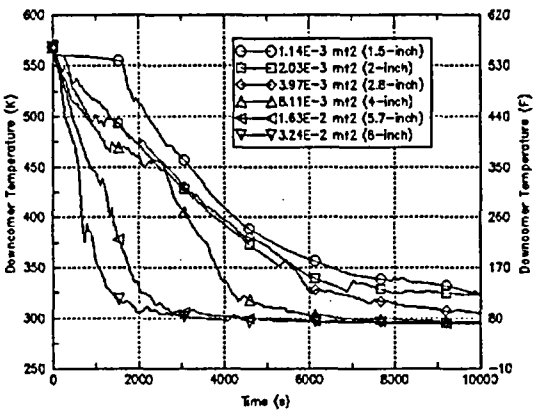

Figure 8.2 The time history of the T_{dc} of the nominal scenarios at different sizes of hot leg LOCA for the Oconee NPP.

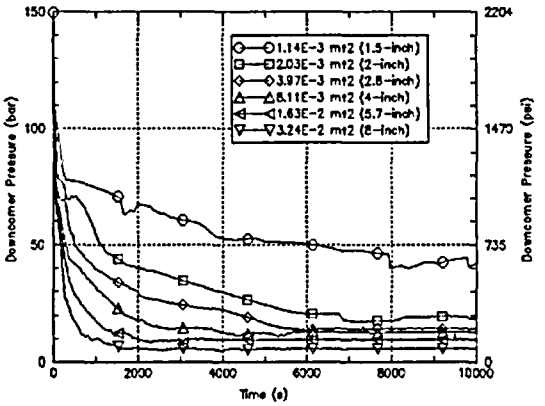

Figure 8.3 The time history of the T_{dc} of the nominal scenarios at different sizes of hot leg LOCA for the Oconee NPP.

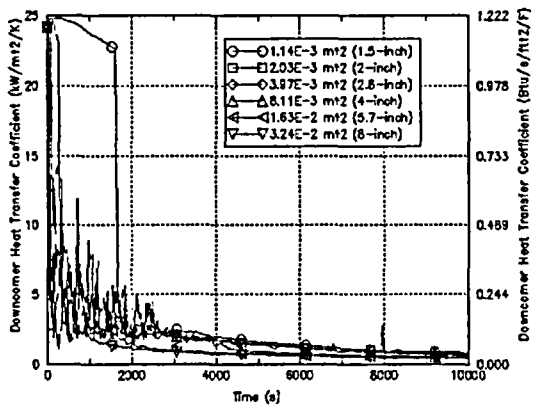

Figure 8.4 The time history of the downcomer heat transfer coefficient of the nominal scenarios at different sizes of hot leg LOCA for the Oconee NPP.

8.2.2 Sensitivities of HPI State and HPI Flow Rate

HPI is one of the important heat sinks, which provides negative heat source, in the early stage of LOCA. HPI injection is usually located at a cold leg a short distance upstream from the downcomer, thus its impact on T_{dc} is direct. In general, HPI failure would increase T_{sen}, especially for small LOCA, in which the high RCS pressure prevents the CFT and LPI from being activated.

Figure 8.5 shows the impact of HPI failure on T_{sen} and on CPF. Two sets of T_{sen} and CPF curves are shown in Figure 8.5. One set represents the nominal scenarios (the baseline scenarios without HPI failure). The other set represents HPI failed scenarios. The differences between the two curves are the sensitivity of HPI failure. It shows that, from a T_{sen} perspective, when the break size is greater than 1.6E-2 m^2 (5.7 inches in diameter), the HPI state has no impact. From a CPF perspective, the HPI state has no effect when

break size is greater than 8E-3 m^2 (4 inches in diameter). Figure 8.5 also shows that PTS risk is negligible if HPI failed at smaller than 4E-3m^2 (2.8 inches in diameter) LOCA and without operator actions.

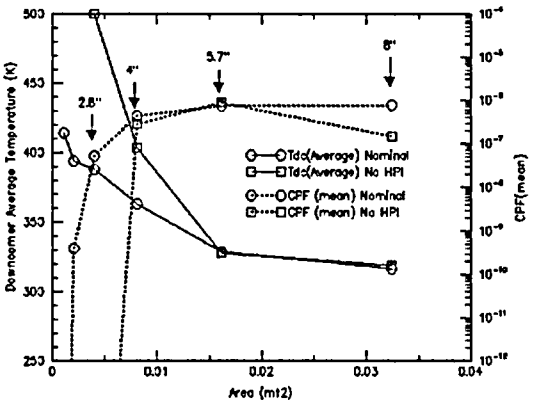

Figure 8.5 The impact of HPI state in T_{sen} and mean CPF. CPFs are calculated based on the embrittlement map used in these analyses, corresponding to 60 effective full power years (EFPY)

Figure 8.6 shows HPI partially failed (nominal, 25% failure, 50% failure, and 100% failure) affecting CPF in the small LOCA region. It shows that, for smaller than 4E-3 m^2 (2.8 inches in diameter) surge line LOCA, reducing 50% HPI flow rate could reduce CPF by two orders of magnitude.

Except for the uncertainty of HPI function state (success, fail on demand, or fail during operation), in this report, 10% flow rate uncertainty is used to represent the uncertainty of modeling of the flow rate. For Oconee NPP, as shown in Figure 8.6, reducing 25% HPI flow rate has little impact on PTS, thus the impact of reducing 10% HPI flow rate is negligible.

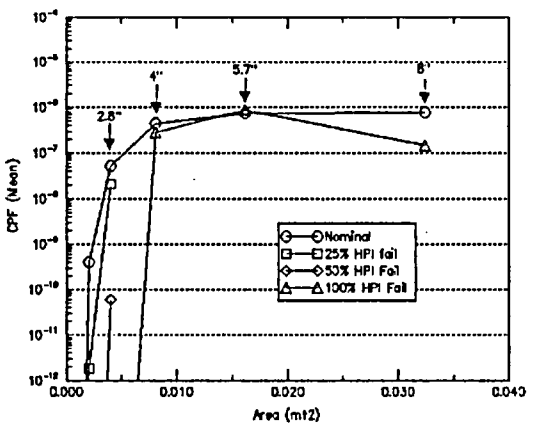

Figure 8.6 The HPI partial failure affect T_{sen} and mean CPF. The 100% HPI failure at break size equal to or less than 2.8 inches causes mean CPF equal to zero, based on the embrittlement map used in these analyses, corresponding to 60 effective full power years (EFPY)

8.2.3 Sensitivity of Decay Heat

Decay heat is the major heat source after RCPs are tripped. Reduction of decay heat would reduce RCS temperature, thus the low decay heat (or hot zero power (HZP)) is expected to increase CPF. Figure 8.7 shows mixed results. At 1.6E-2 m^2 (5.7 inches in diameter) LOCA, instead of increasing CPF the low decay heat decreases CPF more than an order of magnitude. Examining such a difference could provide insight to the relationship between TH and PFM. Figures 8.8 to 8.10 show the time history of the T_{dc}, P_{dc}, and h_{dc} of the two scenarios, low decay heat and full power operations, for 1.6E-2 m^2 (5.7 inches in diameter) LOCA. It shows that, from the TH perspective, it's difficult to explain the CPF results based on the three parameters' trends. The PFM results suggest that the timing of the T_{dc}, both value and rate of change (T_{dc} and dT_{dc}/dt), are important in determining CPF. Since such a combined effect is RPV wall strength dependent, it's beyond the TH scope.

At 1E-3 m^2 (1.5 inches in diameter) LOCA, low decay heat and HPI prevent RCS from loss of subcooling. As a result, RCPs are not tripped. RCPs generate 22 MW energy and circulate RCS coolant that the scenario is not PTS concern.

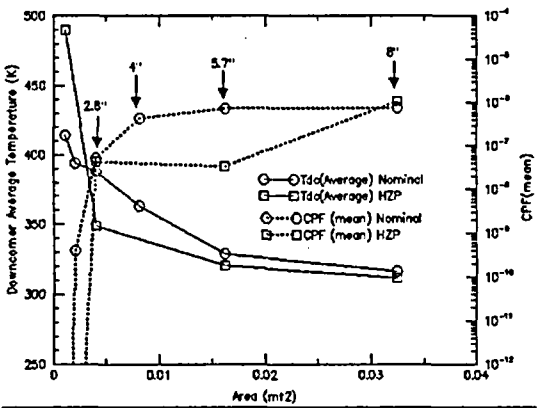

Figure 8.7 The decay heat impact on T_{sen} and mean CPF for the Oconee NPP, based on the embrittlement map used in these analyses, corresponding to 60 effective full power years (EFPY)

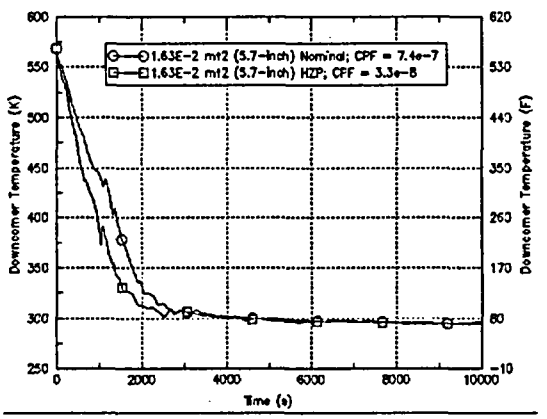

Figure 8.8 The comparison of the T_{dc} time histories of 1.6E-2 m^2 (5.7 inches in diameter) surge line LOCA during full power operation and low decay heat operation for the Oconee NPP.

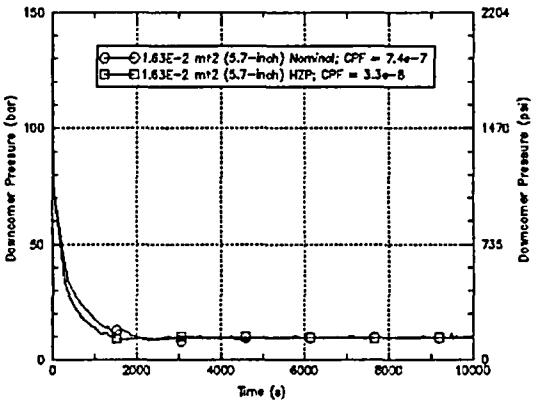

Figure 8.9 The comparison of the P_{dc} time histories of 1.6E-2 m^2 (5.7 inches in diameter) surge line LOCA during full power operation and low decay heat operation for the Oconee NPP.

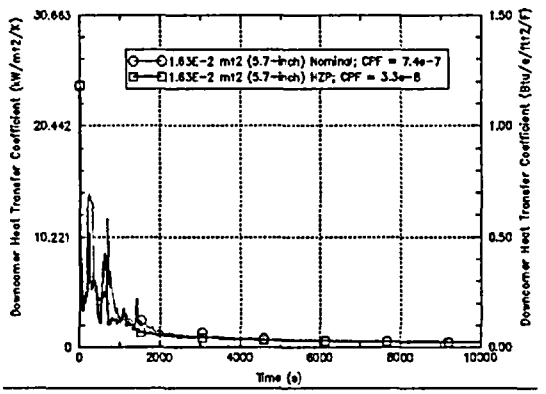

Figure 8.10 The comparison of the h_{dc} time histories of 1.6E-2 m^2 (5.7 inches in diameter) surge line LOCA during full power operation and low decay heat operation for the Oconee NPP.

8.2.4 Sensitivity of Season

Season affects the HPI, CFT, and LPIs' coolant temperatures. The HPI and LPIs' water source is from the refueling water storage tank (RWST), which is located outside of the containment. Their temperatures are significantly dependent on the environmental temperature. The CFTs are located inside the containment, and their temperature is less dependent on the environmental temperature. Nevertheless, the CFT temperature is dependent on season. The continuous temperature distributions are represented by three sets of representative seasonal temperatures as shown in Table 8.2.

Table 8.2 The coolant temperature of the emergency core cooling system at different seasons.

Season / System	Spring/Fall °C (°F)	Summer °C (°F)	Winter °C (°F)
HPI	21.1 (70)	29.4 (85)	4.4 (40)
CFT	26.7 (80)	38.8 (100)	21.1 (70)
LPI	21.1 (70)	29.4 (85)	4.4 (40)

Figure 8.11shows the seasonal impact on T_{sen} and on mean CPF. It shows that winter, spring/fall and summer have the T_{sen} in sequence from the lowest to the highest as expected. The trends of mean CPF in summer and in spring/fall are consistent with the T_{sen} trends. However, Figure 8.11 shows that the mean CPF of winter is lower than that of spring/fall at the break sizes of 1.6E-2 m^2 (5.7 inches in diameter) and 3.2E-2 m^2 (8 inches in diameter). It conflicts with the T_{sen} trends of spring/fall and winter.

Figures 8.12 to 8.15 compare the T_{dc} and P_{dc} of the questionable scenarios with the reference scenarios. Figures 8.12 and 8.13 are the T_{dc} and P_{dc} comparisons of the 1.6E-2 m^2 (5.7 inches in diameter) scenario. Figures 8.14 and 8.15 are the comparisons of the 3.2E-2m^2 (8 inches in diameter) scenario. The comparisons show that the CPF results can hardly be explained from the TH perspective. It requires the knowledge of PFM for more detailed analysis. On the other hand, from the perspective of PTS interest, the mean CPFs are at the order of 1E-7, which might be too small to be PTS interest. Explaining the results might not be necessary.

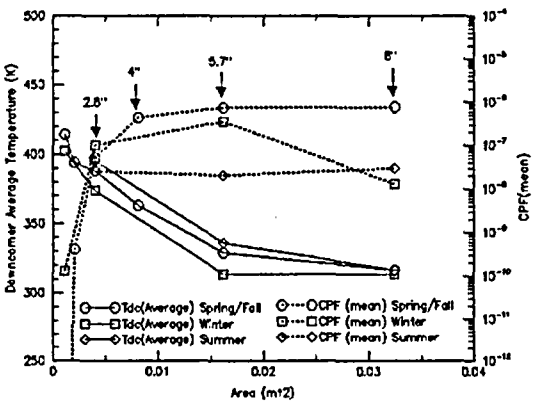

Figure 8.11 Winter impacts on T_{sen} and mean CPF, based on the embrittlement map used in these analyses, corresponding to 60 effective full power years (EFPY)

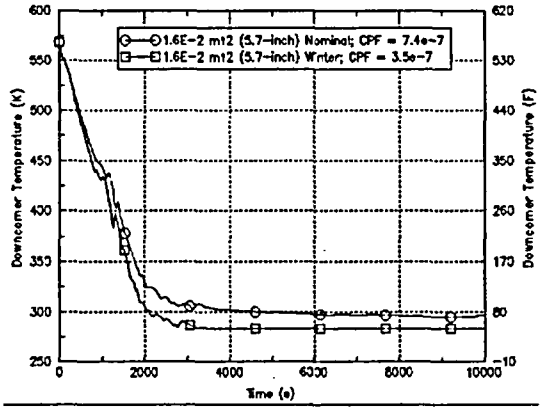

Figure 8.12 The comparison of the T_{dc} time histories of 1.6E-2 m^2 (5.7 inches in diameter) surge line LOCA occurring in spring/fall and winter for the Oconee NPP

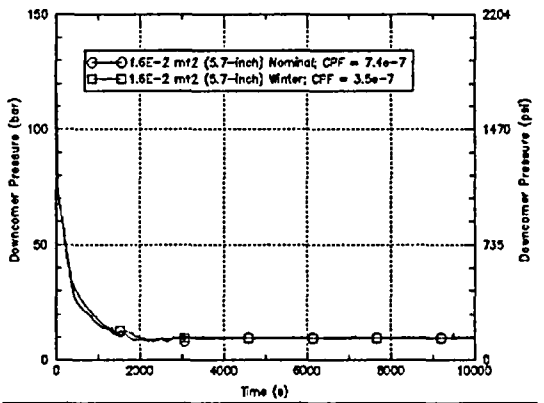

Figure 8.13 The comparison of the P_{dc} time histories of 1.6E-2 m^2 (5.7 inches in diameter) surge line LOCA occurring in spring/fall and winter for the Oconee NPP.

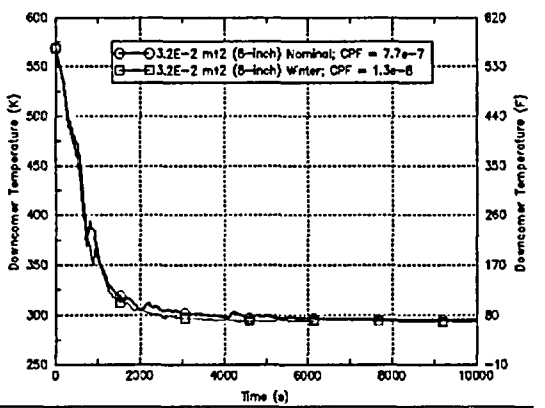

Figure 8.14 The comparison of the T_{dc} time histories of the 3.2E-2 m^2 (8 inches in diameter) surge line LOCA occurring in spring/fall and winter for the Oconee NPP. The LPI temperature of the winter scenario was mistakenly using the spring/fall temperature that resulted in a final temperature 70 °F

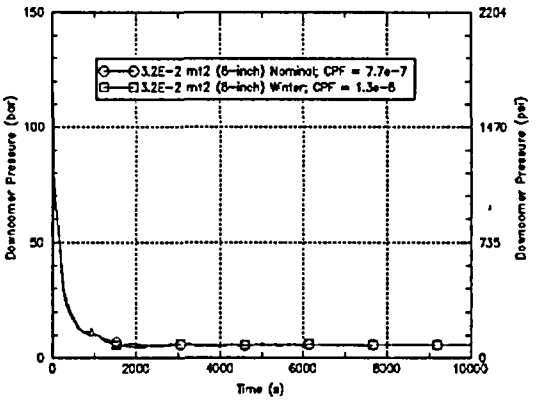

Figure 8.15 The comparison of the P_{dc} time histories of the 3.2E-2 m^2 (8 inches in diameter) surge line LOCA occurring in spring/fall and winter of the Oconee NPP.

8.2.5 Sensitivity of Break Location

Break location is divided into two sections: hot leg section and cold leg section (or before and after the SGs). When the location is at cold leg, the coolant in the RPV could flow from core to downcomer and increase the T_{dc}. Thus, cold leg LOCA is expected to have higher T_{dc} and smaller CPF than hot leg LOCA at the same break size. Figure 8.16 shows that both T_{scn} and mean CPF trends are as expected. It also shows the consistency between the two trends, meaning that lower T_{scn} would result in larger CPF, and a smaller difference in T_{scn} would result in a smaller difference in CPF.

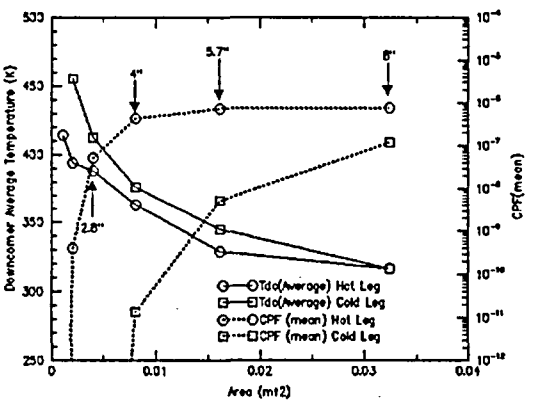

Figure 8.16 Break location impacts on mean CPF for the T_{scn} and Oconee NPP, based on the embrittlement map used in these analyses, corresponding to 60 EFPY.

8.2.6 Sensitivity of RPV Vent Valves States

RVP vent valves (RVVVs) are flapper type valves attached to the outside of the core barrel at the elevation just above the hot leg and cold leg entrances. Eight vent valves with a total open area of 0.8 square meters are in the RPV. In normal operating conditions they are closed. When the core-to-downcomer pressure differential is

reversed, the RVVVs open allowing hot water and/or steam to pass directly into the upper region of the downcomer. This would increase the T_{dc} and decrease CPF. The sensitivity of the RVVV state is assessed at two sizes of LOCA: 4E-3 m^2 (2.8 inches in diameter) and 8E-3 m^2 (4 inches in diameter). It's expected that an RVVV's state has an insignificant effect on CPF when the LOCA size is greater than 8E-3 m^2 (4 inches in diameter).

Figure 8.17 shows that opening RVVVs increases T_{sen}, and closing RVVVs reduces T_{sen}. In this sensitivity study, the opening and closing of the RVVVs occurs at the beginning of the scenarios, and RVVVs remain in the same state till the end of the sequences. Results show that both RVVVs opening and closing reduce CPFs, compared to the nominal sequence. The T_{dc} and P_{dc} trends of the different RVVV states at two different LOCA sizes are shown in Figures 8.18 to 8.21.

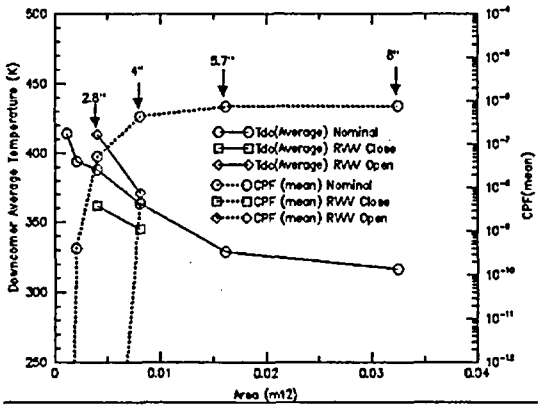

Figure 8.17 RPV vent valve state's impact on T_{sen} and mean CPF for the Oconee NPP, based on the embrittlement map used in these analyses, corresponding to 60 EFPY. The mean CPFs of the RVVV close scenarios are zero.

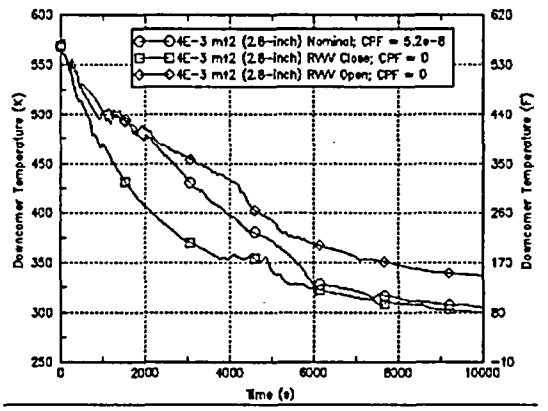

Figure 8.18 The comparison of the T_{dc} time histories of the 4E-3 m^2 (2.8 inches in diameter) surge line LOCA of three different states of RPV vent valves.

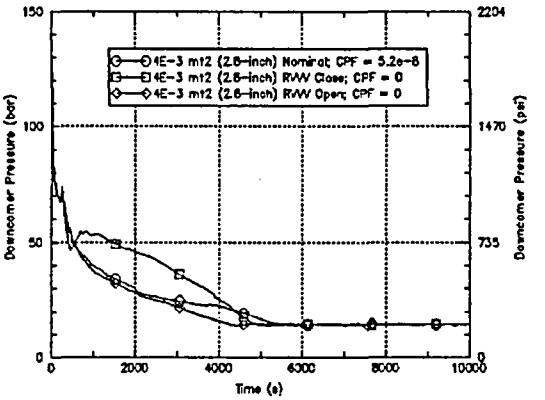

Figure 8.19 The comparison of the P_{dc} time histories of 4E-3 m^2 (2.8 inches in diameter) surge line LOCA of three different states of RPV vent valves.

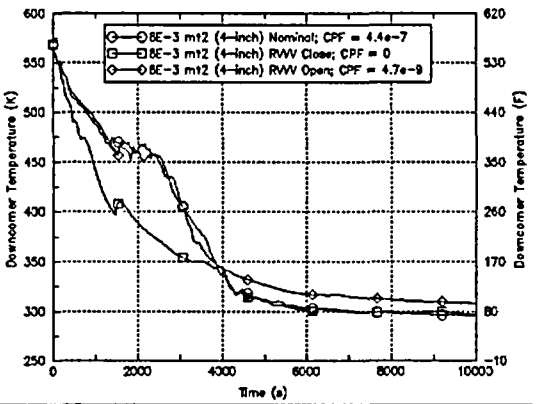

Figure 8.20 The comparison of the T_{dc} time histories of 8E-3 m^2 (4 inches in diameter) surge line LOCA of three different states of RPV vent valves.

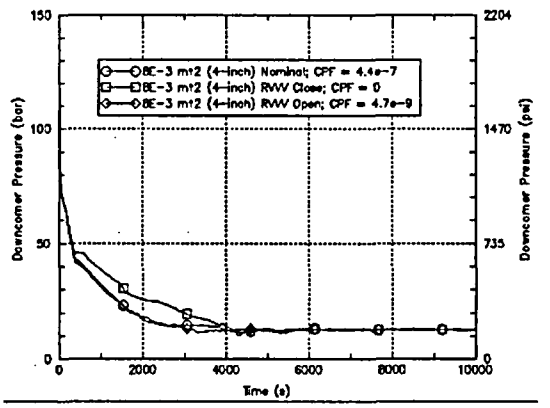

Figure 8.21 The comparison of the P_{dc} time histories of the 8E-3 m^2 (4 inches in diameter) surge line LOCA of three different states of RPV vent valves.

8.2.7 Component Heat Transfer Coefficient Effect

The component heat transfer coefficient (CHTC) affects the heat transfer rate between RCS coolant and the system structure. Before the initiating event, the RCS coolant and system structure are at a heat balance. After the initiating event, the coolant temperature rapidly decreases increasing the heat transfer rate from the system structure to the coolant. A larger CHTC would increase the heat flux. In the sensitivity assessment, plus and minus 30 percent of the nominal heat transfer coefficient is used to represent the upper and lower bounds. Since the CHTC is calculated by RELAP5 based on the dynamics of convection and conduction heat transfer coefficients, it requires changing the RELAP5 source code to assess the CHTC effect directly. That is very troublesome. Instead, changing the components' heat transfer areas is used as an alternative for simulating CHTC effect.

It's expected that a larger CHTC would increase the heat flow from the structure to the RCS coolant, causing a faster decrease in structure temperature thus a larger CPF. However, the FAVOR calculation takes inputs from the coolant instead of from the structure (T_{dc} and h_{dc} instead of RPV wall temperature) to calculate CPFs, which would generate inverse results since larger CHTC results in higher T_{dc} thus smaller CPF. Using the indirect indication inputs could cause misinterpretation of the results. Figure 8.22 shows the effect of CHTC.

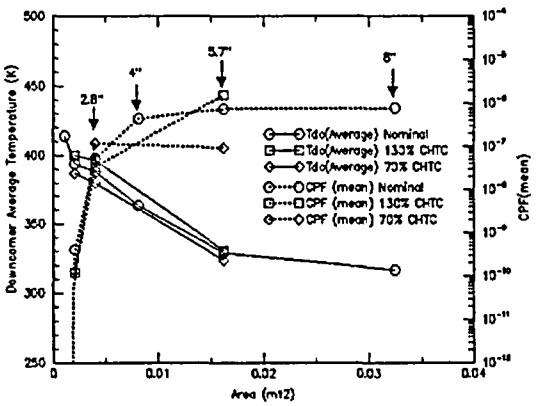

Figure 8.22 Impact of a 30% increase of component heat transfer coefficient on T_{sen} and mean CPF for the Oconee NPP, based on the embrittlement map used in these analyses, corresponding to 60 EFPY.

8.2.8 Intra-Loop Recirculation Flow Effect

The intra-loop recirculation flow is caused by RELAP5 numerical errors (see discussion in chapter 6). The recirculation flow causes the coolant in a cold leg to be reheated at the lower SG plume, and the heated coolant flows to the downcomer through the other cold leg. Thus, intra-loop flow recirculation is expected to increase the T_{sen} and to reduce the CPF. The recirculation flow can be stopped by applying large RCP reverse flow coefficients (High K). Figure 8.15 shows the intra-loop recirculation effect on T_{sen} and CPF. The trends are as expected.

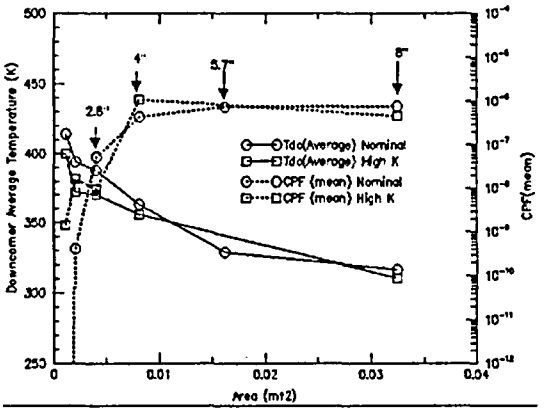

Figure 8.23 Intra-loop recirculation flow impacts on T_{sat} and mean CPF, based on the embrittlement map used in these analyses, corresponding to 60 effective full power years (EFPY)

8.2.9 Sensitivities of PZR SRV Reseat Timing and HPI Throttling Timing

Sections 8.2.1 to 8.2.8 discuss the key parameters relevant to the scenarios in which the primary system breach can not be isolated. For the scenarios with isolable primary system breach, such as PZR SRV stuck open scenarios, additional factors need to be considered, including the time lapse of breach isolation and the time lapse of isolating HPI. Since these two factors are dependent, their effects need to be discussed together.

Figures 8.25 and 8.26 compares the CPFs due to the combined effect of the PZR SRV reseating time (50 and 100 minutes) and the HPI throttling timing of events occurring during full power and low decay heat operations, respectively. The results show some insights. First, early valve reseating could reduce PTS significantly, especially for the SRV stuck open during low decay heat operation scenarios. Reseating SRV in less than 50 minutes could significantly reduce PTS risk. Second, early (less than 10 minutes) HPI throttling could reduce CPF by more than two orders of magnitude. Third, if HPI is not throttled before 10 minutes after it can first be throttled, the timing of throttling has little effect on CPF. The HPI throttling criteria is based on the operating area. Second, early (within several minutes) throttling HPI could also reduce CPF by a magnitude of a couple orders. However, the HPI throttle timing become unimportant if the HPI is not throttled within 10 minutes.

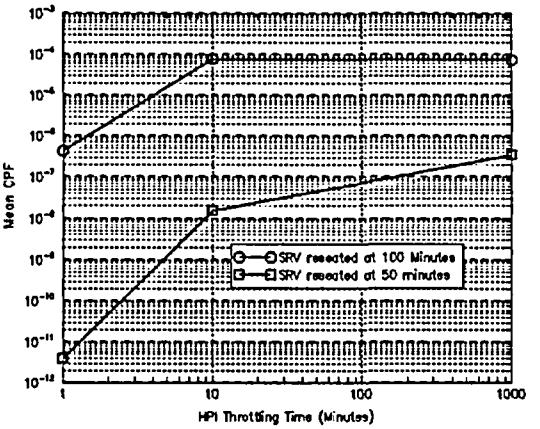

Figure 8.24 The mean CPFs of varying PZR SRV reseating times and HPI throttling times for the initiating event occurring during full power operation.

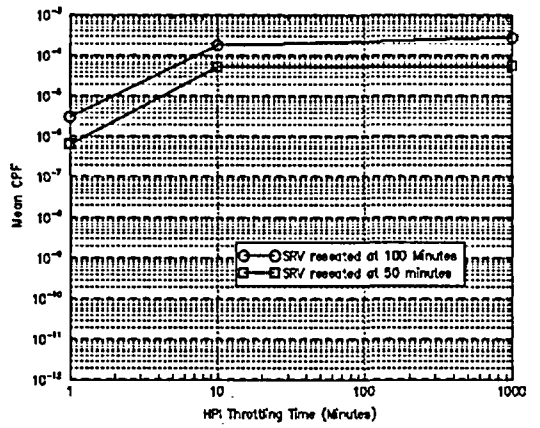

Figure 8.25 The mean CPFs of varying PZR SRV reseating times and HPI throttling times for the initiating event occurring during low decay heat operation.

8.3 Parameters Ranking

Section 8.2 discusses different parameters' sensitivities that can be used for parameters' importance ranking. Figures 8.26 to 8.29 compare the key parameter sensitivity in T_{sen} and mean CPF at different LOCA sizes for the Occonee-1 NPP. Figures 8.30 to 8.33 are Beaver valley results. The table on the right hand side of each figure ranks the parameter importance based on T_{sen}. Figures 8.26 to 8.33 show that the trends of T_{sen} and mean CPF are not consistent with each other for fixed break size, which is in contrast with the trends seen in Section 8.2. They show generally good consistency of the T_{sen} and mean CPF trends for a fixed parameter at different break sizes.

Some observations are discussed. First, trends of T_{sen} and CPF show coherence when the break size is large LOCA (e.g., at 1.6 m^2/5.7 inch and 3.2m^2/8 inch LOCAs). The incoherence occurs at small LOCA (e.g., 4E-3m^2/2.8-inch and 8E-3m^2/4-inch LOCAs). In small LOCA scenarios, the pressure effect might not be negligible, since the use of

T_{sen} assumes that the pressure effect in the same event category is constant. Second, T_{sen} is calculated based on the averaged T_{dc} for a long period of time (10,000 seconds). It does not provide sufficient resolution to reflect the differences. Third, uncertainty of FAVOR code might contribute to the inconsistency.

In the FAVOR code, $T_{dc}(t)$ and $dT_{dc}(t)/dt$ are used for CPF calculation. Figure 8.34 plots the minimum T_{dc} against CPF of all Oconee sensitivity study scenarios. It shows the trend that scenarios with minimum lowest-T_{dc} usually have larger CPF; however, this statement is not always true. Figures 8.35 and 8.36 plot the lowest $dT_{dc}(t)/dt$ against CPF in 5 minute and in 10 minute time intervals after T_{dc} is below 422 °K (300 °F). They show that, in general, rapid T_{dc} decrease is not good but there is no significant relationship. The timing effect of T_{dc} and dT_{dc}/dt is another important factor. Certainly it is also dependent on material toughness and flaws distribution. It seems that except for running FAVOR code, there is no simple way to predict the CPF of a scenario with required accuracy. Figure 8.37 shows that Oconee, Beaver Valley, and Palisade have similar but not exactly identical trends for the CPF against the LOCA size. The Palisade NPP has its maximum CPF at about 8E-3 m^2 (4 inches in diameter). Beaver Valley tends to have its maximum CPF at larger than 3.2E-2m^2(8 inches in diameter). Oconee seems to have its maximum CPF between 8E-3m^2 and 3.2E-2m^2 (4 and 8 inches in diameter). This indicates that uncertainty in material related plant specifics has significant contribution to PTS risk.

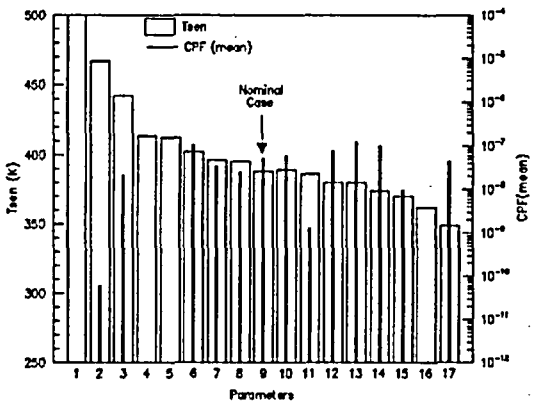

Figure 8.26 The plot of T_{sen} against mean CPF of the key parameters of the Oconee-1 NPP 2.8-inch LOCA.

1 100% HPI failure
2 50% HPI failure
3 25%HPI failure
4 RVVVs Open
5 Cold Leg LOCA
6 90%m(HPI)
7 130% CHTC
8 Summer
9 Nominal
10 p(CFT)-=50 psi
11 p(CFT)+=50 psi
12 110%(mHPI)
13 70% CHTC
14 winter
15 Hi K
16 RVVVs Close
17 low decay heat

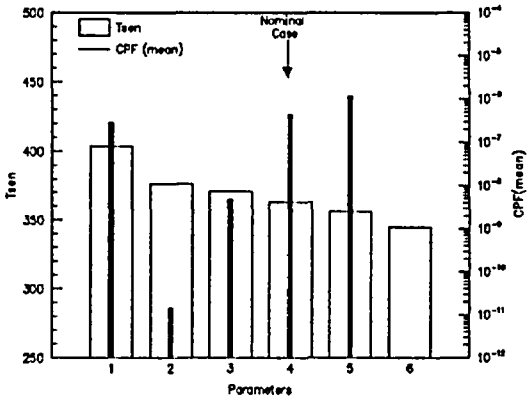

Figure 8.27 The plot of T_{sen} against mean CPF of the key parameters of the Oconee-1 NPP 4-inch LOCA

1 100% HPI Failure
2 CL LOCA
3 VV Open
4 Nominal
5 Hi K
6 VV Close

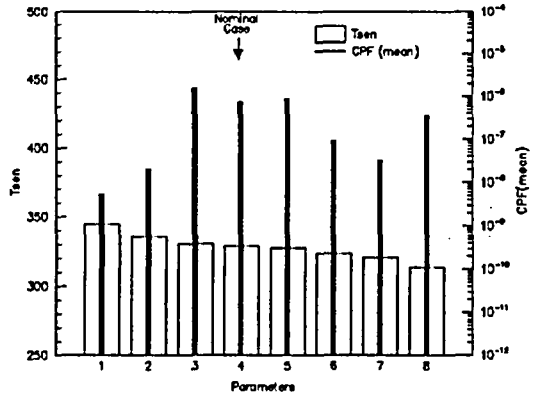

Figure 8.28 The plot of T_{sen} against mean CPF of the key parameters of the Oconee-1 NPP 5.7-inch LOCA.

1 Cold Leg LOCA
2 summer
3 130% CHTC
4 Nominal
5 100% HPI failure
6 70% CHTC
7 low decay heat
8 Winter

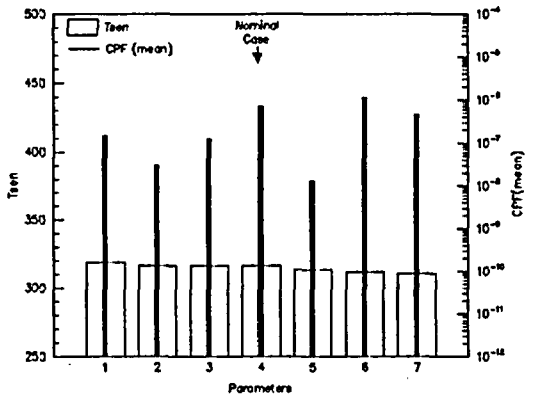

1 100% HPI failure
2 summer
3 Cold Leg LOCA
4 Nominal
5 winter
6 low decay heat
7 High K

Figure 8.29 The plot of T_{sen} against mean CPF of the key parameters of the Oconee-1 NPP 8-inch LOCA.

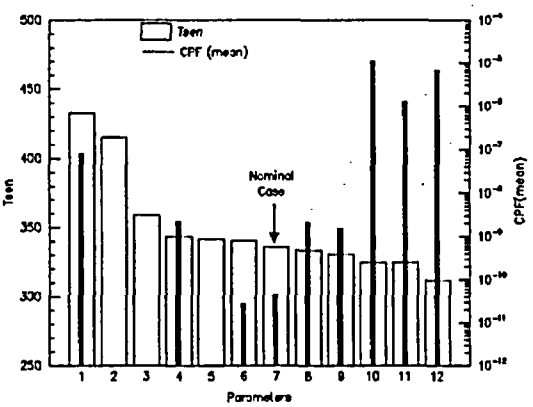

1 100% HPI failure
2 Cold Leg LOCA
3 70% Break Area
4 summer
5 130% CHTC
6 90%m(HPI)
7 Nominal
8 110%(mHPI)
9 70% CHTC
10 130% Break Area low decay
11 heat(.7%) low decay
12 heat(.2%)

Figure 8.30 The plot of T_{sen} against mean CPF of the key parameters of the Beaver Valley NPP 2.8-inch LOCA

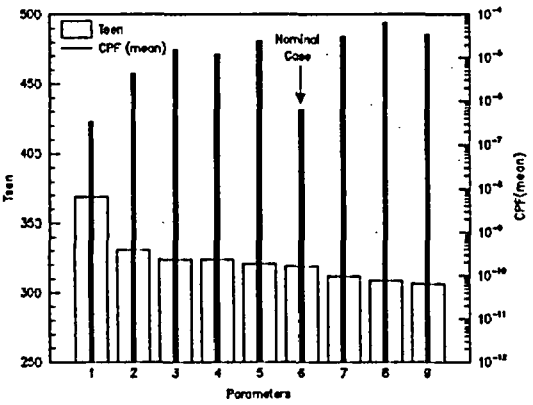

1 Cold Leg LOCA
2 summer
3 70% Break Area
4 130% CHTC
5 70% CHTC
6 Nominal low decay
7 heat(.7%) low decay
8 heat(.2%)
9 130% Break Area

Figure 8.31 The plot of T_{sen} against mean CPF of the key parameters of the Beaver Valley NPP 4-inch LOCA

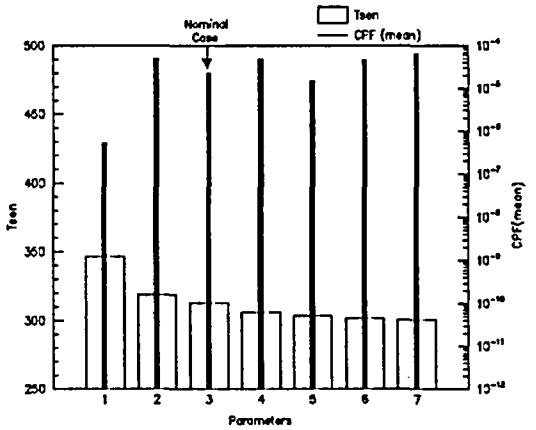

1 CL LOCA
2 summer
3 Nominal
4 70% Break Area
5 low decay heat(.7%)
6 low decay heat(.2%)
7 130% Break Area

Figure 8.32 The plot of T_{sen} against mean CPF of the key parameters of the Beaver Valley NPP 5.7-inch LOCA

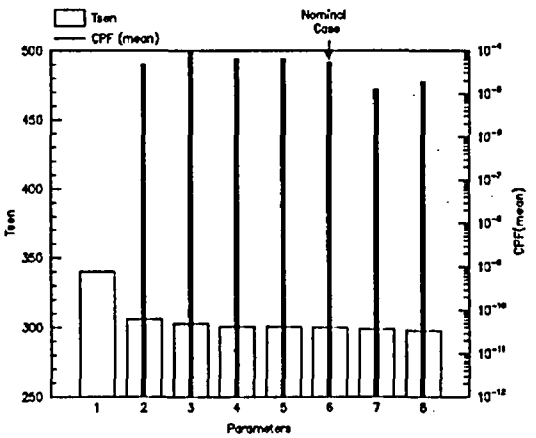

1 CL LOCA
2 70% Break Area
3 summer
4 130% CHTC
5 130% Break Area
6 Nominal
7 low decay heat(.7%)
8 low decay heat(.2%)

Figure 8.33 The plot of T_{sen} against mean CPF of the key parameters of the Beaver Valley NPP 8-inch LOCA

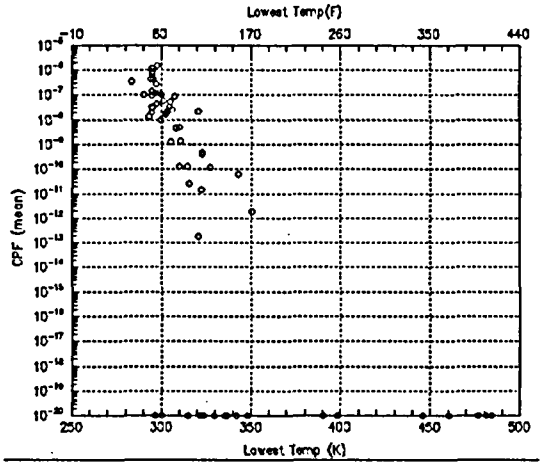

Figure 8.34 The plot of lowest Tdc against the CPF of the sensitivity study scenarios of the Occonee-1 NPP.

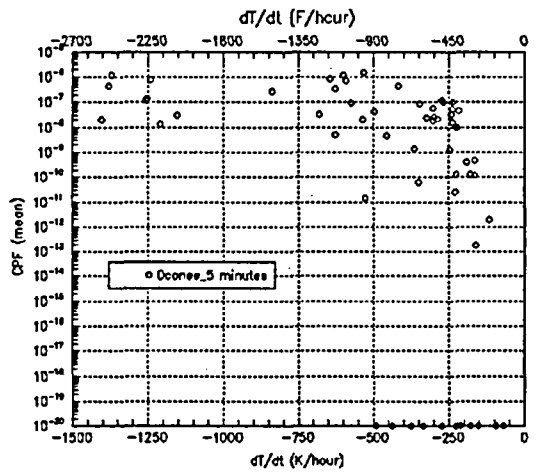

Figure 8.35 The plot of the lowest dT_{dc}/dt against CPF of the sensitivity study scenarios of the Occonee-1 NPP. The data is calculated when Tdc is less than 422 °K (300 °F) and the calculating time interval is five minutes.

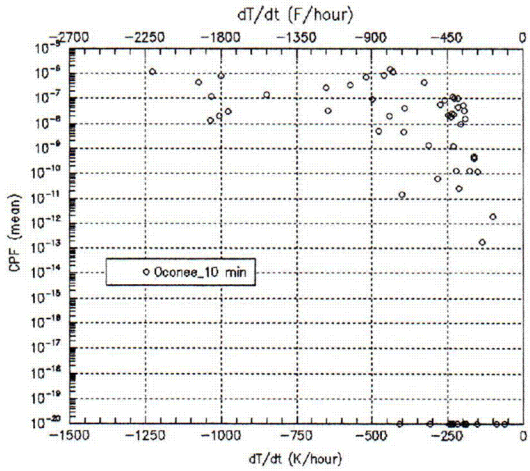

Figure 8.36 The plot of the lowest dT_{dc}/dt against CPF of the sensitivity study scenarios of the Occonee-1 NPP. The data is calculated when Tdc is less than 422 °K (300 °F) and the calculating time interval is ten minutes.

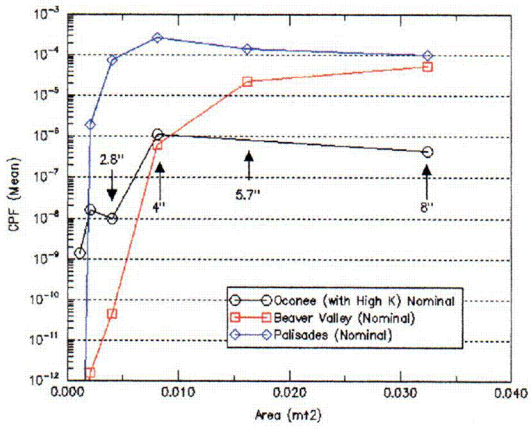

Figure 8.37 The plot of CPF against LOCA size at surge line for the Oconee, Beaver, and Palisade NPPs.

References

Almenas K., K.M. diMarzo, Z. Wang, and Y.Y. Hsu "The Phenomenology of a Small Break LOCA in a Complex Thermal Hydraulic Loop", Nuclear. Engineering & Design, vol 110, pp. 107-116 (1988)

Arcieri, W. C., R. M. Beaton, T. M. Lee and D. Bessette (2001). RELAP5 Thermal Hydraulic Analysis to Support PTS Evaluations for the Oconee-1 Nuclear Power Plant. Washington DC, U.S. Nuclear Regulatory Commission. NUREG/CR-XXXX

Bass, B. R., C. E. Pugh, J. Sievers and H. Schulz (1999). International Comparative Assessment Study of Pressurized Thermal Shock in Reactor Pressure Vessels. Washington d.C., U.S. Nuclear Regulatory Commission. NUREG/CR-6651

Boyack, B. E., I. Catton, R. B. Duffey, P. Griffith, K. R. Katsma, G. S. Lellouche, S. Levy, U. S. Rohatgi, G. E. Wilson, W. Wuleff and N. Zuber (1990). "Quantifying Reactor Safety Margins Part1: An Overview of the Code Scaling, Applicability, and Uncertainty Evaluation Methodology." Nuclear Engineering and Design **119**: 1-15.

Boyd, C. F. and T. Dickson (1999). Impact of the Heat Transfer Coefficient on Pressurized Thermal Shock, U.S. Nuclear Regulatory Commission. NUREG-1667

Burns, T. J., R. D. Cheverton, G. F. Flanagan, J. D. White, D. G. Ball, L. B. Lamonica and R. Olson (1986). Preliminary development of an Integrated Approach to the Evaluation of Pressurized Thermal Shock as Applied to the Oconee Unit 1 Nuclear Power Plant. Washington D.C., U.S. Nuclear Regulatory Commission. NUREG/CR-3770

Cullen, A. C. and H. C. Frey (1999). Probabilistic Techniques in Exposure Assessment. New York, Plenum Press.

Determan, J. C. and C. E. Hendrix (1991). Development of a SCDAP/RELAP5/MOD3 Model of Oconee 1 for Use With The Nuclear Plant Analyzer. Idaho Falls, EG&E Idaho. EGG-EAST_9793

Dickson, T. L., R. D. Cheverton, J. W. Bryson and B. R. Bass (1993). Pressurized Thermal Shock probabilistic Fracture Mechanics Sensitivity Analysis for Yankee Rowe Reactor Pressure Vessel. Washington DC, U.S. Nuclear Regulatory Commission. NUREG/CR-5782, August 1993

Frey, H. C. and S. R. Patil (2002). "Identification and Review of Sensitivity Analysis Methods." Risk Analysis **22**(3): 553-578.

Hanson, D. J., O. R. Meyer, H. S. Blackman, W. R. Nelson and B. P. Hallbert (1987). Evaluation of Operational Safety at Babcock and Wilcox Plants. Volumes 1&2. Washington D.C., U.S. Nuclear Regulatory Commission. NUREG/CR-4966

Henry, R. E. and H. K. Fauske (1971). "The Two-Phase Critical Flow of One Component Mixtures in Nozzles, Orifices and Steam Tubes." Journal of Heat Transfer **93**: 724-737.

Ikonen, K. (1995). Shallow crack effect on brittle fracture of RPV during pressurized thermal shock, Finnish Centre for Radiation and Nuclear Safety, Helsinki. STUK-YTO-TR-98; DE97616026

Mahaffy, J. H. (1981). "A Stability Enhancing Two-P\Step Method for Fluid Flow Calculations." Journal of Computational Physics **40**: 329-341.

Palmorse, D. (1999). Demonstration of Pressurized Thermal Shock Thermal-Hydraulic Analysis with Uncertainty. Washington DC, U.S. Nuclear Regulatory Commission. NUREG/CR-5452, March 1999

Pugh, C. E. and B. R. Bass (2001). Review of Large-Scale Fracture Experiments Relevant to Pressure Vessel Integrity Under Pressurized Thermal Shock Conditions. Washington DC, U.S. Nuclear Regulatory Commission. NUREG/CR-6699, January 2001

Queral, C., J. Mulas and C. G. de la Rua (2000). Analysis of the RELAP5/M)D3.2.2beta Critical Flow Models and Assessment Against Critical Flow Data from the Marviken Tests. Washington DC, U.S. Nuclear Regulatory Commission. NUREG/IA-0186, July 2000

Quick, K. S. (1994). Oconee Unit 1 Pressurized Water Reactor RELAP5/MOD3 Input Model. Washington DC, U.S. Nuclear Regulatory Commission. DOC Contract No. DE-AC07-76IDO1570, August 1994

Ransom, V. H. and D. L. Hicks (1984). "Hyperbolic Two-Pressure Models for Two-Phase Flows." Journal of Computational Physics **53**: 124-151.

Ransom, V. H. and J. A. Trap (1980). The RELAP5 Chocked Flow Model and Application to a Large Scale Flow Test. ANS/ASME/NRC Int. Top. Meeting, Saratoga Springs, NY.

Riemke, R. and B. Johnsen (1994). The Recirculation flow Anomaly. Washington DC, U.S. Nuclear Regulatory Commission. NUREG-EAST-9365, January 1994

Rosdahl, O. and D. Caraher (1986). Assessment of RELAP5/MOD2 Against Critical Flow Data From Marvikken. Washington DC, U.S. Nuclear Regulatory Commission. NUREG/IA-0007, Setp. 1986

Rosenthal, J. (2001). Status of Thermal Hydraudic PTS Calculations, Internal Memorandum US Nuclear Regulatory Commission. August 20, 2001

Selby, D. L., D. G. Ball, R. D. Cheverton, G. F. Flanagan and P. N. Austin (1985). Pressurized Thermal Shock Evaluation of the H. B. Robinson Unit 2 Nuclear Power Plant. Washington DC, U.S. Nuclear Regulatory Commission. NUREG/CR-4183V, Sept 1985

Selby, D. L., D. G. Ball, R. D. Cheverton, G. F. Flanagan, W. T. Hensley, J. D. White, P. A. Austin, D. Bozarth, L. B. Lamonica, A. McBride, J. H. Jo, P. Gherson, K. Iyer, H. P. Nourbakhsh, T. G. Theofanous, P. Humphreys, L. D. Phillips, D. Embrey and L. S. Abbott (1984). Pressurized Thermal Shock Evaluation of the Calvert Cliffs Unit 1 Nuclear Power Plant (DRAFT). Washington DC. NUREG/CR-4022, October 9, 1984

Theofanous, T. G. and H. Yan (1991). Unified Interpretation of One-Fifth to Full Scale Thermal Mixing Experiments Related to Pressurized Thermal Shock. Washington D.C., U.S. Nuclear Regulatory Commission. NUREG/CR-5677

Wang, Z. and K. Almenas (1989). "A Methodology Quantifying the Range of Applicability of Scaling Laws." Nuclear Science & Engineering **102**(1): 101-113.

Wang Z., K. Almenas, M. diMarzo, Y.Y. Hsu and C. Unal. "Impact of Rapid Condensations of Large Vapor Spaces on Natural Circulation in Integral Systems", Nucl. Eng. & Des., Vol. 133, pp 285-300, (1992)

Weisman, J. and A. Tentner (1978). "Models for Estimation of Critical Flow in Two-Phase Systems." Proceedings of Nuclear Energy 2: 183-197.

Appendix A Uncertainty Characteristics and Classification

This Appendix discusses TH-based uncertainty characteristics and classifications. The mass and energy are the two essential parameters to classify PTS relevant phenomena. Section A.1 classifies uncertainty based on the uncertainty propagation mode. Three modes of uncertainty propagation are classified: damped, proportional, and augmented. The important PTS risk factor, RCS flow state, is classified based on the modes of uncertainty propagation. The RCS flow states include forced circulation, natural circulation, and flow stagnation. Section A.2 classifies RCS flow state based on the change of coolant inventory and energy inside RCS. Section A.3 discusses flow state at different percentages of RCS inventory loss for a LOCA scenario.

A.1 Characteristics of Uncertainty Propagation

The following sections discuss the uncertainty ranges of T_{dc} caused by the uncertainty of different parameters. Three types of the T_{dc} uncertainty behaviors are classified: **damped, proportional,** and **augmented** (Table A.1).

The most prevalent, (in terms of number of PRA determined scenarios and their probability) is the damped transformation mode. This is also the consequence of the dominant nature of $\dot{Q}_{sg}$. Basically, as long as the secondary side remains intact and natural or forced circulation is maintained, the TH conditions of the primary side will be determined by the conditions in the steam generators. Perturbations occurring in the primary side will then have little effect. For example, even large variations (on the order of factors of 2 or more) in the decay heat will, for this category of transients, produce minor variations in T_{dc}.

The proportional transformation mode is associated primarily with malfunctions on the secondary side. The energy removed by the steam generators, $\dot{Q}_{sg}$, is by far the dominant heat sink, and the uncertainty in its magnitude is transformed proportionally into uncertainties of T_{dc}. Another condition for which uncertainty is transmitted proportionally concerns the temperature difference between the fluid temperature at SG exit and the downcomer when HPI is operating, and RCPs are shut off. This difference is determined by the relative HPI and loop circulation flows. The uncertainties in these parameters therefore are reflected proportionally in the uncertainty of the temperature difference between $T_{SG\text{-}out}$ and T_{dc}.

Finally, there is the category of transients for which the uncertainties can be augmented. Phenomena that can cause this transformation mode are a two-phase fluid state in the primary and a possibility that flow stagnation can occur. The 'augmentation' is introduced by the uncertainty associated with flow stagnation, which, in turn, depends on the sizable uncertainties associated with the evaluation of two-phase choked flow. Sections A.1.1 to A.1.3 discuss the damped, proportional, and augmented uncertainty transmissions.

Transformation type	Conditions and Parameters
DAMPED $\delta BC \Rightarrow$ Plant Response $\Rightarrow \delta T_{dc}$	• When SGs remain intact, and natural or forced circulation is maintained => $\dot{Q}_{dec}$, $\dot{W}$&T_f of MFW, AFW, HPI flow & temp., SB LOCA flow
PROPORTIONAL $\delta BC \Rightarrow$ Plant Response $\Rightarrow \delta T_{dc}$	• When P_{sec} is NOT controlled => e.g., TBV flow area, and valves open timing and time lapse • When RCPs are OFF, and $\dot{Q}_{SG} \cong 0$ => HPI flow rate and temp.
AUGMENTED $\delta BC \Rightarrow$ Plant Response $\Rightarrow \delta T_{dc}$	• When primary side flow stagnation occurs =>Break flow rate, HPI flow rate and temp.

Table A.1 Classification of uncertainties according to their impact

A.1.1 Damped Uncertainty Transmission

The HPI-PORV feed-bleed transient is well suited to illustrate the response of the T_{dc} parameter for conditions when the primary system is liquid solid and the source/sink terms are reasonably well known. System pressure for this type of transient remains fixed at the PORV set-point pressure [for Oconee ~170 bar (2460 psia)]. At such a high pressure HPI flow is relatively low and is not able to remove the decay energy during the first ~6000 sec. The energy balance of the primary system is thus determined by two sources $\dot{Q}_{dec}$ and $\dot{Q}_{RCP}$ (when the RCPs are running) and by two sinks $\dot{Q}_{SG}$ and the negative enthalpy flow due to the HPI stream.

For this type of transient it is the energy source side of the balance equation that can vary over a wider range and is thus subject to a larger uncertainty. An illustration of this is shown in Figure A.1, which depicts four possible time transients of the total source. The uppermost curve represents $\dot{Q}_{dec}$ plus $\dot{Q}_{RCP}$, where the decay energy is evaluated after an effectively 'infinite' operation time at full power. This means that at the time the reactor trips, the decay products have reached an equilibrium condition. The second curve includes $\dot{Q}_{RCP}$ as before, but it is assumed that the reactor is tripped at hot zero power (HZP) and therefore the fission product buildup is still far from equilibrium. As shown, the difference in decay power generation is substantial; moreover, it increases with time after shut down. This is so because the shorter-lived fission products approach an equilibrium build-up faster than the longer lived ones. For the lower two curves it is assumed that the RCPs have been tripped, thus the heat source consists of $\dot{Q}_{dec}$ alone. As

Figure A.1 illustrates, the magnitude of the source varies significantly and for times longer than 1 hour, the difference between the limiting values can approach a factor of six. T_{dc} is determined by energy balance, thus it is appropriate to enquire what effect this large variation has on the downcomer temperature.

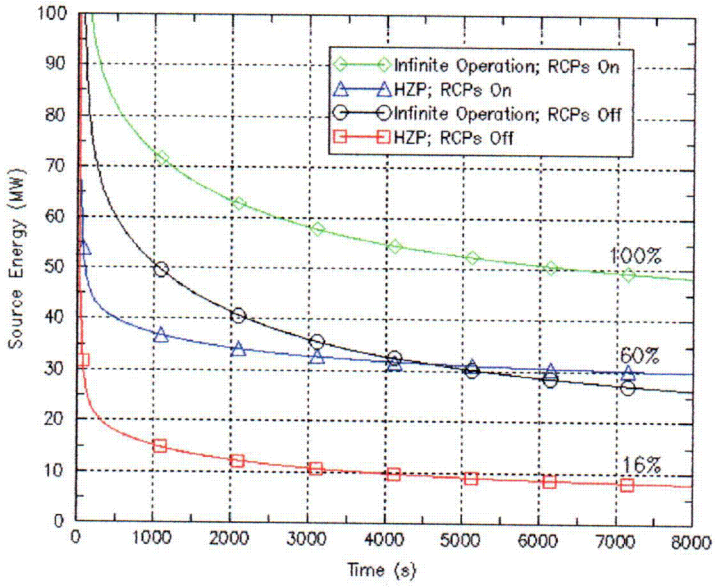

Figure A.1 Range of variation of energy source (decay heat + RCPs)

Note that in contrast to some other safety related parameters (e.g. the fuel temperature), for PTS studies the direction of a 'conservative' $\dot{Q}_{dec}$ is reversed. For PTS concerns it is a low $\dot{Q}_{dec}$ value, which, other conditions being comparable, leads to lower temperatures and thus to more severe PTS conditions. The magnitude of this influence is evaluated using RELAP5 for four nearly identical transients, in which the reactor trips without other system/component failure and no operators' actions take place. They differ only in the magnitude of the time dependent total energy source and RCPs' states. The results, as reflected in T_{dc}, are shown in Figure A.2 for the case where RCPs are operating and in Figure A.3 for the RCPs tripped condition.

In Figure A.2, the temperature scale is significantly expanded so that the low amplitude oscillation (on the order of 1 °K) is magnified. Even then the two curves in Figure A.2, that represent different sources, differences of up to 40% can hardly be distinguished. Similarly for the natural circulation transients depicted in Figure A.3, which are characterized by energy sources differing by more than a factor of 3, the resulting temperature difference is less than 3 °K.

C35

The meaning of the 'damped' uncertainty propagation mode is thus illustrated. This effect is produced by hugely over-designed SGs. From the SG point of view, the sources and sinks on the primary side could vary by almost an order of magnitude before the SG to primary temperature difference would increase appreciably. For PTS analysis this implies that as long as the SG conditions are controlled, they will determine the fluid conditions on the primary side. For such transients, TH and boiling condensation (BC) condition uncertainties will not influence the PTS relevant parameters and thus do not matter.

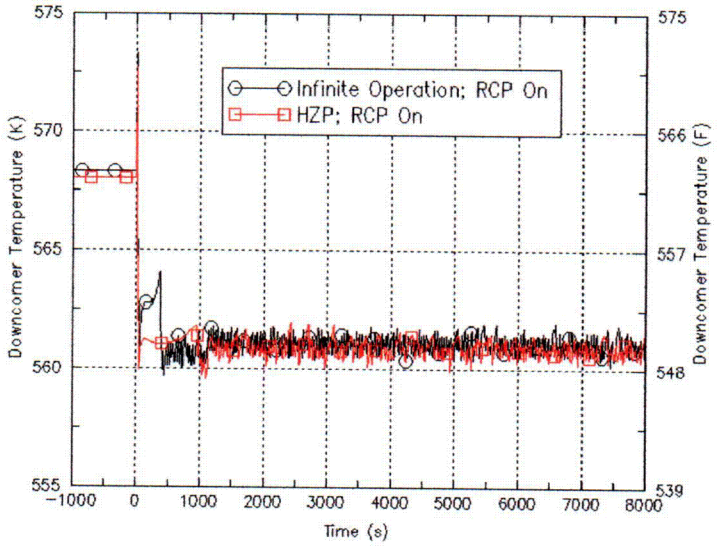

Figure A.2 T_{dc} traces for reactor is tripped after infinite time interval of operation and at hot zero power operation with RCPs operating

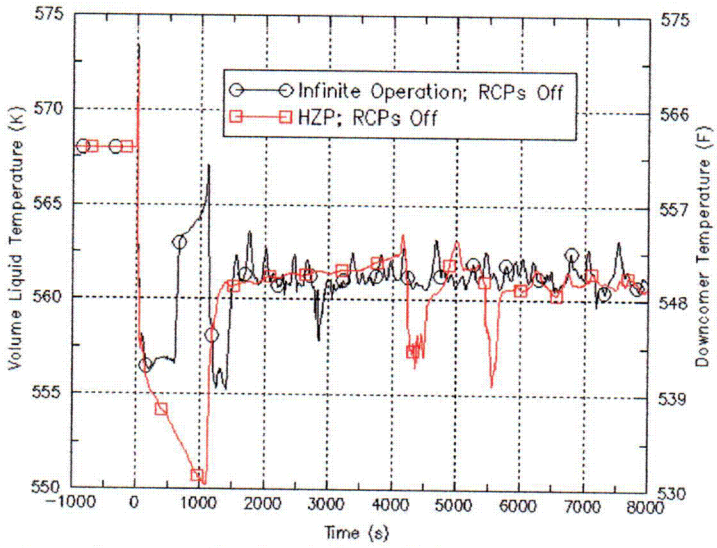

Figure A.3 T_{dc} traces for reactor is tripped after infinite time interval of operation and at hot zero power operation with RCPs tripped right after reactor trips

C36

A.1.2 Proportional Uncertainty Transmission

In order to avoid semantic confusion, it should be noted that in this study the term 'proportional' is employed to mean 'of a similar order of magnitude'. Specifically it implies that the uncertainty range of an independent variable (e.g. an imposed boundary condition like the flow area of a TBV) has an impact on the PTS relevant variables that is of a similar order of magnitude. Admittedly, this is not a precise definition, but, as shown by the examples, it is a useful one. In this sub-section it is illustrated by evaluating the effect that the failure of two TBVs (as compared to one TBV) has on the computed T_{dc} transient.

The chosen initiating event implies that for these transients $\dot{Q}_{sc}$ cannot be controlled. A reference to the uncertainty classification table (Table A.2) shows that the dominant parameters contributing to the uncertainty are A_{SG}, the un-controlled flow area from the SGs and $\dot{Q}_{dc}$ in the "parameter uncertainty" column, and the computed rate of mass and energy flow in the 'model' uncertainty column. Assuming the same $\dot{Q}_{dc}$ applies to both transients and that the 'model' uncertainty exerts an equivalent influence, the changes in the boundary conditions thus are reduced to a change in the flow area. For the first transient, representing two TBVs stuck open per SG, the total break area in the secondary side is 0.0622 m^2 (2 × 0.102 ft^2). The second transient, representing one TBV stuck open per SG, has half of the secondary side break area of the first transient's (0.0311 m^2). This is a larger relative change then will be encountered when considering the variations due to BC uncertainties and thus represents a severe test of the 'proportional' propagation concept.

For the transient in which a single TBV fails, the intact SG becomes an energy source and all of the energy must be ejected through the SG with the stuck open TBV. Figure A.4 shows that the pressures of both SGs (upper curve in the figure) closely track each other. This is an additional illustration of the exceptionally large heat transfer area that is available. As shown in Figure A.5, the downcomer temperatures in both cases closely follow the SG secondary side temperature. The fluid temperature difference in the downcomer caused by the change in SG outflow area is ~30 °K, and this difference remains remarkably constant for the time period from 2000 to 8000 seconds. The presented case study thus shows that a change of ~.031 m^2 in the outflow area produces a change of ~30 °K in T_{dc}.

The illustrative example establishes a proportionality relationship between the outflow area in an SG and the temperature in the downcomer, however, the units of the parameters in question are so different that the reasons for this are not immediately apparent. A qualitative explanation can be gained by again considering Figure A.4. A change in the outflow area of the SG increases the energy loss term of the SG vapor region, and since the energy source terms and the heat capacities for both cases are equivalent, this produces a proportional decrease in pressure. The SGs are at saturated conditions, thus the pressure change can be translated into a change in SG temperature. In Figure A.6 it is shown that the absolute value of the ΔT can be estimated along the saturation line. As shown, the inferred temperature change is ~30 °K. Since the primary

system temperature closely follows the secondary temperature and since for this transient HPI is not activated, this is close to the fluid temperature change in the downcomer.

Table A.2 Classification of PTS Relevant Transients Based on Propagation of Uncertainties

Event Category (Dominant Energy Sinks)	TH Propagation of Uncertainty	Circulation Mode	Dominant Factor Contributing to Uncertainty	
			Boundary Condition	Code Model
$\dot{Q}_{SG}$ – controlled (HPI-PORV)	T_{dc} - damped P - controlled	Forced Circulation	P_{sec} - T_{sec}	
$\dot{Q}_{SG}$ – controlled HPI-PORV	$T_{sg,ex}$. damped P - controlled $\Delta T_{SG\text{-}dc}$ proportional	Natural Circulation	$P_{sec} - T_{sec}$ $\dot{W}_{HPI}$, T_{HPI}	$\dot{W}_{circ}$
$\dot{Q}_{SG}$ – uncontrolled 1.-depressurized 2. - overcooled (HPI-PORV)	T_{dc} - proportional P - proportional $\Delta T_{SG\text{-}dc}$ proportional	Forced Circulation (Natural Circulation)	1) $A_{SG\text{-}flow}$, $\dot{Q}_{dc}$ 2) $\dot{W}_{fw}$, T_{fw}, $\dot{Q}_{dc}$ ($\dot{W}_{HPI}$, T_{HPI})	$\dot{W}_{brk}$, $\dot{Q}_{brk}$ $\dot{W}_{circ}$
$\dot{Q}_{SG}$ – not avail. $\dot{Q}_{brk} > \dot{Q}_{dc}$ HPI	T_{dc} - augmented P - proportional	Natural Circulation with potential flow stagnation	A_{brk}, $\dot{Q}_{dc}$, A_{vv} $\dot{W}_{HPI}$, T_{HPI}	$\dot{W}_{brk}$, $\dot{Q}_{brk}$ $\dot{W}_{vv}$

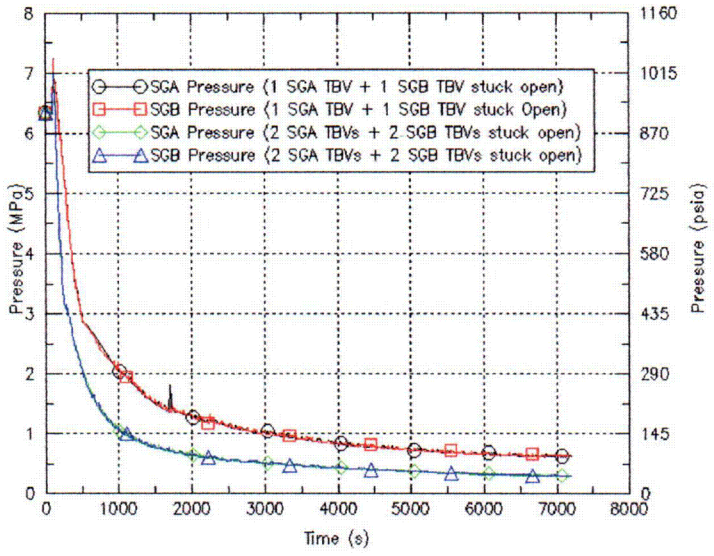

Figure A.4 The two SGs secondary side pressures for 2 and 1 TBVs stuck open per SG

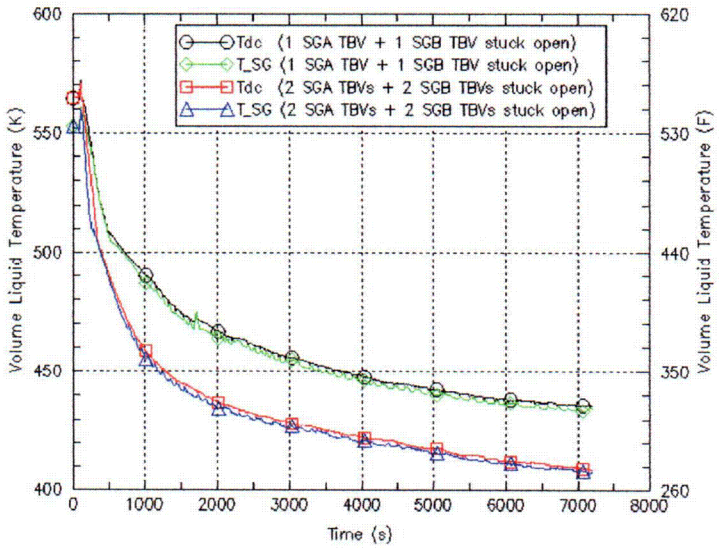

Figure A.5 The SG secondary side tube exit temperature and RCS downcomer temperature in the cases where 2 and 1 TBV(s) are stuck open per SG. It shows that the downcomer temperature closely follows the SG secondary side temperature.

C37

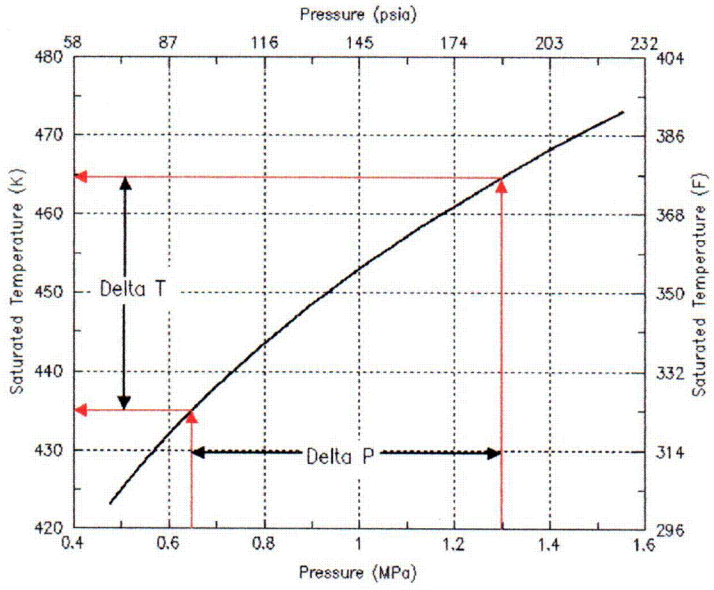

Figure A.6 Estimated delta T by reflecting delta p through saturation line

A.1.3 Augmented Uncertainty Transmission

The TH analysis uncertainty issue is considerably more complicated for transients in which the primary system is breached and regions within the primary become two-phase for significant time segments. The state of the fluid for such transients can be far from thermal equilibrium, and the TH results then depend strongly on the correct evaluation of energy/mass transfer rates. The volume averaged approach employed by codes, such as RELAP5 or TRAC then becomes a contributor to the uncertainty of the analytical results. An additional factor contributing significantly to the uncertainty is that for a range of conditions, a change in the system wide flow pattern can be initiated by the loss of the SG heat sink. This leads to termination of circulation flow, also called 'flow-stagnation'. The purpose of the example presented in this section is to illustrate what is meant by the term 'augmented uncertainty'.

The concept is best illustrated by a direct example. Figure A.7 shows the computed downcomer temperatures for two SB-LOCA events that are identical in all aspects except for the size of the break. For the upper T_{dc} trace the break area is 1.21e-4 m^2 (equivalent to 1.54 inches in diameter.), and for the lower trace it is 1.49e-4 m^2 (equivalent to 1.71 inches in diameter). The absolute difference in the break size is thus ~2.8e-5 m^2, whereas the downcomer fluid temperature difference at 5000 sec amounts to ~100 °K (compare that to 0.031 m^2 and 30 °K in the previous example). Clearly in this case, qualitatively different phenomena drive the transformation of a boundary condition difference into a divergence of the analytical results. The phenomenon in question is the possibility for 'flow-stagnation' that occurs for the larger break and does not occur for the smaller. Note that the difference in the break areas could very well be smaller and still produce this effect. No effort was made to find the 'smallest' area difference, because the values

chosen for the illustrative example already have a smaller difference than the uncertainty band imposed on this parameter by the boundary condition and model uncertainties.

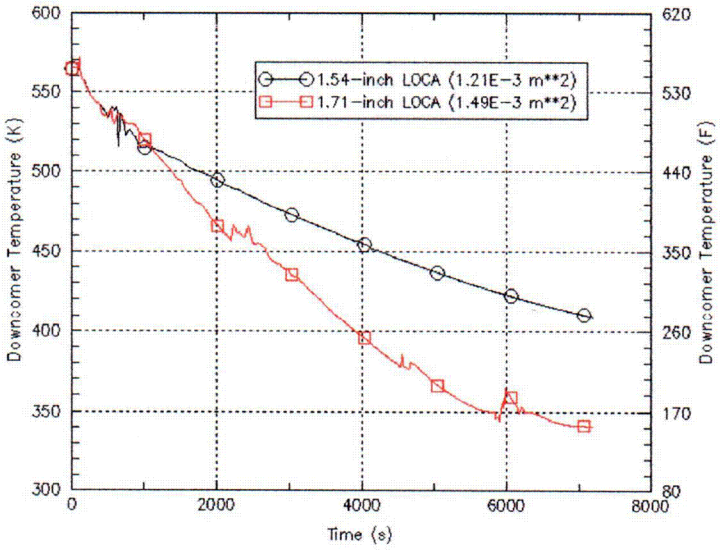

Figure A.7 T_{dc} traces for surge line break with break sizes of 1.49E-3 m^2 (1.71 inches in diameter) and 1.21E-3 m^2 (1.54 inches in diameter). No other system/component failure, and no operators' response actions are involved.

Table A.2 provides a summary of the uncertainty categories and their dependence on boundary and analytical uncertainties. The first column lists the possible modes for the propagation of uncertainties of the PTS relevant parameters. Note that besides the two main parameters T_{dc} and P_{dc}, it also includes $\Delta T_{SG\text{-}dc}$, the difference in temperature between the fluid exiting from the SG and the fluid entering the downcomer. The distinction is useful because for some transients T_{SG}, the exiting temperature from the SG can be determined by SG conditions, however, if the RCPs are shut-off and HPI is flowing, the temperature decrease of the fluid entering the downcomer is influenced by HPI parameters and the rate of circulatory flow. The second and third columns list the dominant energy sinks operative for the transient and the circulation mode of the primary system.

Essential information for further analysis is provided in the split fourth column, which lists the parameters that affect the uncertainties of T_{dc} and P_{dc}. They are divided into parameter uncertainty and model uncertainty. The parameter uncertainty includes uncertainty of the decay energy ($\dot{Q}_{dec}$), the HPI temperature (T_{HPI}), and the feed water flow rate ($\dot{W}_{fw}$). Note that some parameters, e.g. the HPI flow rate ($\dot{W}_{HPI}$) are not completely independent of the computed fluid state in the primary system and thus, to a degree, are also subject to 'model' uncertainty. The classification follows what is judged to be the 'dominant' characteristic.

On the 'model' uncertainty side is the computed circulatory flow ($\dot{W}_{circ}$) for natural circulation conditions. The circulation rate with RCPs running is not included, because it is so large in comparison to shutdown condition sinks/sources, that any uncertainty in its absolute value does not influence the PTS relevant parameters. Significant modeling uncertainties can be associated with the calculated mass ($\dot{W}_{out}$) and energy outflow rates ($\dot{Q}_{out}$) through breaks or un-closed valves. For conditions where flow stagnation occurs, internal circulation through the RVVV's (Reactor Vessel Vent Valves) becomes possible. Therefore the vent valve area ($A_{eff\text{-}VV}$) is included in the parameter uncertainty column; and the computed flow through the valves ($\dot{W}_{VV}$) is included in the 'model' column.

A.2 Classification of RCS Circulation Modes

The RCS circulation mode change is the main factor for transients having augmented Tdc propagation. This section discusses the uncertainty criteria of changing RCS circulation mode.

Except for limited times during overcooling transients, the primary system can include two-phase fluid regions only if it is breached. A two-phase fluid condition has a significant effect on the response of the plant and on the magnitude of the uncertainties associated with the evaluation of this response. The uncertainty margin becomes considerably wider because of the following reasons:

1. The uncertainties of the boundary conditions are larger for two-phase fluid conditions. This is the case because the boundary condition having the largest impact on transient response is the break flow rate, that strongly depends upon the size, location and nature of the break opening, and the condition of the fluid near the break. All of these parameters are subject to sizable uncertainties.

2. The presence of a break in the primary system introduces an additional energy sink. If this energy sink is larger then $\dot{Q}_{circ}$, the un-controlled depressurization of the primary system becomes independent of the SGs. The primary system can then become 'decoupled' from the SGs, which means that circulation flow will cease. For such conditions the mass/energy balance in the cold leg-downcomer region changes drastically. This places the evolution of T_{dc} on a qualitatively different development path, in effect, a bifurcation of the T_{dc} trace occurs.

3. The modeling of two-phase flow regimes and the associated empirical correlations determining mass/energy transfer rates for two-phase conditions have larger uncertainty bands than for single phase flows.

4. At stagnation or low flow conditions the forces driving natural circulation become very small, this emphasizes the effect of numerical oscillations. Numerical oscillations, especially oscillations in parallel flow channels, can introduce un-physical mixing.

An example of a bifurcated T_{dc} transient was presented in Figure A.7. The term can be applied to this example since the BC's (the break size) for both transients shown in the figure fall within the uncertainty range of this parameter and thus are, in a sense, interchangeable. As shown, the difference in T_{dc} values between a transient that does not experience flow stagnation and one that does increases with time, therefore the uncertainty range associated with T_{dc} increases as well. Note, that such an augmentation of the uncertainty applies for all transients that approach conditions at which flow stagnation could occur. In the example shown, it applies not just for the trace for which flow stagnation exists, but also for the transient for which such a condition was not calculated. As long as BC and model uncertainties encompass a range which could lead to flow stagnation, propagated uncertainties will be the augmented type. A key issue in the analysis of two-phase transients is therefore the evaluation of conditions for which flow-stagnation is possible.

The main criterion for classifying SB-LOCA transients is the relative magnitude of the mass/energy loss rate through the break in comparison to the mass/energy source terms. That is the case because a necessary pre-condition for the persistence of two-phase regions in the primary system and of flow stagnation is not just the presence of a break, but a break of sufficient size so that mass/energy is depleted at a rate so that:

A. Mass can not be replaced by HPI flow,
B. Net energy removal rate through the break exceeds the decay energy source.

This criterion leads to a four-fold grouping of two-phase transients as shown in Table A.3. The classification of the table is based on the relative magnitude of the energy/mass removal terms compared to the HPI flow rate and the decay energy. The net enthalpy flow rate in the table is given by $\dot{Q}_{brk} - \dot{Q}_{HPI}$, (the break enthalpy flow minus the enthalpy added by the HPI stream), and the corresponding mass flow rates are $\dot{W}_{brk}$ and $\dot{W}_{HPI}$. Starting with the smallest break size, the four categories are:

Table A.3 Classification of two-phase transients

Transient Category	Break Energy/Mass Flow Rate		Energy/Mass Sources	Flow Stagnation Probability
A	$\dot{Q}_{brk} - \dot{Q}_{IIPI}$ $\dot{W}_{brk}$	< <	$\dot{Q}_{dec}$ $\dot{W}_{HPI}$	No flow stagnation
B	$\dot{Q}_{brk} - \dot{Q}_{IIPI}$ $\dot{W}_{brk}$	< >	$\dot{Q}_{dec}$ $\dot{W}_{HPI}$	Flow stagnation possible, but intermittent
C	$\dot{Q}_{brk} - \dot{Q}_{IIPI}$ $\dot{W}_{brk}$	> >	$\dot{Q}_{dec}$ $\dot{W}_{HPI}$	Flow stagnation possible and could be prolonged
D	$\dot{Q}_{brk} - \dot{Q}_{IIPI}$ $\dot{W}_{brk}$	>> >>	$\dot{Q}_{dec}$ $\dot{W}_{HPI}$	Flow stagnation certain but P_{sys} decreases rapidly

A. If the break is sufficiently small so that both the mass and energy flows are smaller then the corresponding sources, then no long-term two-phase conditions will be present. Even if a short-term void in the primary system occurs during the initial depressurization phase, the inventory will recover and pressurizer control can be maintained. In spite of the presence of a small break, this transient category belongs to the class of 'primary system liquid solid' transients.

B. If the break is sufficiently large that gradual depletion of inventory will occur, but the energy lost through the break is less then the decay energy input, then flow stagnation becomes possible, but it will be intermittent. For OTSG type plants the TH response for such LOCA is quite complex and is characterized by several distinct flow states. Periods of flow stagnation become possible, however, they will last for relatively brief time periods (brief in comparison to the time constants of the RPV wall). That is so because as long as $(\dot{Q}_{brk} - \dot{Q}_{IIPI}) < \dot{Q}_{dec}$, the energy of the primary system increases when flow is interrupted and system pressure rises. As pressure increases, the temperature difference $T_{sat} - T_{dc}$ increases as well and the system moves further from an equilibrium condition. A T-H system cannot depart from equilibrium indefinitely. In some locations (e.g. upper downcomer and at higher inventory losses, also in the cold leg region) steam is in close proximity to cooler water. With increasing pressure, the probability of a rapid condensation event increases as well. These events generate local pressure differences that induce large flows and mixing of the liquid inventory. This leads to more evenly distributed temperatures, thus, from the PTS concern point of view, these events are beneficial. A variety of condensation events have been observed in several test facilities, and they are described in a number of references [Wang, 1992 #968;Bankoff, 1980 #560].

C. The potentially most serious state from the PTS standpoint is the condition in which the energy removed by break flow is somewhat larger, but of the same order of magnitude as the decay energy, and the HPI input rate is less then the

break mass flow. For this set of conditions the primary liquid level and the pressure decrease gradually. When the pressure falls below the pressure of the secondary, natural circulation is terminated and the SG heat sink is lost. However, since break flow alone can remove the energy supplied by $\dot{Q}_{dc}$, pressure does not rise. The non-equilibrium state of the system thus does not increase, and this condition can persist for long time periods. This combination of break and HPI flows can lead to potentially dangerous conditions from the PTS point of view, during which the entering cold HPI liquid reduces the fluid temperature in the downcomer, while system pressure remains relatively high.

D. Finally, for the last category break flows are sufficiently large so that both pressure and system fluid temperatures, including T_{dc}, decrease rapidly. The answer to the question whether the combination of the P_{dc} & T_{dc} parameters lead to conditions that are PTS relevant, depends on the definition of the end result ('crack propagation' or 'driving the crack through the wall') and on the outcome of PFM analysis.

In PTS studies conducted in the past, two-phase transients were classified using an informal three fold scheme, which considered breaks to be either 'very small', 'PTS relevant' or 'large'. The following justification was employed:

1) Very small breaks were eliminated because for such breaks, control of pressure is maintained and thus can be kept above the pressure of the secondary system (present category A).
2) LOCA's caused by breaks which lead to a relatively rapid depressurization (assumed to be larger then 2" in diameter) where eliminated because of low final pressures (category D).
3) The intermediate SBLOCA, for which the pressure remains sufficiently high and T_{dc} decreases, were considered to be 'PTS relevant'. In most past studies a ~ 2-inch in diameter break (~.002 m^2) [Fletcher, 1984 #573;Palmorse, 1999 #890] was taken as representative and most analytical effort was devoted to these transients.

As far as can be ascertained, no clear quantitative criteria were proposed to define the bounding values of the T_{dc} and P_{dc} variables for this classification scheme. This study differs from the previous ones in that the BC and model uncertainties are considered in evaluating the range of break sizes for which flow stagnation can occur. This broadens the range of breaks that could lead to stagnation.

A.3 Characteristics of Inventory Based Two-Phase Flow States in OTSG PWR's

For transients for which HPI flow is smaller than break flow, a gradual decrease of net primary system inventory occurs. Liquid levels in the RPV, the HLs and the tube side of the SGs decrease. As they drop, the collapsed liquid levels encounter flow geometry discontinuities. This leads to changes in local and system wide flow regimes. As liquid inventory is lost, vapor volumes first appear in the RPV dome and at the top of the HLs. The first location for the collection of vapor is the RPV dome. It is a dead end volume fed directly by rising vapor from the core. Once saturation pressures are reached, vapor

will also appear in the upper regions of the HLs. With increasing loss of inventory the primary system will pass through the following sequential flow regimes:

8% to 15% inventory loss

The vapor dome down to the HL entrance represents ~8 % of the primary system inventory. At this level of inventory, the vapor volume fills the RPV dome and some vapor is present in the vertical rising section of the HLs. The elevation difference between the core and the top of the HL, is such that even if steam does not penetrate into the HL entrance, some steam still can be present in the HL because the saturated liquid will flash as it travels upwards. It reaches the candy cane as a bubbly flow that is accelerated due to the lower density of the two-phase mixture. As long as condensation surfaces are available in the SG, at this inventory level phase separation does not occur and flow is maintained.

An issue worth mentioning is that the described behavior can be altered by the presence of incondensable. Flow blockages created by the accumulation of incondensable behave quite differently from those created by the accumulation of vapor. Vapor flow blockages can be removed by changes in system pressure and/or changes of local temperature. On the other hand, once incondensable segregates, it can be removed only by inertia driven flow. In the candy cane flow geometry this requires fluid velocities which generate distributed flow regimes.

From ~15 to ~30% inventory loss

At this level of inventory loss, sufficient vapor is available to fill the RPV dome and the top of the HLs. Now flow blockage of the HLs can occur. Resulting flow stagnation can be long term if $\dot{Q}_{decay} < \dot{Q}_{break}$ otherwise system pressure rises after the flow stagnates, and vapor is compressed leading to condensation, and the period of stagnation is relatively short. For these conditions a dynamic flow regime develops. The event sequence producing periodic phases of flow stagnation followed by periods of flow surges has the following physical interpretation:

A) start with the end of the 'flow- surge' phase during which sub-cooled water from the downcomer enters the core region.
B) This leads to a quenching of boiling.
C) the system pressure falls and water in the HL flashes filling the candy canes and shutting off flow to both SGs, thus losing the SG heat sink.

Flow is terminated. Subsequently decay heat raise the core water temperature, and boiling resumes. The vapor region in the RPV dome expands increasing system pressure and displacing hot water downward. The higher pressure in the RPV forces hot water and steam through the RVVV's into the upper region of the downcomer and to the entrance of the CLs. Simultaneously the increased pressure and displaced water reduces the vapor volume in the candy cane. The steam entering the upper region of the CL encounters subcooled water; this can generate a 'condensation implosion' event. The local condensation rate then increases dramatically, the local pressure decreases suddenly, and the generated pressure difference draws colder water to the RPV, quenching core boiling. Then the cycle is repeated. This flow regime has been

documented by Wang et al [Wang, 1989 #969] and is the IRM (Interruption-Resumption-Mode).

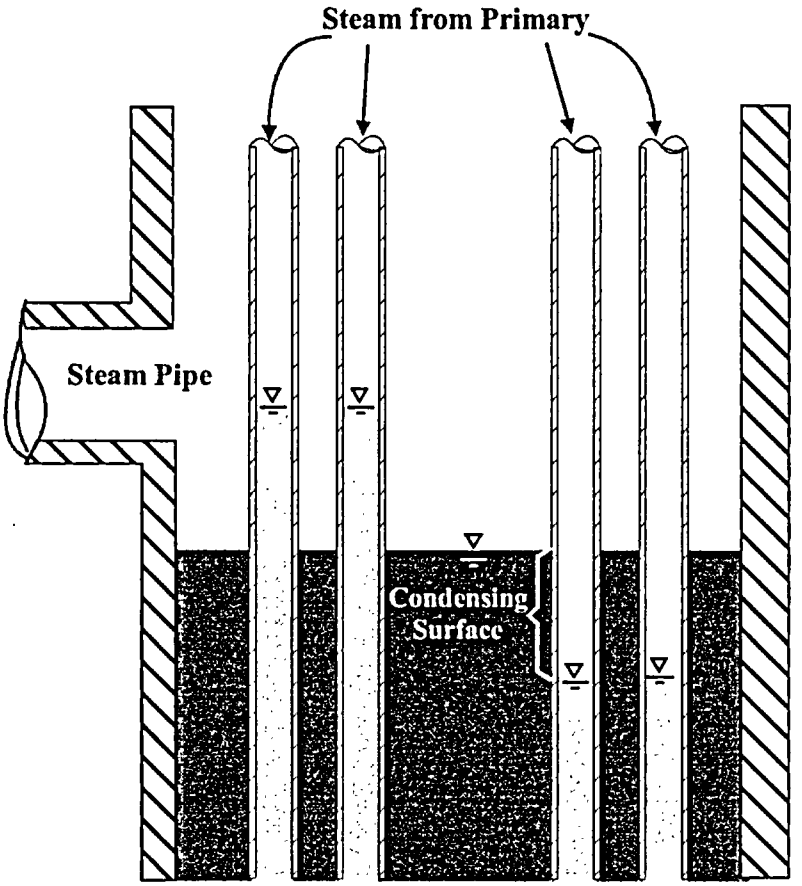

Figure A.8 Primary system inventory level dependent SG condensation surface

From ~30% to 45% inventory loss. Low elevation feed water.
How the system responds to a larger net inventory loss depends on the location at which feed water is introduced (sprays or regular feed-water introduction) into the secondary system. By the time inventory losses approach ~25%, the collapsed primary liquid level in the OTSG approaches the elevation reached by the liquid level in the secondary. System response will first be described for the low feed water introduction point.

When inventory loss has progressed to the point that the collapsed liquid level approaches the lower lip of the HL entrance, the system wide flow regime is altered. The upper third of the primary system is now filled entirely with steam and energy transport is determined by the availability of a condensing surface in the SG. The primary liquid level in the OTSG tubes settles down to the same level as in the RPV. System response

then depends upon the secondary liquid level on the shell side of the OTSG. If this level is higher then the collapsed primary level, the system enters the BCM (Boiling-Condensing Mode); if it is lower, the SG heat sink is lost and flow stagnates. The physical reason for this response is shown schematically in Figure A.8. If the relative inventory levels are such that the collapsed liquid level inside the tubes is higher then the liquid on the secondary system (left side illustration of Figure A.8), no condensation surface is available and heat-transfer to the SG is terminated. However, if inventory loss proceeds further, so that the liquid level in the tubes falls below the secondary system level (right side illustration of Figure A.8), energy transfer to the SG is resumed. For these conditions, flow stagnates for the time that is required for the loss of sufficient primary system inventory, so that a condensing surface is exposed.

From ~30% to 45% inventory loss. High elevation feed water.
If the feed water is introduced in the form of a spray at the elevated location, flow interruption due to unequal secondary and primary system liquid levels will not occur. The steam on the primary system of an OTSG will be condensed in the upper regions of the OTSG reached by the feed water spray. The transition to BCM will occur at higher primary system inventory levels and will be more gradual.

If a condensing surface is available after the upper part of the primary system is voided, energy/mass transfer occurs in the BCM (Boiling condenser Mode) regime. In this operating mode, liquid boils in the RPV, moves as steam to the OTSG and returns as liquid condensate. Because of the high latent heat of water, the rate of condensate flow in the CL is low, however, the energy transfer capability of this mode is high, therefore the system pressure will decrease rapidly towards levels set by the saturation temperature of the condensing surface.

Appendix B Effect of Heat Transfer Coefficient on the Evaluation of the Temperature Gradient Within the RPV Wall

The impact of h(t) on the evaluation of temperature gradients within the RPV wall has been considered in several previous studies, most recently in a study by Boyd and Dickson [Boyd, 1999 #415]. The main conclusion of the studies is that heat transfer to and from the RPV wall is determined primarily by the internal, conductive resistance, that is, energy transfer with the RPV wall is conduction limited. The impact of h(t), as well as the computational uncertainties that are associated with h(t) is therefore limited. This section considers the range and variation of h(t), and its dependence on the the bulk properties of the fluid, primarily on $T_{dc}(t)$.

The evaluation of the convective resistance at a vertical wall is a classical energy transport problem that is treated in all basic heat transfer texts. Depending on how fluid convection is generated two distinct convective modes are recognized:

1) Forced circulation. As the name implies, for this condition the fluid velocity field in front of the wall is imposed externally. The empirical correlations employed for this condition use the Re and Pr numbers.

2) Natural convection. For this condition the velocity field is generated by the temperature difference between the wall surface and the bulk fluid. The correlations used to obtain the Nu number then depend on the Gr (or Ra) numbers.

For some flow conditions the distinction is not clear cut, and 'mixed conditions' between natural and forced circulation are possible. Such conditions can occur during PTS relevant transients during which the circulation rate decreases significantly. Additional phenomena which can complicate the evaluation of h(t) include entrance effects, the length dimension used to characterize the flow field (it can be different for the Re and Gr numbers), characteristics of the flow field for time varying conditions and others. The evaluation of an adequate h(t) can thus be fairly complicated; this is then also reflected in the associated uncertainties. However, as noted, the major resistance to energy transfer into the thick RPV walls is the internal thermal diffusivity. Therefore, second order effects which influence h(t) can be disregarded. For PTS computations, it is sufficient to consider the generic variation of h(t) over the parameter's range of interest.

The dependence of h(t) on the bulk fluid temperature is shown schematically in Figure B-1. The solid line shows a generic variation of $T_{dc}(t)$ during a transient, the dotted lines the resulting potential family of h(t) curves. As illustrated in the figure, a transient which results in a cool-down of the downcomer region will also lead to lower h(t) values. Even if the fluid velocity does not change (that will be true if RCP's are operating), h(t) will decrease because of temperature dependent changes of viscosity and the Pr number. Over the temperature range of interest to PTS transients, this decrease can be up to 50%. If the RCP's are tripped during the transient, the velocity of the fluid in the downcomer

drops sharply and the decrease in the magnitude of h(t) will be considerably steeper. For the 'pumps off' condition, natural circulation forces determine fluid velocity. This can be the natural circulation flow of the primary system, or (when flow stagnation is approached) the local natural circulation that is generated by the temperature difference between the bulk fluid and the fluid in the boundary layer near the wall. For circulation flows, lower values of fluid velocity are correlated with a faster $T_{dc}(t)$ decrease rate.

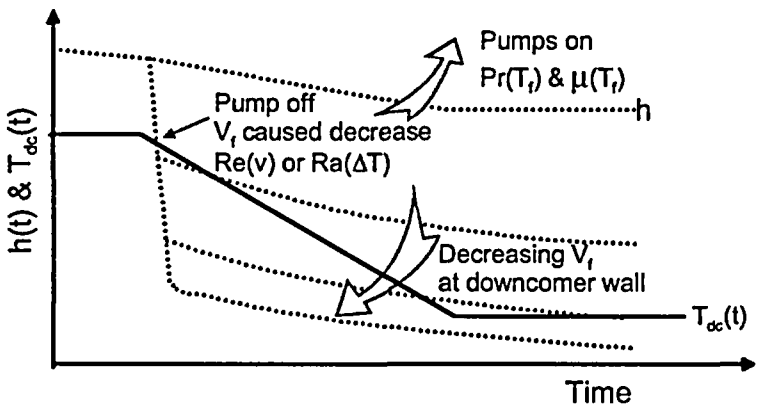

Figure B.1 Generic relationship between $T_{dc}(t)$ and $h_{dc}(t)$

Quantitative examples of h(t) dependence on $T_{dc}(t)$ and the local fluid velocity are evaluated using the correlations and algorithms employed in RELAP5. The code uses the classical Dittus-Boelter relationship for forced circulation flows and the Gr number dependent Churchill-Chu relationship for conditions where the predominant fluid motion is generated by internal natural circulation (RELAP5 manual, Vol. 4). The upper limit of forced circulation h(t) values occurs when the RCP's are operating. Coolant flows as well as velocities are then high (~18000 kg/s total flow, ~7 m/s fluid velocity in the downcomer). This leads to large Re numbers (on the order of ~28000) and to very large h(t) values (on the order of ~25000 W/m^2 K, or ~4400 BTU/hr ft^2 F). For such h(t) magnitudes the surface resistance becomes completely negligible. Of more practical interest are the 'forced' h(t) values when the RCP's are tripped and system flow is by natural circulation. That is not a contradiction in terms, since from the RPV wall point of view, what counts is whether the fluid in front of it is moved by an external driving force, or whether it has to be generated by a wall surface – to fluid temperature difference. Circulations that are driven by density differences in the core region and the SG's are as much 'external' to the RPV wall as circulation imposed by RCP's. They differ only in the magnitude of the fluid velocity.

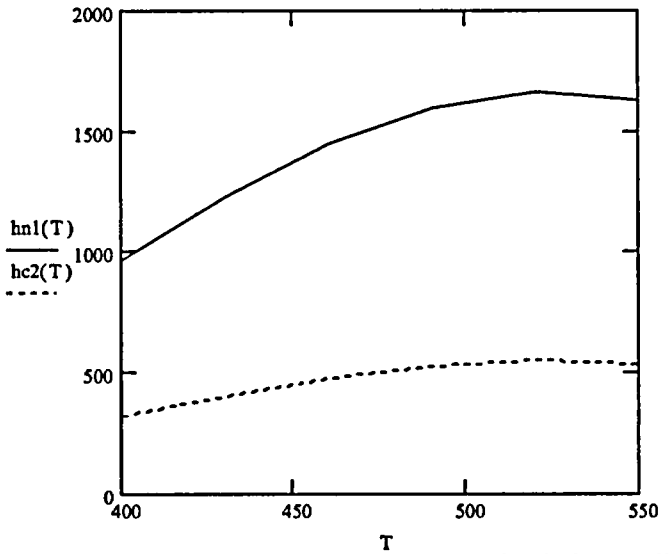

Figure B.2 Range of downcomer h(t) for external natural circulation conditions

The range of downcomer h(t) values generated by external natural circulation is shown in Figure B.2. Two bounding traces are presented as a function of fluid temperature. The upper trace corresponds to a circulation rate of ~440 kg/s, this represents flow shortly after shutdown when the decay energy is high. The lower trace shows a lower limit of ~110 kg/s that would apply when the decay energy is quite low. As shown, the range is from ~1500 to ~400 W/m^2 K (270 to 70 BTU/hr ft^2 F).

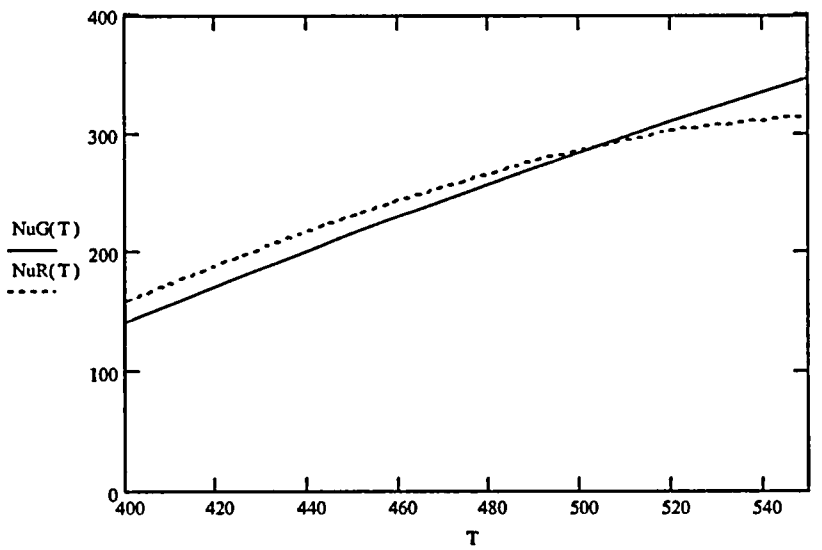

Figure B.3 Nu number dependence on Tdc(t) for the forced and natural circulation correlations. Where NuG(T) is the Nu number calculated from Churchill-Chu relationship. NuR(T) is the Nu number calculated from Dittus-Boelter relationship.

The bottom trace shown in Figure B.2 is a lower limit in two respects. It is limited by the rate of external natural circulation and by the internal circulation generated by a fluid to surface temperature difference. The switchover in the correlations from the local 'forced' to the internal 'natural' circulation occurs when the Gr number becomes larger then the square of the Re number. An example of Nu number dependence on $T_{dc}(t)$ for flow conditions at which the switchover occurs is shown in Figure B3. For this example, $Gr > Re^2$ when the local fluid velocity is ~.12 m/s and the wall surface to $T_{dc}(t)$ temperature difference is ~3° K. The figure shows that both correlations exhibit quite similar trends with respect to the local fluid temperature.

The switchover conditions illustrated in Figure B3 imply that for the duration of most transients, RELAP5 will choose the 'forced' circulation option. At a relatively low flow velocity of .12 m/s, a surface to bulk temperature difference of $\delta T_S > 3°K$ is required before the Gr-Ra number relationship is chosen. Since the thick RPV wall is conduction limited, the fluid to surface δT_S will generally be low (on the order of several degrees); h(t) is then determined by an Re number correlation and is proportional to $V_f^{0.8}$, where V_f is the bulk fluid velocity and, as illustrated in Figure B.2, it depends also on fluid temperature.

To complete a quantitative overview of the h(t) range, Fig B.4 shows the variation of h(t) determined using the Churchill-Chu correlation employed in RELAP5. Note that in this case the driving force is the 'internal' temperature difference between the fluid and the wall surface and is thus independent of external circulation. It applies therefore also for the case of complete flow stagnation. As shown in Figure B.4, when the surface-to-fluid temperature difference drops down to ~0.5 K, the magnitude of h(t) is on the order of ~600 W/m2 K. Based on the results presented in Figs B.2 and B.4, this value can be taken as a lower bound for h(t).

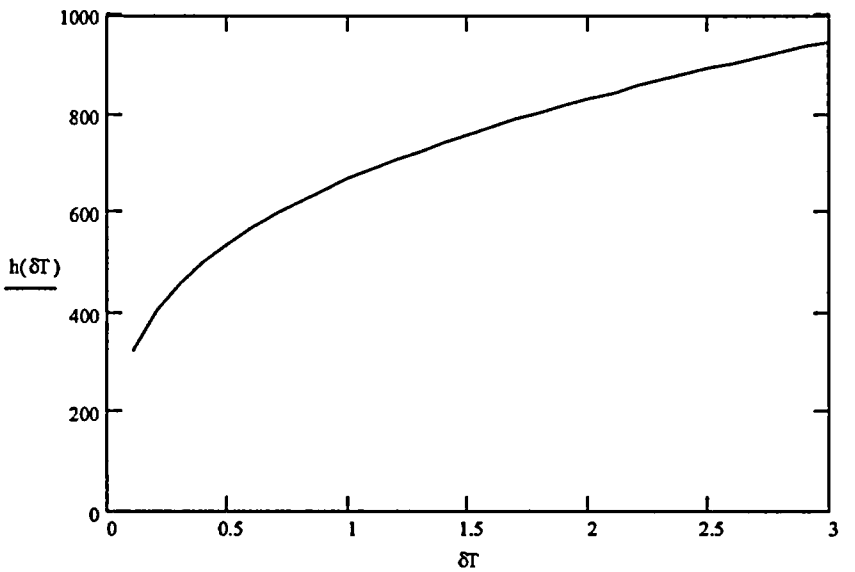

Figure B.4 $h_{(\Delta T)}$ determined by internal natural circulation vs fluid to surface ΔT

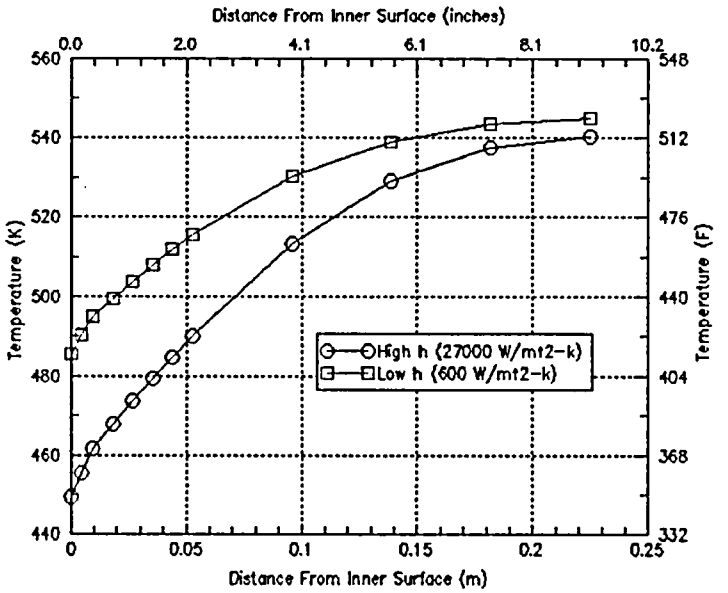

Figure B.5 Temp. distribution in RPV Wall

The effect of the entire possible range of h(t) values is shown in Fig B.5, which presents RELAP5 computed temperature distributions within the RPV wall 400 sec after a step temperature change of 100 K. The high (~27000 W/m^2 K) and low (~600 W/m^2 K) limiting values of h(t) are employed. Comparisons of the external and internal thermal resistances to the centerline of the RPV wall yields Bi numbers of 2 and 70 for the two cases. This confirms the conclusion reached by Boyd and Dickson (Boyd, 99) that energy transfer from the RPV wall is conduction limited over the entire possible range of h(t) values. The evaluation of temperature gradients within the wall then depends principally on the fluid temperature $T_{dc}(t)$, and the uncertainties associated with the evaluation of h(t) have a small influence. As long as the h(t) value supplied to PFM computations is of the right order of magnitude, the effect of its uncertainty can be disregarded.

Appendix C Primary System to SG Temperature Differences

It has been repeatedly noted in this study that for shutdown conditions the SG's are greatly over designed, an important consequence of this being that, as long as the SG's are available, the primary system liquid temperature will closely follow the temperature of the secondary side. This Appendix presents a quantitative analysis that verifies this conclusion.

The simulation of NPP transients by employing the RELAP5 code usually models secondary-to-primary heat transfer by representing the SG tube walls as a distinct solid region. As should be expected, the thermal time constants of the thin tube wall are quite short (on the order of 2 - 4 sec), and compared to the time constants of the RPV wall, they can be disregarded. This means that for purposes of PTS analysis, it is completely acceptable to assume that the SG tube wall is always at thermal equilibrium. The energy transfer rate across this wall can then be represented by:

$$\dot{Q}_{SG}(t) = \sum_{n=1}^{N} h_{eff,n}(t)\, A_n \left[T_{prim,n}(t) - T_{sec,n}(t)\right] \qquad \text{Eq. C.1}$$

Where N is the total number of segments used in the analysis and $h_{eff,n}$ is the 'effective' heat transfer coefficient for segment n, obtained from:

$$\frac{1}{h_{eff,n}} = \frac{1}{h_{prim,n}} + \frac{\Delta X_{tb}}{K_{tb}} + \frac{1}{h_{sec,n}} \qquad \text{Eq. C.2}$$

Where:

Δx_{tb} = tube thickness
K_{tb} = conductivity
$h_{prim,\,i}$ = heat transfer coefficient on primary side in sequence *i*
$h_{sec,\,i}$ = heat transfer coefficient on secondary side in sequence *i*

The RELAP5 computation of h values on the primary and secondary side employs complex algorithms. These algorithms choose the flow regime at time t (dependent on fluid state, velocity etc), on the basis of the flow regime they choose an empirical correlation that can depend on a variety of variables; finally, for cases where transitions occur, they can apply time averages. Note that this process is explicit, that is, the h applied for time interval t is based on the conditions determined for time interval t-δt. Unsurprisingly, such a complex process is burdened with many uncertainties. These include uncertainty in the choice of the flow regime, uncertainty in the appropriateness of the empirical correlation, the uncertainty in the code determined variables employed in the correlation, and finally, uncertainties imposed by the finite difference nature of the code and the explicitness of the computation. The clarification and quantification of these uncertainties is a formidable task.

Fortunately, because of the large 'over-designed' heat transfer surface area available in the SG's, the impact of these uncertainties on the temperature of the primary system liquid exiting from the SG's is small. The reason for this is illustrated by the following expression:

$$T_{pr,o}(t) = T_{sec} - \delta T \qquad \text{Eq. C.3}$$

Where $T_{pr,o}(t)$ is the temperature of the primary system liquid exiting from the SG and δT is the temperature difference between the primary and secondary. If the secondary side conditions are controlled, then all of the uncertainties associated with the evaluation of SG to primary energy transfer rates will be reflected in the value of δT. If δT is small in relation to T_{sec} then the impact of the associated uncertainties will be small as well. This is illustrated quantitatively in figures B1 to C.3

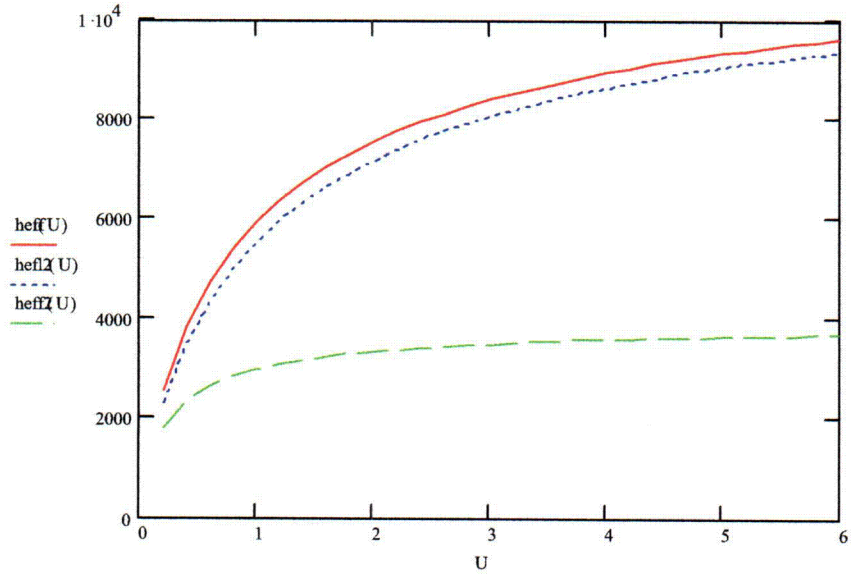

Figure C.1 h_{eff} as a function of liquid flow velocities in tubes

Of the three heat transfer resistances shown in eq. C.2 that determine the effective heat transfer coefficient h_{eff}, the largest is the forced convection resistance inside the tubes. It depends strongly on the fluid velocity, therefore Figure C.1 presents h_{eff} as a function of the liquid velocity in the tubes. Nominal velocities with RCP's operating are ~5 m/s; for natural circulation conditions, this drops down to ~0.1 to 0.2 m/s. The small difference between the two upper traces is caused by the possible variation of the heat transfer resistance on the secondary side. On the secondary side, boiling will take place and RELAP5 uses the Chen correlation for nucleate boiling or the modified Unal-Lahey correlation for bubbly flow (the most prevalent operation mode). The range extends over h values from ~5000 to 30000 W/m^2 K. The impact of this broad range on h_{eff} is small because the external resistance usually represents a small fraction of the total resistance. For completeness a third h_{eff} trace is included for the case where film boiling occurs at

C40

the external surface. Under shutdown conditions, the heat fluxes are not sufficiently large for film boiling, so this trace represents an outside bounding value.

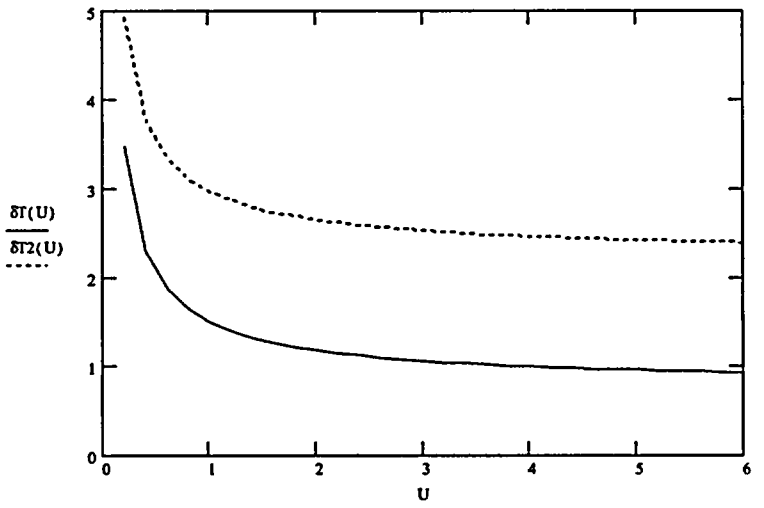

Figure C.2 Primary to sec. temperature difference (vs. tube side liq. velocity)

The liquid velocity dependant variation of h_{eff} is seen to be appreciable, as shown in Figure C.2, this is proportionally reflected in the range of the computed primary to secondary temperature differences. As noted, uncertainties associated with the employed correlations or the computation method will also be reflected in the evaluated magnitude of δT. However, for PTS analysis it is the absolute temperature of the fluid that is of interest. An example of how this parameter changes for the case where secondary temperature is maintained at 560 K and h_{eff} varies over its possible range is shown in Figure C.3.

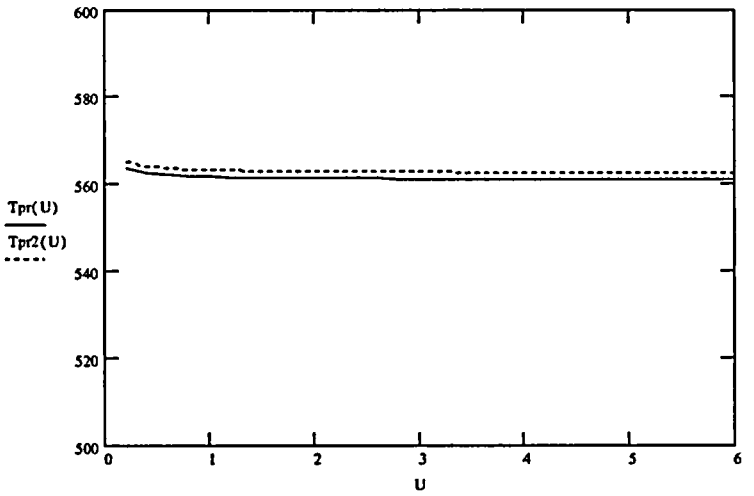

Figure C.3 Primary side Temperature exiting SG (vs. tube side liq. velocity)

Appendix D Program in Calculating Expected Uncertainty Indication Temperature

The C++ computer program written for calculating the linear multiple factor combine impact is included. The "Main.cpp" is the main program. The "TFactor.cpp" and "TFactor.h" define a class for calculation.

```
////////////////////////////////////////////////////////////////////////////////////////////////////////////////////////
// Main.cpp : Defines the entry point for the console application.
// Author: Y.H. Chang 10/14/2001
// Use linear relationship to calculate expected average downcomer temperature
// for Oconee thermal-hydraulic uncertainty study
////////////////////////////////////////////////////////////////////////////////////////////////////////////////////////
#include "stdafx.h"
#include "TFactor.h"
#include <iostream>
#include <vector>
#define ref 285.4243
typedef vector<TFactor> Clsf;
using namespace std;
int main(int argc, char* argv[])
{
    int ii, count;
    Clsf lsf0, lsf1, lsf2, lsf3, lsf4, lsf5, lsf6, lsf7, lsf8, lsf[42];
    Clsf::iterator itr0, itr1, itr2, itr3, itr4, itr5, itr6, itr7, itr8, itr;
    TFactor *factor_ptr;
    string t_name, str;
    double t_prob;
    double t_temp;
    bool not_found;
    //input data ("description", temp, probability)
    //Season
    factor_ptr = new TFactor("Winter", 264.8161, 0.25);
    lsf0.push_back(*factor_ptr);
    factor_ptr = new TFactor("Nom", ref, 0.50);
    lsf0.push_back(*factor_ptr);
    factor_ptr = new TFactor("Summer", 290.0, 0.25);
    lsf0.push_back(*factor_ptr);
    //p(CFT)
//  factor_ptr = new TFactor("p(CFT)+=50psi", 234.3168, 0.1);
//  lsf1.push_back(*factor_ptr);
    factor_ptr = new TFactor("", ref, 1.0);
    lsf1.push_back(*factor_ptr);
//  factor_ptr = new TFactor("p(CFT)-=50psi", 237.5232, 0.1);
//  lsf1.push_back(*factor_ptr);
    //m(HPI)
    factor_ptr = new TFactor("110%m(HPI)", 258.0331, 0.1);
    lsf2.push_back(*factor_ptr);
    factor_ptr = new TFactor("", ref, 0.8);
    lsf2.push_back(*factor_ptr);
    factor_ptr = new TFactor("90%m(HPI)", 291.304, 0.1);
    lsf2.push_back(*factor_ptr);
    //Model Uncertainty
    factor_ptr = new TFactor("130%A", 269.8725, 0.25);
```

```
        lsf3.push_back(*factor_ptr);
        factor_ptr = new TFactor("", ref, 0.5);
        lsf3.push_back(*factor_ptr);
        factor_ptr = new TFactor("70%A", 300.9761, 0.25);
        lsf3.push_back(*factor_ptr);
        //VV state
        factor_ptr = new TFactor("VVClose", ref - 50.0, 0.25);
        lsf4.push_back(*factor_ptr);
        factor_ptr = new TFactor("", ref, 0.5);
        lsf4.push_back(*factor_ptr);
        factor_ptr = new TFactor("VVOpen", ref + 50.0, 0.25);
        lsf4.push_back(*factor_ptr);
        //Heat transfer rate
        factor_ptr = new TFactor("130%HTR", 294.3794, 0.1);
        lsf5.push_back(*factor_ptr);
        factor_ptr = new TFactor("", ref, 0.8);
        lsf5.push_back(*factor_ptr);
        factor_ptr = new TFactor("70%HTR", 268.5074, 0.1);
        lsf5.push_back(*factor_ptr);
        //Loop flow resistance
//      factor_ptr = new TFactor("200%Resis", 234.2071, 0.10);
//      lsf6.push_back(*factor_ptr);
        factor_ptr = new TFactor("", ref, 1.0);
        lsf6.push_back(*factor_ptr);
        //HZP
        factor_ptr = new TFactor("HZP", 256.5954, 0.02);
        lsf7.push_back(*factor_ptr);
        factor_ptr = new TFactor("", ref, 0.98);
        lsf7.push_back(*factor_ptr);
        //ColdLeg
        factor_ptr = new TFactor("CL", 393.069, 0.5);
        lsf8.push_back(*factor_ptr);
        factor_ptr = new TFactor("", ref, 0.5);
        lsf8.push_back(*factor_ptr);
//
        ofstream fout1("all.txt", ios::out);
        for(itr0 = lsf0.begin(); itr0 != lsf0.end(); itr0++){
            for(itr1 = lsf1.begin(); itr1 != lsf1.end(); itr1++){
                for(itr2 = lsf2.begin(); itr2 != lsf2.end(); itr2++){
                    for(itr3 = lsf3.begin(); itr3 != lsf3.end(); itr3++){
                        for(itr4 = lsf4.begin(); itr4 != lsf4.end(); itr4++){
                            for(itr5 = lsf5.begin(); itr5 != lsf5.end(); itr5++){
                                for(itr6 = lsf6.begin(); itr6 != lsf6.end(); itr6++){
                                    for(itr7 = lsf7.begin(); itr7 != lsf7.end(); itr7++){
                                    for(itr8 = lsf8.begin(); itr8 != lsf8.end(); itr8++){
                                        str = itr0->getName();
                                        t_name = str;
                                        if(str.length() > 0){
                                            t_name += ';';
                                        }
                                        str = itr1->getName();
                                        if(str.length() > 0){
                                            t_name += str;
                                            t_name += ';';
                                        }
                                        str = itr2->getName();
```

```
                        if(str.length() > 0){
                            t_name += str;
                            t_name += ';';
                        }
                        str = itr3->getName();
                        if(str.length() > 0){
                            t_name += str;
                            t_name += ';';
                        }
                        str = itr4->getName();
                        if(str.length() > 0){
                            t_name += str;
                            t_name += ';';
                        }
                        str = itr5->getName();
                        if(str.length() > 0){
                            t_name += str;
                            t_name += ';';
                        }
                        str = itr6->getName();
                        if(str.length() > 0){
                            t_name += str;
                            t_name += ';';
                        }
                        str = itr7->getName();
                        if(str.length() > 0){
                            t_name += str;
                            t_name += ';';
                        }
                        str = itr8->getName();
                        if(str.length() > 0){
                            t_name += str;
                            t_name += ';';
                        }
t_prob = itr0->getProbability() * itr1->getProbability() * itr2->getProbability() *
          itr3->getProbability() * itr4->getProbability() * itr5->getProbability() *
          itr6->getProbability() * itr7->getProbability()* itr8->getProbability();
t_temp = itr0->getTemp() + itr1->getTemp() + itr2->getTemp() + itr3->getTemp() +
          itr4->getTemp() + itr5->getTemp() + itr6->getTemp() + itr7->getTemp()
          + itr8->getTemp() - 8.0 * ref;
//write to the all.txt file
    fout1 << t_temp << '\t' << t_prob << '\t' << t_name << '\n';
    factor_ptr = new TFactor(t_name, t_temp, t_prob);
                        not_found = true;
                        count = 0;
                        do {
                            if (t_temp <= 90.0 + count * 10.0 || count >= 40){
                                lsf[count].push_back(*factor_ptr);
                                not_found = false;
                            }
                            count ++;
                        }while (not_found);
                        }
                    }
                }
            }
```

```
                        }
                    }
                }
            }
        }
        fout1.close();
        ofstream fout("PTS_prob.txt", ios::out);
        for(ii = 0; ii <= 41; ii++){
            if (lsf[ii].size() > 0){
                t_temp = 0.0;
                t_prob = 0.0;
                for(itr = lsf[ii].begin(); itr != lsf[ii].end(); itr++){
                    t_temp += itr->getTemp() * itr->getProbability();
                    t_prob += itr->getProbability();
                }
                t_temp /= t_prob;
                fout << t_temp << '\t' << t_prob << '\n';
            }
        }
        fout.close();
        return 0;
}




//////////////////////////////////////////////////////////////////////
// TFactor.cpp: implementation of the TFactor class.
//
//////////////////////////////////////////////////////////////////////

#include "stdafx.h"
#include "TFactor.h"

TFactor::TFactor()
{

}
TFactor::TFactor(string c_name, double c_temp, double c_prob){
        Name = c_name;
        Temp = c_temp;
        Probability = c_prob;
}
TFactor::~TFactor()
{

}
string TFactor::getName() const {return Name;}
double TFactor::getTemp() const {return Temp;}
double TFactor::getProbability() const {return Probability;}
void TFactor::output(){
        cout << Name << '\t' << Temp << '\t' << Probability << '\n';
}
void TFactor::setName(string c_name){Name = c_name;}
void TFactor::setTemp(double c_temp){Temp = c_temp;}
```

```
void TFactor::setProbability(double c_probability){Probability = c_probability;}



//////////////////////////////////////////////////////////
// TFactor.cpp: implementation of the TFactor class.
//
//////////////////////////////////////////////////////////

#include "stdafx.h"
#include "TFactor.h"
TFactor::TFactor()
{

}
TFactor::TFactor(string c_name, double c_temp, double c_prob){
	Name = c_name;
	Temp = c_temp;
	Probability = c_prob;
}
TFactor::~TFactor()
{

}
string TFactor::getName() const {return Name;}
double TFactor::getTemp() const {return Temp;}
double TFactor::getProbability() const {return Probability;}
void TFactor::output(){
	cout << Name << '\t' << Temp << '\t' << Probability << '\n';
}
void TFactor::setName(string c_name){Name = c_name;}
void TFactor::setTemp(double c_temp){Temp = c_temp;}
void TFactor::setProbability(double c_probability){Probability = c_probability;}
```

Appendix E Parameters Sensitivities Assessment in Conditional Probability of Failure

Tables E1 and E2 list the scenarios for sensitivity study. Table E3 shows FAVOR calculation results of the scenarios listed in Tables E1 and E2.

Table E.1 The RELAP5-gamma calculation for surge line or HL LOCA related sensitivity runs

Break Size	1.5"	2"	2.828"	4"	5.656"	8"
Nominal	NRC(S64)	NRC(S65)	NRC(S66)	NRC(S67)	NRC(S68)	NRC(S69)
Winter*	UMD (S1)		UMD (S20)		UMD (S45)	UMD(S52)
Summer*			UMD (S21)		UMD (S46)	UMD(S53)
P(CFT) += 50 psi			UMD (S22)			
P(CFT) –= 50 psi			UMD (S23)			
110% m(HPI) RCPON	UMD (S3)		UMD (S24)			
110% m(HPI) RCPOFF	UMD (S63)					
90% m(HPI)	UMD (S4)		UMD (S25)			
HPI Failed and Recovered (@~7000 sec)			UMD (S26)			UMD(S54)
HPI Failed and Recovered (@~1000 sec)			UMD (S27)			
HPI Failed and Recovered (@~2000 sec)			UMD (S28)			
100 % HPI Failed			UMD(S29)	UMD(S41)	UMD(S48)	UMD(S55)
25% HPI Failed	UMD (S7)	UMD (S11)	UMD(S30)			
50% HPI Failed	UMD (S8)	UMD (S12)	UMD(S31)			
HZP	UMD (S9)		UMD/NRC (U32)		NRC(S49)	UMD(S56)
Vent Valve Close			UMD(S33)	UMD(S42)		
Vent Valve 2/6 Open			UMD(S34)			
Vent Valve 4/6 Open			UMD(S35)			
Vent Valve 6/6 Open			UMD(S36)	UMD(S43)		
High CL Reverse Flow Resistance	UMD (S10)	NRC (S13)	NRC/UMD U(S37)	NRC(S44)		UMD(S57)
130% Components Heat Transfer Coefficient		NRC (S14)	UMD(S38)		UMD(S50)	
70% Components Heat Transfer Coefficient		NRC (S15)	UMD(S39)		UMD(S51)	
200% Loop Flow Resistance		NRC (S16)				
200% Bypass Flow Area		NRC (S17)				
Zero Bypass Flow Area		NRC (S18)				
No heat structure		NRC (S19)				

*In winter, t(HPI) = 4.4 °C (40 °F), t(CFT) = 21.1 °C (70 °F), and t(LPI) = 4.4 °C(40 °F);
in summer, t(HPI)= 29.4 °C (85 °F), t(CFT) = 37.8 °C (100 °F), and t(LPI) = 29.4 °C (85 °F);
in spring and fall, t(HPI) = 21.1 °C (70 °F), t(CFT) = 26.7 °C (80 °F), and t(LPI) = 21.1 °C (70 °F)

Table E.2 The RELAP5-gamma calculation for CL LOCA related sensitivity runs

Break Size	2"	2.828"	4"	5.656"	8"
Cold Leg LOCA	NRC(S58)	UMD(S59)	NRC(S60)	NRC(S61)	UMD(S62)

Summary of PFM Analysis Results for Oconee Sensitivity Transients evaluated at 60 EFPY as requested* by ISL and University of Maryland

*(in e-mail dated 12/13/2002 from Bill Arcieri to Terry Dickson)

(183550 simulated RPVs)

Table E.3 Summary of PFM Analysis Results for Oconee Sensitivity Transients evaluated at 60 EFPY

Transient count	Sequence number	Min temp	Last temp	Min press	Last press	CPImn[1] @ 60 EFPY	CPFmn[2] @ 60 EFPY
1	S1	98.06	105.58	0.501	0.586	2.1988e-08	1.2656e-10
	S3	411.79	411.79	0.841	0.942		
2	S4	117.82	117.82	0.521	0.622	4.9057e-10	1.8331e-13
3	S7	167.22	171.37	0.434	0.434	0	0
4	S8	398.28	410.58	0.531	0.532	0	0
5	S9	342.76	342.76	0.619	0.807	0	0
6	S10	99.36	102.0	0.595	0.619	5.2303e-8	1.3915e-9
7	S11	171.89	171.89	0.240	0.240	3.7005e-9	1.8959e-12
	S12	406.75	406.75	0.383	0.386		
8	S13	85.00	85.00	0.240	0.255	3.6612e-7	1.5543e-8
9	S14	129.00	129.00	0.248	0.276	3.1774e-8	1.1900e-10
10	S15	106.00	106.00	0.238	0.262	2.2790e-8	1.2721e-10
11	S16	121.00	122.00	0.249	0.261	5.1878e-8	4.8016e-10
12	S17	123.00	123.00	0.247	0.261	0	0
13	S18	107.00	125.00	0.234	0.255	0	0
14	S19	76.30	77.50	0.243	0.276	2.6365e-6	4.5335e-8
15	S20	63.17	63.17	0.195	0.213	3.1057e-6	9.7699e-8
16	S21	91.48	91.48	0.195	0.213	1.0569e-6	2.5023e-8
17	S22	89.38	89.38	0.190	0.211	2.1358e-6	1.2381e-9
18	S23	82.29	82.29	0.190	0.213	1.8625e-6	5.9338e-8
19	S24	94.25	94.25	0.185	0.212	2.8639e-6	8.4526e-8
20	S25	80.99	80.99	0.192	0.213	2.7899e-6	1.0346e-7
21	S26	257.18	257.18	0.243	0.249	0	0
22	S27	85.13	85.13	0.192	0.213	9.3238e-7	1.824e-8
23	S28	86.60	86.60	0.192	0.212	1.0585e-6	2.2964e-8
	S29	368.99	387.72	0.207	0.216		
24	S30	117.88	117.88	0.184	0.211	1.0867e-6	2.0924e-8
25	S31	157.86	157.86	0.206	0.206	3.1315e-8	6.0909e-11
26	S32	75.28	75.61	0.187	0.214	2.1251e-6	4.2877e-8
27	S33	80.65	81.51	0.174	0.214	0	0
28	S34	133.50	137.00	0.199	0.213	0	0
29	S35	144.08	145.66	0.198	0.213	0	0
30	S36	146.59	146.59	0.202	0.213	0	0
31	S37	79.71	79.71	0.181	0.212	4.9910e-7	9.5720e-9
32	S38	88.45	88.45	0.194	0.210	1.4176e-6	3.3340e-8
33	S39	77.80	77.80	0.190	0.213	3.9684e-6	1.1794e-7
34	S41	75.62	75.62	0.142	0.171	9.8851e-6	2.7947e-7
35	S42	74.36	74.36	0.154	0.187	0	0
36	S43	95.21	95.21	0.170	0.190	5.2822e-7	4.7073e-9
37	S44	71.80	72.30	0.178	0.187	2.9483e-5	1.1286e-6
38	S45	50.50	50.50	0.122	0.141	2.0722e-5	3.5354e-7
39	S46	86.03	86.05	0.125	0.142	1.2086e-6	2.0188e-8
40	S48	71.40	71.50	0.114	0.143	1.9606e-5	8.5612e-7
41	S49	71.00	71.00	0.129	0.143	1.8850e-6	3.2900e-8
42	S50	75.90	75.90	0.117	0.145	3.2253e-5	1.5249e-6
43	S51	70.65	70.94	0.125	0.143	3.3954e-6	9.1492e-8
44	S52	68.40	68.70	0.067	0.084	1.7955e-6	1.3133e-8
45	S53	71.78	72.20	0.073	0.084	9.2895e-6	2.9244e-8
46	S54	70.62	70.62	0.068	0.084	1.2866e-6	2.0263e-8
47	S55	71.06	71.06	0.054	0.069	7.5060e-6	1.4628e-7
48	S56	70.63	70.74	0.063	0.084	2.9429e-5	1.1231e-6

49	S57	70.46	70.46	0.062	0.084	3.1633e-5	4.4701e-7
50	S58	242.85	242.85	0.306	0.314	0	0
51	S59	155.39	155.39	0.190	0.213	0	0
52	S60	120.00	121.00	0.158	0.189	2.2932e-8	1.4088e-11
53	S61	90.00	117.00	0.109	0.132	3.5977e-7	5.1615e-9
54	S62	74.30	75.60	0.067	0.083	1.0653e-5	1.2319e-7
55	S63	107.69	107.69	0.690	0.846	5.4924e-9	2.4874e-11
56	S64	119.41	119.50	0.589	0.620	0	0
57	S65	121.00	124.00	0.256	0.274	5.6471e-8	4.0944e-10
58	S66	89.10	89.10	0.197	0.212	1.6999e-6	5.1780e-8
59	S67	72.60	72.60	0.162	0.189	1.2689e-5	4.4349e-7
60	S68	70.80	74.00	0.124	0.143	2.1934e-5	7.4101e-7
61	S69	70.7	71.0	0.069	0.084	2.5649e-5	7.7173e-7

Mean value of conditional probability of crack initiation
Mean value of conditional probability of RPV failure (penetration to 90% of wall considered as failure)

Note: The PFM analysis was performed for 183550 simulated RPVs where each simulated RPV had an average of 7937 postulated flaws. This analysis took approximately 11 days on a 1.7 GHz Pentium 4. The results for each transient were reasonably well converged.

Appendix F Description the Official NRC TH Runs for Oconee NPP

This appendix provides the descriptions of all the official NRC TH runs for Oconee-1 PT, and placing these runs in the PTS event classification matrix in Tables D.1 and D.2, respectively. The UMD performed TH runs listed in Tables 6.2 to 6.4 as well as specific runs for studying certain phenomenon are not included.

Table F.1 The descriptions of the NRC official TH runs for Oconee-1 (Arcierir, 2001)

Oconee Case List (11/28/01)									
Case Number	Case Type	Primary Side Failure	Secondary Side Failure	Operator Action	LDH	Hi K	Mod of	PRA	Comments
1	LOCA	2.54 cm (1 inch) surge line break	None	None	No	No	N/A		
2	LOCA	3.59 cm (1.414 in) surge line break	None	None	No	No	N/A		
3	LOCA	5.08 cm (2 in) surge line break	None	None	No	No	N/A	x	
4	LOCA	7.183 cm (2.828 in) surge line break	None	None	No	No	N/A	x	
5	LOCA	10.16 cm (4 inch) surge line break	None	None	No	No	N/A	x	
6	LOCA	3.59 cm (1.414 in) cold leg break	None	None	No	No	N/A		
7	LOCA	5.08 cm (2 inch) cold leg break	None	None	No	No	N/A		
8	LOCA	2.54 cm (1 inch) surge line break	1 stuck open safety valve in SG-A	None	No	No	N/A	x	
9	LOCA	2.54 cm (1 inch) surge line break	2 stuck open safety valves in SG-A	None	No	No	N/A		
10	LOCA	3.59 cm (1.414 inches) surge line break	2 stuck open safety valves in SG-A	None	No	No	N/A		
11	LOCA	2.54 cm (1 inch) surge line break	1 stuck open safety valve in SG-A	HPI terminated when subcooling margin exceeds 55.6 K (100° F)	No	No	N/A		
12	LOCA	2.54 cm (1 inch) surge line break	1 stuck open safety valve in SG-A	HPI throttled to maintain 27.8 K (50° F) subcooling margin	No	No	N/A	x	
13	LOCA	2.54 cm (1 inch) surge line break	2 stuck open safety valves in SG-A	HPI terminated when subcooling margin exceeds 55.6 K (100° F)	No	No	N/A		
14	LOCA	3.59 cm (1.414 in) surge line break	None	Operator is assumed to trip the reactor coolant pumps at 2.778 K (5° F) subcooling.	No	No	N/A		
15	LOCA	2.54 cm (1 in) surge line break with HPI Failure	None	At 15 minutes after transient initiation, operator opens all TBVs to lower primary system pressure and allow CFT and LPI injection.	No	No	N/A	x	
16	LOCA	2.54 cm (1 in) surge line break	None	None	Yes	No	N/A		
17	LOCA	2.54 cm (1 in) surge line break	1 stuck open safety valve in SG-A	None	Yes	No	N/A		
18	TT/RT	None	SG level control system failure causes SG overfill.	Operator is assumed to shut off the emergency feedwater system when the level reaches 96% operating range.	No	No	N/A		
19	TT/RT	None	SG level control system failure causes SG overfill. EFW continues running and the SGs flood and remain flooded.	Operator throttles EFW, maintaining flooded SGs without flooding the steam lines.	No	No	N/A		
20	TT/RT	None	One stuck open TBV in SG-A	The operator throttles HPI to maintain a level of 5.59 m (220 in) in the pressurizer	No	No	N/A		
21	TT/RT	None	None	None	No	No	N/A		
22	TT/RT	Stuck Open PORV	None	None	No	No	N/A		
23	TT/RT	None	SG level control system failure causes SG overfill. EFW continues running and the SGs flood and remain flooded.	Operator trips MFW and turbine driven EFW. Motor driven EFW remains running.	No	No	N/A		Same as 19?
24	TT/RT	None	SG level control system failure	Operator trips MFW when water enters the steam lines.	No	No	N/A		

			causes SG overfill. MFW continues running and the SGs flood.						
25	MSLB	None	MSLB with trip of turbine driven emergency feedwater by the MSLB circuitry.	None	No	No	N/A		
26	MSLB	None	MSLB without trip of turbine driven emergency feedwater	None	No	No	N/A		
27	MSLB	None	MSLB without trip of turbine driven emergency feedwater	Operator throttles HPI to maintain 50° F (27.8 K) subcooling margin.	No	No	N/A	x	
28	TT/RT	None	1 stuck open safety valve in SG-A	None	No	No	N/A	x	
29	TT/RT	None	1 stuck open safety valve in SG-A and a second stuck open safety valve in SG-B	None	No	No	N/A	x	
30	TT/RT	None	1 stuck open safety valve in SG-A	None	Yes	No	N/A	x	
31	TT/RT	None	1 stuck open safety valve in SG-A and a second stuck open safety valve in SG-B	None	Yes	No	N/A	x	
32	TT/RT	None	SG level control system failure causes SG overfill. MFW continues running and the SGs flood.	Operator trips MFW when water enters the steam lines. Operator also throttles HPI (throttling criteria is 50°F subcooling and 120" pressurizer level)	No	No	N/A		
33	TT/RT	None	One stuck open TBV in SG-A. Valve reseates in 10 minutes.	None	No	No	N/A		
34	TT/RT	Stuck open pressurizer Safety Valve	None	None	No	No	N/A	x	
35	TT/RT	None	1 stuck open safety valve in SG-A	Operator throttles HPI to maintain 27.8 K (50° F) subcooling or 304.8 cm (120 in) of level in the pressurizer, whichever is controlling.	No	No	N/A		
36	TT/RT	None	1 stuck open safety valve in SG-A and a second stuck open safety valve in SG-B	Operator throttles HPI to maintain 27.8 K (50° F) subcooling or 304.8 cm (120 in) level in the pressurizer, whichever is controlling.	No	No	N/A	x	
37	TT/RT	None	1 stuck open safety valve in SG-A	Operator throttles HPI to maintain 27.8 K (50° F)) subcooling or 304.8 cm (120 in) level in the pressurizer, whichever is controlling	Yes	No	N/A	x	
38	TT/RT	None	1 stuck open safety valve in SG-A and a second stuck open safety valve in SG-B	Operator throttles HPI to maintain 27.8 K (50° F) subcooling or 304.8 cm (120 in) level in the pressurizer, whichever is controlling.	Yes	No	N/A	x	
39	SGTR	None	SGTR with a stuck open SRV in SG-A. A reactor trip is assumed to occur at the time of the tube rupture.	None.	No	No	N/A		
40	SGTR	None	SGTR. A reactor trip is assumed to occur at the time of the tube rupture.	Operator uses pressurizer sprays to depressurize.	No	No			
41	TT/RT	Stuck open pressurizer safety valve. Valve reseates at 6000 secs (RCS low pressure point).	None	None	No	No	N/A	x	
42	TT/RT	Stuck open pressurizer safety valve. Valve reseates at 6000 secs.	None	None	Yes	No	N/A	x	
43	TT/RT	Stuck open PORV. Valve reseates at 400 sec (RCS low pressure point)	None	None	No	No	N/A		
44	LOCA	2.54 cm (1 in) surge line break with HPI Failure		At 15 minutes after initiation, operators open all TBVs to depressurize the system to the CFT setpoint. When	No	No	N/A	x	

				the CFTs are 50 percent discharged, HPI is assumed to be recovered. The TBVs are assumed remain open for the duration of the transient.					
45	TT/RT	None	Loss of MFW and EFW. At ~30 minutes after operator starts HPI and opens the PORV, EFW is restored. Normal EFW level control is assumed.	Operator starts primary system "feed and bleed" cooling by starting the HPI and opening the PORV at RCS pressure > 2275 psia. Operator also trips one RCP in each steam generator loop (if 0.27 K (0.5° F) subcooling margin is reached, the remaining two RCPs are tripped). The operator then closes the PORV and throttles HPI to maintain 55 K (100° F) subcooling.	No	No	N/A		
46	TT/RT	None	Loss of MFW and EFW. At ~30 minutes after operator starts HPI and opens the PORV, EFW is restored. Normal EFW level control is assumed.	Operator starts primary system "feed and bleed" cooling by starting the HPI and opening the PORV at RCS pressure > 2275 psia. Operator also trips one RCP in each steam generator loop (if 0.27 K (0.5° F) subcooling margin is reached, the remaining two RCPs are tripped). The operator then closes the PORV but fails to throttle HPI.	No	No	N/A		
47	TT/RT	None	Loss of MFW and EFW. At ~30 minutes after operator starts HPI and opens the PORV, EFW is restored. EFW level control fails where the steam generators are overfilled and remain overfilled but water does not enter the steam lines.	Operator starts primary system "feed and bleed" cooling by starting the HPI and opening the PORV at RCS pressure > 2275 psia. Operator also trips one RCP in each steam generator loop (if 0.27 K (0.5° F) subcooling margin is reached, the remaining two RCPs are tripped).	No	No	N/A		
48	TT/RT	None	Loss of MFW and EFW. At ~30 minutes after operator starts HPI and opens the PORV, EFW is restored. Normal EFW level control is assumed.	Operator starts primary system "feed and bleed" cooling by starting the HPI and opening the PORV at RCS pressure > 2275 psia. Operator also trips one RCP in each steam generator loop (2.7 K (5° F) subcooling margin is reached, the remaining two RCPs are tripped). The operator then closes the PORV and throttles HPI to maintain 55 K (100° F) subcooling.	No	No	N/A		
49	TT/RT	None	Loss of MFW and EFW.	Operator opens the TBV to depressurize the secondary side to below the condensate booster pump shutoff head so that these pumps feed the steam generators. Booster pumps are assumed to be uncontrolled so that the steam generators are overfilled. Booster pump flow is then assumed to be terminated. Operator throttles HPI to maintain ~ 55 K (100° F) subcooling and a pressurizer level of 254 cm (100 in) or more. The operator also throttles the TBVs to maintain 3.45 MPa (500 psi) secondary side pressure.	No	No	N/A		
50	TT/RT	None	Loss of MFW and EFW.	Operator opens all TBV to depressurize the secondary side to below the condensate booster pump shutoff head so that these pumps feed the steam generators. Booster pumps are assumed to be uncontrolled so that the steam generators are filled to the top. Booster pump flow is then assumed to be terminated. Operator throttles HPI to maintain ~ 55 K (100° F) subcooling and a pressurizer level of 254 cm (100 in) or more. The TBVs are kept fully opened due to operator error.	No	No	N/A		
51	TT/RT	None	Loss of MFW and EFW.	Operator opens the TBV to depressurize the secondary side to below the condensate booster pump shutoff head so that these pumps feed the steam generators.	Yes	No	N/A		

				Booster pumps are assumed to be uncontrolled so that the steam generators are filled to the top. Booster pump flow is then assumed to be terminated. Operator throttles HPI to maintain ~ 100oF subcooling and a pressurizer level of 100 inches or more. The operator throttles the TBVs to maintain 500 psi secondary side pressure.					
52	LOCA	14.37 cm (5.656 in) surge line break	None	None	No	No	N/A	x	
53	LOCA	20.32 cm (8 inch) surge line break	None	None	No	No	N/A	x	
54	LOCA-IIi K	5.08 cm (2 in) surge line break	None	None	No	Yes	3	x	
55	LOCA-IIi K	7.183 cm (2.828 in) surge line break	None	None	No	Yes	4	x	
56	TT/RT-IIi K	Stuck open pressurizer safety valve.	None	None	No	Yes	34	x	
57	TT/RT	None	Two stuck open safety valves in SG-A.	Operator isolates EFW in SG-A.	No	No	N/A		
58	LOCA-IIi K	10.16 cm (4 inch) surge line break	None	None	No	Yes	5		
59	TT/RT	None	2 stuck open safety valves in SG-A	Operator throttles HPI to maintain 27.8 K (50oF) subcooling or pressurizer level of 304.8 cm (120 inches), whichever is limiting. The operator stops emergency feedwater flow to SG-A at 15 minutes after accident initiation.	No	No	N/A		
60	TT/RT	None	2 stuck open safety valves in SG-A	Operator throttles HPI to maintain 27.8 K (50° F) subcooling or pressurizer level of 304.8 cm (120 inches), whichever is limiting. Assume that the operator stops emergency feedwater flow to SG-A at 15 minutes after accident initiation.	Yes	No	N/A		
61	MSLB	None	MSLB with shutdown of the MFW and the turbine driven EFW pumps by the MSLB circuitry.	Operator stops motor driven EFW flow to the affected steam generator after 10 minutes.	No	No	N/A		
62	MSLB	None	MSLB with shutdown of the MFW and the turbine driven EFW pumps by the MSLB circuitry. Break occurs in the containment so that RCP trip occurs due to a containment isolation signal at 1 minute after break initiation.	None	No	No	N/A		
63	LOCA-S	5.08 cm (2 in) surge line break. Core flood tank temperature of 294 K(70°F). Nominal temperature is 300 K (80° F)	None	None	No	No	3	x	
64	LOCA-S	5.08 cm (2 in) surge line break. Core flood tank temperature of 310 K(100°F). Nominal temperature is 300 K (80° F)	None	None	No	No	3	x	
65	LOCA-S	5.08 cm (2 in) surge line break. HPI temperature of 278 K (40° F). Nominal temperature is 294 K (70° F)	None	None	No	No	3	x	
66	LOCA-S	5.08 cm (2 in) surge line break. HPI temperature of 300 K (80° F). Nominal temperature is 294 K (70° F).	None	None	No	No	3	x	

67	LOCA-S	5.08 cm (2 in) surge line break. Increased effective heat transfer coefficient used (1.3 x HTC).	None	None	No	No	3	x	
68	LOCA-S	5.08 cm (2 in) surge line break. Decreased effective heat transfer coefficient used (0.7 x HTC).	None	None	No	No	3	x	
69	LOCA-S	5.08 cm (2 in) surge line break. Increased loop flow resistance to reduce natural circulation (100 % increase).	None	None	No	No	3	x	
70	LOCA	5.08 cm (2 inch) surge line break	None	None	Yes	No	3	x	
71	LOCA-S	5.08 cm (2 in) surge line break. Reduced vent valve resistance (delta-P) to opening (Factor of 0.5).	None	None	No	No	3	x	
72	LOCA-S	5.08 cm (2 in) surge line break. No vent valve function.	None	None	No	No	3	x	Same as 80
73	LOCA	14.366 cm (5.656 in) surge line break	None	None	Yes	No	52	x	
74	LOCA	2.54 cm (1 in) surge line break with HPI Failure	None	At 15 minutes after transient initiation, the operator opens all turbine bypass valves to lower primary system pressure and allow core flood tank and LPI injection.	Yes	No	15	x	
75	LOCA	2.54 cm (1 in) surge line break with HPI Failure	None	At 15 minutes after sequence initiation, operators open all TBVs to depressurize the system to the CFT setpoint. When the CFTs are 50 percent discharged, HPI is assumed to be recovered. The TBVs are assumed remain opened for the duration of the transient.	Yes	No	44	x	
76	LOCA	3.81 cm (1.5 in) surge line break	None	None	No	No	N/A	x	
77	TT/RT	None	One stuck open TBV in SG-A. Valve reseates in 20 minutes.	Operator throttles HPI to maintain 558 cm (220 in) level in the pressurizer.	No	No	N/A		
78	LOCA-S	5.08 cm (2 in) surge line break. No heat structures.	None	None	No	No	3		
79	LOCA-S	5.08 cm (2 in) surge line break. No heat structures and no vent valve function.	None	None	No	No	3		
80	LOCA-S	5.08 cm (2 in) surge line break. No vent valve function.	None	None	No	No	3		Same as 72
81	LOCA	5.08 cm (2 inch) surge line break with HPI Failure	None	At 15 minutes after transient initiation, operator opens all TBVs to lower primary system pressure and allow CFT and LPI injection.	No	No	15	x	
82	LOCA	2.54 cm (1 in) surge line break with HPI Failure	None	At 15 minutes after initiation, operator opens all TBVs to lower primary pressure and allow CFT and LPI injection. When the CFTs are 50% discharged, HPI is recovered. At 3000 seconds after initiation, operator starts throttling HPI to 5°F subcooling and 100" pressurizer level.	No	No	44	x	
83	TT/RT	Stuck open pressurizer safety valve. Valve reseates at 6000 secs.	None	After valve reseates, operator throttles HPI 1 minute after 5°F subcooling or 100" pressurizer level is reached (throttling criteria is 5°F subcooling and 100" pressurizer level)	No	No	41	x	
84	TT/RT	Stuck open pressurizer safety valve.	None	After valve reseates, operator throttles HPI 10 minutes	No	No	41	x	

		Valve reseates at 6000 secs.		after 5°F subcooling or 100" pressurizer level is reached (throttling criteria is 5°F subcooling and 100" pressurizer level)					
85	TT/RT	Stuck open pressurizer safety valve. Valve reseates at 3000 secs.	None	After valve reseates, operator throttles HPI 1 minute after 5°F subcooling or 100" pressurizer level is reached (throttling criteria is 5°F subcooling and 100" pressurizer level)	No	No	41	x	
86	TT/RT	Stuck open pressurizer safety valve. Valve reseates at 3000 secs.	None	After valve reseates, operator throttles HPI 10 minutes after 5°F subcooling or 100" pressurizer level is reached (throttling criteria is 5°F subcooling and 100" pressurizer level)	No	No	41	x	
87	TT/RT	Stuck Open Pressurizer SRV and HPI Failure	None	At 15 minutes after initiation, operator opens all TBVs to lower primary pressure and allow CFT and LPI injection. When the CFTs are 50% discharged, HPI is recovered. The HPI is throttled 20 minutes after 5°F subcooling or 100" pressurizer level is reached (throttling criteria is 5°F subcooling and 100" pressurizer level).	No	No	41	x	
88	TT/RT	Stuck Open Pressurizer SRV and HPI Failure	None	At 15 minutes after initiation, operator opens all TBVs to lower primary pressure and allow CFT and LPI injection. When the CFTs are 50% discharged, HPI is recovered. The SRV is closed 5 minutes after HPI recovered. HPI is throttled at 1 minute after 5°F subcooling or 100" pressurizer level is reached (throttling criteria is 5°F subcooling and 100" pressurizer level).	No	No	87	x	
89	TT/RT	None	Loss of MFW and EFW.	Operator opens all TBVs to depressurize the secondary side to below the condensate booster pump shutoff head so that these pumps feed the steam generators. Booster pumps are assumed to be initially uncontrolled so that the steam generators are overfilled (240 inches startup level). Operator controls booster pump flow to maintain SG level at 30 inches (startup level) due to continued RCP operation. Operator also throttles HPI to maintain ~ 100oF subcooling and a pressurizer level of 100 inches or more. The TBVs are kept fully opened due to operator error.	No	No	50	x	
90	TT/RT	None	2 stuck open safety valves in SG-A	Operator throttles HPI 20 minutes after 5°F subcooling or 100" pressurizer level is reached (throttling criteria is 5°F subcooling and 100" pressurizer level).	No	No	29	x	
91	SGTR	None	SGTR with a stuck open SRV in SG-B. A reactor trip is assumed to occur at the time of the tube rupture. Stuck safety relief valve is assumed to reseat 10 minutes after initiation.	Operator trips RCP's 1 minute after initiation. Operator also throttles HPI 10 minutes after 5°F subcooling or 100" pressurizer level is reached (assumed throttling criteria is 5°F subcooling or 100" pressurizer level).	No	No	39	x	
92	TT/RT	Stuck open pressurizer safety valve. Valve reseates at 6000 secs .	None	After valve reseates, operator throttles HPI at 1 minute after 5°F subcooling or 100" pressurizer level is reached (throttling criteria is 5°F subcooling and 100" pressurizer level).	Yes	No	41 and 83	x	
93	TT/RT	Stuck open pressurizer safety valve. Valve reseates at 6000 secs.	None	After valve reseates, operator throttles HPI 10 minutes after 5°F subcooling or 100" pressurizer level is reached (throttling criteria is 5°F subcooling and 100"	Yes	No	41 and 84	x	

				pressurizer level).					
94	TT/RT	Stuck open pressurizer safety valve. Valve reseates at 3000 secs.	None	After valve reseates, operator throttles HPI 1 minute after 5°F subcooling or 100" pressurizer level is reached (throttling criteria is 5°F subcooling and 100" pressurizer level).	Yes	No	41 and 85	x	
95	TT/RT	Stuck open pressurizer safety valve. Valve reseates at 3000 secs.	None	After valve reseates, operator throttles HPI 10 minutes after 5°F subcooling or 100" pressurizer level is reached (throttling criteria is 5°F subcooling and 100" pressurizer level).	Yes	No	41 and 86	x	
96	TT/RT	Stuck Open Pressurizer SRV and HPI Failure	None	At 15 minutes after initiation, operator opens all TBVs to lower primary pressure and allow CFT and LPI injection. When the CFTs are 50% discharged, HPI is recovered. HPI is throttled 20 minutes after 5°F subcooling or 100" pressurizer level is reached (throttling criteria is 5°F subcooling and 100" pressurizer level).	Yes	No	41 & 87	x	
97	TT/RT	Stuck Open Pressurizer SRV and HPI Failure	None	At 15 minutes after initiation, operator opens all TBVs to lower primary pressure and allow CFT and LPI injection. When the CFTs are 50% discharged, HPI is recovered. SRV is closed at 5 minutes after HPI is recovered. HPI is throttled at 1 minute after 5°F subcooling or 100" pressurizer level is reached (throttling criteria is 5°F subcooling and 100" pressurizer level).	Yes	No	87 and 88	x	
98	TT/RT	None	Loss of MFW and EFW.	Operator opens all TBVs to depressurize the secondary side to below the condensate booster pump shutoff head so that these pumps feed the steam generators. Booster pumps are assumed to be initially uncontrolled so that the steam generators are overfilled (240 inches startup level). Operator controls booster pump flow to maintain SG level at 30 inches (startup level) due to continued RCP operation. Operator also throttles HPI to maintain ~ 100oF subcooling and a pressurizer level of 100 inches or more. The TBVs are kept fully opened due to operator error.	Yes	No	50 and 89	x	
99	MSLB	None	MSLB with trip of turbine driven EFW by MSLB Circuitry.	HPI is throttled 20 minutes after 5°F subcooling or 100" pressurizer level is reached (throttling criteria is 5°F subcooling and 100" pressurizer level).	No	No	27	x	
100	MSLB	None	MSLB with trip of turbine driven EFW by MSLB Circuitry	Operator throttles HPI 20 minutes after 5°F subcooling or 100" pressurizer level is reached (throttling criteria is 5°F subcooling and 100" pressurizer level).	Yes	No	27 and 99	x	
101	MSLB	None	MSLB with trip of turbine driven EFW by MSLB Circuitry	None	Yes	No	27	x	
102	TT/RT	None	2 stuck open safety valves in SG-A	Operator throttles HPI 20 minutes after 2.77 K (5°F) subcooling or 254 cm (100 in) pressurizer level is reached (throttling criteria is 2.77 K (5°F) subcooling and 100" pressurizer level).	Yes	No	29 and 90	x	
103	SGTR	None	SGTR with a stuck open SRV in SG-B. A reactor trip is assumed to occur at the time of the tube rupture. Stuck safety relief valve is assumed to reseat 10 minutes after initiation.	Operator trips RCP's 1 minute after initiation. Operator also throttles HPI 10 minutes after 2.77 K (5° F) subcooling or 254 cm (100 in) pressurizer level is reached (assumed throttling criteria is 2.77 K (5°F) subcooling or 254 cm (100 in) pressurizer level).	Yes	No	39 and 91	x	

104	LOCA	3.59 cm (1.414 in) surge line break	None	None	Yes	No	2	x	
106	LOCA	7.18 cm (2.828 in) surge line break	None	None	Yes	No	4	x	
107	LOCA-Hi K	2.54 cm (1 inch) surge line break	2 stuck open safety valves in SG-A	HPI terminated when subcooling margin exceeds 55.6 K (100o F)	No	Yes	13		
108	TT/RT-Hi K	Stuck open pressurizer Safety Valve	None	None	No	Yes	34	x	Duplicate of 56
109	TT/RT-Hi K	Stuck open pressurizer Safety Valve. Valve reseates at 6000 secs (RCS low pressure point).	None	None	No	Yes	41	x	
110	LOCA-Hi K	5.08 cm (2 inch) surge line break with HPI Failure	None	At 15 minutes after transient initiation, operator opens both TBV to lower primary system pressure and allow CFT and LPI injection.	No	Yes	81	x	
111	LOCA-Hi K	2.54 cm (1 in) surge line break with HPI Failure	None	At 15 minutes after initiation, operator opens all TBVs to lower primary pressure and allow CFT and LPI injection. When the CFTs are 50% discharged, HPI is recovered. At 3000 seconds after initiation, operator starts throttling HPI to 5°F subcooling and 100" pressurizer level.	No	Yes	82	x	
112	TT/RT-Hi K	Stuck open pressurizer Safety Valve. Valve reseates at 6000 secs.	None	After valve reseates, operator throttles HPI 1 minute after 5°F subcooling or 100" pressurizer level is reached (throttling criteria is 5°F subcooling and 100" pressurizer level)	No	Yes	83	x	
113	TT/RT-Hi K	Stuck open pressurizer Safety Valve. Valve reseates at 6000 secs.	None	After valve reseates, operator throttles HPI 10 minute after 5°F subcooling or 100" pressurizer level is reached (throttling criteria is 5°F subcooling and 100" pressurizer level)	No	Yes	84	x	
114	TT/RT-Hi K	Stuck open pressurizer Safety Valve. Valve reseates at 3000 secs.	None	After valve reseates, operator throttles HPI 1 minute after 5°F subcooling or 100" pressurizer level is reached (throttling criteria is 5°F subcooling and 100" pressurizer level)	No	Yes	85	x	
115	TT/RT-Hi K	Stuck open pressurizer Safety Valve. Valve reseates at 3000 secs.	None	After valve reseates, operator throttles HPI 10 minutes after 5°F subcooling or 100" pressurizer level is reached (throttling criteria is 5°F subcooling and 100" pressurizer level)	No	Yes	86	x	
116	TT/RT-Hi K	Stuck Open Pressurizer SRV and HPI Failure	None	At 15 minutes after initiation, operator opens all TBVs to lower primary pressure and allow CFT and LPI injection. When the CFTs are 50% discharged, HPI is recovered. The HPI is throttled 20 minutes after 5°F subcooling or 100" pressurizer level is reached (throttling criteria is 5°F subcooling and 100" pressurizer level).	No	Yes	87	x	
117	TT/RT-Hi K	Stuck Open Pressurizer SRV and HPI Failure	None	At 15 minutes after initiation, operator opens all TBV to lower primary pressure and allow CFT and LPI injection. When the CFTs are 50% discharged, HPI is recovered. The SRV is closed 5 minutes after HPI recovered. HPI is throttled at 1 minute after 5°F subcooling or 100" pressurizer level is reached (throttling criteria is 5°F subcooling and 100" pressurizer level).	No	Yes	88	x	
118	LOCA-Hi K	5.08 cm (2 inch) surge line break	None	None	Yes	Yes	70	x	
119	LOCA-Hi K	2.54 cm (1 in) surge line break with HPI Failure	None	At 15 minutes after transient initiation, the operator opens all turbine bypass valves to lower primary	Yes	Yes	74	x	

				system pressure and allow core flood tank and LPI injection.					
120	LOCA-Hi K	2.54 cm (1 in) surge line break with HPI Failure	None	At 15 minutes after sequence initiation, operators open all TBVs to depressurize the system to the CFT setpoint. When the CFTs are 50 percent discharged, HPI is assumed to be recovered. The TBVs are assumed remain opened for the duration of the transient.	Yes	Yes	75	x	
121	TT/RT-Hi K	Stuck open pressurizer Safety Valve. Valve reseates at 6000 secs	None	Operator throttles HPI at 1 minute after 5°F subcooling or 100" pressurizer level is reached (throttling criteria is 5°F subcooling and 100" pressurizer level).	Yes	Yes	92	x	
122	TT/RT-Hi K	Stuck open pressurizer Safety Valve. Valve reseates at 6000 secs.	None	Operator throttles HPI 10 minutes after 5°F subcooling or 100" pressurizer level is reached (throttling criteria is 5°F subcooling and 100" pressurizer level).	Yes	Yes	93	x	
123	TT/RT-Hi K	Stuck open pressurizer Safety Valve. Valve reseates at 3000 secs.	None	Operator throttles HPI 1 minute after 5°F subcooling or 100" pressurizer level is reached (throttling criteria is 5°F subcooling and 100" pressurizer level).	Yes	Yes	94	x	
124	TT/RT-Hi K	Stuck open pressurizer Safety Valve. Valve reseates at 3000 secs.	None	Operator throttles HPI 10 minutes after 5°F subcooling or 100" pressurizer level is reached (throttling criteria is 5°F subcooling and 100" pressurizer level).	Yes	Yes	95	x	
125	TT/RT-Hi K	Stuck Open Pressurizer SRV and HPI Failure	None	At 15 minutes after initiation, operator opens all TBVs to lower primary pressure and allow CFT and LPI injection. When the CFTs are 50% discharged, HPI is recovered. HPI is throttled 20 minutes after 5°F subcooling or 100" pressurizer level is reached (throttling criteria is 5°F subcooling and 100" pressurizer level).	Yes	Yes	96	x	
126	TT/RT-Hi K	Stuck Open Pressurizer SRV and HPI Failure	None	At 15 minutes after initiation, operator opens all TBVs to lower primary pressure and allow CFT and LPI injection. When the CFTs are 50% discharged, HPI is recovered. SRV is closed at 5 minutes after HPI is recovered. HPI is throttled at 1 minute after 5°F subcooling or 100" pressurizer level is reached (throttling criteria is 5°F subcooling and 100" pressurizer level).	Yes	Yes	97	x	
127	SGTR-HiK	None	SGTR with a stuck open SRV in SG-B. A reactor trip is assumed to occur at the time of the tube rupture. Stuck safety relief valve is assumed to reseat 10 minutes after initiation.	Operator trips RCP's 1 minute after initiation. Operator also throttles HPI 10 minutes after 5°F subcooling or 100" pressurizer level is reached.	Yes	Yes	103	x	
128	LOCA-HiK	7.18 cm (2.828 in) surge line break	None	None	Yes	Yes	106	x	
129	LOCA	10.16 cm (4 inch) cold leg break	None	None	No	No	N/A		
130	LOCA	14.37 cm (5.656 in) cold leg break	None	None	No	No	N/A		
131	LOCA	10.16 cm (4 inch) surge line break	None	None	Yes	No	5	x	
132	LOCA	20.32 cm (8 inch) surge line break	None	None	Yes	No	53	x	
133	LOCA-HiK	10.16 cm (4 inch) surge line break	None	None	Yes	Yes	131	x	
134	LOCA-HiK	20.32 cm (8 inch) surge line break	None	None	Yes	Yes	132	x	
135	LOCA-S	8.53 cm (3.36 in) surge line break (Break flow area reduced by 30%	None	None		No			

		from 10.16 cm (4 in) break). Vent valves do not function.							
136	LOCA-S	4.34 cm (1.71 in) surge line break (Break flow area increased by 30% from 3.81 cm (1.5 in) break). Winter conditions assumed (HPI, LPI temp = 277 K (40° F) and CFT temp = 294 K (70° F)).	None	None	No	No	N/A		
137	TT/RT-S	TT/RT with stuck open pzr SRV (valve flow area reduced by 30 percent). Summer conditions assumed (HPI, LPI temp = 302 K (85° F) and CFT temp = 310 K (100° F)). Vent valves do not function.	None	None	No	No	N/A		
138	TT/RT-S	TT/RT with stuck open pzr SRV. Summer conditions assumed (HPI, LPI temp = 302 K (85° F) and CFT temp = 310 K (100° F)).	None	None	No	No	N/A		
139	TT/RT-S	TT/RT with partially stuck open pzr SRV (flow area equivalent to 1.5 in diameter opening). HTC coefficients increased by 1.3.	None	None	No	No	N/A		
140	TT/RT-S	TT/RT with stuck open pzr SRV. SRV assumed to reseat at 3000 secs. Operator does not throttle HPI.	None	None	No	No	N/A		
141	LOCA-HiK	8.19 cm (3.22 in) surge line break (Break flow area increased by 30% from 7.18 cm (2.828 in) break).	None	None	No	Yes	N/A	x	
142	LOCA-HiK	6.01 cm (2.37 in) surge line break (Break flow area decreased by 30% from 7.18 cm (2.828 in) break).	None	None	No	Yes	N/A	x	
143	LOCA-HiK	7.18 cm (2.828 in) cold leg break.	None	None	No	Yes	N/A	x	
144	LOCA-HiK	8.53 cm (3.36 in) surge line break (Break flow area reduced by 30% from 10.16 cm (4 in) break). Vent valves do not function.	None	None	No	Yes	135	x	
145	LOCA-HiK	4.34 cm (1.71 in) surge line break (Break flow area increased by 30% from 3.81 cm (1.5 in) break). Winter conditions assumed (HPI, LPI temp = 277 K (40° F) and CFT temp = 294 K (70° F)).	None	None	No	Yes	136	x	
146	LOCA-HiK	TT/RT with stuck open pzr SRV (valve flow area reduced by 30 percent). Summer conditions assumed (HPI, LPI temp = 302 K (85° F) and CFT temp = 310 K (100° F)). Vent valves do not function.	None	None	No	Yes	137	x	
147	TT/RT-Hi K	TT/RT with stuck open pzr SRV.	None	None	No	Yes	138	x	

		Summer conditions assumed (HPI, LPI temp = 302 K (85° F) and CFT temp = 310 K (100° F)).							
148	TT/RT-Hi K	TT/RT with partially stuck open pzr SRV (flow area equivalent to 1.5 in diameter opening). HTC coefficients increased by 1.3.	None	None	No	Yes	139	x	
149	TT/RT-Hi K	TT/RT with stuck open pzr SRV. SRV assumed to reseat at 3000 secs. Operator does not throttle HPI.	None	None	No	Yes	140	x	

Table F.2. The placement of the official NRC TH runs in the PTS event classification matrix

Primary Side / Secondary Side	Intact	Small Breach (X < ~1.5")	Medium Breach (X > ~1.5")

Neither SG breach nor SG overfed	A1B1 21(Rx trip)	A2B1_1 1 (1" surge line) 16 (#1 + HZP) 22 (PZR PORV SO, 1.1") 2 (1.4" surge line) 14 (#2 + RCP trip) 104 (#2 + HZP) 6 (1.4" CL) 43 (PZR PORV SO, valve reseated @ 400 seconds) 46 (F&B + loss /recovery of FW)	76 (1.5" surge line) 136 (1.5", break area += 30%, RCPs trip) 145 (#136 + Hi CL Rev. K) 3 (2" surge line) 105 (#3 + HZP) 54 (#3, Hi CL Rev. K) 63 (#3, t(CFT) = 70 F) 64 (#3, t(CFT) = 100 F) 65 (#3, t(HPI) = 40 F) 66 (#3, t(HPI) = 80 F) 67 (#3, 130 % heat transfer coeff. in all components after RCPs trip) 68 (#3, 70% heat transfer coeff. in all components after RCPs trip) 69 (#3, 200% flow resistance) 70 (#3, HZP) 118 (#70 + Hi CL Rev. K) 71 (#3, 200% bypass flow) 72 (#3, zero bypass flow) 78 (#3, No heat structure) 79 (#3, No heat structure + VVs closed) 80 (#3, VVs closed) 7 (2" CL){0} 4 (2.828" surge line) 55 (#4 + Hi CL Rev. K) 106 (#4 + HZP) 128 (#106 + Hi CL Rev. K) 141 (#4 with increased 30% break area + Hi CL Rev. K) 142 (#4 with reduced 30% break area + Hi CL Rev. K) 5 (4" surge line) 58 (#5, Hi CL Rev. K) 129 (4" cold leg) 143 (#129 + Hi CL Rev. K) 135 (#4, break area -= 30%, VV Closed) 144 (#135 + Hi CL Rev. K) 131 (#4 + HZP) 133 (#131 + Hi CL Rev. K) 34 (PZR-SRV, 2.54") 56 (#34 + Hi. Rev. K) 137 (#34, Open area -= 30% + Summer + VV Close) 146 (#137 + Hi CL Rev. K) 138 (#34 + summer) 147 (#138 + Hi CL Rev. K) 139 (PZR SRV Stuck open area = 1.5", Comp HTC *= 130%, RCPs trip) 148 (#139 + Hi CL Rev. K) 108 (same as 56) 41 (PZR-SRVs reseat at 100 minutes) 109 (#41 + Hi CL Rev. K) 42 (#41 + HZP) 140 (PZR-SRVs reseat at 50 minutes) 149 (#140 + Hi CL Rev. K) 52 (5.656" surge line) 73 (#52 + HZP) 130 (5.656" Cold Leg) 53 (8" surge line) 132 (#53 + HZP) 134 (#132 + Hi CL Rev. K)

		A2B1_2 40 (SGTR) 45 (F&B < 2000 s) 48 (F&B, PZR PORV reseated @ 2000 seconds)	A3B1_2 83 (PZR SRV SO. SRV reseated at 100 min, HPI throttled 1 min after 5F subcool and 100" PZR level) 112 (#83 + Hi CL Rev. K) 92 (#83 + HZP) 121 (#92 + Hi CL Rev. K) 84 (PZR SRV SO. SRV reseated at 100 min, HPI throttled 10 min after 5F subcool and 100" PZR level) 113 (#84 + Hi CL Rev. K) 93 (#84 + HZP) 122 (#93 + Hi CL Rev. K) 85 (PZR SRV SO. SRV reseated at 50 min, HPI throttled 1 min after 5F subcool and 100" PZR level) 114 (#85 + Hi CL Rev. K) 94 (#85 + HZP) 123 (#94 + Hi CL Rev. K) 86 (PZR SRV SO. SRV reseated at 50 min, HPI throttled 10 min after 5F subcool and 100" PZR level) 115 (#86 + Hi CL Rev. K) 95 (#86 + HZP) 124 (#95 + Hi CL Rev. K)
		A2B1_3	A3B1_3
		A2B1_4	A3B1_4
One SG Breach	A1B2_1*	A2B2_1 8 (1" surge line + SGA 1SV) 17 (#8 + HZP) 9 (1" surge line, SGA 2SVs) 10 (1.4" surge line, SGA 2SVs) 28 (F&B, 1SG SV SO) 30 (#28 + HZP) 39 (SGTR + SGB 1SV) 57 (2 SVs, SGA EFW isolated)	A3B2_1
	A1B2_2 20 (1TBV) 33 (1TBV, t_{dpi_ctrl} = 10 min) 35 (1SV) 37 (#35 + HZP) 27 (MSLB) 101 (#27 + HZP)	A2B2_2 11 (1" surge line, 1SV, HPI_{trip}) 12 (1" surge line, 1SV) 13 (1" surge line, SGA 2SVs, HPI trip when subcool > 100F) 107 (#13 + Hi CL Rev. K) 59 (2 SVs, $HPI_{throttled}$, SGA EFW stopped at 15 min) 60 (#59 + HZP) 90 (SGA 2 SVs SO, HPI throttled @ 20 min after it can be throttled) 102 (#90 + HZP) 91 (SGA TR+ 1SGB SV SO and reseated @ 10 min after initiation + RCP tripped @ 1 min + HPI throttled @ 10 min after it can be throttled) 103 (#91 + HZP) 127 (#103 + Hi CL Rev. K) 99 (MSLB + HPI throttled 20 min after it can be throttled) 100 (#99 + HZP)	A3B2_2

	A1B2_3 61 (MSLB, TD EFW & MFW stopped. MD EFW to bad SG is tripped at 10 min) 62 (MSLB, TD EFW & MFW tripped, RCPs tripped at 1 min)	A2B2_3	A3B2_3
	A1B2_4	A2B2_4	A3B2_4
Two SGs Breach	A1B3_1*	A2B3_1 29 (2SVs) 31 (#29 + HZP)	A3B3_1
	A1B3_2 36 (2SVs) 38 (#36 + HZP)	A2B3_2	A3B3_2
	A1B3_3	A2B3_3 15 (1" + 4 TBVs fully open) 74 (#15 + HZP) 119 (#74 + Hi CL Rev. K) 77 (1 TBV SO and reseated @ 20 min, HPI is stopped @ ~15 min)	A3B3_3 81 (2" surge line, 4 TBVs opened @ 15 min) 110 (#81 + Hi CL Rev. K)
	A1B3_4	A2B3_4 44 (1" + 4 TBVs Opened @ 15 min, HPI recovered when CFTs are 50% discharged) 75 (#44 + HZP) 120 (#75 + Hi CL Rev. K) 82 (1" + 4 TBVs Opened @ 15 min, HPI recovered when CFTs are 50% discharged, HPI throttled @ 50 min) 111 (#82 + Hi CL Rev. K)	A3B3_4 87 (PZR SRV SO, HPI fail, 4 TBVs opened @ 15 min, HPI was recovered when CFT are 50% discharged; HPI was throttled @ 20 min after available) 116 (#87 + Hi CL Rev. K) 96 (#87 + HZP) 125 (#96 + Hi CL Rev. K) 88 (PZR SRV SO, HPI fail, 4 TBVs opened @ 15 min, HPI was recovered when CFT are 50% discharged; SRV reseated 5 min after HPI was recovered, HPI throttled 1 min after available). 117 (#88 + Hi CL Rev. K) 97 (#88 + HZP) 126 (#97 + Hi CL Rev. K)
SG(s) Overfed	A1B4_1*	A2B4_1 47 (F&B, loss/recover FW, EFW OF)	A3B4_1
	A1B4_2	A2B4_2	A3B4_2
	A1B4_3 18 (EFW, 96%) 19 (EFW, level maintained at 100%) 23 (EFW) 24 (MFW OF, MFW tripped when water enters MSL) 32 (MFW OF, MFW tripped when water enters MSL, same as #24)	A2B4_3	A3B4_3
	A1B4_4	A2B4_4	A3B4_4

SG(s) Breach + SG(s) Overfed	A1B5_1*	A2B5_1 25 (MSLB, 32.6", AFW_{motor} + MFW overfeed brk SGs, intact SG lvl maintain at 50%) 26 (MSLB, 32.6", AFW_{motor} + AFW_{fb}, MFW overfeed brk SGs, intact SG lvl maintain at 50%)	A3B5_1
	A1B5_2 89 (F&B, + 4 TBVs are opened and HPI is throttled after RCS pressure reaches 2275 psi) 98 (#89 + HZP)	A2B5_2 49 (4 TBVs throttled to maintain SGs pressure at 3.45 Mpa + SGs overfed to 100% then stop FW) 50 (4TBVs + SGs overfed to 100% then stop FW) 51 (#49 + HZP) {0}	A3B5_2
	A1B5_3	A2B5_3	A3B5_3